2017 Synthesis and Processing Science Principal Investigators' Meeting

Gaithersburg Marriott Washingtonian Center, Gaithersburg, MD

November 7-9, 2017

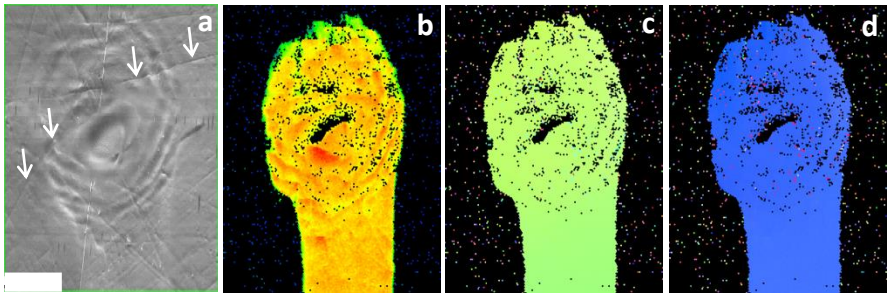

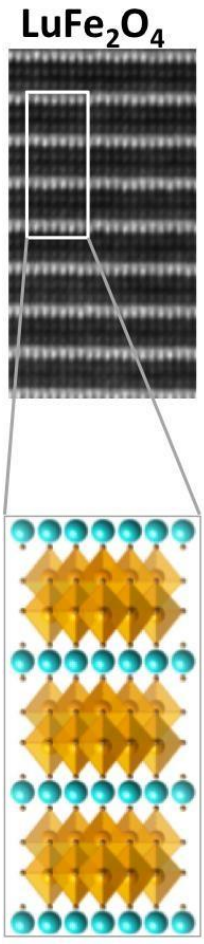

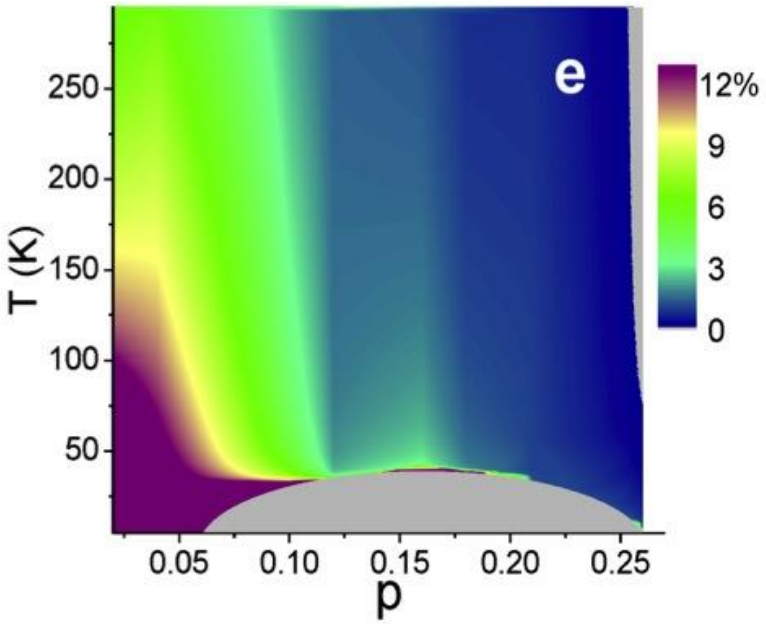

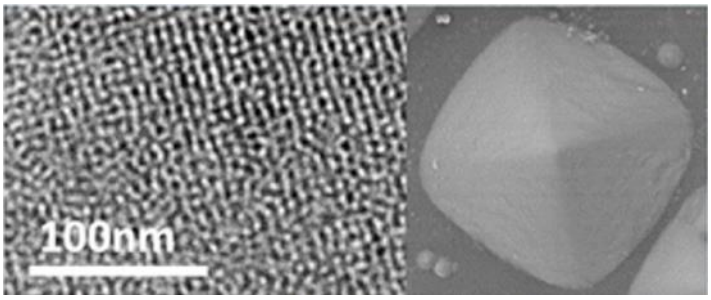

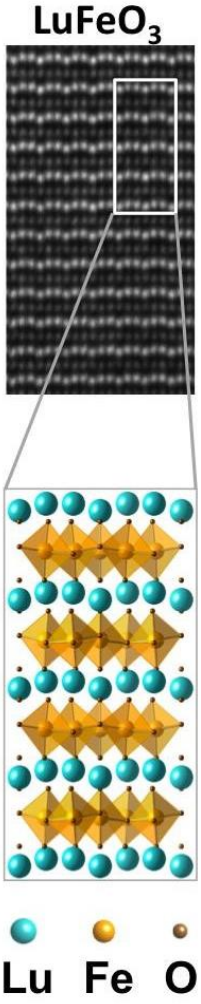

U.S. DEPARTMENT OF ENERGY | Office of Science

Office of Basic Energy Sciences
Materials Sciences and Engineering Division

Cover

Top: Demonstration of single crystal growth via solid-to-solid transformation, as confirmed by persisting scratches (arrows in SEM micrograph, **(a)**), even after glass → crystal conversion. The single crystal nature of laser crystallized Sb_2S_3 within glass matrix is established by electron backscatter diffraction mapping (**b-d**). *Sci. Rep.* **6**, 23324 (2016). (Courtesy: Himanshu Jain, Lehigh University)

Right Middle: High-angle annular dark field scanning transmission electron microscopy (HAADF-STEM) images of the m=0 ($LuFe_2O_4$) and m=∞ ($LuFeO_3$) end-members of a new family of room-temperature multiferroics: $(LuFeO_3)_m/(LuFe_2O_4)_1$ superlattices. Corresponding schematics of these crystal structures are also shown. *Nature* **537**, 523 (2016). (Courtesy: Darrell Schlom, Cornell University)

Center: The figure shows the temperature (T) and doping (r) dependence on the magnitude of the electronic nematicity, $r_T(max)/\langle r \rangle$--the spontaneous breaking of the crystal rotational symmetry in electron transport. *Nature* **547**, 432 (2017). (Courtesy: Ivan Božović, Brookhaven National Laboratory)

Bottom: Left: TEM image of cracked silicate with $Pm\bar{3}n$ pore symmetry along the [110] direction. Right: SEM of growth of pyramidal array on Si(100) after two cycles of 2 h reaction at 100°C. *ACS Nano* **10**, 8670 (2016). (Courtesy: Jun Liu, Pacific Northwest National Laboratory)

This document was produced under contract number DE-SC0014664 between the U.S. Department of Energy and Oak Ridge Associated Universities.

The research grants and contracts described in this document are supported by the U.S. DOE Office of Science, Office of Basic Energy Sciences, Materials Sciences and Engineering Division.

Table of Contents

University Grants' Abstracts

FOREWORD

This abstract book comprises the scientific content of the 2017 Synthesis and Processing Science Principal Investigators' Meeting sponsored by the U.S. Department of Energy, Office of Science, Office of Basic Energy Sciences, Materials Sciences and Engineering (MSE) division. The meeting, held on November 7–9, 2017, at the Marriott Washingtonian, Gaithersburg, Maryland, is the sixth principal investigators' meeting on this topic and is one among a series of research theme-based principal investigators' meetings being held by the MSE division.

The purpose of this principal investigators' meeting is to bring together all of the researchers funded in the Synthesis and Processing Science core research activity so they can get a firsthand look at the broad range of materials science research that is being supported in this important research area. The meeting will serve as a forum for the discussion of new results and research highlights, thus fostering a greater awareness of significant new advances in the field and the research of others in the program. The confidential and collegial meeting environment is intended to provide unique opportunities to develop new collaborations among PIs, and new ideas. In addition, the meeting affords BES program managers an opportunity to assess the state of the entire program at one time on a periodic basis, in order to chart future directions and identify new programmatic needs.

This year's meeting focuses on three topics within the Synthesis and Processing Science portfolio:
Accelerated materials discovery; mechanistic control of synthesis; and integrating theory, computation, and in situ characterization. While this is one way of organizing and presenting the research within this broad portfolio, there are many other synergies that could be highlighted and will be considered at future meetings.

Let me take this opportunity to express my thanks to all the meeting attendees, for their active participation and sharing their ideas and new research results. Special thanks are given to the Meeting Chairs, Michael Arnold and Nancy Dudney, for their dedicated efforts and invaluable assistance towards organizing this meeting. Finally, this meeting would not be possible without the logistical support from Teresa Crockett at DOE-MSE as well as Linda Severs at Oak Ridge Institute for Science and Education (ORISE).

Bonnie Gersten
Program Manager, Synthesis and Processing Science
Materials Sciences and Engineering Division
Office of Basic Energy Sciences
Office of Science
U.S. Department of Energy

This page is intentionally blank.

2017 DOE BES MSE Synthesis and Processing Science Principal Investigators' Meeting

The Synthesis and Processing Science Program (S&PS) supports basic research for developing techniques to synthesize materials with desired structure, function, or behavior; to understand the physical phenomena that underpin materials synthesis; and to develop in situ monitoring. The S&PS program is one of ten programs within the Materials Sciences and Engineering Division at BES with the emphasis of the S&PS program being on the synthesis of materials by physical means. The need to identify and efficiently process materials for many varied energy related applications has motivated the recent Basic Research Needs Workshop on Synthesis Science for Energy Relevant Technology, held in May 2016 and summarized in the report: https://science.energy.gov/~/media/bes/pdf/reports/2017/BRN_SS_Rpt_web.pdf. The meeting was chaired by Jim De Yoreo, with assistance from David Mandrus and Lynda Soderholm. The workshop report distilled many important panel discussion topics down to 4 priority research directions (PRDs).

While this biannual BES PIs' meeting seeks to foster increased integration and collaboration, this year there is also the opportunity to capture and evaluate the insight provided by the Synthesis Science BRN report. With this view, the program is organized to reflect how the current portfolio of research programs aligns and maps onto 3 of the 4 PRDs from the report. We hope this provides interesting points of discussion as we seek to continually boost the impact of our research in this area, moving towards the ultimate goal of achieving predictive synthesis for a variety of important classes of materials. The BRN report states this concisely as progressing 'from the art-of-synthesis to the science-of-synthesis'.

Adopting language from the BRN report, the topical sessions for organization of the meeting, and some crosscutting issues we want to explore, are:

1. **Accelerated Materials Discovery** *Materials discovery is crucial for progress in science and technology, but how will the new materials of the future be created? And where should we look for them?*
2. **Mechanistic Control of Synthesis** *How can we develop a fundamental understanding of the processes by which reactants assemble into products and how can they be controlled? Can we access metastable ordered phases that are formed during synthesis but subsequently dissolve or transform before equilibrium is reached?*
3. **Integrating Theory, Computation and In Situ Characterization** *How can characterization, theory, and computation be combined to make the leap from predictive understanding of existing materials to predictive control enabling radically new molecules and materials?*

Accelerate materials discovery by exploiting extreme conditions, complex chemistries and molecules, and interfacial systems (Sessions 1 and 2)

In the BRN report, accelerated materials discovery opportunities were parsed into two approaches:

(1) Explore regions of extreme conditions that have not been extensively explored. This includes investigation of new growth tools and environments for fabrication of films and single crystals.

It also includes low temperature synthesis whereby a rich variety of new materials can be kinetically stabilized, being formed using, for example, chimie douce methods or mechanochemical and electrochemical processing.

(2) Develop new synthesis and materials using complex chemistries and control of interfaces that address systems beyond simple binary and ternary compounds. The report also challenges research to look beyond homogeneous crystalline materials to probe meso and nanoscale assemblies and distributions where properties are no longer based on the discrete unit cell.

Both research paths are represented in work underway for the Synthesis and Processing Science program. Well defined and in some cases unique conditions and tools are used to process thin films, single crystals, and meso structured composites. While the ultimate properties and intended application of the materials are not ignored, the synthesis or assembly pathways are characterized so we can make informed choices towards tailoring the reactants and process conditions, all with the goal of accelerated materials discovery and identifying new classes of materials. Additionally, novel materials are created as superlattices and nanopatterned structures, as controlled assemblies of particles from solution, as the crystal growth of complex oxides, and by electrodeposition.

Achieve mechanistic control of synthesis to access new states of matter (Sessions 3 and 4)

The reactions to form materials on surfaces, or within a condense phase, generally involve many complex but largely unknown steps along a reaction pathway. If studied at all, work is restricted to determining the rate limiting or initiation site in order to control the properties of the final product. A wealth of information is buried in the reaction pathway, which if interrogated, is expected to lead to more precise and efficient optimization of known materials and to new and as yet unimagined classes of metastable and kinetically stabilized materials.

(1) Synthesis by design: How materials form
The experimental and computational challenge to access details of synthesis mechanisms requires in situ tools or combination of tools as well as the ability to handle and analyze massive amount of data. Success may determine for example the precise time in the reaction path where a change in conditions or composition can alter the synthesis path and ultimate product.

(2) Discovering new molecules and materials: Intermediates and phase space
This describes the effort to look beyond the understanding and control of the synthesis pathway to discover new metastable or kinetically stable substances that typically transform or dissolve before equilibrium is reached. Such intermediates occur in all synthetic routes currently used to produce materials. This provides the opportunity to identify new molecules and materials far from equilibrium.

As is true in general, most programs in the Synthesis and Processing Science portfolio are focused on understanding the mechanisms during the synthesis processing. Examples of detailed characterization tracking all the species along the synthesis, not just of the final product, are evident. This is leading to detailed *understanding* of adsorption, templating, nucleation, growth, coarsening, and aggregation processes which then feedback to tailor the outcome by changes in

the template and precursors. Materials range from elemental to more complex multicomponent systems where the elemental processes are increasingly complex. Achieving mechanistic *control*, however, is still elusive for most studies, as is capturing transient intermediate materials or promoting competing pathways.

Integrate emerging theoretical, computational, and in situ characterization tools to achieve directed synthesis with real-time adaptive control (Session 5)

Technically it is very challenging to characterize, understand, model, and ultimately control a complex synthesis reaction. Just a few of the hurdles noted in the BRN report include needs for: highly specialized characterization equipment, real-time streaming data processing, and effective theoretical analysis of a complex energy landscape.

(1) Innovative approaches: Multimodal in situ characterization probes
To characterize the structure, chemical composition, and defects associated with the intermediate or final products during synthesis requires multiple probes. Further, these probes often have to be applied to extreme conditions of temperature, corrosiveness, high pressure and the like. Advances in TEM and scanning probe imaging, optical and NMR spectroscopy, and environmental cells for neutron and x-ray probes may all provide tools to reveal hidden processes during synthesis.

(2) Theory and simulation: Real time interpretation of in situ data to predictively guide the synthesis process
Particularly for solid and condensed matter systems, there are knowledge gaps for which theoretical frameworks do not exist. An example is the process of crystal growth by coalescence of nanoparticles. Developing computer simulations to handle such complex conditions and materials as they evolve during synthesis is very challenging. Additionally, to provide means to adjust the synthesis process and ultimately predict the pathways requires rapid analysis of in situ information and rapid simulation for real time control.

Most programs in the portfolio, either routinely or at appropriate stages of the study, utilize one or multiple specialized in situ characterization methods to follow the full reaction pathway. Many take advantage of DOE user facilities and either design or utilize special processing equipment and chambers tested at these facilities. Similarly, when tractable, theory and modeling are employed to describe the species and processes that occur during synthesis. All of this is with an eye to predicting the effects of changes in the reactants and conditions for synthesis and processing towards the ultimate predictive control of the synthesis. With further development of the rapid computation methods, real time data analysis will lead to real time control of the synthesis and processing reactions.

This page is intentionally blank.

Synthesis and Processing Science
Principal Investigators' Meeting Agenda

Meeting Chairs:
Nancy Dudney (Oak Ridge National Lab) and **Michael Arnold** (Univ. of Wisconsin–Madison)

Tuesday, November 7, 2017	
7:00 – 7:50am	*****Breakfast*****
7:50 – 8:00am	**Meeting Chairs: Nancy Dudney and Michael Arnold** **Program Manager: Bonnie Gersten** *Introductory Remarks*
Session I	***Chair: Scott Chambers,*** *Pacific Northwest National Laboratory* *Accelerated Materials Discovery*
8:00 – 8:20am	**Ivan Božović,** Brookhaven National Laboratory *Why is Tc in cuprates so high?*
8:20 – 8:30am	*Discussion*
8:30 – 8:50am	**Chang-Beom Eom,** University of Wisconsin–Madison *Novel synthesis of quantum epitaxial heterostructures by design*
8:50 – 9:00am	*Discussion*
9:00 – 9:20am	**Yingge Du,** Pacific Northwest National Laboratory *Controlling ion intercalation induced topotactic phase transitions in oxide thin films*
9:20 – 9:30am	*Discussion*
9:30 – 10:00am	****Break****
10:00 – 10:20am	**Jung Han, Yale University** *Nanoscale selective growth and microstructural control of III-nitride*
10:20 – 10:30am	*Discussion*
10:30 – 10:50am	**Zhiqiang Mao,** Tulane University *Novel low dimensional ternary transition metal chalcogenides with semiconducting and topological semimetallic properties*
10:50 – 11:00am	*Discussion*
11:00 – 11:30am	**Poster Introductions for Session I**
11:30 – 1:00pm	****Working lunch**** **Introductory remarks by Helen Kerch**, Acting Team Lead for Materials Discovery, Design and Synthesis; **CRA Updates by Bonnie Gersten**, Program Manager, Synthesis and Processing Science (S&PS) CRA

1:00 – 2:30pm	**Poster Session 1**
Session 2	**Chair: Jay Switzer,** Missouri Science and Technology *Accelerated Materials Discovery (continued)*
2:30 – 2:50pm	**Ni Ni,** University of California, Los Angeles *Synthesis and characterization of topological semimetals*
2:50 – 3:00pm	*Discussion*
3:00 – 3:20pm	**Rongying Jin,** Louisiana State University *Investigating structure-property relationship in correlated transition-metal compounds*
3:20 – 3:30pm	*Discussion*
3:30 – 4:00pm	****Break****
4:00 – 4:20pm	**Jim De Yoreo,** Pacific Northwest National Laboratory *Basic research needs for synthesis science for energy technologies workshop*
4:20 – 4:30pm	*Discussion*
4:30 – 5:30pm	**Group Breakouts**—six group breakout sessions to discuss new opportunities for S&PS that were brought out in the BRN report. **See Breakout Group Assignments agenda for designated group leaders and breakout group assignments.**
5:30 – 7:00pm	**Poster Session 1, continued**
7:00 – 8:30pm	****Working Dinner**** Bonnie Gersten speaker on new opportunities and collaborative exchanges in Synthesis Science
	Wednesday, November 8, 2017
7:00 – 8:00am	****Breakfast****
Session 3	**Mechanistic Control of Synthesis** Chair: **David Geohegan**, Oak Ridge National Laboratory
8:00 – 8:20am	**Himanshu Jain,** Lehigh University *Engineering the lattice of single crystal grown in glass*
8:20 – 8:30am	*Discussion*
8:30 – 8:50am	**Peter Voorhees,** Northwestern University *The morphology of two-phase mixtures: From nanoporous gold to spinodal ordering*
8:50 – 9:00am	*Discussion*
9:00 – 9:20am	**Daniel Shoemaker,** University of Illinois, Urbana-Champaign *In-situ scattering of exploratory inorganic synthesis and metathesis*
9:20 – 9:30am	*Discussion*

9:30 – 10:00am	****Break****
Session 3	**Mechanistic Control of Synthesis** (continued)
10:00 – 10:20am	**Jun Liu,** Pacific Northwest National Laboratory *General synthetic approaches based on interfacially driven nucleation and assembly*
10:25 – 10:30am	*Discussion*
10:30 – 10:50am	**Jim De Yoreo,** Pacific Northwest National Laboratory *Ion pairs, complexes and clusters: Probing the species that lead to nucleation*
10:50 – 11:00am	*Discussion*
11:00 – 11:30am	**Poster Session 2 Introductions**
11:30 – 1:00pm	****Working Lunch**** Bonnie Gersten speaker: New opportunities discussions in Synthesis Science
1:00 – 2:30pm	**Poster Session 2**
Session 4	**Chair: Guangwen Zhou**, State University of New York at Binghamton *Mechanistic Control of Synthesis (continued)*
2:30 – 2:50pm	**Stacey Bent,** Stanford University *Mechanisms of nucleation and growth in atomic layer deposition*
2:50 – 3:00pm	*Discussion*
3:00 – 3:20pm	**Francisco Zaera,** University of California–Riverside *The surface chemistry of atomic layer deposition (ALD) processes*
3:20 – 3:30pm	*Discussion*
3:30 – 4:00pm	****Break****
4:00 – 4:20pm	**Michael Tringides,** Ames Laboratory *Tuning graphene properties with metal growth on and under graphene*
4:20 – 4:30pm	*Discussion*
4:30 – 4:50pm	**Michael Arnold,** University of Wisconsin–Madison *Anisotropic synthesis of semiconducting graphene*
4:50– 5:00pm	*Discussion*
5:00 – 7:00pm	**Poster Session 2,** continued
7:00 – 8:30pm	****Working Dinner**** Bonnie Gersten speaker on new opportunities and collaborative exchanges in Synthesis Science

Thursday, November 9, 2017	
7:00 – 8:00am	****Breakfast****
8:00 – 8:45am	**Each breakout group leader presents (7.5 min each)**
Session 5	**Chair: Kristen Fichthorn**, Pennsylvania State University *Integrating Theory, Computation and In Situ Characterization*
8:45– 9:05am	**Lynden Archer,** Cornell University *Stabilizing electrochemical interfaces in viscoelastic liquid electrolytes*
9:05 – 9:15am	*Discussion*
9:15 – 9:35am	**Dongsheng Li,** Pacific Northwest National Laboratory *Influence of crystal orientation and molecular details on long-range dispersion forces underlying aggregation and co-alignment between crystals*
9:35 – 9:45am	*Discussion*
9:45 – 10:05am	**Eli Sutter,** University of Nebraska–Lincoln *Exploring and embracing heterogeneity in atomically thin energy materials*
10:05 – 10:15am	*Discussion*
10:15 – 10:45am	****Break****
10:45 – 11:05am	**Max Lagally,** University of Wisconsin–Madison *Group IV nanomembranes and sheets: New synthesis, alloys, and composites*
11:05 – 11:15am	*Discussion*
11:15 – 11:35am	**Feng Liu,** University of Utah *Ubiquitous ideal Rashba-Dresselhaus spin-orbit coupling effect in screw dislocation of semiconductors*
11:35 – 11:45am	*Discussion*
11:35 – 12:00pm	**Meeting Chairs: Nancy Dudney and Michael Arnold** **Program Manager: Bonnie Gersten** *Closing Remarks*
12:00pm	**Adjourn**

Synthesis and Processing Science Principal Investigators' Meeting

Breakout Group Assignments
Tuesday, November 7, 2017

Group Ia: **Accelerated Materials Discovery**

Discussion Leader: Rongying Jin, Louisiana State University

Scribe: Ferdinand P. Poudeu, University of Michigan

Location: Main auditorium (front right)

Team Members:
1. Zhiqiang Mao, Tulane University
2. Joshua Zide, Delaware University
3. Jay Switzer, Missouri Science & Technology
4. Ni Ni, University of California–Los Angles
5. Richard Lunt, Michigan State University
6. Jiang Wei, Tulane University
7. David Young, Louisiana State University

Group Ib: **Accelerated Materials Discovery**

Discussion Leader: Darrell Schlom, Cornell University

Scribe: Tiffany Kaspar, Pacific Northwest National Laboratory

Location: Main auditorium (back left)

Team Members:
1. Michael Arnold, University of Wisconsin–Madison
2. Ivan Božović, Brookhaven National Laboratory
3. Yingge Du, Pacific Northwest National Laboratory
4. Chang-Beom Eom, University of Wisconsin–Madison
5. Jung Han, Yale University
6. Max Lagally, University of Wisconsin–Madison
7. Scott Chambers, Pacific Northwest National Laboratory

Group IIa: **Mechanistic Control of Synthesis**

Discussion Leader: Jun Liu, Pacific Northwest National Laboratory

Scribe: Andrei Fedorov, Georgia Tech

Location: Main auditorium (middle left)

Team Members:
1. Michael Tringides, Ames Laboratory
2. Francisco Zaera, University of California–Riverside
3. Guangwen Zhou, State University of New York–Binghamton
4. Volkmar Dierolf, Lehigh University
5. David Geohegan, Oak Ridge National Laboratory
6. John Hart, Massachusetts Institute of Technology
7. Miaofang Chi, Oak Ridge National Laboratory
8. Cai-Zhuang Wang, Ames Laboratory

Group IIb: **Mechanistic Control of Synthesis**

Discussion Leader: Katsuyo Thornton, University of Michigan

Scribe: Daniel Shoemaker, University of Illinois, Urbana-Champaign

Location: Main auditorium (middle right)

Team Members:
1. James De Yoreo, Pacific Northwest National Laboratory
2. Mark Ediger, University of Wisconsin–Madison
4. Himanshu Jain, Lehigh University
5. Alexandra Navrotsky, University of California–Davis
6. Stacey Bent, Stanford University
7. Kai Xiao, Oak Ridge National Laboratory
8. Brian Benicewicz, University of South Carolina

Group IIIa: **Integrating Theory, Computation and In Situ Characterization**

Discussion Leader: Ralph Napolitano, Ames Laboratory

Scribe: Amy Clarke, Colorado School of Mines

Location: Dining room (table group IIIa)

Team Members:
1. Lynden Archer, Cornell University
2. Nancy Dudney, Oak Ridge National Laboratory
3. Tobias Hanrath, Cornell University
4. Feng Liu, University of Utah
5. Eli Sutter, University of Nebraska–Lincoln
6. Peter Voorhees, Northwestern University
7. Dongsheng Li, Pacific Northwest National Laboratory

Group IIIb: **Integrating Theory, Computation and In Situ Characterization**

Discussion Leader: Kristen Fichthorn, Pennsylvania State University

Scribe: Mina Yoon, Oak Ridge National Laboratory

Location: Dining room (table group IIIb)

Team Members:
1. Hanchen Huang, Northeastern University
2. Sanat Kumar, Columbia University
3. Eugene Olevsky, San Diego State University
4. Linda Schadler, Rensselaer Polytechnic University
5. Boris Yakobson, Rice University
6. Peter Sutter, University of Nebraska–Lincoln
7. Maria Sushko, Pacific Northwest National Laboratory
8. Gabriel Veith, Oak Ridge National Laboratory

Synthesis and Processing Science Principal Investigators' Meeting

POSTER SESSION I
Tuesday, November 7, 2017

1. **Tiffany C. Kaspar**, Ryan B. Comes, Steven R. Spurgeon, Peter V. Sushko, and Scott A. Chambers **(intro)**, PNNL, *Emergent Properties of Oxide Superlattices*

2. **Scott A. Chambers**, Yingge Du, Timothy C. Droubay, Tiffany C. Kaspar, Steven R. Spurgeon, Peter V. Sushko, Mark E. Bowden, and Kelsey A. Stoerzinger **(intro)**, PNNL, *Novel Functionality through Controlled Synthesis of Epitaxial Oxide Heterostructures*

3. **Yingge Du**, Zhenzhong Yang, Phuong-Vu Ong, and Le Wang, PNNL, *Controlling Ion Intercalation Induced Topotactic Phase Transitions in Oxide Thin Films*

4. **I. Božović**, J. Wu, and A. Bollinger, BNL, *Molecular Beam Epitaxy of Superconducting Oxides*

5. **Chang-Beom Eom**, University of Wisconsin–Madison, *Novel Synthesis of Quantum Epitaxial Heterostructures by Design*

6. **Darrell Schlom (intro**), Cornell University, *Utilizing Synthesis Science to Create New Ruddlesden-Popper Ferroelectrics with Ultra-Low Dielectric Loss*

7. **Jung Han**, Yale University, *Nanoscale Selective Growth and Microstructural Control of III-Nitride*

8. **Joshua Zide (intro)**, University of Delaware, *The Path to Growth of Metal/Semiconductor Nanocomposite Materials by Liquid Phase Epitaxy*

9. **Jay Switzer (intro)**, Missouri S&T, *Producing Ordered, Transparent, and Flexible Substrates for Electronics by Epitaxial Lift-Off of Electrodeposited Single-Crystal Gold Foils*

10. **Rongying Jin**, Louisiana State University, *Investigating Structure-Property Relationship in Correlated Transition-Metal Compounds*

11. Zhiqiang Mao and **Jiang Wei (intro)**, Tulane University, *Novel Exotic Properties of Two-Dimensional Atomic Crystals of Layered Ternary Transition Metal Chalcogenides*

12. **Ni Ni**, University of California–Los Angles, *Synthesis and Characterization of Topological Semimetals*

13. **Pierre Ferdinand Poudeu (intro)**, Ctirard Uher, University of Michigan, and Anton Van der Ven**,** University of California–Santa Barbara, *Enhanced Thermoelectric Performance in Hierarchical Nanostructured Semiconductors*

14. **Daniel Shoemaker**, University of Illinois–Urbana-Champaign, *Chalcogenide and Oxide Syntheses Expedited with Pre-reactions, Fluxes, and Computation*

15. **Alexandra Navrotsky (intro)**, University of California–Davis, *Thermodynamic Limitations on Synthesis and Stability of Hybrid Perovskites for Energy Applications*

16. **Nancy Dudney** and Miaofang Chi **(intro)**, ORNL, *Elucidating Phase Evolutions of Solid Electrolytes during Synthesis and Interface Fabrication.*

17. Robert L. Sacci, **Gabriel M. Veith**, Miaofang Chi, Ke An, Chelsea Xi, Robert Schmidt, and Nancy Dudney **(intro)**, ORNL, *Understanding Growth Mechanisms of Ionically Conductive Metastable Phases*

18. **Eugene Olevsky (intro),** San Diego State University, *All-Materials-Inclusive Net Shape Flash Spark Plasma Sintering*

19. **Lynden Archer**, Cornell University, *Electrodeposition of Metals in Viscoelastic Liquid Electrolytes*

20. **Mark Ediger (intro)**, University of Wisconsin–Madison, *Stability, Structure, and Molecular Orientation in Organic Glasses Produced by Physical Vapor Deposition*

21. **Linda Schadler (**Rensselaer Polytechnic Institute), **Sanat Kumar** (Columbia University), and Brian Benicewicz (University of South Carolina) **(intro)**, *Using Crystallization to Control Filler Dispersion and Vice Versa in Polymer Nanocomposites*

22. **Richard Lunt (intro)**, Michigan State University, *Quasiepitaxial Growth of Organic Crystalline Thin-Films*

23. **Stacey Bent**, Stanford University, *Mechanisms of Nucleation and Growth in Atomic Layer Deposition*

24. **Francisco Zaera**, University of California–Riverside, *The Surface Chemistry of Atomic Layer Deposition (ALD) Processes*

Synthesis and Processing Science Principal Investigators' Meeting

POSTER SESSION II
Wednesday, November 8, 2017

1. Peter Voorhees (Northwestern University) and **Katsuyo Thornton** (University of Michigan) (**intro**), *The Morphology of Two-Phase Mixtures: From Nanoporous Gold to Spinodal Ordering*

2. **Amy Clarke (intro)**, Colorado School of Mines, *Multiscale Prediction and Control of Metallic Alloy Solidification Dynamics*

3. K.-M. Ho, **M.J. Kramer**, M.I. Mendelev, **R.E. Napolitano**, R.T. Ott, P.K. Ray, X. Song, C.Z. Wang, and W. Wang **(intro),** Ames Laboratory, *Ordering in Glass-Forming Metallic Liquids: Crystal Motifs and Connections to Phase Selection*

4. K.-M. Ho, **M.J. Kramer**, M.I. Mendelev, **R.E. Napolitano**, R.T. Ott, P.K. Ray, X. Song, C.Z. Wang, and W. Wang, Ames Laboratory, *Prediction of Phase Transformations in Metallic Alloys Far From Equilibrium*

5. Himanshu Jain and **Volkmar Dierolf (intro)**, Lehigh University, *Laser Fabrication of Single Crystal Architecture in Glass of Noncongruent Composition*

6. **Guangwen Zhou (intro)**, State University of New York, *Atomic-Step-Induced Local Nonequilibrium Effects on Surface Oxidation*

7. **Tobias Hanrath**, Paulette Clancy, and Lena Kourkoutis **(intro)**, Cornell University, *Fabricating Single Crystal Quantum Dot Solids by Inkjet Printing*

8. **Kristen Fichthorn (intro**), Pennsylvania State University, *Thermodynamics and Kinetics of Nanocrystal Growth: Investigations of Silver and Copper*

9. **Maria Sushko (intro)**, PNNL, *Combining Theory and In-Situ Characterization to Understand Non-Classical Nucleation Processes in Synthesis*

10. **Jun Liu**, PNNL, *Controlling Materials Evolution through Interfacial Interactions and Reactivity*

11. **James De Yoreo**, PNNL, *Ion Pairs, Complexes and Clusters: Probing the Species that Lead to Nucleation*

12. **Peter Sutter (intro)** and Eli Sutter, University of Nebraska, *Exploring and Embracing Heterogeneity in Atomically Thin Energy Materials*

13. **Dongsheng Li**, PNNL, *Crystal Growth through Monomer Addition, Particle Attachment, and Strain Realization*

14. **Andrei Fedorov (intro)**, Georgia Institute of Technology, *Using Multi-Phase Energetic Precursor Jets to Enable New Modes of Focused Electron Beam Induced Processing (FEBIP)*

15. **Hanchen Huang (intro)**, Northeastern University, *Theoretical Framework of Nanorod Growth*

16. **David Geohegan (intro)**, **Mina Yoon, Kai Xiao**, Alex Puretzky, Gyula Eres, Gerd Duscher, Christopher M. Rouleau, M. Mahjouri-Samani, M. Tian, K. Wang, X. Li, and W. Tennyson, ORNL, *Growth Mechanisms and Controlled Synthesis of Nanomaterials (ERKCS81): Understanding the Nonequilibrium Assembly of Functional Nanostructures and Thin Films from Metastable "Building Blocks"*

17. **Kai Xiao (intro)**, **David B. Geohegan**, **Mina Yoon**, Alex Puretzky, Gyula Eres, Gerd Duscher, Christopher M. Rouleau, M. Mahjouri-Samani, M. Tian, K. Wang, X. Li, and W. Tennyson, ORNL, *Growth Mechanisms and Controlled Synthesis of Nanomaterials (ERKCS81): Toward Synthetic Control over Heterogeneity and Functionality in Two-Dimensional Materials*

18. **Mina Yoon (intro)**, **David B. Geohegan**, **Kai Xiao**, Alex Puretzky, Gyula Eres, Gerd Duscher, Christopher M. Rouleau, M. Mahjouri-Samani, M. Tian, K. Wang, X. Li, and W. Tennyson, ORNL, *Growth Mechanisms and Controlled Synthesis of Nanomaterials (ERKCS81): Atomistic Modeling Coupled with In Situ Diagnostics of the Formation and Transformation of Oxide Nanostructures and 2D Materials*

19. **John Hart (intro)**, Massachusetts Institute of Technology, *Mechanical Modulation of Graphene and Carbon Nanotube Synthesis and Processing*

20. **Michael Arnold**, University of Wisconsin–Madison, *Anisotropic Synthesis of Semiconducting Graphene (and Atomically Thin Graphene Templates for Directing the Synthesis of Block Copolymers and Semiconductors)*

21. **Michael Tringides**, Ames Laboratory, *2-D Layer Quantum Materials by Controlling Graphene Metal Intercalation*

22. **Max Lagally**, University of Wisconsin–Madison, *Group IV Nanomembranes, Sheets, and Composites: Measuring Unique Properties*

23. **Feng Liu**, University of Utah, *Computational Design of Topological Semimetals*

24. **Boris Yakobson (intro)**, Rice University, *Mapping the Synthetic Routes for 2-Dimensional Materials: Bridging Micro and Macro*

Laboratory Projects' Abstracts

Project title: Molecular Beam Epitaxy of Superconducting Oxides

PIs: Ivan Bozovic, Jie Wu (Brookhaven National Laboratory, Upton NY 11973)

1. Program Scope

The mechanism of high-temperature superconductivity (HTS) is one of the most important problems in Condensed Matter Physics. Some basic questions – what are the spin and the charge of free carriers, the nature of superconducting transition and the effective interaction that causes electron pairing - are still open. To address these questions, we use atomic-layer ('digital') molecular beam epitaxy (MBE) to synthesize single-crystal HTS films as well as multilayers and superlattices with atomically perfect interfaces, and manufacture tunnel junctions, field-effect devices, and HTS nano-structures. Experimenting with these, we discovered HTS interface superconductivity, the Giant Proximity Effect, HTS in a single CuO_2 layer, existence of small (local) electron pairs, their (de)localization at the superconductor-insulator quantum phase transition, and electronic nematicity. These results significantly impact research on HTS and more broadly on strongly-correlated materials.

2. Recent Progress

2.1. The nature of *S-I* transition and of the 'insulating' state.

To clarify the nature of the insulating ground state, we studied[1] the Hall effect in LSCO samples doped near the quantum critical point at $x \approx 0.06$. Dramatic fluctuations in the Hall resistance appear below $T_{CG} \approx 1.5$ K and increase as the sample is cooled down further, signaling quantum critical behavior (Fig. 1). We explored the doping dependence by studying a combinatorial LSCO library in which the Sr content is varied in extremely fine steps, $\Delta x \approx 0.00008$. We observed that quantum charge fluctuations wash out when superconductivity emerges but can be restored when the latter is suppressed by applying a magnetic field, showing that the two instabilities compete for the ground state. In the anomalous 'insulator' phase, charge carriers form local pairs that are organized in glassy charge clusters[2]

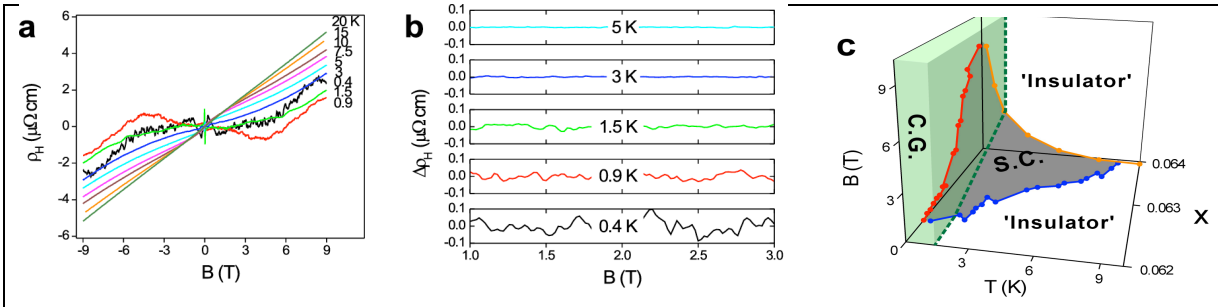

Fig. 1. Charge-cluster glass (CCG) behavior in 'insulating' LSCO. Below $T_{CG} = 1.5$ K, the Hall resistance shows erratic behavior, switching, hysteresis, and memory effects. With doping, this state gives way to the d-wave superconductivity. Magnetic field suppresses superconducting fluctuations and promotes the CCG state.

2.2 The (anomalous) nature of superconducting state in LSCO

Using an improved mutual inductance technique[3], we measure the temperature and doping dependence of the magnetic penetration depth λ with absolute accuracy better than 1%. Using ALL-MBE we engineer the samples at the atomic-layer level to ensure that the active (superconducting) layer thickness is sharply defined.[4-7] We have studied well over 2,000 single-crystal LSCO films; this large statistics allow us to clearly identify intrinsic behavior.

In Fig. 2a, we show the doping dependence of $\lambda(T)$ covering densely the entire overdoped side of the LSCO phase diagram. For few most heavily overdoped films, in Fig. 2b we show N_{s0}, the corresponding 2D superfluid density at $T \rightarrow 0$, expressed as the number of holes per one CuO_2 unit. The values of $N_{s0} \equiv N_s(T \rightarrow 0)$ are extremely small, as low as 1% of the total mobile carrier density. Fig. 2c shows the dependence of T_c on N_{s0}.

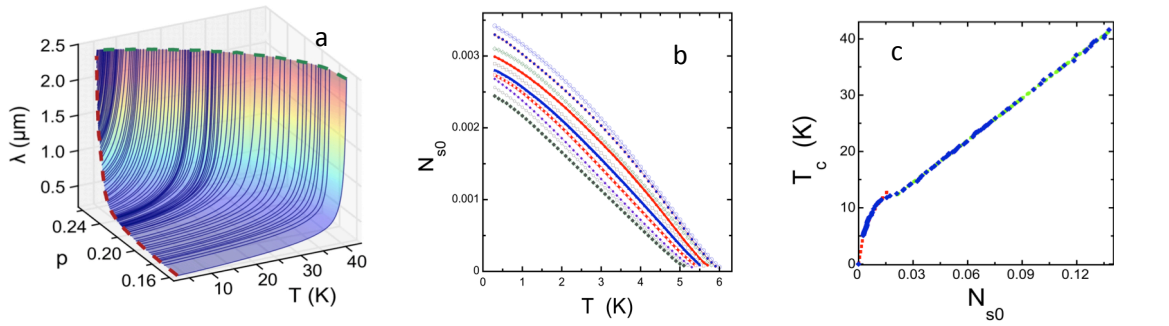

Fig. 2. a, The dependence of the penetration depth (λ) on temperature (T) and doping (p). b, The dependence of N_{s0} on T for $p = 0.25$ (top) to $p = 0.255$ (bottom). c, The dependence of T_c on N_{s0} (error bars < markers).

These findings cannot be explained within the standard Bardeen-Cooper-Schrieffer (BCS) theory. Rather, T_c appears to be essentially controlled by the superfluid density, i.e., just by the kinematics. This points to Bose-Einstein condensation (BEC) of small, local pairs — which, however, appear to coexist with and give way to free fermions as the doping is increased. Cuprates may be the first example of electronic BEC.

2.3 The (anomalous) nature of the normal state in LSCO

The fact that the standard BCS description fails dramatically on the overdoped side implies that the normal state cannot be a simple Fermi liquid. This is indeed confirmed by our recent discovery that in single-crystal LSCO films a spontaneous voltage (V_T) develops transverse to the electrical current.[8] The effect is intrinsic, substantial, and robust — present from T_c up to the room temperature, for every doping, in every film and device (out of thousands we have tested). If the current direction is rotated in-plane by an angle ϕ, V_T oscillates as $\sin(2\phi)$, breaking the fourfold-rotation symmetry. The amplitude of oscillations is strongly peaked near T_c, and it decreases with doping. We have shown[8] that these are manifestations of in-plane anisotropy in the electronic transport — the so-called 'electronic nematicity'.[9-11] The big surprise is that the

director is not pinned to the crystal lattice; the orthorhombic lattice distortion plays little or no role. Rather than as an ordinary Fermi Liquids, cuprates behave as Fermi Liquid Crystals.

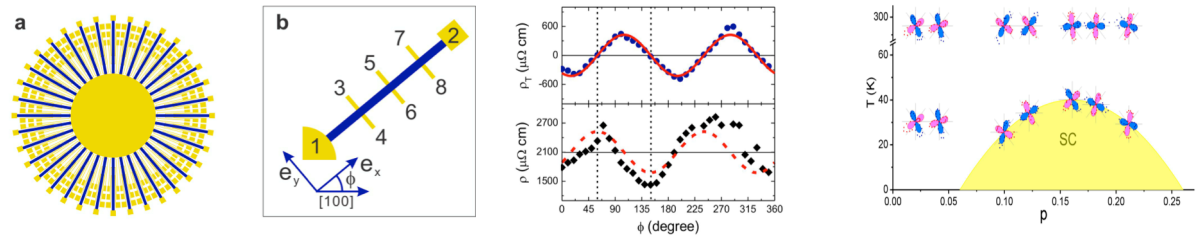

Figure 3: **a,** The 'sunbeam' lithography pattern, with 36 Hall bars; the angle between two successive bars is 10°. **b,** A schematic drawing of a single Hall bar. **c**, Angular dependences of transverse (ρ_T) and longitudinal resistivity and (ρ) in an underdoped ($p = 0.04$) LSCO film at the temperature $T = 30$ K. **d**, ρ_T as a function of doping, temperature and azimuth angle (ϕ), in polar coordinates (normalized for clarity).

3. Future Plans

Investigation of the mechanism of HTS in cuprates. Our results described above have shed some new light on the mystery of HTS in cuprates. However, they pose new questions. Is the root cause of HTS the electronic Bose-Einstein condensation of small (local) pairs? Are local pairs the 'nematogens' responsible for the observed electronic xy-nematicity, and for Marginal Fermi Liquid behavior? Why do T_c and the superfluid density decrease with overdoping — because the density of bosons (local pairs of holes) decreases, while the density of free fermions increases? Are the bosonic and fermionic fractions related to antinodal and nodal regions of the ***k***-space, respectively? To answer these important questions, we will investigate further the electronic nematicity by studying the angle-resolved transverse resistance (ARTR) in LSCO films on substrates deliberately miscut at a larger angle, bulk LSCO single crystals, other cuprates, as well as other complex oxides such as $LaNiO_3$, $La_{2-x}Sr_xNiO_4$, and Sr_2RuO_4.

Comparative study of cuprates and pnictides using OASIS. In collaboration with J. C. Davis and T. Valla, we will use OASIS, the new capability at BNL that combines an oxide MBE, a non-oxide MBE, ARPES and SI-STM modules, integrated into one interconnected ultrahigh vacuum system. This will enable us to systematically investigate what features of the normal and the superconducting states are similar in cuprates and pnictides.

Search for novel (high-T_c) superconductor materials. By electrolyte gating we can induce a high density of charge carriers in a very thin layer next to the surface. We will apply this technique to dope various 2D quantum materials. We will also explore materials in which local (but mobile) pairs may form, including naturally or artificially layered metallic oxides with strong in-plane covalency, materials in which bipolarons are believed or proposed to form, etc.

Search for novel Interface superconductivity. Our discovery[4] of interface superconductivity with $T_c > 50$ K has attracted much interest, yet a number of questions are still open. One is the mechanism of large (> 25%) enhancement of T_c in LSCO-LCO bilayers as compared to single-phase LSCO films and bulk crystals. We will study this by all the techniques at our disposition:

atomic-layer engineering, Zn δ-doping, combinatorial spread, electrolyte field effect, measuring $R(T)$, $R_H(T)$, $n_s(T)$, I-V characteristics, etc.,[1-8] and attempt to understand the origins of T_c enhancement in interface superconductivity.

A more ambitious project is to search for HTS in so-far unexplored interfaces in bilayer or superlattice heterostructures in which one constituent material is an insulator that sustains some low-energy bosonic excitations that could act as a 'glue' to pair the mobile electrons in a nearby layer that is metallic intrinsically or after mobile charge carriers are induced by charge transfer. These excitations could be excitons, as suggested long ago by W. Little[12] and V. L. Ginzburg[13-4], as well as plasmons, high-frequency phonons, soft phonons due to an incipient CDW or ferroelectric order, fluctuations of ferro- or antiferro-magnetic order, etc.

References

1. J. Wu, A. T. Bollinger, Y.-J. Sun and I. Božović, "Hall Effect in quantum critical charge-cluster glass", *Proceedings of the US National Academy od Science* 113, 4284 (2016).
2. X. Shi, D. Popović, C. Panagopoulos, G. Logvenov, A. T. Bollinger and I. Božović "Dynamically heterogeneous insulating state in $La_{2-x}Sr_xCuO_4$", *Nature Mater.* 12, 47 (2013).
3. I. Božović, J. Wu, X. He and A. T. Bollinger, "Dependence of critical temperature in overdoped copper oxides on superfluid density", *Nature* 536, 309 (2016).
4. A. Gozar, G. Logvenov, L. Fitting Kourkoutis, A. T. Bollinger, L. A. Giannuzzi, D. A. Muller and I. Bozovic, "High-temperature interface superconductivity between metallic and insulating copper oxides", *Nature* 455, 782 (2008).
5. G. Logvenov, A. Gozar and I. Bozovic, "High-Temperature Superconductivity in a Single Copper-Oxygen Plane", *Science* 326, 699–702 (2009).
6. A. T. Bollinger, G. Dubuis, J. Yoon, D. Pavuna, J. Misewich and I. Božović, "Superconductor–insulator transition in $La_{2-x}Sr_xCuO_4$ at the pair quantum resistance", *Nature* 472, 458 (2011).
7. J. Wu, O. Pelleg, G. Logvenov, A. T. Bollinger, Y.-J. Sun, G. S. Boebinger, M. Vanević, Z. Radović and I. Božović, "Anomalous independence of interface superconductivity from carrier density", *Nature Mater.* 12, 877-881 (2013).
8. J. Wu, A. T. Bollinger, X. He and I. Božović, "Spontaneous breaking of rotational symmetry in copper oxide superconductors", *Nature* 547, 432-436 (2017).
9. E. Fradkin, S. A. Kivelson, M. J. Lawler, J. P. Eisenstein and A. P. Mackenzie, "Nematic Fermi Fluids in Condensed Matter Physics", *Ann. Rev. Cond. Mat. Phys.* 1, 153 (2010).
10. M. J. Lawler, K. Fujita, J. Lee, A. R. Schmidt, Y. Kohsaka, C. K. Kim, H. Eisaki, S. Uchida, J. C. Davis, J. P. Sethna and E.-A. Kim, "Intra-unit-cell electronic nematicity of the high-T_c copper-oxide pseudogap states", *Nature* 466, 347 (2010).
11. K. Fujita, C. K. Kim, I. Lee, J. Lee, M. H. Hamidian, I. A. Firmo, S. Mukhopadhyay, H. Eisaki, S. Uchida, M. J. Lawler, E.-A. Kim, J. C. Davis, "Simultaneous Transitions in Cuprate Momentum-Space Topology and Electronic Symmetry Breaking", *Science* 344, 612 (2014).
12. W. A. Little, "Possibility of synthesizing an organic superconductor". *Phys. Rev.* A 134, 1416 (1964).
13. V. L. Ginzburg, "On surface superconductivity", *Phys. Lett.* 13, 101 (1964).
14. V. L. Ginzburg, "On two-dimensional superconductors", *Phys. Scr.* T27, 76 (1989).

FY 2016 and FY2017 Journal Publications

Publications led by this FWP

1. J. Wu, A. T. Bollinger, X. He and I. Božović, "Spontaneous breaking of rotational symmetry in copper oxide superconductors", ***Nature*** 547, 432 (2017).
2. X. Leng, J. Pereiro, J. Strle, G. Dubuis, A. T. Bollinger, A. Gozar, N. Litombe, D. Pavuna and I. Božović, "Insulator to Metal Transition in WO_3 Induced by Electrolyte Gating", ***NPJ Quantum Materials*** 2, 35 (2017).
3. A. Gozar, N. E. Litombe, J. E. Hoffman and I. Božović, "Optical Nanoscopy of High-T_c Cuprate Nano-Constriction Devices Patterned by Helium Ion Beams", ***Nano Letters*** 17, 1582 (2017).
4. J. Wu, V. Lauter, H. Ambaye, X. He and I. Božović, "Search for ferromagnetic order in overdoped copper-oxide superconductors", ***NPJ Scientific Reports*** 7, 45896 (2017).
5. I. Božović, X. He, J. Wu and A. T. Bollinger, "What is strange about high-temperature superconductivity in cuprates?", Internat. J. Mod. Phys. B (2017).
6. V. A. Gasparov, L. Drigo, A. Audouard, X. He and I. Božović, "Study of high-T_c interface superconductivity in $La_{1.55}Sr_{0.45}CuO_4/La_2CuO_4$ heterostructures at high fields and frequencies", Internat. J. Mod, Phys. B (2017).
7. I. Božović, X. He, J. Wu and A. T. Bollinger, "On the origin of high-temperature superconductivity in cuprates", (invited keynote) in Oxide-based Materials and Devices VIII, edited by F. H. Teherani, D. C. Look, D. J. Rogers, Proc. SPIE Vol. 10105, 1010502.
8. S. Dietrich, W. Mayer, S. Byrnes, S. Vitkalov, A. Sergeev, A. T. Bollinger and I. Božović, "Microwave nonlinear response of oxide superconducting films in the Berezinskii-Kosterlitz-Thouless state", (invited) *in Oxide-based Materials and Devices VIII*, edited by F. H. Teherani, D. C. Look, D. J. Rogers, Proc. SPIE Vol. 10105, 101051S (2017).
9. A. Gozar, P. Abbamonte and I. Božović, "Strong off-diagonal polarizability and electron-lattice coupling in high-temperature superconductors", (invited) In *Oxide-based Materials and Devices VIII*, edited by F. H. Teherani, D. C. Look and D. J. Rogers, Proc. SPIE Vol. 10105, 101050B (2017).
10. I. Božović, J. Wu, X. He and A. T. Bollinger, "Is there a path from cuprates towards room-temperature superconductivity?", (invited) Quantum Stud.: Math. Found. Published online Sept. 1 (2017) DOI 10.1007/s40509-017-0126-x
11. I. Božović, X. He, J. Wu and A. T. Bollinger, "The demise of superfluid stiffness in overdoped $La_{2-x}Sr_xCuO_4$ films grown by molecular beam epitaxy", (invited) J. Supercond. Nov. Magn. 30, 1345 (2017).
12. D. Pavuna, G. Dubuis, A. T. Bollinger, J. Wu, X. He and I. Božović, "On Local Pairs vs. BCS: Quo Vadis High-T_c Superconductivity?", (invited) J. Supercond. Nov. Magn. 30, 731 (2017).
13. J. Wu, A. T. Bollinger, Y. Sun and I. Božović, "Ground State of Underdoped Cuprates in Vicinity of Superconductor-to-Insulator Transition", (invited) J. Supercond. Nov. Magn. 30, 1073 (2017).
14. Z. Radović, M. Vanević, J. Wu, A. T. Bollinger and I. Božović, "Interface superconductivity in cuprates defies Fermi-Liquid description", (invited) J. Supercond. Nov. Magn. 30, 725 (2017).
15. I. Božović, J. Wu, X. He and A. T. Bollinger, "Dependence of critical temperature in overdoped copper oxides on superfluid density", ***Nature*** 536, 309 (2016).

16. I. Božović, "High-temperature superconductivity: a conventional conundrum", ***Nature Physics*** 12, 22 (2016).
17. J. Wu, A. T. Bollinger, Y.-J. Sun and I. Božović, "Hall Effect in quantum critical charge-cluster glass", ***PNAS - Proceedings of the US National Academy od Science*** 113, 4284 (2016).
18. X. Leng, A. T. Bollinger and I. Božović, "Purely electronic mechanism of electrolyte gating of indium tin oxide thin films", ***NPJ Scientific Reports*** 6, 31239 (2016).
19. X. He, A. Gozar, R. Sundling and I. Božović, "High-precision measurement of magnetic penetration depth in superconducting films", Rev. Sci. Instr. 87, 113903 (2016).
20. V. A. Gasparov, L. Drigo, A. Audouard, X. He and I. Božović, "Magnetic field dependence of high-T_c interface superconductivity in $La_{1.55}Sr_{0.45}CuO_4$-La_2CuO_4 heterostructures", Phys. Rev. B 94, 014507 (2016).
21. A. T. Bollinger, J. Wu, and I. Božović, "Rapid Synthesis of Complex Oxides by Combinatorial Molecular Beam Epitaxy", APL Materials 4, 053205 (2016).
22. A. Gozar and I. Božović, "High temperature interface superconductivity", Physica C 521, 38 (2016).
23. I. Božović and A. T. Bollinger, "Two-dimensional superconductivity in the cuprates revealed by atomic-layer-by-layer molecular beam epitaxy", Superconduct. Sci. Tech. 29, 103001 (2016).
24. V. A. Gasparov, X. He, G. Dubuis, D. Pavuna, N. D. Kushch, E. B. Yagubskii, J. A. Schlueter and I. Božović, "Magnetic field, frequency and temperature dependence of complex conductance of ultrathin $La_{1.65}Sr_{0.45}CuO_4/La_2CuO_4$ films and the organic superconductors k-(BEDT-TTF)2Cu[N(CN)2]Br", Internat. J. Mod. Phys. B 29, 1542012 (2015). Published: 20 Oct 2015.
25. V. A. Gasparov and I. Božović, "Complex conductance of ultrathin $La_{2-x}Sr_xCuO_4$ films and heterostructures", Low Temp. Phys. 41, 965 (2015). Published: Nov 2015.

Collaborative publications

26. G. Dubuis, Y. Yacoby, H. Zhou, X. He, A. T. Bollinger, D. Pavuna, R. Pindak and I. Božović, "Oxygen Displacement in Cuprates under Ionic-Liquid Field-Effect Gating", Scientific Reports 6, 32378 (2016).
27. K. Zou, S. Mandal, S. Albright, R. Peng, D. Kumah, G. Simon, O. Dagdeviren, X. He, I. Božović, U. Schwarz, E. Altman, D. Feng, F. J. Walker, S. Ismail-Beigi and C. H. Ahn, "The role of double TiO_2 layers at the interface of FeSe/ $SrTiO_3$ superconductors", Phys. Rev. B 93, 180506(R) (2016).
28. D. Meyers, H. Miao, A. C. Walters, V. Bisogni, R. S. Springell, M. d'Astuto, M. Dantz, J. Pelliciari, H. Huang, J. Okamoto, D. J. Huang, J. P. Hill, X. He, I. Božović, T. Schmitt and M. P. M. Dean, "Doping dependence of the magnetic excitations in $La_{2-x}Sr_xCuO_4$", Phys. Rev. B 95, 075139 (2017).

Novel functionality and emergent properties through controlled synthesis of epitaxial oxide heterostructures

Scott A. Chambers, Peter V. Sushko, Yingge Du, Tiffany C. Kaspar, Timothy C. Droubay, Steven R. Spurgeon. Pacific Northwest National Laboratory, Richland, WA

Program Scope

We explore fundamental phenomena related to electron-hole pair creation, propagation, and lifetime in model complex oxide epitaxial films, heterojunctions and superlattices. Understanding these phenomena paves the way for effective and scientifically informed use of oxides in photovoltaics and photoelectrochemistry. Our materials are synthesized with state-of-the-art control and purity using molecular beam epitaxy for the purpose of understanding the intricate relationships that exist between composition, structure and functional properties. The resulting material systems are characterized using a variety of methods aimed at determining composition, global and local structure, and the kinds and quantities of defects present. Electronic, optical, magnetic and magnetoelectronic properties are measured and interpreted in light of realistic, as opposed to idealized, models of the material system. Deep insight is gained by coupling experiment with classical and quantum mechanical modeling efforts. A key goal is an in-depth understanding of how defects influence properties, and can be harnessed and controlled for useful purposes.

Recent Progress

We will be presenting two posters at the PI meeting:

1. Novel functionality through controlled synthesis of epitaxial oxide heterostructures.

In this work, we used molecular beam epitaxy (MBE) to grow *p*-$La_{0.9}Sr_{0.1}CrO_3$ on *n*-$SrTiO_3$(001) and demonstrated that the resulting heterojunctions exhibit a type-II staggered band alignment, as determined by *in situ* x-ray photoelectron spectroscopy (XPS), and rectifying *I-V* behavior. The ideality factors (n) are high ($n \geq 8$), and there is some reverse-bias leakage current that increases with increasing temperature.[1] These anomalies were correlated with the presence of substitutional defects that form at the interface as a result of cation intermixing. In the process of characterizing the interface composition by scanning transmission electron microscopy (STEM) and related techniques, energy dispersive spectroscopy (STEM/EDS) and electron energy loss spectroscopy (STEM/EELS), we made significant progress in understanding probe beam delocalization and its effect on apparent interface widths at perovskite heterojunctions.[2]

We also showed that epitaxial *n*-$SrTiO_3$ (*n*-STO) can be grown on *p*-Ge(001) without unwanted GeO_x formation at the interface, and that the resulting heterostructure exhibits a type-II staggered band alignment, as determined by *in situ* XPS.[3] In the process of determining band alignment, we discriminated between two candidate physical causes of core-level peak broadening that can occur: (i) the presence of built-in potentials,[4] and, (ii) chemical shifts associated with surface and/or interface formation. In this case, surface hydroxide formation due to the interaction of residual water vapor in the MBE chamber with SrO on the surface results in a second set of weak spin-orbit peaks in the Sr 3d spectrum, leading to peak broadening that

might otherwise be interpreted as signaling the presence of a built-in potential in the STO. Angle-resolved XPS allowed us to rule out the presence of built-in potentials and confirmed that $Sr(OH)_2$ was present on the surface. The measured band alignment allows electrons photogenerated in Ge to run energetically downhill through the STO and into an aqueous electrolyte solution to drive the hydrogen evolution reaction. This conclusion was very recently confirmed with photoconversion experiments in which 630 nm light was coupled to a potentiostat in our *in situ* N_2-purged photoelectrochemistry system appended to the MBE/XPS system. Our initial measurements indicate that the incident light-to-photocurrent conversion efficiency is 14% under applied bias.

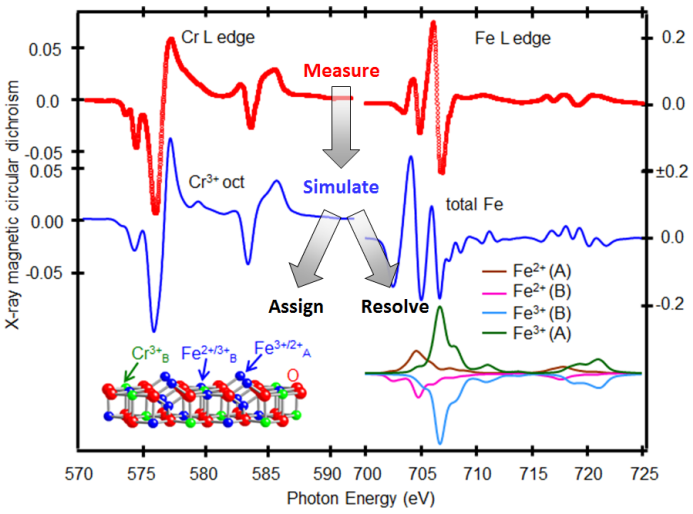

Fig. 1 – Measured (red) and calculated (blue) Cr and Fe L-edge XMCD spectra for $CrFe_2O_4$. The total Fe dichroism is well represented by the sum of contributions for Fe^{2+} and Fe^{3+} in the *A* sites and *B* sites of the inverse spinel lattice whereas the Cr dichroism consists of a single signature resulting from Cr^{3+} at the *B* sites.

Using a growth protocol we developed for epitaxial magnetite, $Fe_3O_4(001)$,[5, 6] we grew and determined the properties of epitaxial chromium ferrite, $Fe_2CrO_4(001)$.[7] We found that growing with a 2:1 Fe:Cr flux ratio on lattice matched MgO(001) results in half the *B* sites being occupied by Cr^{3+}, with the other half of the *B* sites and all *A* sites containing Fe in an equal mix of Fe^{2+} and Fe^{3+}. This change in composition converts the host magnetite lattice from a half-metal to a semiconducting ferrimagnet that absorbs strongly in the visible range. X-ray magnetic circular dichroism (XMCD) measured at the APS reveals that the spin alignment in the *A* and *B* sublattices is the same as it is in Fe_3O_4 (see Fig. 1). Of the many possible compositions for $Fe_{3-x}Cr_xO_4$, our first-principles modeling suggested that x = 1 should lead to strong visible light absorption, making the material of interest for visible light harvesting. This prediction was verified experimentally. This alloy showed better photoconductive properties than any others we have synthesized since starting this research thrust. Our modeling also showed that hopping conductivity between Fe^{2+} and Fe^{3+} is greatly facilitated by a non-random distribution of Fe and Cr in the B sublattice. Significantly, the presence of nanoscale patches of *B*-site Cr rich and *B*-site Fe rich $Fe_{3-x}Cr_xO_4$ leads to a low-energy path for hopping conductivity. Our very recent STEM/EELS results confirm the presence of such compositional irregularities in $Fe_2CrO_4(001)$. In addition, Fe_2CrO_4 is ferromagnetic up to at least 400K, making it of interest for spintronics.

2. Emergent properties of oxide superlattices

Complex oxide superlattices comprised of dissimilar materials exhibit a wide range of novel structural, electronic, and magnetic properties due to the high density of interfaces present in such

thin films. The large number of interfaces in epitaxial superlattices can give rise to emergent properties within the interior of the multilayer that may not be present (or measureable) at a single interface. The precise, atomic-level details of these interfaces determine the emergent properties, but there is poor understanding of local ordering in such systems and of how surface termination and band alignment affect the overall superlattice behavior. These phenomena can only be investigated in high-quality, epitaxial superlattices synthesized by an atomically-precise deposition technique such as molecular beam epitaxy.

In 2013, we confirmed that the surface termination of epitaxial Cr_2O_3 differs from that of epitaxial Fe_2O_3,[8] which likely leads to the observed non-commutative band offsets that differ by ~0.4 eV depending on the order of deposition.[9] Building on this, in our current work[10] we deposited epitaxial Fe_2O_3/Cr_2O_3 superlattices on Al_2O_3 (0001). We observed a built-in potential in the superlattice structure that arises from the non-commutative band alignments at each interface. Importantly, we could significantly reduce the magnitude of the built-in potential by purposefully altering the precise atomic ordering at the Fe_2O_3/Cr_2O_3 interfaces. Enhanced photoconductivity (PC) was measured for a thick Fe_2O_3 epitaxial film capped with an $(Fe_2O_3)_3$-$(Cr_2O_3)_3$ SL compared to a film capped with an $(Fe_{0.5}Cr_{0.5})_2O_3$ alloy (Fig. 2); this enhancement was attributed to efficient electron–hole separation in the SL as a result of the band alignment. The Fe–O–Cr bonds at the SL interfaces also redshifted the onset of photoconductivity to ~1.5 eV. Exploiting the band alignment and photoabsorption properties of Fe_2O_3-Cr_2O_3 SLs holds promise to increase the efficiency of hematite-based photo electrochemical water splitting.

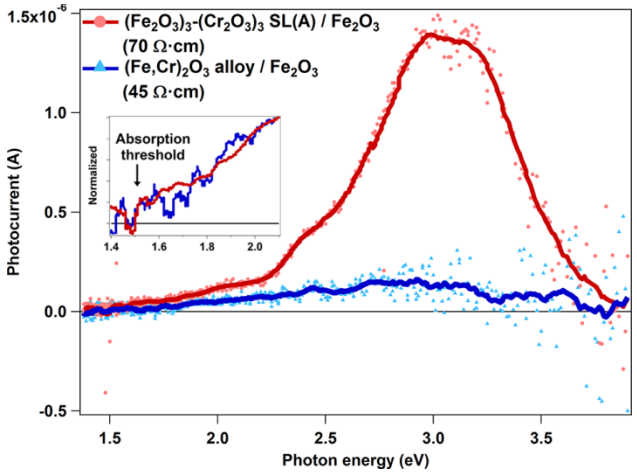

Fig 2 - PC spectra for capped Fe_2O_3 thin films. A strong photocurrent is observed for Fe_2O_3 capped with a Fe_2O_3/Cr_2O_3 SL, while a weaker photoinduced signal is observed for the alloy-capped film.

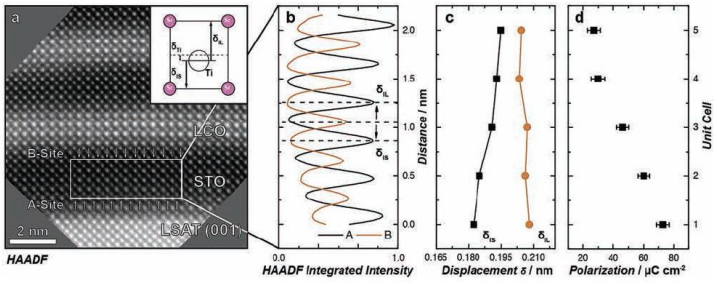

Fig. 3 – STEM-HAADF measurement of local polarization (Ti displacement) in the STO layer of a LCO/STO superlattice.

Epitaxial superlattices of $LaCrO_3/SrTiO_3$ (LCO/STO) present the unique opportunity to explore the effect of the built-in potential which arises in the polar LCO layer when deposited on non-polar STO. We found[11] that in LCO/STO superlattices with precisely-tailored atomic ordering at the interfaces, the built-in potential in the LCO layer could induce a similar potential in the STO layer, as well as a ferroelectric-like polar distortion of the Ti cations in the layer (Fig. 3). This induced polarization was predicted by DFT simulations of the superlattice structure. In further work,[12] we thoroughly characterized the non-idealities in the LCO/STO superlattice structure, including interfacial non-stoichiometry, Cr valence changes, and

the presence of oxygen vacancies, with STEM-EELS, atom probe tomography (APT), and XPS. We found that excess La ions in the LCO layer of the superlattice contribute free carriers to the neighboring STO layers, while excess Cr ions promote the formation of interfacial oxygen vacancies. These vacancies produce a combination of Cr^{2+} and Ti^{3+} ions while also preventing the formation of a Cr^{4+} hole that was predicted by density functional theory calculations to screen the built-in polarization in the superlattice.

Future Plans

Going forward, we have developed a comprehensive research plan aimed at developing methods to control the kinetics of formation and final ground-state properties of oxide heterostuctures. We will test two hypotheses:

1. *Functional properties of epitaxial heterostructures are influenced and can be controlled by lattice structure, cation site occupancies and distributions and defects.*
2. *Unique, persistent metastable structures, and the corresponding electronic states, can be achieved through control of assembly pathways by tuning growth parameters, such as metal atom fluxes and the temporal overlaps of these fluxes.*

Successfully addressing these two hypotheses will enable new degrees of control in the synthesis of complex oxide heterostructures. By investigating a well-rounded mix of optical, electronic, magnetic and photochemical phenomena, this program will facilitate a holistic, fundamental understanding of these materials at a level appropriate for BES sponsored research. Specific materials systems to be investigated include, but are not limited to, *n*-$SrZr_xTi_{1-x}O_3$/*p*-Ge(001), $Sr_xLa_{1-x}FeO_3$/*n*-$SrTiO_3$(001) and *n*-Fe_2CrO_4/*p*-$FeTi_2O_4$(001) and $Fe_{3-x}Cr_xO_4$/NiO(001).

References

[1] Y. Du, C. Li, K. H. L. Zhang, M. E. McBriarty, S. R. Spurgeon, H. S. Mehta, and D. Wu, Appl. Phys. Lett. **111**, 063501 (2017).

[2] S. R. Spurgeon, Y. Du, and S. A. Chambers, Microsc. Microanal. **23**, 513 (2017).

[3] S. A. Chambers, Y. Comes, S. R. Spurgeon, and P. V. Sushko, Appl. Phys. Lett. **110**, 082104 (2017).

[4] S. A. Chambers, in *Hard X-ray Photoelectron Spectroscopy*, edited by J. Woicik (Springer, 2016), Vol. 59, p. 341.

[5] Y. Gao and S. A. Chambers, J. Cryst. Growth **174**, 446 (1997).

[6] Y. Gao, Y. J. Kim, and S. A. Chambers, J. Mater. Res. **13**, 2003 (1998).

[7] S. A. Chambers, T. C. Droubay, T. C. Kaspar, I. H. Nayyar, M. E. McBriarty, S. M. Heald, D. J. Keavney, M. E. Bowden, and P. V. Sushko, Adv. Funct. Mater. **27**, 1605040 (2017).

[8] T. C. Kaspar, S. E. Chamberlin, and S. A. Chambers, Surf Sci. **618**, 159 (2013).

[9] S. A. Chambers, Y. Liang, and Y. Gao, Phys. Rev. B **61**, 13223 (2000).

[10] T. C. Kaspar, D. K. Schreiber, S. R. Spurgeon, M. E. McBriarty, G. M. Carroll, D. R. Gamelin, and S. A. Chambers, Adv. Mater. **28**, 1616 (2016).

[11] R. B. Comes, S. R. Spurgeon, S. M. Heald, D. M. Kepaptsoglou, L. Jones, P. V. Ong, M. E. Bowden, Q. M. Ramasse, P. V. Sushko, and S. A. Chambers, Adv. Mater. Int. **3**, 1500779 (2016).

[12] R. B. Comes, S. R. Spurgeon, D. M. Kepaptsoglou, M. H. Engelhard, D. E. Perea, T. C. Kaspar, Q. M. Ramasse, P. V. Sushko, and S. A. Chambers, Chem. Mater. **29**, 1147 (2017).

Publications over the past two years

1. P. Xu, T.C. Droubay, J.S. Jeong, K.A. Mkhoyan, P.V. Sushko, S.A. Chambers, and B. Jalan, "*Quasi two-dimensional ultra-high carrier in a complex oxide broken-gap heterojunction*," Adv. Mater. Int. **3**, 1500432 (2016). DOI: 10.1002/admi.201500432
2. S.A. Chambers, "*Probing perovskite interfaces and superlattices with x-ray photoemission spectroscopy*," invited book chapter for Hard X-ray Photoelectron Spectroscopy (HAXPES), J. Woicik, ed. Springer Series in Surface Sciences, Vol. **59**, 341-380 (2016). DOI:10.1007/978-3-319-24043-5_14
3. R.B. Comes, T.C. Kaspar, S.M. Heald, M.E. Bowden, and S.A. Chambers, "*Infrared optical absorption in low-spin Fe^{2+}-doped $SrTiO_3$*," J. Phys. Cond Mat. **28**, 035901 (2016). https://doi.org/10.1088/0953-8984/28/3/035901
4. T.C. Kaspar, D.K. Schreiber, S.R. Spurgeon, M.E. McBriarty, G.M. Carroll, D.R. Gamelin, and S.A. Chambers, "*Built-in Potential in Fe_2O_3-Cr_2O_3 Superlattices for Improved Photoexcited Carrier Separation*," Adv. Mater. **28**(8) 1616-1622 (2016). DOI: 10.1002.adma.201504545
5. R.B. Comes, S.R. Spurgeon, S.M. Heald, D.M. Kepaptsoglou, L. Jones, P.V. Ong, M.E. Bowden, Q.M. Ramasse, P.V. Sushko, S.A. Chambers, "*Interface-induced polarization in $SrTiO_3$-$LaCrO_3$ superlattices*," Adv. Mater. Int. **3**(10) 1500779 (2016). DOI:10.1002/admi.201500779
6. Y. Du, G. Li, E.W. Peterson, J. Zhou, X. Zhang, R. Mu, Z. Dohnalek, M. Bowden, I. Lyubinetsky, and S.A. Chambers, "*Iso-oriented monolayer α-MoO_3(010) films epitaxially grown on $SrTiO_3$(001)*," Nanoscale **8**, 3119-3124 (2016). DOI: 10.1039/C5NR07745A
7. S.A. Chambers, T.C. Kaspar, A. Prakash, G. Haugstad, and B. Jalan, "*Band alignment at epitaxial $BaSnO_3$/$SrTiO_3$(001) and $BaSnO_3$/$LaAlO_3$(001) heterojunctions*," Appl. Phys. Lett. **108**, 152104 (2016). DOI: http://dx.doi.org/10.1063/1.4946762
8. S.R. Spurgeon, Y. Du, T. Droubay, A. Devaraj, X. Sang, P. Longo, P. Yan, P.G. Kotula, V. Shutthanandan, M.E. Bowden, J.M. LeBeau, C. Wang, P.V. Sushko, and S.A. Chambers, "*Competing pathways for nucleation of the double perovskite structure in the epitaxial synthesis of La_2MnNiO_6*," Chem. Mater. **28**(11) 3814-3822 (2016). DOI: 10.1021/acs.chemmater.6b00829
9. P. Xu, Y. Ayino, C. Cheng, V.S. Pribiag, R.B. Comes, P.V. Sushko, S.A. Chambers, and B. Jalan, "*Predictive control over charge density in the two-dimensional electron gas at the polar/non-polar $NdTiO_3$/$SrTiO_3$ interface*," Phys. Rev. Lett. **117** 106803 (2016). DOI:10.1103/PhysRevLett.117.106803
10. T.C. Kaspar, P.V. Sushko, M.E. Bowden, S.M. Heald, A. Papadogianni, C. Tschammer, O. Bierwagen, and S.A. Chambers, "*Defect compensation by Cr vacancies and oxygen interstitials in Ti^{4+}-doped Cr_2O_3 epitaxial thin films*," Phys. Rev. B **94** 155409 (2016). DOI:https://doi.org/10.1103/PhysRevB.94.155409
11. R.B. Comes and S.A. Chambers, "*Interface structure, band alignment and built-in potentials at $LaFeO_3$/n-$SrTiO_3$ heterojunctions*," Phys. Rev. Lett. **117** 226802 (2016). DOI:10.1103/PhysRevLett.117.226802
12. I.H. Nayyar, S.E. Chamberlin, T.C. Kaspar, N. Govind, S.A. Chambers and P.V. Sushko, "*Effect of doping and chemical ordering on the optoelectronic properties of complex oxide semiconductors: Fe_2O_3 – V_2O_3 solid solutions and hetero-structures*," Phys. Chem. Chem. Phys. **19** 1097-1107 (2017). DOI:10.1039/C6CP06087K

13. S.A. Chambers, T.C. Droubay, T.C. Kaspar, I.H. Nayyar, M.E. McBriarty, S.M. Heald, D.E. Keavney, P.V. Sushko, and M.E. Bowden, "*Electronic and optical properties of a semiconducting spinel – Fe_2CrO_4*," Adv. Funct. Mater. **27**(9) 1605040 (2017). DOI: 10.1002/adfm.201605040
14. R.B. Comes, S.R. Spurgeon, D.M. Kepaptsoglou, M.H. Engelhard, D.E. Perea, T.C. Kaspar, Q.M. Ramasse, P.V. Sushko, and S.A. Chambers, "*Probing the origin of interfacial carriers in $SrTiO_3$-$LaCrO_3$ Superlattices*," Chem Mater. **29**(3) 1147-1155 (2017). DOI:10.1021/acs.chemmater.6b04329
15. S.A. Chambers, Y. Du, R.B. Comes, S.R. Spurgeon, and P.V. Sushko, "*The effects of core-level broadening in determining band alignment at the epitaxial $SrTiO_3$(001)/p-Ge(001) heterojunction*," Appl. Phys. Lett. **110** 082104 (2017). DOI: http://dx.doi.org/10.1063/1.4977422
16. S.R. Spurgeon, Y. Du, and S.A. Chambers, "*Measurement error in atomic-scale scanning transmission electron microscopy—energy-dispersive x-ray spectroscopy (STEM-EDS) mapping of a model oxide interface*," Microscopy and Microanalysis **23**(3) 513-517 (2017). DOI:10.1017/S1431927617000368
17. K.A. Stoerzinger, R.B. Comes, S.R. Spurgeon, S. Thevuthasan, K. Ihm, E. J. Crumlin, and S.A. Chambers, "*Influence of $LaFeO_3$ surface termination on water reactivity*," J. Phys. Chem. Lett. **8**(5) 1038-1043 (2017). DOI: 10.1021/acs.jpclett.7b00195
18. Yingge Du, Chen Li, Kelvin H. L. Zhang, Martin E. McBriarty, Steven R. Spurgeon, Hardeep S. Mehta, Di Wu, Scott A. Chambers, "*An all-perovskite p-n junction based on transparent conducting p-$La_{1-x}Sr_xCrO_3$ epitaxial layers*", Appl. Phys. Lett. **111**, 063501 (2017). DOI: http://dx.doi.org/10.1063/1.4997410.
19. Steven R. Spurgeon and Scott A. Chambers, "*Atomic-scale Characterization of oxide interfaces and superlattices using scanning transmission electron microscopy*", book chapter in Encyclopedia of Interface Chemistry: Surface Science and Electrochemistry (2017). DOI: 10.1016/B978-0-12-409547-2.12877-X.

Nucleation and Self-Assembly of Hierarchical Materials: Predicting Pathways, Dynamics and Outcomes

Jim De Yoreo, Marcel Baer, Jaehun Chun, Karl Mueller, Chris Mundy, and Peter Pauzauskie, Pacific Northwest National Laboratory

Program Scope

The objective of this project is to develop a predictive understanding of the mesoscale principles connecting atomistic structure to the macroscopic dynamics that control synthesis via multi-step nucleation pathways and nanoparticle assembly. We are achieving this objective through 1) synthesis of nano-materials that exhibit non-classical pathways and represent distinct classes of molecular interactions, 2) *in situ* TEM, AFM, surface vibrational spectroscopy and NMR characterization, and 3) theory and simulation of speciation pathways, cluster formation, nucleation, solution-solid interfacial structure, the forces between particles, and particle assembly dynamics. We are applying these approaches to simple materials systems including: AlOOH clusters on mica (001), supersaturated $CaCO_3$ solutions, polysilicate frameworks that nucleate along complex chemical reaction pathways, and $NaYF_4$ and TiO_2 nanorods that assemble via oriented attachment of primary particles whose phases are distinct form the final phase. The outcome will be a predictive description of non-classical crystallization that crosses scales to seamlessly connect atomic scale details to mesoscopic collective behavior through the development of models of reduced complexity. Here we focus on our studies of nucleation.

Recent Progress

The dynamics of AlOOH cluster populations: Classical nucleation theory predicts precursors to nucleation are small unstable clusters that form spontaneously *via* statistical-fluctuations.[1] However, recent studies suggest pathways to nucleation are complex, involving aggregation of large, stable clusters or formation of liquid-like precursors.[2] Researchers have attempted to directly detect precursors to nucleation in order to test these various models; unfortunately, the species present prior to nucleation are either too small or scarce to be unambiguously detected using methods like *in situ* TEM or X-ray scattering. However, recent advances with *in situ* AFM now allow for solution imaging of surfaces at atomic resolution.[3] Here we utilize *in situ* AFM to investigate epitaxial nucleation of AlOOH (gibbsite) on mica. The results (Fig. 1) show that, at 25°C and low pH, there is a dynamic population of atomic species, which appear to reside at the cation sites. As pH is increased to drive crystallization, a dynamic population of clusters forms consisting of a classical distribution plus a large excess narrowly distributed about a diameter of 1-2 nm. The dependence of cluster number density on pH and Al concentration indicates the initial species are $Al(OH)_2^{1-}$. DFT simulations predict these species will dominate due to a local pH increase, which also creates high supersaturation. As temperature is increased to 46°C, the surface becomes covered with irregular-shaped clusters ~ 1 to 20 nm in diameter, as well as highly-transient species of small dimension. At 60°C the

clusters evolve into crystalline islands comprised of a monolayer of gibbsite; these coalesce and coarsen with time. Our findings suggest a crystallization pathway differing from traditional views of nucleation *via* rare, dispersed clusters built from monomeric species, but instead suggests involvement of ion coordination complexes, the existence of special cluster sizes, and crystallization occurring by condensation of a relatively dense adsorbate layer.

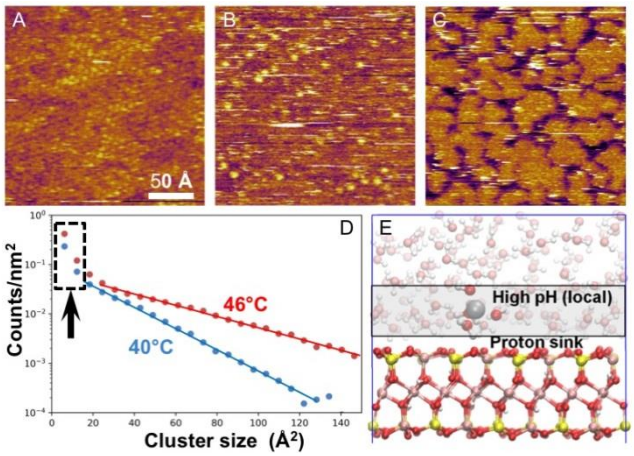

Fig. 1 – (A-C) AFM showing evolution from atomic adsorbates (A) to clusters (B) to gibbsite (C). (D) Cluster size distributions showing "classical" log-linear dependence and excess near 1nm (dashed box). (E) Snapshot from DFT simulation predicting high pH near interface leading that creates high local supersaturation.

Solution species in $CaCO_3$ supersaturated solutions: One of the challenges to predicting nucleation is that cluster formation starts with ion pairing, which requires atomistic simulations at the level of DFT, but growth of critical clusters and beyond is an ensemble outcome requiring statistical analyses. We developed an approach that enables us to bridge these scales and applied it to $CaCO_3$ solutions (Fig. 2). Recent studies suggest these solutions contain significant populations of large, stable clusters prior to nucleation, which is claimed to proceed by aggregation of these "pre-nucleation clusters", rather than by classical monomer-by-monomer addition to unstable clusters resulting from inherent thermal fluctuations.[4] We first obtained potentials of mean force for ion pairing from DFT and used them to create a coarse grain solution model. A new computational method based on aggregation-volume-bias Monte Carlo (AVBMC) was then used to develop statistical-mechanically converged estimates for the free energy of formation of clusters and predict: 1) their populations in solution, 2) effective surface energies, 3) evolution of solution composition during titration experiments and 4) Ca^{2+} x-ray adsorption near edge spectra

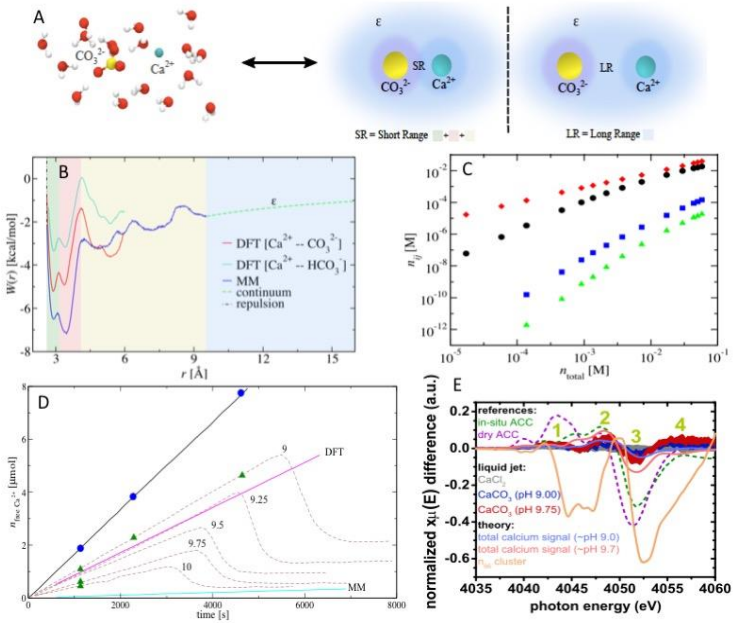

Fig. 2 – (A) Atomistic and reduced $CaCO_3$ model. (B) PMFs for ion pairing from DFT vs. MD (C) Distribution of species predicted by AVBMC. (E) Comparison of XANES spectra to spectra from hydrated and dry amorphous $CaCO_3$ (ACC) and predicted spectra for populations in (C) as well as large species predicted by others.

(XANES), which probe the local chemical environment of Ca^{2+} ions solution. Our results predict that the solutions will be dominated by ions and ion pairs and that larger clusters will be exceeding rare. Moreover, they predict titration curves and XANES data that are in good agreement with reported data over a wide pH range, as well as classical dependencies of cluster formation energy on size that give a reasonable valued for the effective surface energy. Thus, our results lead to a classical picture of calcium carbonate nucleation from solution in which the formation of large clusters is a rare event and occurs through ion-by-ion addition up a classical free energy barrier.

Pre-nucleation pathways of polysilicates: Polysilicates represent a class of framework structures that utilize cage-like building blocks to form larger structures.[5] Moreover, silicates are well known for their ease of polymerization to form solution species more complex than simple ions or ion complexes. Finally, ^{29}Si NMR is an effective technique for defining polysilicate speciation in solution. Consequently, they provide a good model system to explore pre-nucleation species and chemical reaction pathways that lead to formation of complex framework lattices. Using ^{29}Si NMR to identify species and quantify relative concentrations of tetramethylammonium (TMA) silicates, we find that simple Q^0 species dominate at 5 min, but by 72 hours full octahedral $Q^3{}_8$ cages that define the basic unit of the crystal comprise 83% of the species (Fig. 3). Pulsed-Field Gradient (PFG) Stimulated Echo measurements of chemically specific diffusion show that solvent exchange is rapid and crucial to cluster formation and transformation. MD simulations similarly find, that the basic unit of the crystal exists in solution as a fluctuating cluster.

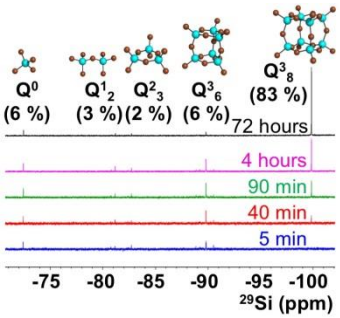

Fig. 3 – ^{29}Si NMR spectra of polysilicate solution showing speciation change with time.

Future Plans

We plan to complete our experimental analysis of AlOOH cluster dynamics and polysilicate chemical reaction paths and extend our multiscale computational approach to both of these cases. In addition, we will incorporate new results we are obtaining on the structure of water and distribution of ions at the mica surface from surface vibrational spectroscopy and frequency modulated AFM into our computational models[6] to produce a true atomic-scale view of nucleation that, nonetheless, predicts ensemble pathways and rates. We will also continue to apply a similar *in situ* experimental and multi-scale simulations approach to the process of oriented attachment.

References

1 Legg, B. A. & De Yoreo, J. J., *J. Chem. Phys.*, **145**, 211921 (2016).
2 De Yoreo, J. J. *et al.*, *Science* **349**, aaa6760 (2015).
3 Fukuma, T. & Jarvis, S. P., *Rev Sci Instrum* **77**, 043701 (2006).
4 Gebauer, D. & Colfen, H., *Nano Today* **6**, 564-84, (2011).

5 Cordes, D. B., Lickiss, P. D. & Rataboul, F., *Chem. Rev.* **110**, 2081-173, (2010).
6 Prakash, A., Pfaendtner, J., Chun, J. H. & Mundy, C. J., *J. Phys. Chem. C* **121**, 18496-504, (2017).

Publications

B.A. Legg, J.J. De Yoreo, The Energetics of Prenucleation Clusters in Lattice Solutions. *J. Chem. Phys.* **145**, 211921 (2016) doi.org/10.1063/1.4964489

M. D. Baer and C. J. Mundy, Local aqueous solvation structure around Ca^{2+} during $Ca^{2+} \cdots Cl^-$ pair formation. *J. Phys. Chem. B* **120**, 1885-1893, (2016). DOI. 10.1021/acs.jpcb.5b09579

X. Zhou, B. E. Smith, P. B. Roder, and P. J. Pauzauskie, Laser Refrigeration of Ytterbium-Doped Sodium–Yttrium–Fluoride Nanowires. *Adv. Mat.*, **28**, 8658-8662 (2016) doi: 10.1002/adma.201600406

J.J. De Yoreo and N.A.J.M Sommerdijk, Investigating processes of materials formation via liquid phase and cryogenic TEM. *Nature Reviews Mater.* **1**, 16035 (2016). doi:10.1038/natrevmats.2016.35

D. Li, J. Chun, D. Xiao, W. Zhou, H. Cai, L. Zhang, K. M. Rosso, C. J. Mundy, G. K. Schenter, J. J. De Yoreo, Trends in mica–mica adhesion reflect the influence of molecular details on long-range dispersion forces underlying aggregation and coalignment. *Proc. Nat'l Acad. Sci*. **114**, 7537-7542 (2017). DOI/10.1073/pnas.1621186114

A. Prakash, J. Pfaendtner, J. Chun, and C. J. Mundy, Quantifying the Molecular-Scale Aqueous Response to the Mica Surface. *J. Phys. Chem. C*, **121**, 18496–18504 (2017)

J.J. De Yoreo, N.A.J.M. Sommerdijk and P.M. Dove, Nucleation pathways in electrolyte solutions. *in* A.E.S. van Driessche, M. Kellermeier, L.G. Benning and D. Gebauer, Eds., New perspectives on mineral nucleation and growth: From solution precursors to solid materials, (Springer International, New York, 2017)

K. Henzler, E.O. Fetisov, M. Galib, M.D. Baer, C. B.1, J.M. Xto1, B.A. Legg, S. Pin, J.L. Fulton, G.K. Schenter, N. Govind, J.I. Siepmann, C.J. Mundy, T. Huthwelker, J.J. De Yoreo, Supersaturated calcium carbonate solutions are classical. *Sci. Adv.* (In revision).

Controlling ion intercalation induced topotactic phase transitions in oxide thin films

Yingge Du, Pacific Northwest National Laboratory

Program Scope

The overarching goal of this program is to *understand, predict, and ultimately control ion transport and topotactic phase transition processes occurring in structurally ordered transition metal oxide (TMO) thin films*. TMOs with interconnected, ordered vacant lattice sites enable facile, synchronous electron/ion intercalation reactions, and have been extensively investigated for energy conversion and storage applications, particularly for use as solid-state electrolytes, mixed electronic/ionic conductors, electrocatalysts, and electrodes in batteries and fuel cells.[1-3] A topotactic phase transition (TPT), in which the final crystal lattice is closely related to that of the original material, may occur through the displacement and exchange of atoms as a result of intercalation. The fundamental questions we investigate are highly relevant to energy conversion and storage technologies, as such fundamental processes govern the mass-transport properties and failure mechanisms of widely used energy materials. TPTs occurring at the forefront of many catalytic reactions and electrode/electrolyte interfaces are often responsible for many of the challenges (e.g., safety concern due to volume expansion and capacity decrease after cycling due to loss of desired structure/phase) found in lithium ion batteries and solid oxide fuel cells.

We will investigate structurally and compositionally well-defined complex oxide films and thin-film based devices that will enable the facile intercalation of either small cations (e.g., Li^+, Na^+, and Ca^{2+}) or oxygen anions (O^{2-}). Our team will bring together 1) state-of-the-art synthesis of epitaxial oxide thin films and heterostructures by molecular beam epitaxy (MBE) and pulsed laser deposition (PLD); 2) detailed *in situ/in operando* characterization of the superstructures, film/substrate, film/film, film/vacuum, and film/solvent interfaces, and their evolution as a function of interfacial strain, doping level, and processing conditions; and 3) *ab initio* modeling of defect formation, structural ordering, and phase transition pathways and kinetics within the studied materials. The specific aims of this research are to: 1) correlate atomic-scale structural evolution, mesoscale topotactic phase transition, and macroscopic mass transport characteristics as TPTs occur; 2) understand how doping and interfacial strain can be used to modify the onset (e.g., temperature, electrochemical potential), dynamics, intermediate states, and trajectories of TPTs.

Recent Progress

The team secured an EMSL user proposal support (10/01/16-10/01/17) shortly after the DOE Award was received. The needed instrument resources were granted, with an extra $40K in staff support. Postdocs currently supported by this program are Drs. Zhenzhong Yang (100%, on thin film growth and *in situ* TEM), Le Wang (70%, on thin film growth, characterization, and property measurement), and Phuong-Vu Ong (50%, on *ab initio* simulations). We have started

collaborations with beamline scientists at Advanced Photon Source (APS) to investigate the detailed structures of the films.

The first two bullet points below are key proof-of-concept accomplishments for this Award. A portion of these results were used as preliminary data in the early career research proposal, and the two papers listed were accepted before the Award was made.

• Elucidated Li-ion intercalation and subsequent conversion reaction processes in a model electrode material, WO_3, through direct structural and chemical imaging using *in situ* transmission electron microscopy (TEM).These findings are of general importance to the predictive design and synthesis of next generation battery materials.

Y. He, M. Gu, H. Xiao, L. Luo, Y. Shao, F. Gao, Y. Du,* S. X. Mao*, and C. Wang*, "Atomistic conversion reaction mechanism of WO_3 in secondary ion batteries of Li, Na, and Ca", *Angewandte Chemie International Edition* **55**, 6244 (2016).

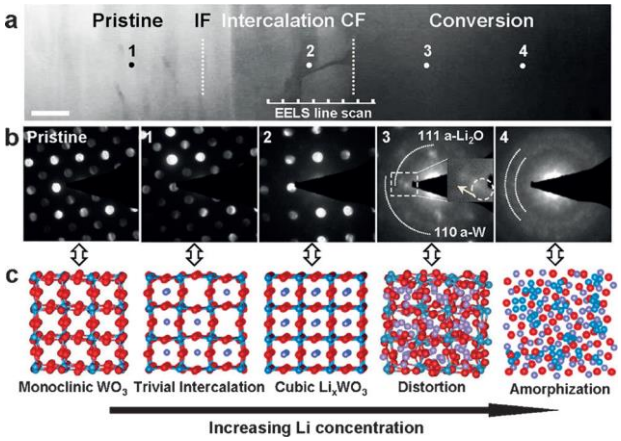

Fig. 1. a) High angle annular dark field (HAADF) scanning transmission electron microscopy (STEM) image of the reaction front. Scale bar, 50 nm. b) Nano beam diffractions (NBD) from the pristine sample and across the conversion front (CF). c) Structure and crystal symmetry evolution with increasing Li concentration in the Li_xWO_3 lattice as indicated by the corresponding NBDs.

• Synthesized and characterized MoO_3 thin films with tailored phases, structures, and properties. This is a critical step as such model materials enable us to further study fundamental Li intercalation and reaction processes as proposed.

Y. Du,* G. Li, E. W. Peterson, J. Zhou, X. Zhang, R. Mu, Z. Dohnalek, M. Bowden, I. Lyubinetsky and S. A. Chambers, "Iso-oriented monolayer α-MoO_3(010) films epitaxially grown on $SrTiO_3$(001)", *Nanoscale*, **8**, 3119 (2016).

• Carried out *ab initio* simulations to better understand defect formation, diffusion, and ordering processes that may ultimately lead to phase transitions observed in the Li_xWO_3 and $SrCrO_{3-\delta}$ systems. These work were supported by this program. Please see 1 and 2 in the publication list.

Future Plans

We are currently preparing three manuscripts that are initiated and led by this program, with materials focusing on $SrCrO_{2.8}$, $SrFeO_{2.5}$, and $LiCoO_2$, respectively. Going forward, we will

be pursuing *in situ* study of the strain effect on the phase stability of MBE-grown $SrFeO_{2.5}$ and $SrCrO_{2.8}$ films by ETEM and STEM. In addition, we will investigate the Li diffusion processes and interface evolution occurring at the solid-solid interface between $LiCoO_2$ and solid state electrolyte deposited by PLD.

References

1. Robert Schöllhorn, "Reversible Topotactic Redox Reactions of Solids by Electron/Ion Transfer", *Angewandte Chemie International Edition*, **19** (12), 983 (1980).

2. H. Jeen, W. S. Choi, J. W. Freeland, H. Ohta, C. U. Jung, and H. N. Lee, "Topotactic Phase Transformation of the Brownmillerite $SrCoO_{2.5}$ to the Perovskite $SrCoO_{3-\delta}$", *Advanced Materials*, **25** (27), 3651 (2013).

3. K. H. L. Zhang, P. V. Sushko, R. Colby, Y. Du, M. E. Bowden, and S. A. Chambers, "Reversible nano-structuring of $SrCrO_{3-\delta}$ through oxidation and reduction at low temperature", *Nature Communications*, **5,** 4669, (2014).

Publications

1. Z. Wang, Y. He, M. Gu, Y. Du, S. X. Mao, and C. Wang, "Electron Transfer Governed Crystal Transformation of WO_3 upon Li Ions Intercalation", *ACS Applied Materials & Interfaces*, **8**, 24567 (2016). DOI: 10.1021/acsami.6b06581

2. P. V. Ong, Y. Du, and P. V. Sushko, "Low-Dimensional Oxygen Vacancy Ordering and Diffusion in $SrCrO_{3-\delta}$", *The Journal of Physical Chemistry Letters*, **8**, 1757 (2017). DOI: 10.1021/acs.jpclett.7b00355

3. K. H. L. Zhang, R. Wu, F. Z. Tang, W. W. Li, F. E. Oropeza, L. Qiao, V. K. Lazarov, Y. Du, D. J. Payne, J. L. MacManus-Driscoll, and M. G. Blamire, "Electronic Structure and Band Alignment at the NiO and $SrTiO_3$ p-n Heterojunctions", *ACS Applied Materials & Interfaces* **9**, 26549 (2017). DOI: 10.1021/acsami.7b06025

Ion Transport and Structural Evolution of Solid Electrolytes

Elucidating phase evolutions of solid electrolytes during synthesis and interface fabrication

Miaofang Chi, Cheng Ma, Robert Schmidt, Yan Chen, Ke An, Xiaoming Liu, Robert L. Sacci, Gabriel M. Veith, Chelsea Xi, Nancy Dudney
Center for Nanophase Materials Sciences, Spallation Neutron Source, and the Materials Science and Technology Division, Oak Ridge National Laboratory, Oak Ridge, TN 37831

Program Scope

The goal of this project is to provide a detailed, fundamental understanding of the role of chemistry, crystal structure, and microstructure on the key properties of solid electrolytes under the highly non-equilibrium conditions during operation of electrochemical energy storage (EES) systems. This goal will be achieved through three synergistically arranged aims: (1) Elucidation of the effect of atomic and mesoscale structures on ion transport in solids. (2) Understanding the influence of interfaces and interphases on the ion transport and electron transfer in EES systems. (3) Revealing the structural evolution and interface contact properties of SEIs and electrode-electrolyte interfaces in solid-state electrochemical cells. The bulk and interface properties of the solid electrolytes are determined by rigorous control synthesis conditions, but the properties may further evolve due to chemical and electrochemical reactions. Understanding these complex processes requires *in situ* characterization during synthesis, interface fabrication and electrochemical operation. The program encompasses new materials and compositions, as well as known model materials formed via vapor, solid, and liquid synthesis routes. This includes highly conductive oxides, phosphates, and thiophosphates.

Recent Progress

Tuning conductivity via controlling synthesis conditions. We have demonstrated that mesoscale features, such as domain structures, can be used to create fast ion percolation pathways and result in enhanced ion conductivity in solid electrolytes. In our recent investigation, we are exploring

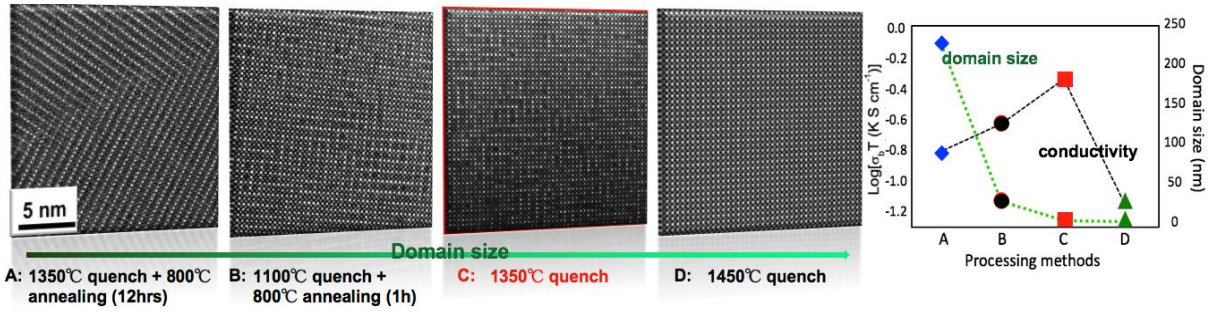

Figure 1 Domains structures in LLTO create fast ion percolation pathways in LLTO. Such domain structure was found to be tunable through adapting different post-synthesis processing conditions, as revealed by scanning transmission electron microscopy (STEM) images (a-d). This work highlights the strategy to tune ion conductivity of superionics through controlled synthesis (unpublished).

how to tune ion conductivity in $Li_{3x}La_{2/3-x}TiO_3$ (LLTO) by controlling mesoscale domain structures through varying synthesis and processing conditions. The domain size in LLTO was successfully tuned from 0 to hundreds of nanometers by adapting different annealing/quenching conditions, resulting in different ionic conduction behavior (**Figure 1**). The maximum ionic conductivity was found to be in the specimen with a domain size of 2-3nm, which combines an

ordering structure within unit cells and a unique domain structure at the mesoscopic scale. The former feature promises the availability of nearby vacancy sites for ions to hop and the latter maximizes ion percolation pathways in three-dimensions. Another example of our research for creating high-performance ion conductors through the control of synthesis parameters was shown in our *in situ* neutron study on $LiNi_{0.5}Mn_{1.5}O_4$ (LNMO) high voltage cathodes (**Figure 2**). By monitoring the phase evolution of LNMO upon annealing, it was found that the material not only experiences phases with different unit cell structures, i.e. structures with ordered /disordered transition metal elements in lattice, but also a new structure that is composed of orientation disordered lattice cells formed during a specific range of annealing time. These phases, though with minute lattice variations, give rise to different electronic structures, leading to notable changes in voltage plateaus during electrochemical cycling. The above two studies demonstrated the significance of probing the evolution of phases and structures as a function of synthesis conditions using *in situ* characterization tools in controlled synthesis research. Future work related to this topic will be focused on understanding how local performance-controlling features, such as grain boundaries and interfaces, evolve at atomic scale during synthesis. By explaining the dynamic elemental diffusion, chemical reactions and phase evolution, as well as the relative roles of kinetic stabilization and thermal relaxations, valuable insights will be gained towards designed synthesis of these critical features.

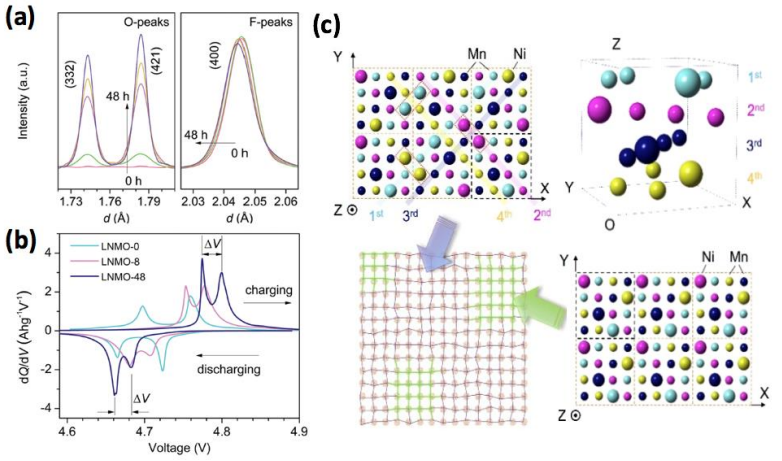

Figure 2 Neutron diffraction reveals the changes in (332), (421) and (400) peaks as a functional of annealing time at 700 ℃ (a); The differential capacity versus voltage curves show that the electrochemical behavior varies with annealing time. The peak separation ΔV is correlated to the density of lattice-cell orientation disorder (LCOD) zones (b); Illustration of the LCOD structure (c). Same lattice cells are arranged in two different ways resulting in local structures with different symmetry. The coexistence of these two arrangements in LNMO forms complex disordered structure at mesoscale [Y. Chen et. al., Adv. Energy Mater. 7, 1601950 (2017)].

<u>Elucidating interphase evolution during interface formation.</u> Heterogeneous ionic interfaces currently represent the most critical features controlling the rate capability and cyclability in energy storage systems. Our knowledge of atomic-scale structure and chemistry during fabrication and operation is currently very limited. This is because of the complexity of interfacial structure and chemistry in real materials systems, where multiple interfacial mechanisms are often involved in, not only mechanical integrity, but also chemical and electrochemical stability and even the formation of space charges. These mechanisms couple with each other in a spatially confined region, resulting in intricate interfacial phenomena that is challenging for both experiments and theory. Elucidating these phenomena and their coupling in model interfaces will significantly help us to seek strategies to form stable and conductive interfaces. In our recent work, through the *in situ* formation of a Li-metal/ $Li_{7-3x}Al_xLa_3Zr_2O_{12}$

(cubic-LLZO) interface inside an electron microscope, the atomic-scale chemical and structural evolution at the interface is revealed (**Figure 3**). Simultaneous implantation of Li^+ and electrons induced a self-limiting stable interfacial phase trans-formation. This interphase effectively prevented further interfacial reactions without compromising the ionic conductivity and the structural compatibility, promising greater stability and conductivity across critical interfaces for Li-metal batteries. Passivation layers are preferred to those formed through chemical decomposition where the multiple reactant phases may potentially introduce inhomogeneous current distributions at the interface upon electrochemical cycling. Taking advantage of intrinsic phase transformations in materials may be used as one strategy to enable the formation of stable and conductive interfaces leading to safe and high-performance batteries. Future work will be focused on exploring the structural and chemical stability of such interphases upon electrochemical cycling.

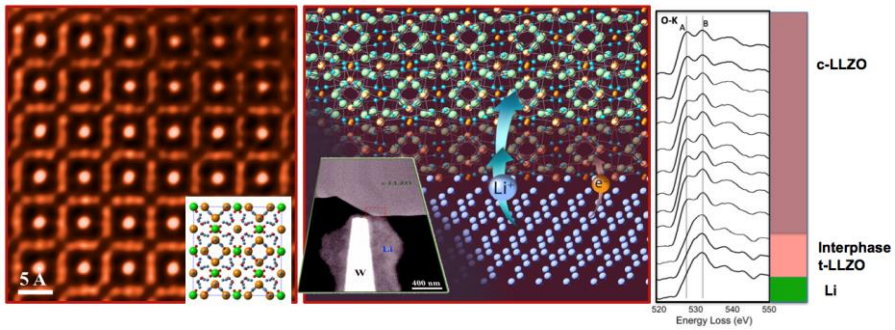

Figure 3 A rapid but self-limiting phase transformation was revealed upon the *in situ* juxtaposition of LLZO with lithium metal inside a STEM. The interphase layer is found to be confined to several unit cells, and is stable over time and upon biasing. Such interfaces promise desirable stability and conductivity for Li-metal batteries. This work highlights the importance of using interfaces and boundaries to explore high-performance metastable phases that may not be easily accessed through conventional bulk synthesis methods [C. Ma, et al., Nano Letters 16(11) 7030, 2016].

<u>Forming functional nano-architectures through self-assembly upon operation</u>. Creating nanoscale architecture in materials has been a widely adopted method to create properties exceeding those of bulk phases for the application of energy conversion and storage. A key challenge in this field is to construct functional nanoarchitectures that are not only compatible with their components, but also are stable upon electrochemical operations, as complex phase evolution and chemical reactions occur. The electrochemical instability in materials indeed is commonly observed during the initial charge/discharge process. In addition to designing materials with more stable structures, an under-researched approach is to take advantage of initial electrochemical cycling to intentionally generate structures that are stable for repeated cycling. Such structures in fact

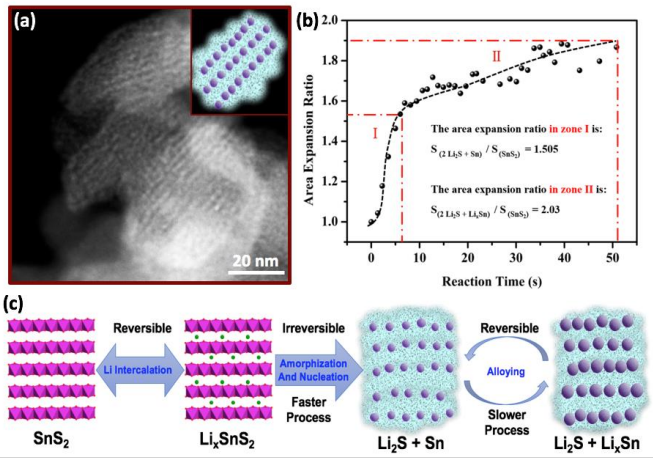

Figure 4 *In situ* TEM observation of the lithiation process of SnS_2 nanoplates reveals the formation of a self-assembled composite framework that consists of well-aligned Sn nanoparticles buried in amorphous lithium sulfide matrix(a); two reaction speeds were identified by tracking the area expansion of individual nanoplates (b); Reaction mechanism and morphology evolution during cycling are illustrated in (c) [K. Yin, et. al., Acc. Chem. Res. 50 (7) 1115 (2017)].

might be metastable and/or not easily created using conventional synthesis approaches. Here, we use SnS_2 nanomaterials as a model system to demonstrate this concept. By simultaneously probing the dynamic lithiation reactions and the correlated morphology evolutions using *in situ* TEM, we found that the lithiation of SnS_2 nanoplates leads to a self-assembled composite framework which is stable during succeeding electrochemical cycling (**Figure 4**). This nanoarchitecture not only provides a buffer to relax the large strain formation due to the volume expansion of the tin nanoparticles in subsequent charging and discharging processes, but also improves the connectivity of the Li_xSn nanoparticles, providing a desired electrical conductivity of the system. This work shows that utilizing initial reactions under operation conditions may serve as a facile route to create materials with nanoscale architectures that offer enhanced properties for energy storage and conversion.

Future Plans

As shown by these examples, there is still much to learn about how precise control of the synthesis refines the crystalline phase and lattice structure to promote facile ion conduction. We will continue to investigate sulfide and oxide solid electrolytes, particularly the meso-scale features which are being revealed for the first time. Studies of the interfaces formed of solid electrolytes contacting lithium and other reversible electrodes will fill a critical knowledge gap. Facile ion transport across such interfaces is critical to practical solid state devices. Future work will aim to integrate our neutron, electron microscopy and electrochemical capabilities to reveal the intrinsic interface stability, ion transport paths, and the role of reaction or barrier layers.

Publications

1. Zhang, M. H., Yin, K. B., Hood, Z. D., Bi, Z, Bridges, C. A., Dai, S., Meng, Y. S., Paranthaman, M. P., and Chi, M. F.,"In situ TEM observation of the electrochemical lithiation of N-doped anatase TiO_2 nanotubes as anodes for lithium-ion batteries," *J Mater Chem A* (2017) (accepted).
2. Nation, L., Li, J. , James, C., Qi, Y., Dudney, N., and Sheldon, B. W.,"In SItu Stress measurements furing electrochemical cycling of lithium-rich cathodes," *Journal of Power Sources* **364** 383 (2017).
3. Yin, K., Zhang, M., Hood, Z. D., Pan, J., Meng, Y. S., and Chi, M. F.,"Self-Assembled Framework Formed During Lithiation of SnS_2 Nanoplates Revealed by in Situ Electron Microscopy," *Accounts of Chemical Research* **50** 1513 (2017).
4. Sun, X. G., Wan, S., Guang, H. Y., Fang, Y. X., Reeves, K. S., Chi, M. F., and Dai, S.,"New promising lithium malonatoborate salts for high voltage lithium ion batteries," *J Mater Chem A* **5** 1233 (2017).
5. Chen, Y., Cheng, Y. Q., Li, J. C., Feygenson, M., Heller, W. T., Liang, C. D., and An, K.,"Lattice-Cell Orientation Disorder in Complex Spinel Oxides," *Adv Energy Mater* **7** (2017).
6. Sharafi, A., Yu, S. H., Naguib, M., Lee, M., Ma, C., Meyer, H. M., Nanda, J., Chi, M. F., Siegel, D. J., and Sakamoto, J.,"Impact of air exposure and surface chemistry on Li-$Li_7La_3Zr_2O_{12}$ interfacial resistance," *J Mater Chem A* **5** 13475 (2017).
7. Chen, Y., Yu, D. J., and An, K.,"Stress-induced charge-ordering process in $LiMn_2O_4$," *Mater Res Lett* **5** 89 (2017).

8. Wang, Z. Y., Santhanagopalan, D., Zhang, W., Wang, F., Xin, H. L. L., He, K., Li, J. C., Dudney, N., and Meng, Y. S.,"In Situ STEM-EELS Observation of Nanoscale Interfacial Phenomena in All-Solid-State Batteries," *Nano Lett* **16** 3760 (2016).
9. Ma, C., Cheng, Y. Q., Yin, K. B., Luo, J., Sharafi, A., Sakamoto, J., Li, J. C., More, K. L., Dudney, N. J., and Chi, M. F.,"Interfacial Stability of Li Metal-Solid Electrolyte Elucidated via in Situ Electron Microscopy," *Nano Lett* **16** 7030 (2016).
10. Wang, H., Hood, Z. D., Xia, Y. N., and Liang, C. D.,"Fabrication of ultrathin solid electrolyte membranes of beta-Li_3PS_4 nanoflakes by evaporation-induced self-assembly for all-solid-state batteries," *J Mater Chem A* **4** 8091 (2016).
11. Ma, C. and Chi, M. F.,"Novel Solid Electrolytes for Li-Ion Batteries: A Perspective from Electron Microscopy Studies," *Front Energy Res* **4** (2016).
12. Wang, H., Chen, Y., Hood, Z. D., Sahu, G., Pandian, A. S., Keum, J. K., An, K., and Liang, C.,"An Air-Stable Na_3SbS_4 Superionic Conductor Prepared by a Rapid and Economic Synthetic Procedure," *Angew Chem Int Edit* **55** 8551 (2016).
13. Ma, C., Cheng, Y. Q., Chen, K., Li, J. C., Sumpter, B. G., Nan, C. W., More, K. L., Dudney, N. J., and Chi, M. F.,"Mesoscopic Framework Enables Facile Ionic Transport in Solid Electrolytes for Li Batteries," *Adv Energy Mater* **6** (2016).
14. Liu, H. D., Chen, Y., Hy, S., An, K., Venkatachalam, S., Qian, D. N., Zhang, M. H., and Meng, Y. S.,"Operando Lithium Dynamics in the Li-Rich Layered Oxide Cathode Material via Neutron Diffraction," *Adv Energy Mater* **6** (2016).
15. Li, Y. C., Paranthaman, M. P., Gill, L. W., Hagaman, E. W., Wang, Y. Y., Sokolov, A. P., Dai, S., Ma, C., Chi, M. F., Veith, G. M., Manthiram, A., and Goodenough, J. B.,"Conduction below 100 degrees C in nominal $Li_6ZnNb_4O_{14}$," *J Mater Sci* **51** 854 (2016).
16. Hood, Z. D., Wang, H., Pandian, A. S., Keum, J. K., and Liang, C. D.,"Li_2OHCl Crystalline Electrolyte for Stable Metallic Lithium Anodes," *J Am Chem Soc* **138** 1768 (2016).
17. Wu, Y., Ma, C., Yang, J. H., Li, Z. C., Allard, L. F., Liang, C. D., and Chi, M. F.,"Probing the initiation of voltage decay in Li-rich layered cathode materials at the atomic scale," *J Mater Chem A* **3** 5385 (2015).
18. Wang, H., Ma, C., Chi, M. F., and Liang, C. D.,"High-Performance Lithium Solid-State Batteries Operating at Elevated Temperature," *Adv Mater Interfaces* **2** (2015).
19. Li, J. C., Zhang, Q. L., Xiao, X. C., Cheng, Y. T., Liang, C. D., and Dudney, N. J.,"Unravelling the Impact of Reaction Paths on Mechanical Degradation of Intercalation Cathodes for Lithium-Ion Batteries," *J Am Chem Soc* **137** 13732 (2015).
20. Hood, Z. D., Wang, H., Li, Y. C., Pandian, A. S., Paranthaman, M. P., and Liang, C. D.,"The "filler effect": A study of solid oxide fillers with beta-Li_3PS_4 for lithium conducting electrolytes," *Solid State Ionics* **283** 75 (2015).
21. Chen, Y., Rangasamy, E., dela Cruz, C. R., Liang, C. D., and An, K.,"A study of suppressed formation of low-conductivity phases in doped $Li_7La_3Zr_2O_{12}$ garnets by in situ neutron diffraction," *J Mater Chem A* **3** 22868 (2015).

Ion Transport and Structural Evolution of Solid Electrolytes
Understanding growth mechanisms of ionically conductive and metastable phases

Robert L. Sacci, Gabriel M. Veith, Miaofang Chi, Ke An, Chelsea Xi, Robert Schmidt, Nancy Dudney
Materials Science and Technology Division, Spallation Neutron Source, and the Center for Nanophase Materials Sciences, Oak Ridge National Laboratory, Oak Ridge, TN 37831

Program Scope

The goal of this project is a detailed, fundamental understanding of the role of synthesis and processing unique to inorganic solid electrolyte materials. For room temperature solid electrolytes, control of the material's phase, meso- and micro-structure, and lattice defects is critical to achieving liquid-like ionic transport through an electrochemically stable host. Solid electrolytes must function under the highly non-equilibrium conditions during operation; identifying novel and superior materials will open up new avenues to securing safe and sustainable electrochemical energy storage (EES) systems such as rechargeable batteries.

In reality, control of the synthesis and processing of solid electrolytes is not completed with the formation of the single-phase conductive membrane or film. The solid electrolyte is further modified during fabrication and operation of the electrochemical cell. When first contacted with highly reactive electrode materials, an interfacial reaction layer forms, often referred to as the solid electrolyte interphase (SEI), which can profoundly alter the ion and electron transfer across the interface. With extended electrochemical cycling, the structure of both the bulk and interface of the solid electrolyte continue to evolve in response to electrochemical and mechanical forces. Understanding the mechanisms leading to the structural evolution in relation to the original synthesis of the electrolyte phase is also elucidated in this program.

The bulk and interface properties of the solid electrolytes are determined by rigorous control synthesis conditions, but the properties may further evolve due to chemical and electrochemical reactions. Understanding these complex processes requires in situ characterization during synthesis, interface fabrication and electrochemical operation. The program encompasses new materials and compositions, as well as known model materials formed via vapor, solid, and liquid synthesis routes. This includes highly conductive oxides, phosphates, and thiophosphates.

Recent Progress

<u>Directing synthesis of novel Li-ion conductors at low temperatures</u>. Understanding reaction pathways and the role of dopants on the stability and ion conductivity of solid electrolytes is critical to predictively synthesizing functional materials. One such class of materials is the anti-perovskites, such as Li_3OBr, which are known to be good ionic conductors, however they are extremely sensitive toward moisture and are difficult to isolate. In this work, novel hydrate-promoted synthesis processes dramatically lower the synthesis temperature of $Li_3O(S)Br$ from 400 ^oC down to 200^oC. Furthermore, sulfur doping improves the purity and ease of synthesis of the perovskite. Interestingly, the S doping also helps to stabilize the materials towards long term exposure to humidity and elevated temperatures. The ionic conductivity of the sulfur doped

materials is similar to that of the undoped Li_3OBr (10^{-3} mS cm^{-1}) with the same energy of activation 0.59 eV. Li_3SBr was far more stable high temperature annealing (500°C for 24 hours, Figure 1) showing only 70% decrease in conductivity, while Li_3OBr loses 98% of conductivity after extended high temperature annealing. Li_3SBr is also stable for over 24 hours in air while Li_3OBr decomposes within seconds due to ambient moisture.

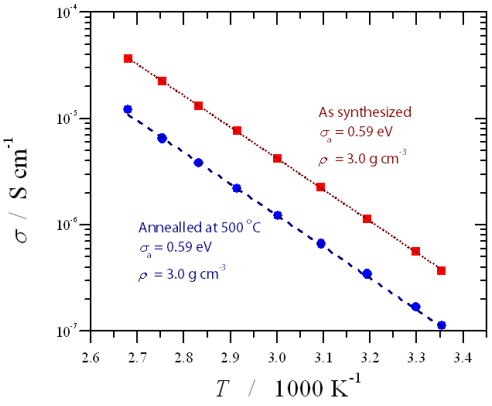

Figure 1 Ionic conductivity of Li3OBr before and after annealing

To explain understand the synthesis mechanism and structure property relationships extensive neutron diffraction and spectroscopy studies were performed along with scanning calorimetry, and optical spectroscopy. We found that direct synthesis from basic compounds (Li_2S or Li_2O and LiBr) occurred only at high temperatures (> 500°C, *in vacu*) and preferentially produced low conductive phases (~10^{-5} mS cm^{-1}). These phases come about due to the sluggish kinetics of the reaction. However, a low temperature route involving refluxing in organic solvents (80-100°C, 3-5hr) weakens the Li-oxide/ sulfide interaction and produces phase pure, highly conductive products. The effects of processing the material in the low temperature pathway (i.e. phonon-ion conduction interaction) are being studied using novel in situ electrochemical impedance neutron spectroscopy technique.

Understanding how reagents mediate reaction mechanism in the formation of ionically conducting garnets. At the common calcining temperatures used for solid state synthesis of $Li_7La_3Zr_2O_{12}$ garnet (LLZO), ~ 1373 K, the material is prone to lithium loss. This is typically compensated by the trial-and-error addition of 5-20% excess lithium precursor. Furthermore, the volatility of lithium creates a lithium concentration gradient in the powder or pellet during calcination often resulting in a mixed phase of both cubic and low ionic conductivity tetragonal phases of the LLZO. In this work, replacing Li_2CO_3 with a relatively stable lithium compound, such as $LiNO_3$, reduces the initial formation temperature of LLZO by 100 K

To understand the origin of this temperature reduction *in situ* neutron diffraction studies were performed and coupled with thermodynamic calculations. Figure 2 shows the refined species from the diffraction as a function of temperature during heating when using Li_2CO_3 (Fig. 2a) and $LiNO_3$ (Fig. 2b) precursors. The amorphous content in each case, shown as a dashed line, is computed as the non-observed fraction after normalizing. Lithium carbonate is the most stable compound in the Li_2CO_3-containing system, which is unsurprising given that its decomposition to Li_2O and CO_2 is slow at temperatures less than 973 K. At 573 K the $LiNO_3$ phase is no longer observed due to melting and onset of the reaction. One surprise from the in situ results was the appearance of the $La_2O_2(CO_3)$ phase in nitrate based synthesis, assumed to be carbon-free. The affinity of some lanthanum-containing compounds, such as LaOOH, La_2O_3 or $La(OH)_3$ to scavenge CO_2 or another carbon source has been noted in the literature. The source of carbon in this reaction was traced to adsorbed CO_2 on the ZrO_2. Detailed experimental (mass spec) analysis and thermodynamic calculations further addressed the CO_2 evolution and phase stability of the carbonate species. Characterization of the LLZO products shows that the nitrate

processing route results in less Li is loss, a higher phase purity and less residual carbon. This is important not only for an efficient synthesis, but also to optimize the Li ion transport and reduce the electronic conductivity.

Identifying the low temperature reaction mechanisms during the formation of metastable alloys. Insertion reactions in electrochemical systems often result in the formation of phases not predicted based on the thermodynamic phase diagrams. This is particularly prevalent during the alloying of Sn and Sb with Na or Li which result in amorphous compounds with clusters of metal and alkali atoms as estimated by NMR and Mössbauer spectroscopies. Understanding the structure and diffusion of these materials is important to the design of new materials and strategies to enable long term cycling stability.

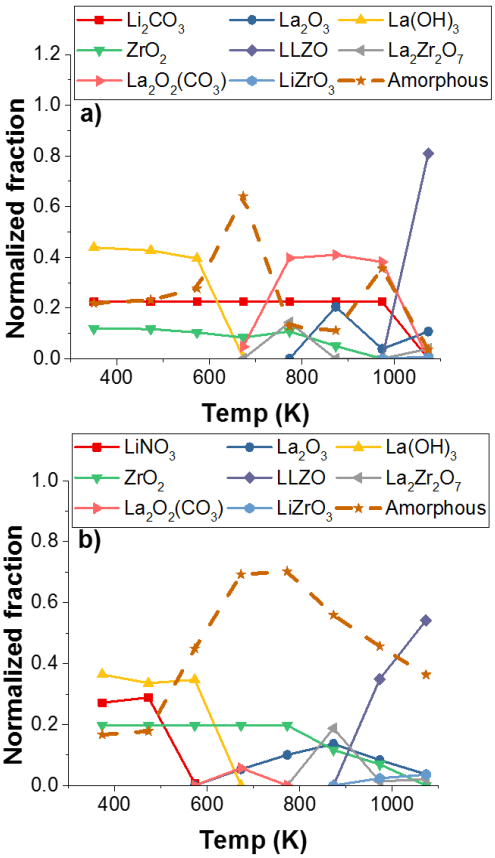

Figure 2. Normalized phase fractions of the crystalline phases from (a) lithium carbonate-containing precursors, and (b) lithium nitrate-containing precursors

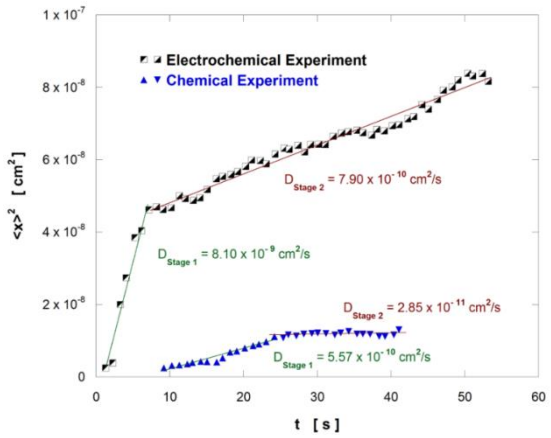

Figure 3. Plot of the sodiated area ($<x>^2$) versus time (t) from the in situ TEM data used to extract sodium diffusion coefficients (D) in SnSb during the chemical and electrochemical biasing experiment.

Thin films of SnSb alloys were vapor deposited on TEM grids for use during *in situ* sodiation reactions. Two types of room temperature sodiation reactions were performed: electro-chemical and solid state. A piece of Na metal was brought in close contact with the electrode and the oxide passivation layer was used as a solid electrolyte in the electrochemistry measurement. For the solid-state reaction the sodium was pushed into the SnSb film to allow direct contact between the two materials.

Upon contact an immediate reaction front was evident as the sodium diffused into the thin film. This reaction front resulted as the crystalline SnSb converted into an amorphous phase as evidenced in the electron diffraction data. After a period of time the reaction slowed considerably and coincided with the formation of crystalline Na_3Sb, Na_9Sn_4, and $Na_{15}Sn_4$. Interestingly thermodynamic modelling predicted the formation of the ternary compounds

Na_5SnSb_3 and Na_8SnSb_4 which were not detected in the diffraction data. Following the reaction front enabled a direct measurement of diffusion where several noticeable trends were identified. First the electrochemical diffusion was about 1 order of magnitude faster than the solid state diffusion. In the electrochemical reaction initially the rates were fast (~8 x 10^{-9} cm^2/sec) during transport in the amorphous phase. Upon crystallization the diffusion rate dropped by an order of magnitude (~8 x 10^{-10} cm^2/sec). Similar changes were measured during the solid state reaction. These studies demonstrate the challenges in understanding reaction mechanisms and likely indicate substantial intrinsic differences in defect density and order which will influence electrode performance.

Future Plans

This research provides a foundation to develop an understanding of how reagents assemble into materials suitable for electrochemical systems. This includes metastable phases which are produced at low temperatures at conditions far from equilibrium by processes such as electrochemical reactions and quenching from a gas phase. There is still much to learn from these materials with regards to how to control atomic rearrangements and how these local structures mediate diffusion of the ions. Future work will address these issues by integrating more advanced neutron and X-ray diffraction and spectroscopy measurements. These studies will be coupled with electron microscopy and theoretical modeling to provide an enabling capability to predict methods to synthesize and control defects within electrochemically functional materials.

Publications (last 2 years)

1. Zhang, M. H., Yin, K. B., Hood, Z. D., Bi, Z, Bridges, C. A., Dai, S., Meng, Y. S., Paranthaman, M. P., and Chi, M. F.,"In situ TEM observation of the electrochemical lithiation of N-doped anatase TiO_2 nanotubes as anodes for lithium-ion batteries," *J Mater Chem A* (2017) (accepted).
2. Nation, L., Li, J. , James, C., Qi, Y., Dudney, N., and Sheldon, B. W.,"In SItu Stress measurements furing electrochemical cycling of lithium-rich cathodes," *Journal of Power Sources* **364** 383 (2017).
3. Yin, K., Zhang, M., Hood, Z. D., Pan, J., Meng, Y. S., and Chi, M. F.,"Self-Assembled Framework Formed During Lithiation of SnS_2 Nanoplates Revealed by in Situ Electron Microscopy," *Accounts of Chemical Research* **50** 1513 (2017).
4. Sun, X. G., Wan, S., Guang, H. Y., Fang, Y. X., Reeves, K. S., Chi, M. F., and Dai, S.,"New promising lithium malonatoborate salts for high voltage lithium ion batteries," *J Mater Chem A* **5** 1233 (2017).
5. Chen, Y., Cheng, Y. Q., Li, J. C., Feygenson, M., Heller, W. T., Liang, C. D., and An, K.,"Lattice-Cell Orientation Disorder in Complex Spinel Oxides," *Adv Energy Mater* **7** (2017).
6. Sharafi, A., Yu, S. H., Naguib, M., Lee, M., Ma, C., Meyer, H. M., Nanda, J., Chi, M. F., Siegel, D. J., and Sakamoto, J.,"Impact of air exposure and surface chemistry on Li-$Li_7La_3Zr_2O_{12}$ interfacial resistance," *J Mater Chem A* **5** 13475 (2017).
7. Chen, Y., Yu, D. J., and An, K.,"Stress-induced charge-ordering process in $LiMn_2O_4$," *Mater Res Lett* **5** 89 (2017).

8. Wang, Z. Y., Santhanagopalan, D., Zhang, W., Wang, F., Xin, H. L. L., He, K., Li, J. C., Dudney, N., and Meng, Y. S.,"In Situ STEM-EELS Observation of Nanoscale Interfacial Phenomena in All-Solid-State Batteries," *Nano Lett* **16** 3760 (2016).
9. Ma, C., Cheng, Y. Q., Yin, K. B., Luo, J., Sharafi, A., Sakamoto, J., Li, J. C., More, K. L., Dudney, N. J., and Chi, M. F.,"Interfacial Stability of Li Metal-Solid Electrolyte Elucidated via in Situ Electron Microscopy," *Nano Lett* **16** 7030 (2016).
10. Wang, H., Hood, Z. D., Xia, Y. N., and Liang, C. D.,"Fabrication of ultrathin solid electrolyte membranes of beta-Li_3PS_4 nanoflakes by evaporation-induced self-assembly for all-solid-state batteries," *J Mater Chem A* **4** 8091 (2016).
11. Ma, C. and Chi, M. F.,"Novel Solid Electrolytes for Li-Ion Batteries: A Perspective from Electron Microscopy Studies," *Front Energy Res* **4** (2016).
12. Wang, H., Chen, Y., Hood, Z. D., Sahu, G., Pandian, A. S., Keum, J. K., An, K., and Liang, C.,"An Air-Stable Na_3SbS_4 Superionic Conductor Prepared by a Rapid and Economic Synthetic Procedure," *Angew Chem Int Edit* **55** 8551 (2016).
13. Ma, C., Cheng, Y. Q., Chen, K., Li, J. C., Sumpter, B. G., Nan, C. W., More, K. L., Dudney, N. J., and Chi, M. F.,"Mesoscopic Framework Enables Facile Ionic Transport in Solid Electrolytes for Li Batteries," *Adv Energy Mater* **6** (2016).
14. Liu, H. D., Chen, Y., Hy, S., An, K., Venkatachalam, S., Qian, D. N., Zhang, M. H., and Meng, Y. S.,"Operando Lithium Dynamics in the Li-Rich Layered Oxide Cathode Material via Neutron Diffraction," *Adv Energy Mater* **6** (2016).
15. Li, Y. C., Paranthaman, M. P., Gill, L. W., Hagaman, E. W., Wang, Y. Y., Sokolov, A. P., Dai, S., Ma, C., Chi, M. F., Veith, G. M., Manthiram, A., and Goodenough, J. B.,"Conduction below 100 degrees C in nominal $Li_6ZnNb_4O_{14}$," *J Mater Sci* **51** 854 (2016).
16. Hood, Z. D., Wang, H., Pandian, A. S., Keum, J. K., and Liang, C. D.,"Li_2OHCl Crystalline Electrolyte for Stable Metallic Lithium Anodes," *J Am Chem Soc* **138** 1768 (2016).
17. Wu, Y., Ma, C., Yang, J. H., Li, Z. C., Allard, L. F., Liang, C. D., and Chi, M. F.,"Probing the initiation of voltage decay in Li-rich layered cathode materials at the atomic scale," *J Mater Chem A* **3** 5385 (2015).
18. Wang, H., Ma, C., Chi, M. F., and Liang, C. D.,"High-Performance Lithium Solid-State Batteries Operating at Elevated Temperature," *Adv Mater Interfaces* **2** (2015).
19. Li, J. C., Zhang, Q. L., Xiao, X. C., Cheng, Y. T., Liang, C. D., and Dudney, N. J.,"Unravelling the Impact of Reaction Paths on Mechanical Degradation of Intercalation Cathodes for Lithium-Ion Batteries," *J Am Chem Soc* **137** 13732 (2015).
20. Hood, Z. D., Wang, H., Li, Y. C., Pandian, A. S., Paranthaman, M. P., and Liang, C. D.,"The "filler effect": A study of solid oxide fillers with beta-Li_3PS_4 for lithium conducting electrolytes," *Solid State Ionics* **283** 75 (2015).
21. Chen, Y., Rangasamy, E., dela Cruz, C. R., Liang, C. D., and An, K.,"A study of suppressed formation of low-conductivity phases in doped $Li_7La_3Zr_2O_{12}$ garnets by in situ neutron diffraction," *J Mater Chem A* **3** 22868 (2015).

Growth Mechanisms and Controlled Synthesis of Nanomaterials (ERKCS81): Understanding the Nonequilibrium Assembly of Functional Nanostructures and Thin Films from Metastable "Building Blocks"

David B. Geohegan,[1] Kai Xiao,[1] Alex Puretzky,[1] Gyula Eres,[2] Mina Yoon,[1]
Gerd Duscher,[2,3] Christopher M. Rouleau,[1]
Postdocs: M. Mahjouri-Samani,[1] M. Tian,[3] K.Wang,[1] X. Li[1], W. Tennyson[1],
[1]Center for Nanophase Materials Sciences and [2]Materials Science and Technology Division, Oak Ridge National Laboratory, Oak Ridge, TN 37831
[3]Dept. of Materials Science and Engineering, Univ. of Tennessee, Knoxville, 37996

Program Scope

The overarching goal of the research program is to understand the link between the growth mechanisms and the resulting structure and properties of nanoscale materials. The emphasis is on the development of real-time methods to induce and probe chemical and physical transformations away from thermodynamic equilibrium, in order to controllably synthesize nanomaterials with enhanced properties resulting from metastable structures. The approach relies on correlating the real-time diagnostic measurements with predictive theoretical methods and post-growth characterization by imaging, spectroscopy, and atomic-resolution analytical electron microscopy, to develop a framework for the controllable synthesis of nanomaterials with desired properties.

Specific aims of the program are: (1) To reveal the kinetic pathways by which "building blocks" are involved in the growth of nanostructures through the development of real-time measurement approaches and modeling. (2) To understand the special role of nonequilibrium growth environments in capturing metastable phases and structures with novel nanoscale properties through the development of new synthesis and processing approaches incorporating in situ diagnostics. (3) To understand the atomistic interactions governing the design and synthesis of nanostructures with specific configurations and functionalities through predictive theory and associated experiments. Key synthesis and processing science challenges are addressed for major nanomaterials classes that are important to DOE's energy mission, including two-dimensional materials, metal oxide photocatalysts, and carbon nanomaterials.

Recent Progress

Addressing the crosscutting challenges in the controllable synthesis of nanostructures and thin films requires identification of the reaction pathways, key precursors, and assembly kinetics on different time scales and different length scales. We use the nonequilibrium features of pulsed laser deposition to address this problem by tuning the ablation process to condense and selectively deliver fluxes of amorphous, ultrasmall nanoparticles (UNPs) that serve as "building blocks" in the assembly of nanostructures, thin films, and 2D crystals that occurs by the non-classical mechanisms of crystallization by particle attachment (CPA). The pulsed laser ablation plume was tuned to produce and selectively deliver nanoparticle fluxes using *in situ,* time-resolved intensified CCD-array imaging and plasma diagnostics in a regime we call "nanoparticle PLD". The nanoparticle PLD process and *in situ* diagnostics are described in Figure 1.[1]

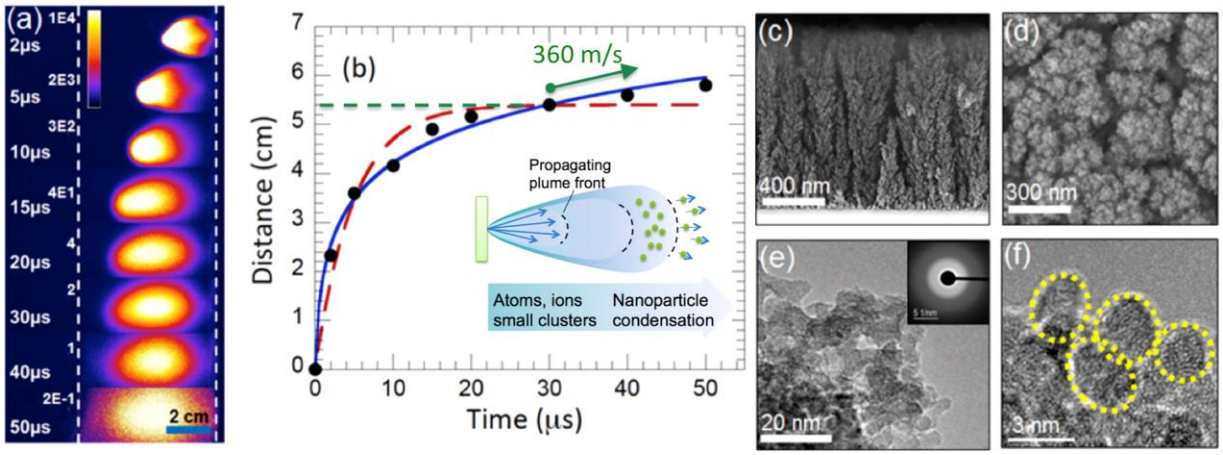

Figure 1. Nanoparticle PLD: Gas-Phase Synthesis and Deposition of Ultrasmall Amorphous Nanoparticles as "Building Blocks" for Crystallization by Particle Attachment Studies of Nanostructure Growth (a) Gated ICCD images of the ablation plume from a TiO_2 target into 200mTorr oxygen show that the substrate (dashed line) at d = 5 cm is just beyond the traditional plume range. In (b) the *R-t* plot for the leading edge of the plasma plume shows this range as defined by a linear drag model (red dashed curve). As shown in the inset, nanoparticles produced during the actual (quadratic drag fit, blue curve) plume expansion have significant velocity and separate from the plasma plume, depositing over time into hierarchical nanoparticle architectures at room temperature (c) side view, (d) top view SEM, (e), (f) TEM, or incorporate sequentially at high temperature into nanostructures and thin films. (Ref. 1)

We find that amorphous, ultrasmall nanoparticles crystallize according to the Ostwald-Lussac law of stages, through a series of transformations toward more stable crystal structures.[2,3] With TiO_2 as a model system, TiO_2 nanostructures grew with a variety of morphologies and crystal structures from anatase nanowires at 400°C, to TiO_2(B) nanosheets at 600°C, to thick anatase nanorods at 800°C. Molecular dynamics simulations revealed that amorphous nanoparticles crystallize within 2 ns at 600°C when contacting a base crystal, but do not sinter into the bulk crystal during this time. Estimates of sintering times range from nanoseconds at 1200°C, to microseconds at 800°C, to hundreds of seconds at 400°C. Figure 2 shows the crystallization and incorporation of the topmost nanoparticle layer of a nanorod deposited at 400°C.[1] Thus, amorphous UNPs can be deposited either: (1) sequentially by PLD at elevated temperatures to kinetically crystallize and sinter into nanostructures or films shot-by-shot, or (2) as aggregates to form mesoporous architectures, then post-annealed to form hierarchical 3D nanostructures with functional phases.

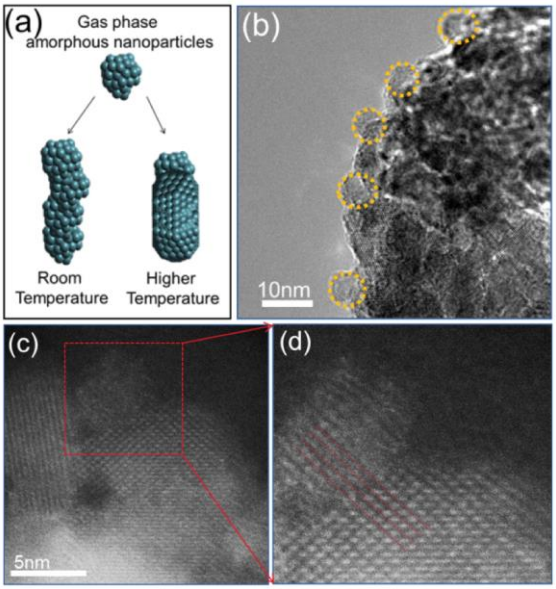

Figure 2. Crystallization by Particle Attachment of Gas-Phase Synthesized TiO_2 nanoparticles by PLD. (a) Schematic shows how amorphous nanoparticles deposit at RT, or crystallize and incorporate into nanostructures. (b) Anatase TiO_2 nanorod grown at 400°C with few ~3nm nanoparticles on surface. (c), (d) Atomic-resolution HAADF STEM images revealed how the nanoparticles have crystallized and are sintering and templating from the crystalline nanorod surface. (Ref. 1)

A particularly interesting phase is black titania, because of a dramatic enhancement of the photocatalytic performance by bandgap narrowing of TiO_2 attributed to self-doping by lattice distortions and defects. By simply annealing the stoichiometric, amorphous titania nanoparticle network films (deposited by PLD at RT as shown in Fig. 1(c,d)) in Ar gas at 700°C, we formed core-shell black titania particles with a perfect rutile core, and a very thin Ti_2O_3 shell. The co-evolution of size, phase, and crystal structure that results in these functional particle networks is a model system that illustrates the fascinating science of CPA from our PLD-synthesized, amorphous TiO_2 building blocks, which we recently unraveled as shown in Fig. 3. The combination of atomic-resolution, HAADF STEM microscopy, SAED, and EELS were used to follow the evolution of the amorphous, ultrasmall "building blocks" into different crystalline phases, including black anatase nanoparticles that form at temperatures as low as 400°C. This 'black anatase' phase is metastable, and begins to form as the first few a-UNPs sinter in Ar, resulting also in a shell of sub-stoichiometric phases such as amorphous Ti_2O_3, as identified by EELS. At higher temperatures, as shown in Fig. 3, we find that more rapid crystallization and phase evolution toward the thermodynamically stable rutile phase competes with the formation of the Ti_2O_3 shell which can hinder alignment and regulate the CPA process. By preventing agglomeration, the Ti_2O_3 shell helps maintain a high surface-to-volume ratio that is beneficial to photocatalytic processes. These results show that the amorphous nanoparticle network represents a highly tunable platform that can transform into a wide range of self-doped defective TiO_2 architectures simply by varying the annealing conditions.

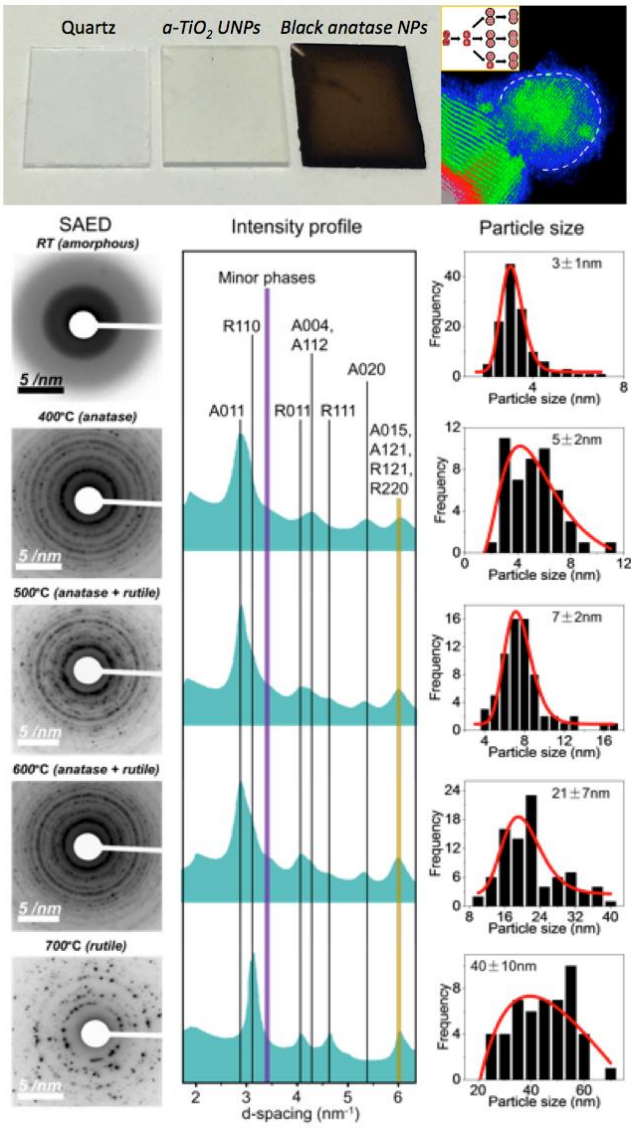

Figure 3. Black anatase to black rutile: evolution of particle size and phase by thermal annealing of a-UNPs of TiO_2 in Ar gas. Top panel shows the color of transparent quartz slides coated with 1μm-thick layer of amorphous TiO_2 nanoparticles by nanoparticle PLD at RT, and after annealing at 400°C in Ar to form black anatase core-shell nanoparticle networks. SAED, EELS, and size distributions show how different phases co-evolve under oxygen-deficient conditions to form a series of phases, culminating in black rutile at 700°C. The dynamics of crystallization and oxygen evolution during sintering can forms unique functional phases and hierarchical networks from the predeposited a-UNP "building blocks". (Ref. 5)

Nanoparticle PLD is a new synthesis and processing approach to deliver stoichiometric ultrasmall "building blocks" of materials for CPA. This is the processing regime we used for the first direct synthesis of 2D crystals by PLD, intentionally depositing GaSe UNPs.[4] These UNPs are stoichiometric and can be "digitally" deposited as feedstock for thermal post-processing, allowing us to grow large 2D single crystals with desired layer number in patterned locations.[5]

Future Plans

The formation of atomic order on the nanoscale is often the key factor determining the emerging properties of complex nanostructures. Crystallization and sintering of ultrasmall nanoparticles deposited cleanly by PLD from the gas phase provides an unprecedented opportunity to understand nanophase evolution through a combination of experiment, *in situ* electron microscopy and scattering techniques, and theory and modeling. We have the opportunity to controllably produce functional metastable phases with *in situ* diagnostic control, and stepwise control the structural evolution with pulsed processing. We must understand crystallization on the *individual* particle level, and co-crystallization and phase evolution during sintering of particle *ensembles.* The results of nanoparticle PLD indicate that nanoparticles can crystallize within nanoseconds, and sinter from ns to thousands of seconds.[1] To understand the faster of these timescales, we are employing rapid heating through rapid CO_2-laser heating of predeposited nanoparticles on susceptors, or UV-pulsed laser processing of the particles directly, in a custom designed *in situ* processing chamber which provides time-resolved optical spectroscopy (Raman, PL, absorption with 5-ns resolution). We will explore nanoparticle phase evolution using tunable ns, ps, and fs lasers through user projects at the CNMS. Coordinated experiments within a special TEM stage that permits laser introduction will observe the structural effects vs. pulse number. We will explore photolytic interactions to induce phase evolution within individual nanoparticles of both a single material (e.g. stoichiometric TiO_2) and nanoparticles containing known stoichiometries of mixed materials (e.g., TiO_2:VO_2). These computationally tractable materials systems will be also explored with recent advances in our global optimization search for stable phases.[6] We plan to simulate the EELS spectra for metastable phases to understand the evolution of unknown phases. We will understand the critical role that strain plays in nanostructure formation with predictive modeling. Neutron scattering is more sensitive to oxygen coordination number than X-ray scattering, so pair distribution functions of gram quantities of oxide nanoparticles will be measured at the SNS to understand how functional phases such as black oxides co-develop from thermal treatments of amorphous precursors. A novel nanoparticle PLD system employing 2 lasers will explore the synthesis of novel mixed phase nanoparticle-based coatings using multiple targets and photolytic processing to incorporate nanoparticle building blocks on a variety of practical substrates, with relevance to additive manufacturing of energy-relevant coatings.

References

1. M. Mahjouri-Samani, M.Tian, A. A. Puretzky, M. F. Chi, K. Wang, G. Duscher, C. M. Rouleau, G. Eres, M. Yoon, J. Lasseter, K. Xiao, and D. B. Geohegan, "Nonequilibrium Synthesis of TiO_2 Nanoparticle "Building Blocks" for Crystal Growth by Sequential Attachment in Pulsed Laser Deposition," *Nano Letters* **17**(8), 4624-4633 (2017).
2. M. Tian, M. Mahjouri-Samani, G. Eres, R. Sachan, M. Yoon, M. F Chisholm, K. Wang, A. A Puretzky, C. M Rouleau, D. B Geohegan, G. Duscher "Structure and Formation Mechanism of Black TiO_2 Nanoparticles", *ACS Nano* **9**(10) 10482 (2015).
3. M. Tian, M. Mahjouri-Samani, K. Wang, A. A. Puretzky, D. B. Geohegan, W. D. Tennyson, N. Cross, C. M. Rouleau, T. A. Zawodzinski, Jr., G. Duscher & G. Eres, "Black Anatase Formation by Annealing of Amorphous Nanoparticles and the Role of the Ti2O3 Shell in Self-Organized Crystallization by Particle Attachment", *ACS Appl. Mater. Interfaces* **9**, 22018 (2017).
4. M. Mahjouri- Samani, R. Gresback, M. Tian, K. Wang, A. A. Puretzky, C. M. Rouleau, G. Eres, I. N. Ivanov, K. Xiao and M. A. McGuire, "Pulsed Laser Deposition of Photoresponsive Two- Dimensional GaSe Nanosheet Networks" *Adv. Funct. Mat.* **24**, 6365 (2014).
5. M. Mahjouri-Samani, M. Tian, K. Wang, A. Boulesbaa, C. M. Rouleau, A.A. Puretzky, M. A. McGuire, B. R. Srijanto, K. Xiao, G. Eres, G. Duscher, and D. B. Geohegan "Digital Transfer Growth of Patterned 2D Metal Chalcogenides by Confined Nanoparticle Evaporation" *ACS Nano* **8**(11), 11567 (2014).
6. E. Inclan, D. Geohegan, and M. Yoon, "A hybrid optimization algorithm for exploring the atomic configurations of TiO_2 nanoparticles," *Comp. Mat. Sci.,(in press*) (2017).

DOE Sponsored Publications in the Last Two Years

1. M. Mahjouri-Samani, M. K. Tian, A. A. Puretzky, M. F. Chi, K. Wang, G. Duscher, C. M. Rouleau, G. Eres, M. Yoon, J. Lasseter, K. Xiao, and D. B. Geohegan, "Nonequilibrium Synthesis of TiO2 Nanoparticle "Building Blocks" for Crystal Growth by Sequential Attachment in Pulsed Laser Deposition," *Nano Letters* **17** (8), 4624-4633 (2017).

2. W. D. Tennyson, M. Tian, A. B. Papandrew, C. M. Rouleau, A. A. Puretzky, B. T. Sneed, K. L. More, G. M. Veith, G. Duscher, T. A. Zawodzinski, D. B. Geohegan, "Bottom up synthesis of boron-doped graphene for stable intermediate temperature fuel cell electrodes" *Carbon*, **123**, 605 (2017).

3. H. Yu, N. Gupta, Z. Hu, K. Wang, B. R. Srijanto, K. Xiao, D. B Geohegan, B. I Yakobson, "Tilt Grain Boundary Topology Induced by Substrate Topography" *ACS Nano*, **11**(9), 8612 (2017).

4. M. G. Stanford, P. R. Pudasaini, E. T. Gallmeier, L. Liang, N. Cross, A. Oyedele, G. Duscher, M. Mahjouri-Samani; K. Wang; K. Xiao; D. B. Geohegan; A. Belianinov, B. G. Sumpter, P. D. Rack, "High conduction hopping behavior induced in transition metal dichalcogenides by percolating defect networks: toward atomically thin circuits", *Adv.Funct. Mat.*, 27, 1702829 (2017).

5. A. B. Papandrew, R. A. Elgammal, M. Tian, W. D. Tennyson, C. M. Rouleau, A. A. Puretzky, G. M. Veith, D. B. Geohegan, and T. A. Zawodzinski, "Nanostructured carbon electrocatalyst supports for intermediate temperature fuel cells: Single-walled versus multi-walled structures," *J Power Sources* **337**, 145 (2017).

6. H-J. Qian, G. Eres & S. Irle Quantum chemical molecular dynamics simulation of carbon nanotube–graphene fusion, *Molecular Simulation* **43**, 1269 (2017).

7. L. Fan, C. B. Jacobs, C. M. Rouleau, and G. Eres, "Stabilizing Ir(001) Epitaxy on Yttria-Stabilized Zirconia Using a Thin Ir Seed Layer Grown by Pulsed Laser Deposition," *Cryst. Growth Des.* **17**, 89 (2017).

8. X. Li, A. A. Puretzky, X. Sang, K.C. Santosh, M. Tian, F. Ceballos, M. Mahjouri-Samani, K. Wang, R. R. Unocic, H. Zhao, G. Duscher, V. R. Cooper, C. M. Rouleau, D. B. Geohegan, K. Xiao, "Transition Metal Dichalcogenides: Suppression of Defects and Deep Levels Using Isoelectronic Tungsten Substitution in Monolayer $MoSe_2$", *Adv. Funct. Mater.* **27**, 1603850 (2017). (invited)(cover)

9. M. Tian, M. Mahjouri-Samani, K. Wang, A. A. Puretzky, D. B. Geohegan, W. D. Tennyson, N. Cross, C. M. Rouleau, T. A. Zawodzinski, Jr., G. Duscher & G. Eres, "Black Anatase Formation by Annealing of Amorphous Nanoparticles and the Role of the Ti2O3 Shell in Self-Organized Crystallization by Particle Attachment", *ACS Appl. Mater. Interfaces* **9**, 22018 (2017).

10. X. Li, J. Dong, J. C. Idrobo, A. A. Puretzky, C. M. Rouleau, D. B. Geohegan, F. Ding, and K. Xiao "Edge-Controlled Growth and Etching of Two-Dimensional GaSe Monolayers" *J. Am. Chem. Soc.* **139**(1), 482 (2017). (Highlight)

11. L. Fan, X. Gao, D. Lee, E.-J. Guo, S. Lee, P. C. Snijders,T. Z. Ward, G. Eres, M. F. Chisholm, and H. N. Lee, "Kinetically Controlled Fabrication of Single-Crystalline TiO_2 Nanobrush Architectures with High Energy {001} Facets" *Adv. Sci.* 1700045 (2017).

12. L. Fan, C. B. Jacobs, C. M. Rouleau, and G. Eres, "Stabilizing Ir(001) Epitaxy on Yttria-Stabilized Zirconia Using a Thin Ir Seed Layer Grown by Pulsed Laser Deposition", *Cryst.*

Growth Des. **17**, 89−94 (2017).

13. Z. Wang, Z. Zhong, S. McKeown Walker, Z. Ristic, J.-Z. Ma, F. Y. Bruno, S. Riccò, G. Sangiovanni, Gyula Eres, N. C. Plumb, L. Patthey, M. Shi, J. Mesot, F. Baumberger and M. Radovic, "Atomically precise lateral modulation of a two-dimensional electron liquid in anatase TiO_2 thin films", *Nano Lett.* **17**, 2561 (2017).

14. C. B. Jacobs, K. Wang , A. V. Ievlev, L. Collins, E. S. Muckley, I. N. Ivanov, "Functional two/three-dimensional assembly of monolayer WS_2 and nickel oxide," *J. of Photonics for Energy* **7(1)**, 014001 (2017).

15. X. Li, M.-W. Lin, L. Basile, S. M. Hus, A. A. Puretzky, J. Lee, Y.-C. Kuo, L.-Y. Chang, K. Wang, J. C. Idrobo, A.-P. Li, C.-H. Chen, C. M. Rouleau, D. B. Geohegan, K. Xiao, "Isoelectronic tungsten doping in monolayer $MoSe_2$ for carrier type modulation", *Adv. Mater.* **28**, 8240 (2016).

16. Z.-J. Wang, J. Dong, Y. Cui, G. Eres, O. Timpe, Q. Fu, F. Ding, R. Schloegl & M.-G. Willinger, "Stacking sequence and interlayer coupling in few-layer graphene revealed by in situ imaging", *Nat. Comm.* **7**, 13256 (2016).

17. A. Boulesbaa, V E Babicheva, K. Wang, I. I Kravchenko, M.-W. Lin, M. Mahjouri-Samani, C. B Jacobs, A. A Puretzky, K.Xiao, I.Ivanov, C. M Rouleau, D. B Geohegan, "Ultrafast Dynamics of Metal Plasmons Induced by 2D Semiconductor Excitons in Hybrid Nanostructure Arrays", *ACS Photonics*, **3**(12) 2389 (2016).

18. A. Boulesbaa, K. Wang, M. Mahjouri-Samani, M. Tian, A. A. Puretzky, I. Ivanov, C. M. Rouleau, K. Xiao, B. G. Sumpter, and D. B. Geohegan, "Ultrafast Charge Transfer and Hybrid Exciton Formation in 2D/0D Heterostructures", *J. Am. Chem. Soc.* **138**(44) 14713 (2016).

19. K. Wang, B. Huang, M. Tian, F. Ceballos, M. W. Lin, M. Mahjouri-Samani, A. Boulesbaa, A. A. Puretzky, C. M. Rouleau, M. Yoon, H. Zhao, K. Xiao, G. Duscher, and D. B. Geohegan, "Interlayer Coupling in Twisted WSe2/WS2 Bilayer Heterostructures Revealed by Optical Spectroscopy," *ACS Nano* **10**(7), 6612-6622 (2016).

20. M. Mahjouri-Samani, L. B. Liang, A. Oyedele, Y. S. Kim, M. K. Tian, N. Cross, K. Wang, M. W. Lin, A. Boulesbaa, C. M. Rouleau, A. A. Puretzky, K. Xiao, M. Yoon, G. Eres, G. Duscher, B. G. Sumpter, and D. B. Geohegan, "Tailoring Vacancies Far Beyond Intrinsic Levels Changes the Carrier Type and Optical Response in Monolayer MoSe2-x Crystals," *Nano Lett.* **16** (8), 5213-5220 (2016).

21. X. Li, M-W. Lin, L. Basile, S. M. Hus, A. A. Puretzky, J. Lee, Y-C. Kuo, L.-Y. Chang, K. Wang, J. C. Idrobo, A.-P. Li, C.-H. Chen, C. M. Rouleau, D. B. Geohegan, K. Xiao, "Isoelectronic tungsten doping in monolayer $MoSe_2$ for carrier type modulation" *Adv Mater.*, **28**, 8240 (2016).

22. B. Yang, M. Mahjouri-Samani, C. M. Rouleau, D. B. Geohegan, K. Xiao, "Pulsed Laser Deposition of Hierarchical TiO_2 for High Performance Perovskite Solar Cells", *Phys. Chem. Chem. Phys.*, **18**, 27067 (2016). (Invited)

23. X. Li, M.-W. Lin, A. A. Puretzky, L. Basilea, K. Wang, J. C. Idrobo, C. M. Rouleau, D. B. Geohegan, K. Xiao, "Persistent photoconductivity in two-dimensional Mo1−xWxSe2–MoSe2 van der Waals heterojunctions", J. Mater. Res. 31, 923 (2016). (Invited)

24. X. Li, M.-W. Lin, J. Lin, B. Huang, A. A. Puretzky, C. Ma, K. Wang, W. Zhou, S. T. Pantelides, C. Miao, I. Kravchenko, J. Fowlkes, C. M. Rouleau, D. B. Geohegan, K. Xiao, "Two-dimensional GaSe/MoSe2 misfit bilayer heterojunctions by van der Waals epitaxy", *Science*

Advances, **2**, E1501882 (2016).

25. K. Share, R. E. Carter, P. Nikolaev, D. Hooper, L. Oakes, A. P. Cohn, R. Rao, A. A. Puretzky, D. B. Geohegan, B. Maruyama, and C. L. Pint, "Nanoscale Silicon as a Catalyst for Graphene Growth: Mechanistic Insight from in Situ Raman Spectroscopy", *J. Phys. Chem. C* **120**, 14180-14186 (2016).

26. A. A. Puretzky, L. Liang, X. Li, K. Xiao, B. G. Sumpter, V. Meunier, and D. B. Geohegan "Twisted $MoSe_2$ Bilayers with Variable Local Stacking and Interlayer Coupling Revealed by Low-Frequency Raman Spectroscopy", *ACS Nano* **10**, 2736 (2016).

27. A. M. Jubb, Y. Jiao, G. Eres, S. T. Retterer, and B. Gu, "Elevated gold ellipse nanoantenna dimers as sensitive and tunable surface enhanced Raman spectroscopy substrates", *Nanoscale*, **8**, 5641 (2016).

28. Z. Yan, L. Chen, M. Yoon, and S. Kumar, "Phonon Transport at the Interfaces of Vertically Stacked Graphene and Hexagonal Boron Nitride Heterostructures", *Nanoscale* **8**, 4037 (2016).

29. M. Tian, M. Mahjouri-Samani, G. Eres, R. Sachan, M. Yoon, M. F Chisholm, K. Wang, A. A Puretzky, C. M Rouleau, D. B Geohegan, G. Duscher "Structure and Formation Mechanism of Black TiO_2 Nanoparticles", *ACS Nano* **9**(10) 10482 (2015).

Growth Mechanisms and Controlled Synthesis of Nanomaterials (ERKCS81): Toward Synthetic Control over Heterogeneity and Functionality in Two-Dimensional Materials

Kai Xiao,[1] David B. Geohegan,[1] Alex Puretzky,[1] Gyula Eres,[2] Mina Yoon,[1] Gerd Duscher,[2,3] Christopher M. Rouleau,[1] Postdocs: M. Mahjouri-Samani,[1] M. Tian,[3] K. Wang,[1] X. Li[1], W. Tennyson[1], [1]Center for Nanophase Materials Sciences and [2]Materials Science and Technology Division, Oak Ridge National Laboratory, Oak Ridge, TN 37831 [3]Dept. of Materials Science and Engineering, Univ. of Tennessee, Knoxville, 37996

Program Scope

The overarching goal of the research program is to understand the link between the growth mechanisms and the resulting structure and properties of nanoscale materials. The emphasis is on the development of real-time methods to induce and probe chemical and physical transformations away from thermodynamic equilibrium, in order to controllably synthesize nanomaterials with enhanced properties resulting from metastable structures. The approach relies on correlating real-time diagnostic measurements with predictive theoretical methods and post-growth characterization by imaging, spectroscopy, and atomic-resolution analytical electron microscopy, to develop a framework for the controllable synthesis of nanomaterials with desired properties.

Specific aims of the program are: (1) To reveal the kinetic pathways by which "building blocks" are involved in the growth of nanostructures through the development of real-time measurement approaches and modeling. (2) To understand the special role of nonequilibrium growth environments in capturing metastable phases and structures with novel nanoscale properties through the development of new synthesis and processing approaches incorporating in situ diagnostics. (3) To understand the atomistic interactions governing the design and synthesis of nanostructures with specific configurations and functionalities through predictive theory and associated experiments. Key synthesis and processing science challenges are addressed for major nanomaterials classes that are important to DOE's energy mission, including two-dimensional materials, metal oxide photocatalysts, and carbon nanomaterials.

Recent Progress

Many classes of two-dimensional (2D) materials have emerged as potential platforms for novel electronic and optical devices, notably the semiconducting 2D transition metal dichalcogenides (TMDs) and their heterostructures. However, several synthesis and processing challenges remain, including scalable synthesis of uniform layers of crystalline 2D materials. Currently, crystals of 2D materials display remarkable heterogeneity, including localized atomistic heterogeneity including vacancies, dopants, and edge terminations, as well as mesoscopic heterogeneity involving misoriented grains, layer orientations, and interactions with substrates and adsorbates. This heterogeneity can strongly influence the

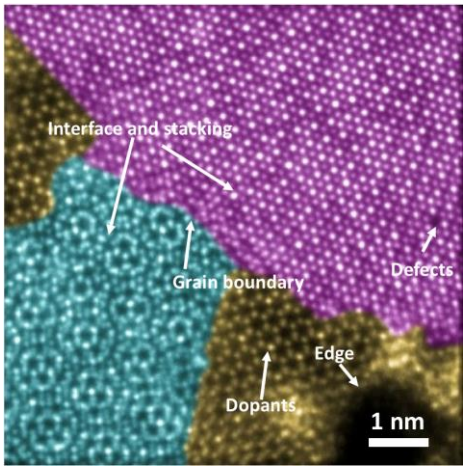

Figure 1 Atomic resolution ADF-STEM image of bilayer W-doped $MoSe_2$ shows the various heterogeneities in 2D materials. (unpublished).

structure and electronic properties in 2D materials, offering at the same time a serious challenge to synthesis control for reliable properties and a tremendous opportunity to tailor functionality. Therefore, fundamental understanding and control of heterogeneity during synthesis and processing is critical to tailor the properties of 2D materials.

Recently we have developed both chemical vapor deposition (CVD) and laser-based synthesis and processing approaches to explore how to exert control over heterogeneity during synthesis including defects, dopants, strain, edges and layers (many of which are represented in Fig. 1) for a variety of 2D crystals. In each case we have characterized the crystals via their optoelectronic properties which we are developing as *in situ* diagnostics to remotely and spectroscopically monitor, understand, and eventually control the growth and heterogeneity of the 2D materials. Briefly, below we review some of the key findings on the interrelationship between controlled synthesis, heterogeneity, and resulting properties.

Isoelectronic doping of 2D TMD crystals:
Isoelectronic substitutional *doping* to form random alloys was shown to be a very promising synthetic strategy to not only modulate carrier type but to suppress defects to enhance photoluminescence. While doping is one of the essential technologies needed in various applications of 2D materials, stable and highly-efficient doping techniques still remain a challenge.

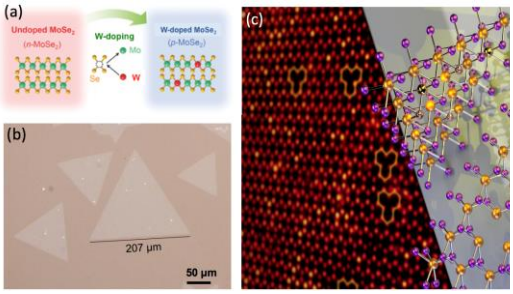

Figure 2 (a) A schematic image of isoelectronic W doping in $MoSe_2$. (b) Optical image of monolayer W doped $MoSe_2$ crystals on a SiO_2 substrate grown by CVD. (c) Atomic resolution ADF-STEM image and atomic model of W-doped $MoSe_2$ to show the suppression of Se vacancies with W doping. X. Li, et al., *Adv. Funct. Mater.* **27**, 1603850 (2017).

In recent work, we demonstrated that isoelectronic doping of 2D crystals of $MoSe_2$ with tunable doping levels of tungsten (from WO_3) produced ideal random alloys of monolayer 2D $Mo_{1-x}W_xSe_2$ by vapor transport growth. We found that isoelectronic doping was not only capable of modulating the carrier type, but also of suppressing defects and dramatically enhancing the photoluminescence and quality of the samples. W-doping suppressed the Se vacancies in monolayer $Mo_{1-x}W_xSe_2$ by 50% compared to those found in pristine CVD $MoSe_2$ (Fig. 2). Isoelectronic doping by CVD therefore provides a controllable and efficient synthetic way to both dope 2D crystals and suppress defects.

Edge-controlled etching and growth of 2D GaSe monolayers:
Etching and growth are complementary processes and usually compete during 2D crystal growth. Recently, by controllably adjusting the balance between deposition and etching during the vapor-phase deposition growth process, we revealed the edge-controlled etching and growth mechanisms of 2D GaSe monolayer crystals, which are not predicted by classical nucleation and growth models. By adjusting the flux of vapor during growth, switching between growth and etching, the shapes of monolayer GaSe crystals grown on TEM grids were recorded to reveal the fastest growing crystal edges (as identified by atomic resolution electron microscopy). As-grown GaSe monolayers generally show triangular shapes and have zigzag edges. However, etching changes the morphology from hexagons or truncated triangles to triangles with their orientation rotated by 60° relative to the parent flakes (Fig. 3). A theoretical model at

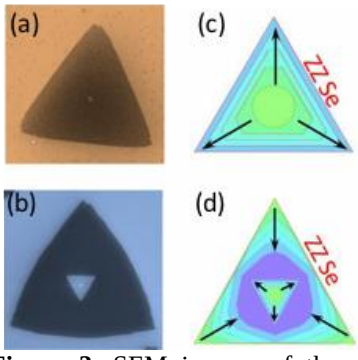

Figure 3. SEM images of the as-grown (a) and etched (b) monolayer GaSe crystals on substrates and simulated growth (c) and etching process (d) by KWC and DFT calculations. X. Li, et al., *J. Am. Chem. Soc.* **139**, 482 (2017).

the atomic level was developed based on Kinetic Wulff Construction theory and density functional theory (DFT) to explain the observed growth morphologies, revealing that zigzag Se edges are the fastest growing edges that determine the GaSe crystal morphologies. Therefore, the growth-etching-regrowth process can not only be used to study the growth mechanism of 2D binary crystals, but also is a promising way to synthesize large, shape-controllable, high-quality single-crystalline 2D crystals and their lateral heterostructures by precisely tuning chemical potentials.

Van der Waals epitaxial growth of 2D misfit heterostructures: The bottom-up, vdW heteroepitaxial growth of 2D crystals is the hope to achieve wafer-scale synthesis of stacked heterostructures with reproducible, energetically-preferred interlayer orientations. However, vdW epitaxy occurs without obvious lattice matching. Recently, we utilized a two-step CVD process to grow 2D GaSe/$MoSe_2$ heterostructures with atomically sharp interfaces and well-defined stacking by vdW epitaxy, despite large lattice mismatch. The deposition rate of GaSe molecules compared to the diffusion rate on the substrate was found to play an important role in controlling whether lateral or vertical heterostructures form. Despite the large lattice difference and disparate periodicities, atomic resolution STEM imaging revealed Moiré patterns that showed highly reproducible alignment of the two lattices. Theoretical simulations of the energetics based on DFT calculations explained that vdW interactions are sufficiently strong to reliably guide vertically stacked GaSe/$MoSe_2$ heterostructures into incommensurate superlattices. Such vertically-stacked vdW GaSe/$MoSe_2$ heterostructures were shown to form p−n junctions with effective transport and separation of photo-generated charge carriers between layers, resulting in a gate-tunable photovoltaic response.

Non-equilibrium laser-based synthesis of nonideal 2D crystals with vacancy levels far beyond intrinsic values: Developing synthesis methods to engineer defects in 2D crystals is a critical step toward understanding how heterogeneity can be harnessed to control the optical and electronic properties of next-generation electronics. Recently we have demonstrated a novel non-equilibrium, laser-based synthesis and processing approach to grow single crystalline, monolayer 2D crystals of $MoSe_{2-x}$ with Se-vacancy concentrations up to 20% – far beyond intrinsic values (as shown in Figure 4). These Se vacancies can be repaired reliably by a follow-on treatment supplying Se by pulsed laser evaporation from a selenium target. With increasing vacancy concenteration, the $MoSe_{2-x}$ crystals changed from n-type to p-type carrier behavior and a new defect-activated phonon band (observed by Raman spectroscopy) emerged, serving as an optical fingerprint of the vacancy concentration in the crystals. First-principles calculations explained the new Raman mode and revealed that the selenium vacancies serve to trap electrons, reducing the Fermi energy to facilitate the production of holes to explain corresponding vacancy-induced electrical and optical transitions.

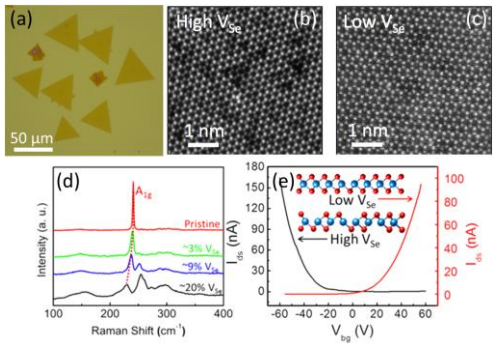

Figure 4. (a) Optical image of highly Se-deficient $MoSe_2$ crystals which can still retain their crystallinity. Atomically resolved Z-contrast STEM images show $MoSe_2$ crystals synthesized with (b) high (~20%) and (c) low (<1%) Se-vacancy concentrations. (d) Evolution of Raman spectra as a function of Se vacancy concentration. (e) Electrical transport properties transition with Se vacancy concentration increasing. M. Mahjouri-Samani, *Nano Lett.*, **16**, 5213 (2016).

In summary, synthesis and processing approaches were explored to understand the evolution of the dominant types of heterogeneity (doping, vacancies, edges, and layers) during synthesis in 2D materials, and their resulting effects on optoelectronic properties. Controllably introducing isoelectronic (metal) dopants or inducing (chalcogen) vacancies from the "bottom-up" were capable of introducing desirable

electronic properties changes in the 2D crystals in what appeared to be highly defective single crystals. With the appropriate deposition flux, van der Waals interactions were found to strongly and reliably guide the growth of 2D crystal heteroepitaxy despite large lattice mismatch. Balancing growth and etching revealed the sensitivity of crystal shape and edge termination to chemical potential. In each case, the optoelectronic signature of the crystals could be correlated to the atomistic heterogeneity revealed by STEM imaging, and will be pursued as *in situ* diagnostics in the next phase of the research.

Future Plans

The spectroscopic optical signatures of heterogeneity we established above (e.g., PL, Raman, reflectivity) offers the opportunity for *in situ* monitoring and control over heterogeneity during growth, doping, etching, and repair of 2D crystals. This will be pursued on two levels: First, at the macroscale through the further development of pulsed laser deposition for 2D materials where we can not only continuously vary the precursor "building blocks" of growth from atomic/molecular flux to laser-generated ultrasmall nanoparticles, with digital control over flux and kinetic energy to probe different reaction pathways, but also monitor and control heterogeneity during synthesis. Second, we will exert rapid variations in temperature, gas environment, and supply of dopant/chalcogen fluxes at the microscale in a high-vacuum optical microscopy chamber with multiple laser access ports capable of providing not only spectroscopic monitoring but of probing the formation of metastable phases via PLD from small targets.

The stability and reconstruction of crystal edges will be studied spectroscopically in the optical microscopy chamber during growth/etching, but also using a hot stage via *in situ* STEM imaging as shown in Figure 5a where preliminary experiments are revealing mechanisms of grain boundary reconstruction and elimination under thermal annealing. These mechanisms are under theoretical investigation, and offer new possibilities for synthesis and processing strategies to recrystallize 2D materials to eliminate grain boundaries at the microscale and mesoscale. Utilizing the new optical microscopy chamber we will pursue local thermal processing from laser heating and photolytic interactions with the 2D crystals to explore control over layer number, crystallinity, size, and adsorbates through explorations of laser thinning, recrystallization, etching, cleaning. To understand the incorporation and interplay of strain during growth of atomically-thin crystals, laser-induced strain, and growth on curved surfaces that exert strain engineering beyond substrate lattice mismatch, will be studied in association with theory (Fig. 5 b, c). Laser synthesis of 2D materials utilizing conversion of predeposited precursor compounds or nanoparticle "building blocks" on substrates will also be explored. High power, ultrafast laser-2D interactions are predicted to offer processing possibilities such as layer-by-layer exfoliation, layer melting, and interlayer bonding which can be pursued within the same microscopy-based processing chamber. Laser introduction within the TEM at UTK is already underway to explore the atomistic evolution of such non-equilibrium deposition of energy in 2D materials, and the processing opportunities they offer.

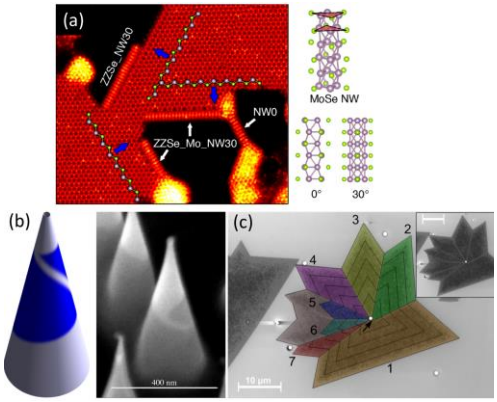

Figure 5. (a) In-situ heating and etching of 2D crystals with edge reconstructions in STEM. Atomic resolution HAADF-STEM image and atomic structure models of the reconstructed MoSe NW formed on the edges.(unpublished) (b) SEM image of monolayer WS_2 crystal grown on conical surface with a theoretical simulated morphology, (c) The single crystal grain splitting during the growth due to the cone-induced strain. H. Yu, et al., *ACS Nano*, **11**(9), 8612 (2017).

DoE Sponsored Publications in the Last Two Years

1. M. Mahjouri-Samani, M. K. Tian, A. A. Puretzky, M. F. Chi, K. Wang, G. Duscher, C. M. Rouleau, G. Eres, M. Yoon, J. Lasseter, K. Xiao, and D. B. Geohegan, "Nonequilibrium Synthesis of TiO2 Nanoparticle "Building Blocks" for Crystal Growth by Sequential Attachment in Pulsed Laser Deposition," *Nano Letters* **17** (8), 4624-4633 (2017).

2. W. D. Tennyson, M. Tian, A. B. Papandrew, C. M. Rouleau, A. A. Puretzky, B. T. Sneed, K. L. More, G. M. Veith, G. Duscher, T. A. Zawodzinski, D. B. Geohegan, "Bottom up synthesis of boron-doped graphene for stable intermediate temperature fuel cell electrodes" *Carbon*, **123**, 605 (2017).

3. H. Yu, N. Gupta, Z. Hu, K. Wang, B. R. Srijanto, K. Xiao, D. B Geohegan, B. I Yakobson, "Tilt Grain Boundary Topology Induced by Substrate Topography" *ACS Nano*, **11**(9), 8612 (2017).

4. M. G. Stanford, P. R. Pudasaini, E. T. Gallmeier, L. Liang, N. Cross, A. Oyedele, G. Duscher, M. Mahjouri-Samani; K. Wang; K. Xiao; D. B. Geohegan; A. Belianinov, B. G. Sumpter, P. D. Rack, "High conduction hopping behavior induced in transition metal dichalcogenides by percolating defect networks: toward atomically thin circuits", *Adv.Funct. Mat.*, 27, 1702829 (2017).

5. A. B. Papandrew, R. A. Elgammal, M. Tian, W. D. Tennyson, C. M. Rouleau, A. A. Puretzky, G. M. Veith, D. B. Geohegan, and T. A. Zawodzinski, "Nanostructured carbon electrocatalyst supports for intermediate temperature fuel cells: Single-walled versus multi-walled structures," *J Power Sources* **337**, 145 (2017).

6. H-J. Qian, G. Eres & S. Irle Quantum chemical molecular dynamics simulation of carbon nanotube–graphene fusion, *Molecular Simulation* **43**, 1269 (2017).

7. L. Fan, C. B. Jacobs, C. M. Rouleau, and G. Eres, "Stabilizing Ir(001) Epitaxy on Yttria-Stabilized Zirconia Using a Thin Ir Seed Layer Grown by Pulsed Laser Deposition," *Cryst. Growth Des.* **17**, 89 (2017).

8. X. Li, A. A. Puretzky, X. Sang, K.C. Santosh, M. Tian, F. Ceballos, M. Mahjouri-Samani, K. Wang, R. R. Unocic, H. Zhao, G. Duscher, V. R. Cooper, C. M. Rouleau, D. B. Geohegan, K. Xiao, "Transition Metal Dichalcogenides: Suppression of Defects and Deep Levels Using Isoelectronic Tungsten Substitution in Monolayer $MoSe_2$", *Adv. Funct. Mater.* **27**, 1603850 (2017). (invited)(cover)

9. M. Tian, M. Mahjouri-Samani, K. Wang, A. A. Puretzky, D. B. Geohegan, W. D. Tennyson, N. Cross, C. M. Rouleau, T. A. Zawodzinski, Jr., G. Duscher & G. Eres, "Black Anatase Formation by Annealing of Amorphous Nanoparticles and the Role of the Ti2O3 Shell in Self-Organized Crystallization by Particle Attachment", *ACS Appl. Mater. Interfaces* **9**, 22018 (2017).

10. X. Li, J. Dong, J. C. Idrobo, A. A. Puretzky, C. M. Rouleau, D. B. Geohegan, F. Ding, and K. Xiao "Edge-Controlled Growth and Etching of Two-Dimensional GaSe Monolayers" *J. Am. Chem. Soc.* **139**(1), 482 (2017). (Highlight)

11. L. Fan, X. Gao, D. Lee, E.-J. Guo, S. Lee, P. C. Snijders,T. Z. Ward, G. Eres, M. F. Chisholm, and H. N. Lee, "Kinetically Controlled Fabrication of Single-Crystalline TiO_2 Nanobrush Architectures with High Energy {001} Facets" *Adv. Sci.* 1700045 (2017).

12. L. Fan, C. B. Jacobs, C. M. Rouleau, and G. Eres, "Stabilizing Ir(001) Epitaxy on Yttria-

Stabilized Zirconia Using a Thin Ir Seed Layer Grown by Pulsed Laser Deposition", *Cryst. Growth Des.* **17**, 89−94 (2017).

13. Z. Wang, Z. Zhong, S. McKeown Walker, Z. Ristic, J.-Z. Ma, F. Y. Bruno, S. Riccò, G. Sangiovanni, Gyula Eres, N. C. Plumb, L. Patthey, M. Shi, J. Mesot, F. Baumberger and M. Radovic, "Atomically precise lateral modulation of a two-dimensional electron liquid in anatase TiO_2 thin films", *Nano Lett.* **17**, 2561 (2017).

14. C. B. Jacobs, K. Wang , A. V. Ievlev, L. Collins, E. S. Muckley, I. N. Ivanov, "Functional two/three-dimensional assembly of monolayer WS_2 and nickel oxide," *J. of Photonics for Energy* **7(1)**, 014001 (2017).

15. X. Li, M.-W. Lin, L. Basile, S. M. Hus, A. A. Puretzky, J. Lee, Y.-C. Kuo, L.-Y. Chang, K. Wang, J. C. Idrobo, A.-P. Li, C.-H. Chen, C. M. Rouleau, D. B. Geohegan, K. Xiao, "Isoelectronic tungsten doping in monolayer $MoSe_2$ for carrier type modulation", *Adv. Mater.* **28**, 8240 (2016).

16. Z.-J. Wang, J. Dong, Y. Cui, G. Eres, O. Timpe, Q. Fu, F. Ding, R. Schloegl & M.-G. Willinger, "Stacking sequence and interlayer coupling in few-layer graphene revealed by in situ imaging", *Nat. Comm.* **7**, 13256 (2016).

17. A. Boulesbaa, V E Babicheva, K. Wang, I. I Kravchenko, M.-W. Lin, M. Mahjouri-Samani, C. B Jacobs, A. A Puretzky, K.Xiao, I.Ivanov, C. M Rouleau, D. B Geohegan, "Ultrafast Dynamics of Metal Plasmons Induced by 2D Semiconductor Excitons in Hybrid Nanostructure Arrays", *ACS Photonics,* **3**(12) 2389 (2016).

18. A. Boulesbaa, K. Wang, M. Mahjouri-Samani, M. Tian, A. A. Puretzky, I. Ivanov, C. M. Rouleau, K. Xiao, B. G. Sumpter, and D. B. Geohegan, "Ultrafast Charge Transfer and Hybrid Exciton Formation in 2D/0D Heterostructures", *J. Am. Chem. Soc.* **138**(44) 14713 (2016).

19. K. Wang, B. Huang, M. Tian, F. Ceballos, M. W. Lin, M. Mahjouri-Samani, A. Boulesbaa, A. A. Puretzky, C. M. Rouleau, M. Yoon, H. Zhao, K. Xiao, G. Duscher, and D. B. Geohegan, "Interlayer Coupling in Twisted WSe2/WS2 Bilayer Heterostructures Revealed by Optical Spectroscopy," *ACS Nano* **10**(7), 6612-6622 (2016).

20. M. Mahjouri-Samani, L. B. Liang, A. Oyedele, Y. S. Kim, M. K. Tian, N. Cross, K. Wang, M. W. Lin, A. Boulesbaa, C. M. Rouleau, A. A. Puretzky, K. Xiao, M. Yoon, G. Eres, G. Duscher, B. G. Sumpter, and D. B. Geohegan, "Tailoring Vacancies Far Beyond Intrinsic Levels Changes the Carrier Type and Optical Response in Monolayer MoSe2-x Crystals," *Nano Lett.* **16** (8), 5213-5220 (2016).

21. X. Li, M-W. Lin, L. Basile, S. M. Hus, A. A. Puretzky, J. Lee, Y-C. Kuo, L.-Y. Chang, K. Wang, J. C. Idrobo, A.-P. Li, C.-H. Chen, C. M. Rouleau, D. B. Geohegan, K. Xiao, "Isoelectronic tungsten doping in monolayer $MoSe_2$ for carrier type modulation" *Adv Mater.*, **28**, 8240 (2016).

22. B. Yang, M. Mahjouri-Samani, C. M. Rouleau, D. B. Geohegan, K. Xiao, "Pulsed Laser Deposition of Hierarchical TiO_2 for High Performance Perovskite Solar Cells", *Phys. Chem. Chem. Phys.*, **18**, 27067 (2016). (Invited)

23. X. Li, M.-W. Lin, A. A. Puretzky, L. Basilea, K. Wang, J. C. Idrobo, C. M. Rouleau, D. B. Geohegan, K. Xiao, "Persistent photoconductivity in two-dimensional Mo1−xWxSe2–MoSe2 van der Waals heterojunctions", J. Mater. Res. 31, 923 (2016). (Invited)

24. X. Li, M.-W. Lin, J. Lin, B. Huang, A. A. Puretzky, C. Ma, K. Wang, W. Zhou, S. T. Pantelides, C. Miao, I. Kravchenko, J. Fowlkes, C. M. Rouleau, D. B. Geohegan, K. Xiao, "Two-

dimensional GaSe/MoSe2 misfit bilayer heterojunctions by van der Waals epitaxy", *Science Advances*, **2**, E1501882 (2016).

25. K. Share, R. E. Carter, P. Nikolaev, D. Hooper, L. Oakes, A. P. Cohn, R. Rao, A. A. Puretzky, D. B. Geohegan, B. Maruyama, and C. L. Pint, "Nanoscale Silicon as a Catalyst for Graphene Growth: Mechanistic Insight from in Situ Raman Spectroscopy", *J. Phys. Chem. C* **120**, 14180-14186 (2016).

26. A. A. Puretzky, L. Liang, X. Li, K. Xiao, B. G. Sumpter, V. Meunier, and D. B. Geohegan "Twisted $MoSe_2$ Bilayers with Variable Local Stacking and Interlayer Coupling Revealed by Low-Frequency Raman Spectroscopy", *ACS Nano* **10**, 2736 (2016).

27. A. M. Jubb, Y. Jiao, G. Eres, S. T. Retterer, and B. Gu, "Elevated gold ellipse nanoantenna dimers as sensitive and tunable surface enhanced Raman spectroscopy substrates", *Nanoscale*, **8**, 5641 (2016).

28. Z. Yan, L. Chen, M. Yoon, and S. Kumar, "Phonon Transport at the Interfaces of Vertically Stacked Graphene and Hexagonal Boron Nitride Heterostructures", *Nanoscale* **8**, 4037 (2016).

29. M. Tian, M. Mahjouri-Samani, G. Eres, R. Sachan, M. Yoon, M. F Chisholm, K. Wang, A. A Puretzky, C. M Rouleau, D. B Geohegan, G. Duscher "Structure and Formation Mechanism of Black TiO_2 Nanoparticles", *ACS Nano* **9**(10) 10482 (2015).

Growth Mechanisms and Controlled Synthesis of Nanomaterials (ERKCS81): Atomistic Modeling Coupled with In Situ Diagnostics of the Formation and Transformation of Oxide Nanostructures and 2D Materials

Mina Yoon,[1] David B. Geohegan,[1] Kai Xiao,[1] Alex Puretzky,[1] Gyula Eres,[2] Gerd Duscher,[2,3] Christopher M. Rouleau,[1]
Postdocs: M. Mahjouri-Samani,[1] M. Tian,[3] K. Wang,[1] X. Li[1], W. Tennyson[1],
[1]Center for Nanophase Materials Sciences and [2]Materials Science and Technology Division, Oak Ridge National Laboratory, Oak Ridge, TN 37831
[3]Dept. of Materials Science and Engineering, Univ. of Tennessee, Knoxville, 37996

Program Scope

The overarching goal of the research program is to understand the link between the growth mechanisms and the resulting structure and properties of nanoscale materials. The emphasis is on the development of real-time methods to induce and probe chemical and physical transformations away from thermodynamic equilibrium, in order to controllably synthesize nanomaterials with enhanced properties resulting from metastable structures. The approach relies on correlating the real-time diagnostic measurements with predictive theoretical methods and post-growth characterization by imaging, spectroscopy, and atomic-resolution analytical electron microscopy, to develop a framework for the controllable synthesis of nanomaterials with desired properties.

Specific aims of the program are: (1) To reveal the kinetic pathways by which "building blocks" are involved in the growth of nanostructures through the development of real-time measurement approaches and modeling. (2) To understand the special role of nonequilibrium growth environments in capturing metastable phases and structures with novel nanoscale properties through the development of new synthesis and processing approaches incorporating in situ diagnostics. (3) To understand the atomistic interactions governing the design and synthesis of nanostructures with specific configurations and functionalities through predictive theory and associated experiments. Key synthesis and processing science challenges are addressed for major nanomaterials classes that are important to DOE's energy mission, including two-dimensional materials, metal oxide photocatalysts, and carbon nanomaterials.

Recent Progress

In this work we use theory to link synthesis with characterization to understand the formation and transformation of atomic order and the resulting electronic structure on different length scales. We use titanium oxide [1-3] as a model system for the class of oxides that are built up of MO_6 octahedral units in stable bulk phases, where the 6 Ti-O bond lengths determine the size and the shape of the octahedral crystal field that governs the Ti *d*-orbital splitting and the resulting electronic structure. The density of octahedral units as well as the distortion of individual octahedra in metastable and stable titanium oxide phases also influences the electronic structure. As the TiO_2 nanopartcle size decreases, structures with low octahedral densities and the distortion of octahedral units become more pronounced. The distortions of the octahedra are characterized by atomic resolution imaging and diffraction, with the corresponding electronic structure determined by EELS. A similar six-fold metal coordination is also present in 2D materials [4,5] of the type MX_2, where M=IVB or VIB metal, and X=S or Se. The presence of the additional electrons changes the crystal field splitting

from octahedral for group IVB metals to trigonal prismatic coordination for VIB metals substantially increasing the structural variety and the range of properties.

A global search algorithm for determining TiO_2 cluster structure and energetic stability

We developed a global structure search algorithm to efficiently explore the configuration space of macromolecular cluster structures that were observed experimentally to form before nucleation of crystalline nanoparticles. Our global structure search algorithm [6] comprised of differential evolution, coupled with the Broyden–Fletcher–Goldfarb–Shanno quasi-Newton optimization algorithm, is used for the purpose of determining the energy stability of the clusters described by Buckingham interatomic potential. The energy stability of the macromolecular structures increases with the number (n) of TiO_2 units as shown in Fig. 1. The first TiO_6 octahedral unit forms for n>15, and the first few TiO_6 are highly distorted and their formation is not necessarily limited to minimum energy pathways. Our *in situ* nanoparticle PLD data imply that agglomeration of these macromolecular clusters leads to formation of 3-5 nm size nanoparticles that remain amorphous at room temperature deposition. [1-3] Although, the NPs appear amorphous by selective area electron (SAED) diffraction, nanobeam electron beam diffraction (NBED) reveals that they possess medium range order corresponding to a large fraction of polyhedrally coordinated Ti atoms.

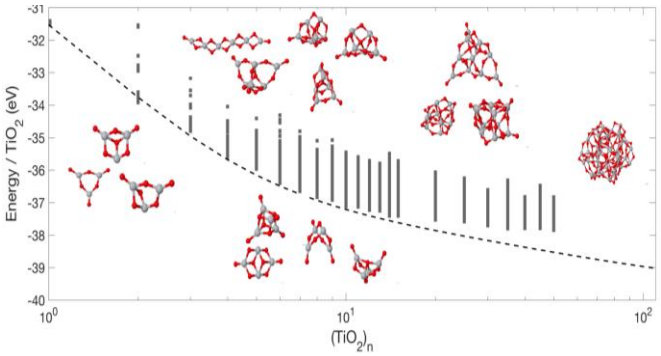

Figure 1. The hybrid algorithm shows that the energy stability of $(TiO_2)_n$ macromolecular clusters increases (dashed line) with size (n). The dashed line is based on interpolation extended to the energy of bulk rutile and the vertical data points for a given n are the energies of meta/stable configurations found by our algorithm [6].

Understanding the spatial and temporal evolution of TiO_2 nanostructure formation by nanoparticle PLD: in situ diagnostics and atomistic simulations

To gain insight into the lengthscales and timescales involved in nanoparticle PLD (for details see ERKCS81 by D. Geohegan *et al.*) we performed molecular dynamics (MD) simulations of a 3-nm amorphous nanoparticle landing on a TiO_2(B) nanocrystal surface (consisting of 19200 atoms) at various temperatures (see Fig. 2 for the snapshots from simulations at T=600°C). We model the growth of crystalline TiO_2 nanostructures of different morphology and phase by the attachment and crystallization of ultrasmall, amorphous TiO_2 nanoparticle "building blocks" formed in the gas phase and deposited by PLD [1]. The MD simulations reveal that the nanoparticle attaches within *t~10 ps*, with some interdiffusion of its atoms into the topmost layer of the TiO_2(B) crystal. The

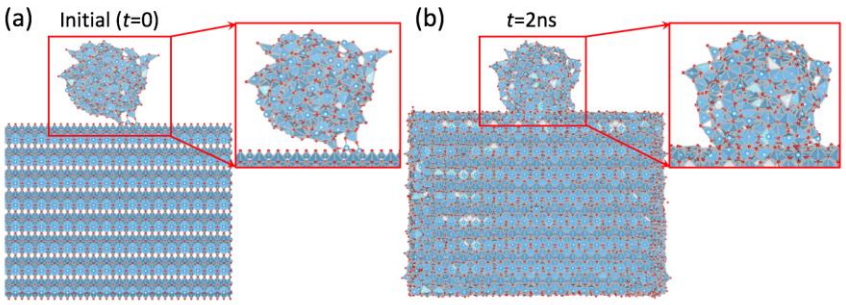

Figure 2. Molecular dynamics simulation of amorphous ultrasmall TiO_2 nanoparticle (NP) attachment and crystallization. (a) A 3-nm-diameter TiO_2 NP arrives to a ~10 nm TiO_2(B) nanocrystal surface, the initial configuration. (b) Snapshot of the attachment and crystallization of the NP after 2 ns at 600 °C [1].

nanoparticle then undergoes crystallization such that within *t*~2 ns as shown in Fig. 1, more than 50% of the atoms have formed TiO_6 octahedra. The evolution of the number of TiO_6 octahedral units and their relative orientation in the nanoparticle is used as a measure of crystallization and tracked as a function of time. We found that the orientational alignment of the octahedra in the nanoparticle strongly correlate with the alignment of the octahedra in the underlying crystal, indicating that the nanoparticle appears to crystallize and template its phase and alignment with that of the underlying crystal within several nanoseconds, even at such relatively low temperatures.

Strain-induced growth of cubic TiO_2 and extension to 2D materials

We observed that electron beam irradiation induces a partial structural transformation of rutile to the TiO_2 cubic phase that occurs in the surface area damaged by the electron beam shown in Fig. 3. To understand the atomistic mechanism driving this transformation, we performed first-principles density functional theory (DFT) calculations. We employed the climb nudged elastic band method to identify transition state pathways starting from the stable rutile phase to much less stable cubic phase. The relatively high energy barrier for the rutile-to-cubic transformation process (>2eV) becomes significantly reduced with increasing strain is applied, with the cubic phase becoming favored above 6% compressive strain. We propose this as a viable mechanism for driving the observed structural transformation near the surface where atoms can freely rearrange. The underlying coupling between substrate and the overlayer is also a mechanism that drives the growth of 2D materials illustrated in Fig. 4.

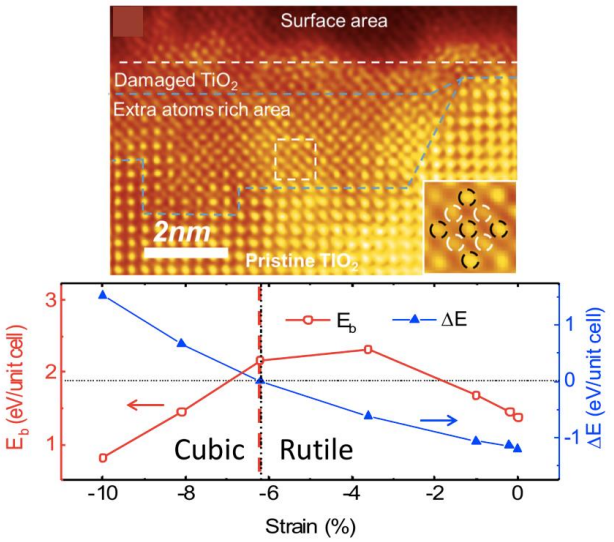

Figure 3. Electron beam induced structural transformation of a black rutile NP surface to a cubic phase (inset) imaged by high angle annular dark field (HAADF). The relative structural stabilities (ΔE: energy difference between cubic and rutile; E_b: energy barrier for transformation) of the cubic and the rutile phase under external strain, where the cubic phase becomes more stable than rutile under 6% compressive strain.

Future Plans

We plan to significantly extend the capability of the current force-field-based global structure search algorithm by coupling it to first-principles calculations for a more accurate description of structural and electronic properties. Our goal is to establish a computational tool that produces results that can be directly compared with experimental data, XRD and SAED for

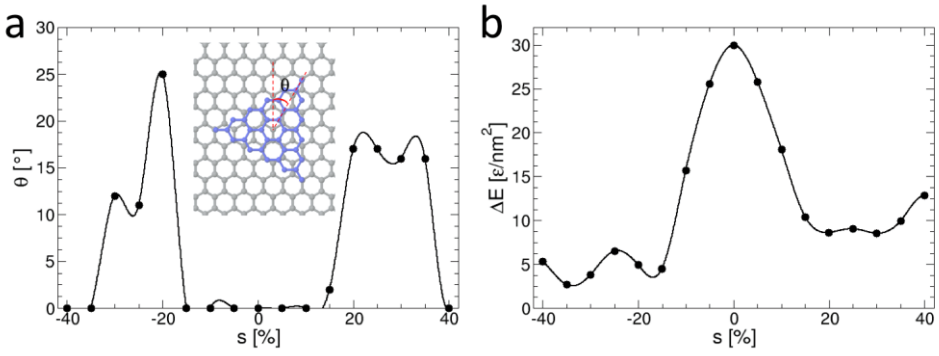

Figure 4. Modeling the epitaxial growth of 2D nanoflakes on substrates. Preferred orientation (θ) (a) and rotational barrier (b) of the nanoflake depending on the substrate induced strain (s).

structural properties and EELS for electronic properties. Our first-principles calculations will be performed by an all-electron first-principles code (FHI-aims), that we highly optimized on the ORNL supercomputer (Titan) with GPU acceleration. By utilizing it we will be able to handle a large-scale sampling of nanoparticles and to perform statistical analysis of calculational big data. We will establish an experiment-theory combined scheme that incorporates the new theoretical capability and *in situ* characterization, which will be applied to understand the non-classical crystal growth mechanisms of NPs and 2D. In the first step that we refer to as chemistry before crystallization we will model the structure of macromolecular clusters that form in the first step of a two-step nucleation process. The collision of these clusters leads to assembly into larger structures and their rearrangement leads to the nucleation of a crystalline phase, which occurs inside such macromolecular clusters. Our experimental results obtained by in situ measurements suggest that this picture initially developed for biomolecular crystallization in solution, is also applicable for inorganic crystal growth such as oxides, and 2D materials on substrates and in vacuum. Our results for the formation of black anatase nanoparticles by crystallization of the core in a disordered shell are a good example for such mechanisms. We also observe that such reorganization and rearrangements occurs on a wide range of length scales in the crystallization of metastable and stable phases by a process known as crystallization by particle attachment (CPA).

We will perform pair distribution function (pdf) measurements by neutron and x-ray scattering and electron diffraction, and by focusing on the formation of MO_6 coordinated units follow the evolution of order in successive states starting from amorphous to crystalline states. We will utilize the theoretical methods that already demonstrated macromolecular cluster formation to determine the macromolecular cluster structures that are the best fit with the measured pdfs. The characteristic features in the pdfs of these clusters will be independently confirmed by atomic resolution TEM, NBEM, EELS for individual particles. In addition we will use theory to interpret and predict the outcome of in situ measurements of structure evolution of model systems, such as annealing in environmental TEM, or neutron and x-ray scattering during annealing of amorphous powders produced by nanoparticle PLD. These general methods for understanding synthesis science will be adjusted to address the unique features of different classes of materials focusing on representative prototype systems for oxides and 2D materials. The addition of dopants, the presence of strain and structural and composition inhomogeneities all influence the basic coordination environment that can be tracked by using theory to perform structural interpretation of the pdf data.

References

1. M. Mahjouri-Samani, M.Tian, A. A. Puretzky, M. F. Chi, K. Wang, G. Duscher, C. M. Rouleau, G. Eres, M. Yoon, J. Lasseter, K. Xiao, and D. B. Geohegan, "Nonequilibrium Synthesis of TiO_2 Nanoparticle "Building Blocks" for Crystal Growth by Sequential Attachment in Pulsed Laser Deposition," *Nano Letters* **17**(8), 4624-4633 (2017).
2. M. Tian, M. Mahjouri-Samani, G. Eres, R. Sachan, M. Yoon, M. F Chisholm, K. Wang, A. A Puretzky, C. M Rouleau, D. B Geohegan, G. Duscher "Structure and Formation Mechanism of Black TiO_2 Nanoparticles", *ACS Nano* **9**(10) 10482 (2015).
3. M. Tian, M. Mahjouri-Samani, K. Wang, A. A. Puretzky, D. B. Geohegan, W. D. Tennyson, N. Cross, C. M. Rouleau, T. A. Zawodzinski, Jr., G. Duscher & G. Eres, "Black Anatase Formation by Annealing of Amorphous Nanoparticles and the Role of the Ti2O3 Shell in Self-Organized Crystallization by Particle Attachment", *ACS Appl. Mater. Interfaces* **9**, 22018 (2017).
4. M. Mahjouri- Samani, R. Gresback, M. Tian, K. Wang, A. A. Puretzky, C. M. Rouleau, G. Eres, I. N. Ivanov, K. Xiao and M. A. McGuire, "Pulsed Laser Deposition of Photoresponsive Two- Dimensional GaSe Nanosheet Networks" *Adv. Funct. Mat.* **24**, 6365 (2014).
5. M. Mahjouri-Samani, M. Tian, K. Wang, A. Boulesbaa, C. M. Rouleau, A.A. Puretzky, M. A. McGuire, B. R. Srijanto, K. Xiao, G. Eres, G. Duscher, and D. B. Geohegan "Digital Transfer Growth of Patterned 2D Metal Chalcogenides by Confined Nanoparticle Evaporation" *ACS Nano* **8**(11), 11567 (2014).
6. E. Inclan, D. Geohegan, and M. Yoon, "A hybrid optimization algorithm for exploring the atomic configurations of TiO_2 nanoparticles," *Comp. Mat. Sci.,(in press*) (2017).

DOE Sponsored Publications in the Last Two Years

1. M. Mahjouri-Samani, M. K. Tian, A. A. Puretzky, M. F. Chi, K. Wang, G. Duscher, C. M. Rouleau, G. Eres, M. Yoon, J. Lasseter, K. Xiao, and D. B. Geohegan, "Nonequilibrium Synthesis of TiO2 Nanoparticle "Building Blocks" for Crystal Growth by Sequential Attachment in Pulsed Laser Deposition," *Nano Letters* **17** (8), 4624-4633 (2017).

2. W. D. Tennyson, M. Tian, A. B. Papandrew, C. M. Rouleau, A. A. Puretzky, B. T. Sneed, K. L. More, G. M. Veith, G. Duscher, T. A. Zawodzinski, D. B. Geohegan, "Bottom up synthesis of boron-doped graphene for stable intermediate temperature fuel cell electrodes" *Carbon*, **123**, 605 (2017).

3. H. Yu, N. Gupta, Z. Hu, K. Wang, B. R. Srijanto, K. Xiao, D. B Geohegan, B. I Yakobson, "Tilt Grain Boundary Topology Induced by Substrate Topography" *ACS Nano*, **11**(9), 8612 (2017).

4. M. G. Stanford, P. R. Pudasaini, E. T. Gallmeier, L. Liang, N. Cross, A. Oyedele, G. Duscher, M. Mahjouri-Samani; K. Wang; K. Xiao; D. B. Geohegan; A. Belianinov, B. G. Sumpter, P. D. Rack, "High conduction hopping behavior induced in transition metal dichalcogenides by percolating defect networks: toward atomically thin circuits", *Adv.Funct. Mat.*, 27, 1702829 (2017).

5. A. B. Papandrew, R. A. Elgammal, M. Tian, W. D. Tennyson, C. M. Rouleau, A. A. Puretzky, G. M. Veith, D. B. Geohegan, and T. A. Zawodzinski, "Nanostructured carbon electrocatalyst supports for intermediate temperature fuel cells: Single-walled versus multi-walled structures," *J Power Sources* **337**, 145 (2017).

6. H-J. Qian, G. Eres & S. Irle Quantum chemical molecular dynamics simulation of carbon nanotube–graphene fusion, *Molecular Simulation* **43**, 1269 (2017).

7. L. Fan, C. B. Jacobs, C. M. Rouleau, and G. Eres, "Stabilizing Ir(001) Epitaxy on Yttria-Stabilized Zirconia Using a Thin Ir Seed Layer Grown by Pulsed Laser Deposition," *Cryst. Growth Des.* **17**, 89 (2017).

8. X. Li, A. A. Puretzky, X. Sang, K.C. Santosh, M. Tian, F. Ceballos, M. Mahjouri-Samani, K. Wang, R. R. Unocic, H. Zhao, G. Duscher, V. R. Cooper, C. M. Rouleau, D. B. Geohegan, K. Xiao, "Transition Metal Dichalcogenides: Suppression of Defects and Deep Levels Using Isoelectronic Tungsten Substitution in Monolayer $MoSe_2$", *Adv. Funct. Mater.* **27**, 1603850 (2017). (invited)(cover)

9. M. Tian, M. Mahjouri-Samani, K. Wang, A. A. Puretzky, D. B. Geohegan, W. D. Tennyson, N. Cross, C. M. Rouleau, T. A. Zawodzinski, Jr., G. Duscher & G. Eres, "Black Anatase Formation by Annealing of Amorphous Nanoparticles and the Role of the Ti2O3 Shell in Self-Organized Crystallization by Particle Attachment", *ACS Appl. Mater. Interfaces* **9**, 22018 (2017).

10. X. Li, J. Dong, J. C. Idrobo, A. A. Puretzky, C. M. Rouleau, D. B. Geohegan, F. Ding, and K. Xiao "Edge-Controlled Growth and Etching of Two-Dimensional GaSe Monolayers" *J. Am. Chem. Soc.* **139**(1), 482 (2017). (Highlight)

11. L. Fan, X. Gao, D. Lee, E.-J. Guo, S. Lee, P. C. Snijders,T. Z. Ward, G. Eres, M. F. Chisholm, and H. N. Lee, "Kinetically Controlled Fabrication of Single-Crystalline TiO_2 Nanobrush Architectures with High Energy {001} Facets" *Adv. Sci.* 1700045 (2017).

12. Z. Wang, Z. Zhong, S. McKeown Walker, Z. Ristic, J.-Z. Ma, F. Y. Bruno, S. Riccò, G.

Sangiovanni, Gyula Eres, N. C. Plumb, L. Patthey, M. Shi, J. Mesot, F. Baumberger and M. Radovic, “Atomically precise lateral modulation of a two-dimensional electron liquid in anatase TiO_2 thin films”, *Nano Lett.* **17**, 2561 (2017).

13. C. B. Jacobs, K. Wang , A. V. Ievlev, L. Collins, E. S. Muckley, I. N. Ivanov, "Functional two/three-dimensional assembly of monolayer WS_2 and nickel oxide," *J. of Photonics for Energy* **7(1)**, 014001 (2017).

14. X. Li, M.-W. Lin, L. Basile, S. M. Hus, A. A. Puretzky, J. Lee, Y.-C. Kuo, L.-Y. Chang, K. Wang, J. C. Idrobo, A.-P. Li, C.-H. Chen, C. M. Rouleau, D. B. Geohegan, K. Xiao, “Isoelectronic tungsten doping in monolayer $MoSe_2$ for carrier type modulation”, *Adv. Mater.* **28**, 8240 (2016).

15. Z.-J. Wang, J. Dong, Y. Cui, G. Eres, O. Timpe, Q. Fu, F. Ding, R. Schloegl & M.-G. Willinger, “Stacking sequence and interlayer coupling in few-layer graphene revealed by in situ imaging”, *Nat. Comm.* **7**, 13256 (2016).

16. A. Boulesbaa, V E Babicheva, K. Wang, I. I Kravchenko, M.-W. Lin, M. Mahjouri-Samani, C. B Jacobs, A. A Puretzky, K.Xiao, I.Ivanov, C. M Rouleau, D. B Geohegan, “Ultrafast Dynamics of Metal Plasmons Induced by 2D Semiconductor Excitons in Hybrid Nanostructure Arrays”, *ACS Photonics,* **3**(12) 2389 (2016).

17. A. Boulesbaa, K. Wang, M. Mahjouri-Samani, M. Tian, A. A. Puretzky, I. Ivanov, C. M. Rouleau, K. Xiao, B. G. Sumpter, and D. B. Geohegan, “Ultrafast Charge Transfer and Hybrid Exciton Formation in 2D/0D Heterostructures”, *J. Am. Chem. Soc.* **138**(44) 14713 (2016).

18. K. Wang, B. Huang, M. Tian, F. Ceballos, M. W. Lin, M. Mahjouri-Samani, A. Boulesbaa, A. A. Puretzky, C. M. Rouleau, M. Yoon, H. Zhao, K. Xiao, G. Duscher, and D. B. Geohegan, "Interlayer Coupling in Twisted WSe2/WS2 Bilayer Heterostructures Revealed by Optical Spectroscopy," *ACS Nano* **10**(7), 6612-6622 (2016).

19. M. Mahjouri-Samani, L. B. Liang, A. Oyedele, Y. S. Kim, M. K. Tian, N. Cross, K. Wang, M. W. Lin, A. Boulesbaa, C. M. Rouleau, A. A. Puretzky, K. Xiao, M. Yoon, G. Eres, G. Duscher, B. G. Sumpter, and D. B. Geohegan, "Tailoring Vacancies Far Beyond Intrinsic Levels Changes the Carrier Type and Optical Response in Monolayer MoSe2-x Crystals," *Nano Lett.* **16** (8), 5213-5220 (2016).

20. B. Yang, M. Mahjouri-Samani, C. M. Rouleau, D. B. Geohegan, K. Xiao, “Pulsed Laser Deposition of Hierarchical TiO_2 for High Performance Perovskite Solar Cells”, *Phys. Chem. Chem. Phys.*, **18**, 27067 (2016). (Invited)

21. X. Li, M.-W. Lin, A. A. Puretzky, L. Basilea, K. Wang, J. C. Idrobo, C. M. Rouleau, D. B. Geohegan, K. Xiao, “Persistent photoconductivity in two-dimensional Mo1−xWxSe2–MoSe2 van der Waals heterojunctions”, J. Mater. Res. 31, 923 (2016). (Invited)

22. X. Li, M.-W. Lin, J. Lin, B. Huang, A. A. Puretzky, C. Ma, K. Wang, W. Zhou, S. T. Pantelides, C. Miao, I. Kravchenko, J. Fowlkes, C. M. Rouleau, D. B. Geohegan, K. Xiao, “Two-dimensional GaSe/MoSe2 misfit bilayer heterojunctions by van der Waals epitaxy”, *Science Advances*, **2**, E1501882 (2016).

23. K. Share, R. E. Carter, P. Nikolaev, D. Hooper, L. Oakes, A. P. Cohn, R. Rao, A. A. Puretzky, D. B. Geohegan, B. Maruyama, and C. L. Pint, “Nanoscale Silicon as a Catalyst for Graphene Growth: Mechanistic Insight from in Situ Raman Spectroscopy”, *J. Phys. Chem. C* **120**, 14180-14186 (2016).

24. A. A. Puretzky, L. Liang, X. Li, K. Xiao, B. G. Sumpter, V. Meunier, and D. B. Geohegan

"Twisted $MoSe_2$ Bilayers with Variable Local Stacking and Interlayer Coupling Revealed by Low-Frequency Raman Spectroscopy", *ACS Nano* **10**, 2736 (2016).

25. A. M. Jubb, Y. Jiao, G. Eres, S. T. Retterer, and B. Gu, "Elevated gold ellipse nanoantenna dimers as sensitive and tunable surface enhanced Raman spectroscopy substrates", *Nanoscale,* **8**, 5641 (2016).

26. Z. Yan, L. Chen, M. Yoon, and S. Kumar, "Phonon Transport at the Interfaces of Vertically Stacked Graphene and Hexagonal Boron Nitride Heterostructures", *Nanoscale* **8**, 4037 (2016).

27. M. Tian, M. Mahjouri-Samani, G. Eres, R. Sachan, M. Yoon, M. F Chisholm, K. Wang, A. A Puretzky, C. M Rouleau, D. B Geohegan, G. Duscher "Structure and Formation Mechanism of Black TiO_2 Nanoparticles", *ACS Nano* **9**(10) 10482 (2015).

In situ TEM study of nanocrystal growth mechanisms: understanding classical and non-classical processes controlling formation of branched nanostructures

PI: Dongsheng Li, Pacific Northwest National Laboratory

Program Scope

The vision of this BES Early Career project is to reveal the unknown molecular mechanisms of mass transport and structural evolution during classical and non-classical processes of nanocrystal synthesis to enable the design of nanostructures with controlled size and morphology, and tailored properties. Specifically, the research investigates two types of growth mechanisms of branched nanowire formation: 1) particle-based growth, particularly oriented attachment (OA) and competition between classical and non-classical mechanisms, specifically, defect induced growth mechanisms, such as screw dislocation-driven trunk growth and vapor-liquid-solid (DD-VLS) branch nucleation and does so in the context of ionic and covalent systems. Representative examples of metal (Ag), metal oxides (TiO_2, OA[1]), and semiconductors (PbSe, DD-VLS[2]) serve as the material systems under investigation. Initial studies focus on TiO_2 to investigate the OA process and the Ag system to study both classical and non-classical mechanisms, such as monomer addition, particle attachment, and defect induced growth.

My specific objectives are:

Objective 1. Establish the source of the driving force for OA, the barrier to OA, and the factors that control them, including surface charge, solvent exclusion, and interface hydration.

Objective 2. Determine the origin of defects, such as screw dislocation and strain related to twin structure, and factors that control it, including temperature and supersaturation

Objective 3. Understand the source of hierarchical organization — i.e., branching at many length scales — during OA and DD-VLS growth and the correlation between branching rate and trunk extension.

Objective 4. Use the knowledge gained from Objectives 1, 2, and 3 to direct growth of nanostructures, specifically hierarchical structure.

Currently, we are working on objectives 1 and 2.

Recent Progress

Influence of crystal orientation and molecular details on long-range dispersion forces underlying aggregation and co-alignment between crystals:

To obtain a mechanistic understanding of OA process, we used atomic force microscopy-based dynamic force spectroscopy with tips (Figure 1A) fabricated from oriented mica and rutile to measure the adhesion forces between mica (001) and TiO_2 (001) surfaces in electrolyte solutions as a function of orientation, temperature, electrolyte type, and electrolyte concentration. For mica, the results reveal a ~60° periodicity (Figure 1B) as well as a complex dependence on electrolyte type and concentration (Figure C and D) and temperature. A continuum model that considers the competition between electrostatic repulsion and van der Waals attraction, augmented by microscopic details that include surface separation, water structure, ion hydration, and charge regulation at the interface, qualitatively reproduces the observed trends and implies that dispersion forces are responsible for establishing co-alignment in the solvent-separated state.

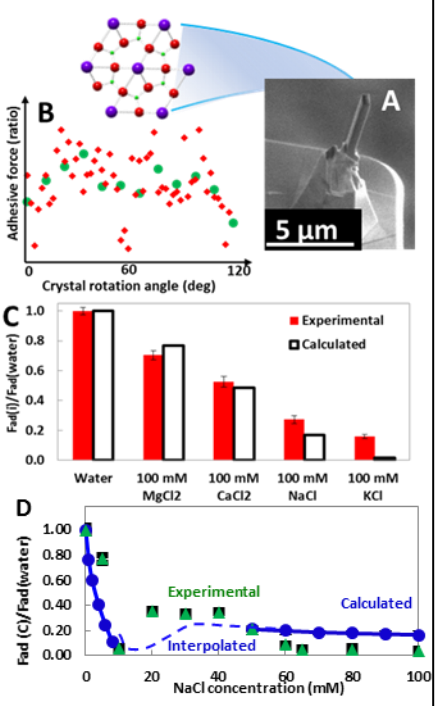

Figure 1. (A) Microscopy image of a customized atomic force microscopy probe with a single-crystal mica (001) tip. (B) ~60° oscillation of adhesive force corresponding to crystal structure. (C, D) Comparison between measured forces and theoretical predictions that couple short-range molecular details (C, ionic species; D, salt concentration) with long-range van der Waals interactions.

For TiO_2 (001), the results reveal a ~90° periodicity in the adhesion force with respect to the lattice mismatch angle (Figure 2A). As with mica, the periodicity is generally consistent with the crystal symmetry, which in this case is due to a square-lattice of Ti^{4+} centers on rutile (001). Due to the under-saturated 4-fold coordinated Ti atoms on the (001) surface, the surface is unstable and will be stabilized by chemisorption and physisorption of water with an ordered structure (Figure 2B). We investigated the effects of H-bond network formation (Figure 2B, C, and D) on the surface using molecular dynamics simulations that incorporate relevant molecular details. The simulations provide a qualitative explanation for the observed orientation-dependence and predict that hydrogen bonding is the main source of adhesion at a short range. Thus we conclude that van der Waals and hydrogen bonding are the

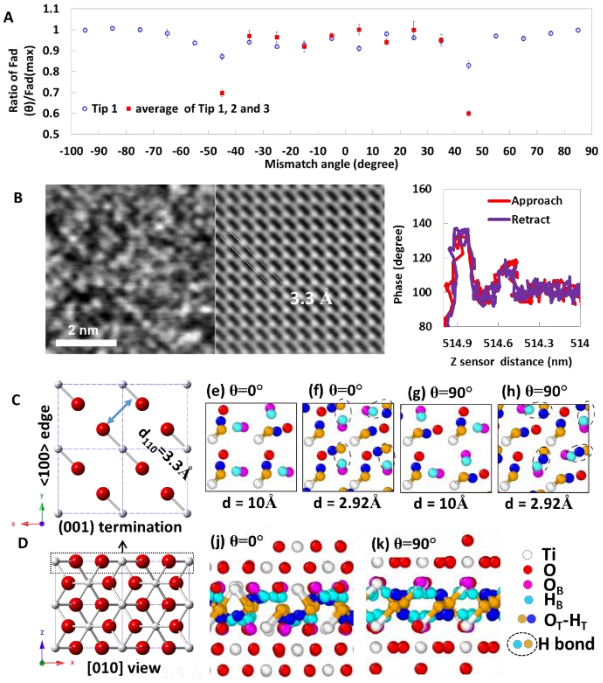

Figure 2. (A) ~90° oscillation of adhesive force corresponding to crystal structure. (B) Water structure on rutile (001) surface. (C) Top and (D) side view of rutile structure with and without water absorption.

origin of adhesion forces between TiO_2 (001) faces

Crystal growth through monomer addition, particle attachment, and strain relaxation:

Using in-situ transmission electron microscopy, we directly observed the growth of Ag nanocubes, nanobars, and particles with twin structures in aqueous solution by classical monomer-by-monomer addition (Figure 3A), non-classical particle attachment processes (Figure 3B), and strain relaxation (Figure 3C), respectively. During the particle attachment process, Ag nanocubes and nanobars were formed via both oriented and non-oriented attachment. Our calculations, along with the observed dynamics of attachment in our experiments, suggest that van der Waals attraction overcomes repulsive hydrodynamic and friction forces and drives the particles toward each other at separations of 10-100 nm. Classical growth was observed to be anisotropic; the resulting asymmetrical shapes constituted intermediate states of Ag nanocube growth. We hypothesize that the temporary symmetry breaking during nanocube growth results from different growth rates on the adjacent (001) surfaces due to a local surface concentration variations caused by the imbalance between the consumption of Ag^+ near the surface and the diffusion of Ag^+ from the bulk to surface.

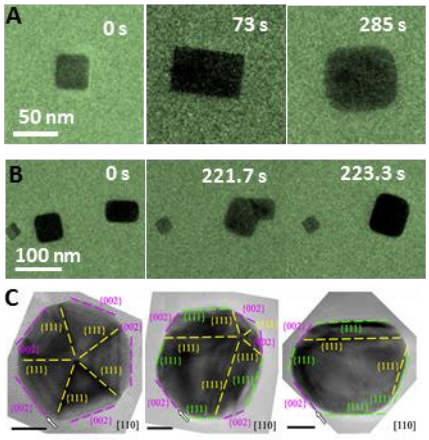

Figure 3. (A) Ag nanocube growth via monomer addition. (B) Ag nanocube growth via particle attachment. (C) Ag nanoparticle growth via strain relaxation.

For Ag particles with twin structures, strain analysis was performed to elucidate the mechanism of symmetry breaking induced by strain relaxation. The results reveal that dodecahedral nanoparticles larger than ~50 nm possessing fivefold twins evolve into asymmetric rhombic pyramids via asymmetric migration of the twin boundaries. The migration is driven by relaxation of lattice strain associated the twins and numerous stacking faults are emitted from the boundary during this process. The rhombic pyramid further evolves into a rhomboid bar due to growth in a specific manner to avoid increasing the strain energy of the crystal.

Future Plans

In the future, we will work on the following investigations.

1. Further investigation of effects of molecular details on long-range dispersion forces underlying aggregation and co-alignment.
2. In situ TEM investigations of OA mechanisms for TiO_2 or FeOOH branched nanowire growth.
3. In situ study of phase transformation from anatase into rutile along with OA during TiO_2 branched nanowire growth.

4. Modification of flow system of gas heating cell to precisely control gas flow rate and pressure, which is needed for studies of PbSe wire growth.
5. In situ investigation of DD-VLS growth mechanism of PbS/PbSe.

References

1. Li, D. *et al.* Growth mechanism of highly branched titanium dioxide nanowires via oriented attachment. *Crystal Growth & Design* **13**, 422-428, doi:10.1021/cg301388e (2013).
2. Lau, Y. K. A., Chernak, D. J., Bierman, M. J. & Jin, S. Formation of PbS nanowire pine trees driven by screw dislocations. *Journal of the American Chemical Society* **131**, 16461-16471, doi:10.1021/ja906499a (2009).

Publications

Published:

1. Li, D. *et al.* Investigating the magnitude and source of orientation-dependent interactions between TiO 2 crystal surfaces. *Nanoscale* **9**, 10173-10177 (2017).
2. Li, D. *et al.* Trends in mica–mica adhesion reflect the influence of molecular details on long-range dispersion forces underlying aggregation and coalignment. *Proceedings of the National Academy of Sciences* **114**, 7537-7542 (2017).
3. Wu, X. *et al.* Dye-Sensitized Core/Active Shell Upconversion Nanoparticles for Optogenetics and Bioimaging Applications. *ACS Nano*, doi:10.1021/acsnano.5b06383 (2016).
4. Li, Z. *et al.* Direct Aqueous-Phase Synthesis of Sub-10 nm “Luminous Pearls” with Enhanced in Vivo Renewable Near-Infrared Persistent Luminescence. *Journal of the American Chemical Society* **137**, 5304-5307, doi:10.1021/jacs.5b00872 (2015).

Under revision:

5. Silver nanocube growth vis anisotropic growth and particle attachment processes revealed by liquid cell transmission electron microscopy, Dongdong Xiao, Zhigang Wu, Miao Song, Dongsheng Li, submitted to Nano research
6. Strain relaxation induced morphological evolution in silver nanoparticles, Miao Song, Zhigang Wu, Dongdong Xiao, Dongsheng Li, submitted to Crystal Growth & Design
7. Fabrication of oriented crystals as force measurement tips via focused ion beam and microlithography methods, Zhigang Wu, Jaehun Chun, Sayandev Chatterjee, Dongsheng Li, submitted to Applied surface science

Molecularly Organized Nanostructural Materials

Jun Liu, Maria Sushko, James De Yoreo, Praveen Thallapally, Jinhui Tao

Pacific Northwest National Laboratory

Program Scope

The goal of this project is to develop innovative approaches employing molecularly directed interfacial reactions to control crystallization and self-assembly of functional nanocomposites for energy applications. The project aims to develop general principle of interface-controlled nucleation and self-assembly to predict and control the synthesis of nanocomposite materials with multiscale structural ordering. This project focuses on interfacially controlled nucleation in synthesizing carbon-metal-metal oxide nanocomposite materials. The knowledge is extended to understand and control self-assembly of materials with both atomic and longer length-scale ordering, and furthermore, to develop principles for synthesizing hierarchical structures through multi-generation homo-epitaxial nucleation processes. State-of-the-art transmission electron microscopy (TEM), atomic force microscopy (AFM), nuclear magnetic resonance (NMR), and other spectroscopy techniques are used to probe the early-stage nucleation processes. Extensive molecular and mesoscale computer modeling are used to elucidate fundamental mechanisms of interfacial binding, nucleation, and self-assembly, and guide the materials synthesis efforts.

Recent Progress

This project is demonstrating the potential of a general synthetic approach for multiscale structural control by manipulating the interfacial nucleation and self-assembly of nanoscale building blocks (Fig. 1a), developing an integrated theoretical and experimental approach, and developing and applying new in situ characterization tools. We developed a theoretical framework for modeling interfacially directed crystallization pathways and a suite of in situ scanning probe and TEM characterization techniques for monitoring nucleation and crystal growth processes. Through a combination of theoretical and experimental research, we have shown that the interfacial solvent structure and ion distributions are critical controls for surface-directed nucleation. Using a model system of gold nanoparticles, we have shown that the correlated fluctuation dynamics of growth solutions in the interfacial region largely dictate nucleation and growth pathways.[2] The project also demonstrated that highly regular 3D porous materials can be produced by using surfactant templating on the substrate and temperature-induced phase transformations in surfactant templates.[1] Finally, the project has demonstrated that the electrochemical properties of electrode materials can be manipulated using novel reaction mechanisms8 and through phase separation and interfacial stabilization to improve the cycling stabilities of electrode materials for batteries.[3]

1. Synthesis across scales. We demonstrated many examples of scalable synthesis based on interfacial control (Fig. 1a). Fig. 1b shows an example in which nucleation and mesoscale self-assembly of sodium silicate pyramids, were both controlled by interfaces.[1] Formation of the mesoscale structure was induced and directed by an atomic-scale epitaxial relationship with a Si (100) substrate. Furthermore, the atomic-scale epitaxial relationship was translated to mesoscale ordering and beyond via a self-assembled surfactant that templated the silicate: well-defined macrocrystals were formed in which mesoscale channels and crystal orientations were precisely aligned.

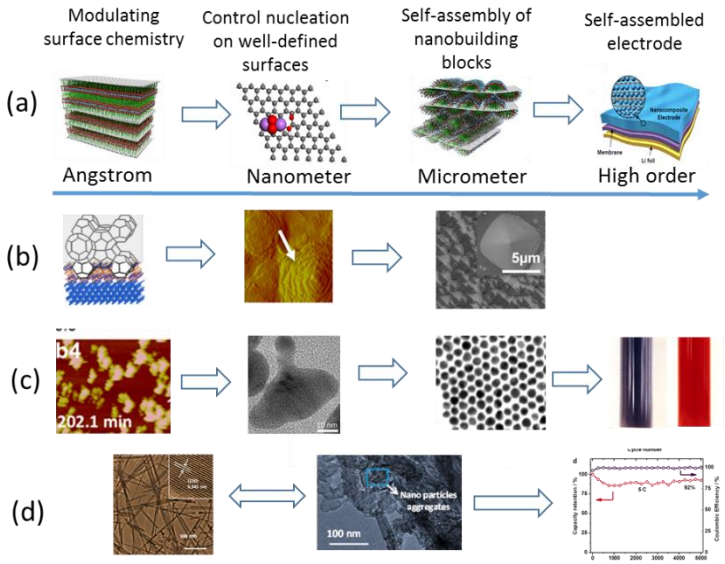

Figure 1. Synthesis across scales. (a) Illustration of the general synthetic approach based on interfacial controlled nucleation and self-assembly developed in this program from controlled nucleation, to secondary crystal growth and self-assembly. (b) Epitaxial growth of well-defined mesophase crystals with precise alignment on atomic, meso and macroscales.[1] (c) Non-classic nucleation mechanism for nanoparticle growth based in situ characterization.[2] (d) New powerful energy storage mechanism based on controlling dissolution and nucleation.[3]

2. Theoretical framework for modeling crystallization pathways. A theoretical framework was developed from first principles to model crystallization pathways. The model couples plane-wave DFT and classical DFT to encompass the complexity of short-range chemical interactions and solution fluctuation dynamics at interfaces. To validate the model as a predictive framework for modeling crystallization pathways, several well-defined examples were used. The test systems included 1) Li electrodeposition on Li metal electrodes, for which the model predicted additive chemistries that induce the transition between dendritic growth and dome-shape clusters;[4] 2) Au-seeded growth in citrate/auric acid solutions undergoing pH-induced transition between classic monomer addition and particle-based crystallization (Fig. 1c);[2] and 3) anatase TiO_2 naoparticles undergoing either oriented attachment or random aggregation depending on the pH of aqueous solutions.[5] Theoretical studies combined with in situ characterization revealed a recurring theme that crystallization pathway selection is linked to the interfacially correlated fluctuation dynamics of the solvent and precursor solution species.

3. Developing and applying new in situ tools. We made a significant effort to develop and apply state-of-art in situ characterization tools. One example is the application of in situ AFM and TEM to show that solution pH can alter the pathway of crystallization, leading to a preference for near-surface nucleation rather than classic growth. Detailed in situ study of gold seeded growth in citrate-containing solutions combined with theoretical modeling gave a comprehensive picture of solvent-controlled nucleation and growth pathways and identified the main driving

forces dictating pathway selection. The results show that the impact of the interface on the nearby solvent can alter the crystallization pathway, thereby leading to a preference for near-surface nucleation (Fig. 1c).[2] Colloidal Au particle growth has played an important role in analyses of nucleation mechanisms based on CNT. The discovery of this non-classical pathway represents significant progress in the field and may lead to new synthetic approaches for more complex nanoparticles.

4. New energy storage materials and mechanisms. We showed we can use interfacial reactions to develop new materials and mechanism to improve the properties of energy storage materials. We demonstrated that with careful design of the initial material and fundamental understanding of the mechanism of structural transformations during ion insertion/deinsertion, detrimental structural changes can be used to stabilize the electrode. Using a combination of in situ characterization and theoretical modeling, we discovered that in antimony-tin alloy electrodes phase separation takes place during the first Mg insertion/deinsertion cycle. Subsequent Mg ion insertion/deinsertion stabilizes the interface between antimony- and tin-rich regions.[6] The antimony interface then stabilizes the electrochemically active tin region for a stable high-capacity Mg ion electrode.

Controlling dissolution and nucleation can also lead to a powerful new energy storage mechanism. Based on this hypothesis, we discovered that a new conversion-type reaction, instead of ion intercalation reaction, for a rechargeable Zn-MnO_2 battery, could enable a novel, aqueous solution based highly stable and reversible battery chemistry.[3] In-depth analysis of the structure and chemistry of zinc-manganese oxide batteries provided insights into the mechanisms that control this process and allowed development of a system with that had a longer battery lifetime. High-resolution imaging of the atomic structure of the manganese oxide battery electrode material when fully discharged shows that the initial pristine, well-defined nanofibers were transformed into short nanorods and nanoparticle aggregates by dissolution and renucleation (Fig. 1d). When recharged, the structure reverts to the crystalline manganese oxide structure.

Future Plans

Future work will focus on the role of solvation and interfacial structures and interactions in local nucleation, secondary nucleation and assembly, and the effect of an external field on interfacial interactions and early nucleation. Future research will be based on four integrated elements: modeling experimental systems with well-defined interfacial structures, extensive characterization of interfaces, in situ and ex situ methods to monitor nucleation and growth processes, and theory to incorporate the effects of interfacial structures and predict nucleation and assembly. This project will focus on three key tasks.

1. Fundamental understanding of the role of solvent in nucleation on well-defined nanostructured substrates. The emphasis will be on the impact of interfacial solvent properties and solution

composition on early stages of nucleation, phase evolution and assembly in complex fluids such as ionic liquids.

2. Electric field-controlled nanocrystal nucleation. The focus will be on exploring how electric field modifies the heterogeneous and homogeneous nucleation processes emphasizing the role of E-field induced change in the particle surface chemistry and the solvation structures near the interfaces in the early stages of nucleation.

3. Higher-order structures through kinetic and thermodynamic control of nucleation and crystal growth. This task will explore and apply principles of interface- and electric field-controlled crystallization and self-assembly to control the pathways leading to complex higher-order structures.

References

(1) Shin, Y, JH Tao, BW Arey, CM Wang, GJ Exarhos, JJ De Yoreo, ML Sushko, J Liu. 2016. "Double epitaxy as a paradigm for templated growth of highly ordered three-dimensional mesophase crystals". ACS Nano, 10, 8670-8675.

(2) Cheng, Y, J Tao, G Zhy, JA Soltis, BA Legg, JJ De Yoreo, ML Sushko, J Liu. "Near surface nucleation and particle mediated growth of colloidal au nanocrystals". (submitted).

(3) Pan, HL, YY Shao, PF Yan, YW Cheng, KS Han, ZM Nie, CM Wang, JH Yang, XL Li, P Bhattacharya, KT Mueller, J Liu. 2016. "Reversible aqueous zinc/manganese oxide energy storage from conversion reactions". Nature Energy, 1. 1-6, 2016.

(4) Ding, F, W Xu, GL Graff, J Zhang, ML Sushko, XL Chen, YY Shao, MH Engelhard, ZM Nie, J Xiao, XJ Liu, PV Sushko, J Liu, JG Zhang. 2013. "Dendrite-free lithium deposition via self-healing electrostatic shield mechanism". Journal of the American Chemical Society, 135, 4450-4456.

(5) Sushko, ML, KM Rosso. 2016. "The origin of facet selectivity and alignment in anatase tio2 nanoparticles in electrolyte solutions: Implications for oriented attachment in metal oxides". Nanoscale, 8, 19714-19725.

(6) Cheng, YW, YY Shao, LR Parent, ML Sushko, GS Li, PV Sushko, ND Browning, CM Wang, J Liu. 2015. "Interface promoted reversible mg insertion in nanostructured tin-antimony alloys". Advanced Materials, 27, 6598.

Publications

(1) Qiu S., Xiao L., Sushko M.L., Han K.S., Shao Y., Yan M., Liang X., Mai L., Feng J., Cao Y., Ai X., Yang H., and Liu J. (2017) Manipulating Adsorption-Insertion Mechanisms in Nanostructured Carbon Materials for High-Efficiency Sodium Ion Storage. Advanced Energy Materials, 7(17), 1700403, 10.1002/aenm.201700403

(2) Cao X.X., Pan A. Q., Liu S. N., Zhou J., Li T. S., Cao G. Z., J. Liu, and S. Q. Liang (2017), Chemical Synthesis of 3D Graphene-Like Cages for Sodium-Ion Batteries Applications. Advanced Energy Materials 1700797. doi:10.1002/aenm.201700797

(3) Medasani, B, J Liu, and ML Sushko (2017). Stable Pt clusters anchored to monovacancies on graphene sheets. MRS Communications, (in press).

(4) Li W.Z., Kovarik, L., Cheng Y., Nie L., Bowden M.E., Liu J., and Wang Y. (2017). Stabilization and transformation of Pt nanocrystals supported on ZnAl2O4 spinel, RSC Advances, 7, 3282-3286, doi: 10.1039/C6RA26159K.Shin Y , Tao J , Arey B W, Wang C ,Exarhos G J, De Yoreo J J, Sushko M L, Liu J 2016. "Double epitaxy as a paradigm for templated growth of highly ordered three-dimensional mesophase crystals" ACS Nano, DOI: 10.1021/acsnano.6b03999.

(6) Huilin Pan, Yuyan Shao, Pengfei Yan, Yingwen Cheng, Kee Sung Han, Zimin Nie, Chongmin Wang, Jihui Yang, Xiaolin Li, Priyanka Bhattacharya, Karl Todd Mueller, Jun Liu, 2016. "Highly reversible aqueous zinc/manganese oxide energy storage from conversion reactions," Nature Energy, 1, 16039. DOI: 10.1038/nenergy.2016.39,

(7) Zhang W , Banerjee D , Liu J , Schaef H T, Crum J V, Fernandez C A, Kukkadapu R K, Nie Z ,Nune S K, Motkuri R K, Chapman K W, Engelhard M H, Hayes J C, Silvers K L, Krishna R ,McGrail B Peter, Liu J ,Thallapally P K 2016. "Redox-Active Metal-Organic Composites for Highly Selective Oxygen Separation Applications" Advanced Materials 28(18): 3572–3577. 10.1002/adma.201600259

(8) Lee YJ , Huang L , Wang H ,Sushko M L, Schwenzer B., Aksay I A, Liu J 2016. "Structural rearrangement and dispersion of functionalized graphene sheets in aqueous solutions" Colloids and Interface Science Communications 8:1-5.

(9) Cheng Y ,Shao Y ,Raju V ,Ji X ,Mehdi B L,Han KS ,Engelhard M H,Li G ,Browning N D, Mueller K T, Liu J 2016. "Molecular Storage of Mg Ions with Vanadium Oxide Nanoclusters" Advanced Functional Materials 26(20): 3446-3453.

(10) Xiao L , Cao Y ,Henderson W A, Sushko M L, Shao Y ,Xiao J ,Wang W ,Engelhard M H, Nie Z ,Liu J 2016. "Hard carbon nanoparticles as high-capacity, high-stability anodic materials for Na-ion batteries" Nano Energy 19(): 279-288. 10.1016/j.nanoen.2015.10.034

(11) Elsaidi S K, Mohamed M H, Schaef H T, Kumar A ,Lusi M , Pham T ,Forrest K A, Space B , Xu W ,Halder G J, Liu J ,Thallapally P K, Zaworotko M J 2015. "Hydrophobic Pillared Square Grids for Selective Removal of CO2 from Simulated Flue Gas" Chemical Communications 51(85):15530-15533. 10.1039/c5cc06577a

(12) Yingwen Cheng, Langli Luo, Li Zhong, Junzheng Chen, Bin Li, Wei Wang, Scott X. Mao, Chongmin Wang, Vincent L. Sprenkle, Guosheng Li, and Jun Liu. 2016. "Highly Reversible Zinc-Ion Intercalation into Chevrel Phase Mo6S8 Nanocubes and Applications for Advanced Zinc-Ion Batteries" ACS Appl. Mater. Interfaces, 2016, 8 (22), pp 13673–13677. DOI: 10.1021/acsami.6b03197

(13) Cheng N ,Shao Y ,Liu J ,Sun X 2016. "Electrocatalysts by Atomic Layer Deposition for Fuel Cell Applications" Nano Energy 10.1016/j.nanoen.2016.01.016

(14) Daniel R. Vissers, Zonghai Chen, Yuyan Shao, Mark Engelhard, Ujjal Das, Paul Redfern, Larry A. Curtiss, Baofei Pan, Jun Liu, and Khalil Amine. 2016. "Role of Manganese Deposition on Graphite in the Capacity Fading of Lithium Ion Batteries" ACS Appl. Mater. Interfaces, 2016, 8 (22), pp 14244–14251. DOI: 10.1021/acsami.6b02061.

(15) Organic Frameworks as Platform. Comments on Inorganic Chemistry 35(1):18-38, doi:10.1080/02603594.2014.976704

(16) Elsaid, S.K., Mohamed M.H., Schaef H.T., Kumar A.,Lusi M., Pham T., Forrest K.A., Space B., Xu W.Q., Halder G.J., Liu J., Zaworotko M.J., Thallapally P.K. (2015) Hydrophobic pillared square grids for selective removal of CO2 from simulated flue gas. Chem. Commun., 51, 15530-15533, doi: 10.1039/C5CC06577A

(17) Cheng Y., Shao Y., Parent L.R., Sushko M.L, Li G., Sushko P., Browning N.D., Wang C.M., and Liu J (2015) Interface Promoted Reversible Mg Insertion in Nanostructured Tin-Antimony Alloys. Advanced Materials 27(42):6598-6605. doi:10.1002/adma.201502378

(18) Lu P.J., Liu J.N., Liang S., Liu J., Wang W.J., Lei M., Tang S., and Yang Q. (2015) Ultrathin Li3VO4 Nanoribbon/Graphene Sandwich-Like Nanostructures with Ultrahigh Lithium ion Storage Properties. Nano Energy 12:709-724. doi:10.1016/j.nanoen.2014.12.019.

(19) Deria P., Gomez-Gualdron D.A., Bury W., Schaef H.T., Wang T.C., Timothy C., Thallapally P.K.,. Sarjeant A.A., Amy A., Snurr R.Q., Hupp J.T., Farha O.K.. (2015) Ultraporous, Water Stable, and Breathing Zirconium-Based Metal-Organic Frameworks with ftw Topology. J. Am. Chem. Soc., 137(40), 13183–13190, doi:10.1021/jacs.5b08860.

Prediction of phase transformations in metallic alloys far from equilibrium

K.M. Ho[a,c], M. J. Kramer[a,b], M.I. Mendelev[a], R.E. Napolitano[a,b], R.T. Ott[a], X.Song[a,d], C.Z. Wang[a]

[a]Materials Science and Engineering Division, Ames Labs DOE

[b]Department of Materials Science and Engineering, Iowa State University

[c]Department of Physics, Iowa State University

[d] Department of Chemistry, Iowa State University

Program Scope

This program area is aimed at understanding the principal structures and mechanisms that govern phase transformations in glass-forming systems. The large departure from equilibrium (i.e. undercooling) attainable in a glass forming system gives rise to a competitive crystallization scenario involving multiple highly driven phases. In addition, sluggish transport and short time scales shift the relative importance of the various kinetic contributors, where *local* atomic ordering, interface structures, and short-range motion become increasingly dominant. In this subtask, we focus on these mechanisms of crystallization and their influence on transition dynamics. Efforts include experimental and computational methods to measure specific properties such as interfacial free energy, interface mobility, and diffusivity, and to examine the mechanisms and multi-scale nucleation and growth phenomena associated with crystallization.

Recent Progress

In our past work [1,2], we showed that all available molecular dynamics (MD) simulation data for the solid-liquid interface (SLI) free energy, γ, for the fcc and bcc metals can be described by the Ewing relation [3], $\gamma = C'_T \rho_s^{2/3} T_m \Delta S_m + C_O \rho_s^{2/3} T_m S_O$, where ΔH_m is the latent heat, ρ_s is the atomic density and S_O is the liquid excess entropy. The first term is associated with the difference in bonding in the liquid and solid phases. The second term describes the structural relaxation in the interface region. Our MD simulation results suggested that C'_T is a universal constant that does not depend on the crystal structure. To test this idea, we determined the SLI free energy for several hcp systems (there has been only one MD simulation study published prior to our work that has determined the SLI free energy for an hcp phase [4]). Figure 1 demonstrates that, indeed, the data for all three crystal lattices can be described by one universal coefficient that is independent of the crystal structure and only one coefficient for each specific crystal structure.

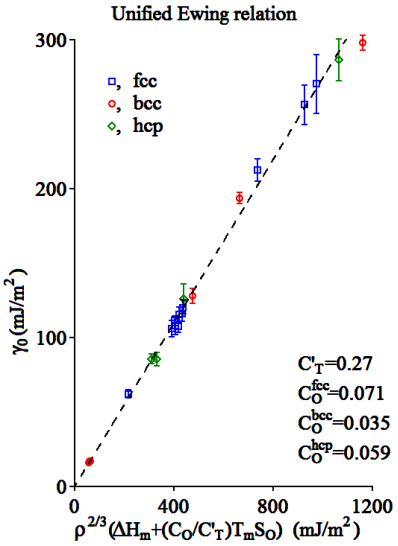

Figure 1. Comparison between the unified Ewing relation and MD simulation data. The data for all studied crystal lattices fall on the same straight line.

Our work provides a simple estimate of SLI free energy (which is very time consuming to determine) based on bulk properties that are easy to determine.

We developed a theoretical model to calculate the first order curvature correction to the SLI free energy based on the interfacial excess thermodynamic properties. We showed that this curvature correction is crucial in predicting the nucleation barrier when the size of the crystal nucleus is small. The thermodynamic driving force was also calculated by combining simulation data with a classical density functional theory. We showed that the classical nucleation theory is capable of predicting the nucleation barrier with excellent agreement to the simulated results when the curvature correction to the interfacial free energy is accounted for.

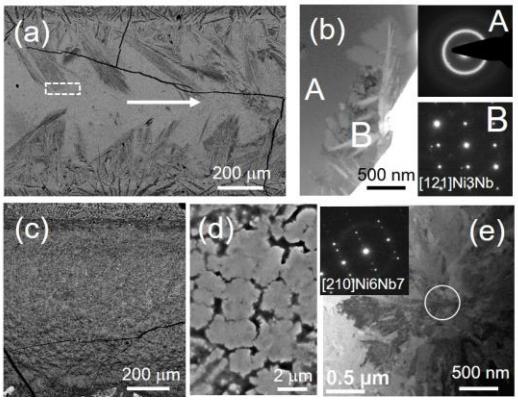

Figure 2. (a) Back-scattered SEM (BS-SEM) image of laser trace for the alloy with x_{Ni}~0.66; arrow directs to the laser movement direction. (b) BF-TEM image of the top dendritic structure marked in (a); SADs A and B are from regions A and B marked in image (b). (c) BS-SEM images of laser trace for the alloy with x_{Ni}~0.56; (d) high magnification of laser trace; (e) BF-TEM and corresponding SAD pattern.

While the SLI migration in single component systems has been intensively studied in the last two decades (e.g., see [5,6]) much less is known about the SLI migration in multi-component systems. We investigated the SLI migration in the Ni-Nb alloy which represents a rare example of a bulk glass forming binary metallic alloy. In the experimental part, we performed surface laser remelting. It was found that when the Ni concentration is about 66 %, there is a dendritic structure on the laser trace surface which grows from the interface between unmelted and melted zones in the direction of laser movement (see Fig. 2a). After removing a sample with a focused ion beam (FIB), transmission electron microscopy (TEM) was used to confirm the structure of the dendritic phase. The selected area diffraction (SAD) patterns indicate that the primary and secondary dendrites are the Ni_3Nb phase (see Fig. 2b). When the Ni concentration is decreased to 56%, the dendritic and amorphous structures do not appear in the same trace (see Fig. 2c). Instead equiaxed crystals are observed on the top of laser trace (see Fig. 2d). TEM analysis of a sample from this region reveals the Ni_6Nb_7 phase (see Fig. 2e). The crystallization proceeds by a radial growth from central nuclei (marked by circle in Fig. 2e) until the crystals impinge upon each other. Thus, the experiment indicates that the SLI mobility of the Ni_6Nb_7 phase is much smaller than that of the Ni_3Nb phase.

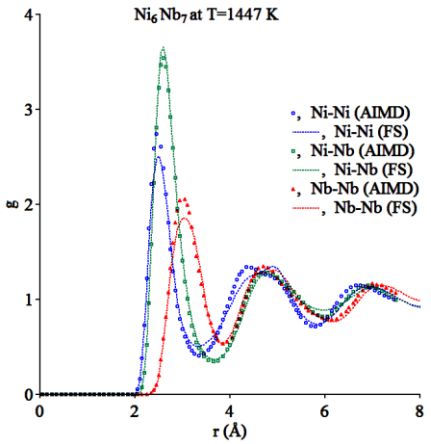

Figure 3. Partial pair correlation functions of the liquid $Ni_{62}Nb_{38}$ alloy.

In order to simulate the SLI migration in the Ni-Nb alloys, we first developed a Finnis-Sinclair (FS) potential [7],

specifically fitting (i) the liquid pair correlation functions obtained from *ab initio* molecular dynamics simulation (see Fig. 3) and (ii) *ab initio* formation energies of metastable crystal phases. Next we performed the MD simulation which showed that the Ni_3Nb phase grows much faster than does the Ni_6Nb_7 phase, in agreement with our experiment.

Up to the present moment, conventional MD-based determination of nucleation rates in metals have been obtained only for pure elements and for very large undercoolings, which are not achievable in experiment. Therefore, any reported attempt to compare the obtained nucleation rate with an experimental value was based on an extrapolation to the experimental conditions. There is also another group of methods where the energy landscape is biased to facilitate nucleation [8,9]. These methods provide valuable information about the free energy landscape, but they do not provide a straightforward method to estimate the nucleation rate. In our approach, we take advantage of the subcritical cluster energetics, where most of the nucleation barrier is associated with the well-below critical regime. To avoid simulating the nearly random walk through this part of the trajectory, we developed a "persistent embryo" method, where the embryo is prevented from re-melting in this regime but becomes unbiased as the cluster size moves closer to the critical size (see Fig. 4). This allowed us to obtain both the critical nucleus size and the attachment rate and, finally, calculate the nucleation rate. Contrary to the previous MD studies, our method can be used at small undercooling, which allowed us to compare the nucleation rates with available experimental data for Ni without using any extrapolation. Moreover, for the first time, we were able to determine the nucleation rate in a good glass-forming alloy ($Cu_{50}Zr_{50}$), where timescales are generally very long, even by experimental standards. Thus, our work opens a new avenue to study solidification under realistic experimental conditions via atomistic computer simulation.

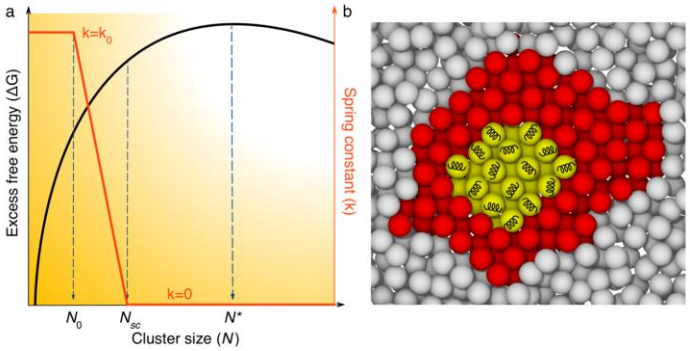

Figure 4. Persistent-embryo method a) Excess free energy (black) and spring constant (red) as a functions of the crystalline cluster size N. N_0 is the number of atoms in the constrained embryo. When the embryo grows, the strength of the spring constant decreases with the cluster size. The spring is completely removed when the cluster size reaches the threshold value, N_{sc}. N^* is the critical size. b) a cross-section of the as-grown crystalline cluster. The yellow atoms with spring icon are the persistent embryo. The red are the as-grown atoms, showing the crystalline packing. The gray are the liquid atoms.

Future Plans

Our strategic goal is to facilitate the intentional realization of materials and structures that are accessible only through pathways involving highly undercooled liquids and glasses. While *ab initio* calculation can predict the *existence* of boundless metastable phases at T=0, the more important challenge lies in determining which are *attainable* and predicting viable *realization*

pathways. Moreover, for many functional materials, the phase morphology and/or microstructure may also be critical. Using the Al-Sm as our principal prototype system, we have demonstrated that processing conditions can be controlled to effect the realization of never-before-seen metastable phases during devitrification of the glass. The transformations are very sensitive to small changes in thermal history and solute content. By understanding the detailed mechanisms that govern nucleation and growth in the high driving force regime, we aim to build a set of theory-based tools to enable specific control of phase selection and structure evolution in these systems. By expanding our scope to other aluminum rare-earth and other more complex alloys, this work will enable prediction and realization of new phases in a range of energy-relevant systems.

To meet this goal our future work will include using a suite of synthesis and processing techniques to systematically investigate phase selection response over a wide range of driving forces to address the follow challenges. We will extend our experimental observations of crystallization kinetics across all temperatures from the melting temperature (or liquidus) to below the glass transition temperature for the Al-Sm, Cu-Ni-Zr and Ni-Nb alloys. Methods will include levitation melting with free cooling, isothermal holding, splat cooling, and triggered growth; laser-trace melting/freezing; and magnetron sputter deposition.

The MD simulations will be used to study the effect of solutes on the nucleation kinetics. Our preliminary studies shows that addition of just a small amount of solutes can change the nucleation rate by orders of magnitude. This approach is especially promising for the alloys containing stoichiometric compounds and provides the tools to direct and control the phase selection. The developed persistent embryo methods will allow us to study such systems in the MD simulation and provide quantitative predictions which will be verified by comparison with our experimental results.

The MD simulations will require using semi-empirical potentials of the interatomic interaction. We have developed a robust technique to develop such potentials for binary alloys. The studies of the effects of solutes on the nucleation kinetics in binary alloys will obviously require semi-empirical potentials for 3-4 component systems. The key components will be to fit the liquid structure and formation energy obtained from *ab initio* calculations and transformation temperature data obtained from experiment. The developed semi-empirical potentials will also be employed to study the thermodynamics of liquid alloys and defects in crystalline phases.

References

[1] S. R. Wilson, K. Gunawardana, and M. I. Mendelev, J. Chem. Phys. **142**, 12, 134705 (2015).
[2] S. R. Wilson and M. I. Mendelev, Model. Simul. Mater. Sci. Eng. **22**, 12, 065004 (2014).
[3] R. H. Ewing, J. Cryst. Growth **11**, 221 (1971).
[4] D. Y. Sun, M. I. Mendelev, C. A. Becker, K. Kudin, T. Haxhimali, M. Asta, J. J. Hoyt, A. Karma, and D. J. Srolovitz, Phys. Rev. B **73**, 024116 (2006).
[5] J. J. Hoyt, M. Asta, and A. Karma, Mater. Sci. Eng. R-Rep. **41**, 121 (2003).
[6] Y. Mishin, M. Asta, and J. Li, Acta Mater. **58**, 1117 (2010).

[7] M. W. Finnis and J. E. Sinclair, Philosophical Magazine a-Physics of Condensed Matter Structure Defects and Mechanical Properties **50**, 45 (1984).
[8] P. R. ten Wolde, M. J. Ruiz-Montero, and D. Frenkel, Physical Review Letters **75**, 2714 (1995).
[9] S. Auer and D. Frenkel, Nature **413**, 711 (2001).

Publications

1. D. G. Quirinale, G. E. Rustan, A. Kreyssig, S. H. Lapidus, M. J. Kramer, and A. I. Goldman, "The Solidification Products of Levitated $Fe_{83}B_{17}$ Studied by High-Energy X-Ray Diffraction," *Journal of Applied Physics*, **120**, 175104 (2016).
2. D. G. Quirinale, A. Kreyssig, S. Saunders, D. Messina, W. E. Straszheim, P. C. Canfield, M. J. Kramer, and A. I. Goldman, "The Solidification of Al-Pd-Mn Studied by High-Energy X-ray Diffraction from Electrostatically Levitated Samples," *Zeitschrift Fur Kristallographie-Crystalline Materials*, **232**, 619-627 (2017).
3. S. R. Wilson and M. I. Mendelev, "A Unified Relation for the Solid-Liquid Interface Free Energy of Pure Fcc, Bcc, and Hcp Metals," *Journal of Chemical Physics*, **144**, 144707 (2016).
4. P. Zhang, L. He, M. F. Besser, Z. Liu, J. Schroers, M. J. Kramer, and P. M. Voyles, "Applications and Limitations of Electron Correlation Microscopy to Study Relaxation Dynamics in Supercooled Liquids," *Ultramicroscopy*, **178**, 125-130 (2017).
5. S. H. Zhou, Y. Huo, and R. E. Napolitano, "Phase Stability for the Pd-Si System: First-Principles, Experiments, and Solution-Based Modeling," *Metallurgical and Materials Transactions A*, **47**, 194-208 (2016).
6. S. H. Zhou, M. J. Kramer, R. T. Ott, and R. E. Napolitano, "[O69] Energetic Investigation of Metastable $Al_{60}Sm_{11-\Omega}$, Al_5Sm-π, Al_4Sm-γ, $Al_{11}Sm_{3-\alpha}$ and Al_4Sm-β Phase Formation," *Calphad*, **51**, 366 (2015).
7. P. Zhang, J. J. Maldonis, M. F. Besser, M. J. Kramer, and P. M. Voyles, "Medium-Range Structure and Glass Forming Ability in Zr-Cu-Al Bulk Metallic Glasses," *Acta Materialia*, **109**, 103-114 (2016).
8. K. G. S. H. Gunawardana and X. Song, Free Energy Calculations of Crystalline Hard Sphere Complexes Using Density Functional Theory, *J.Phys. Chem. B*,**119**, 9160 (2015).
9. B. Shen, Z. Y. Wang, F. Dong, Y. R. Guo, R. J. Zhang, Y. X. Zheng, S. Y. Wang, C. Z. Wang, K. M. Ho, and L. Y. Chen, "Dynamics and Diffusion Mechanism of Low-Density Liquid Silicon," *Journal of Physical Chemistry B*, **119**, 14945-14951 (2015).
10. S. H. Zhou, C. Liu, Y. X. Yao, Y. Du, L. J. Zhang, C. Z. Wang, K. M. Ho, and M. J. Kramer, "Magnetic Bimn-Alpha Phase Synthesis Prediction: First-Principles Calculation, Thermodynamic Modeling and Nonequilibrium Chemical Partitioning," *Computational Materials Science*, **120**, 117-126 (2016).
11. Z. Wang, L. Huang, G. Q. Yue, B. Shen, F. Dong, R. J. Zhang, Y. X. Zheng, S. Y. Wang, C. Z. Wang, M. J. Kramer, K. M, Ho, and L. Y. Chen, "Effects of Oxygen Impurity on Glass-Formation Ability in Zr_2Cu Alloy", *The Journal of Physical Chemistry* B, **120**, 9223-9229 (2016).

Ordering in glass-forming liquids: A critical component in the phase selection pathway

K.M. Ho[c], C.Z. Wang[a,c], M.I. Mendelev[a], R. T. Ott[a], X.Song[a,d], R. E. Napolitano[a,b], M. J. Kramer[a,b]

[a]Materials Science and Engineering Division, Ames Labs DOE

[b]Department of Materials Science and Engineering, Iowa State University

[c]Department of Physics, Iowa State University

[d]Chemistry Department, Iowa State University

Program Scope

The unique feature surrounding transformation kinetics in glass-forming systems is the development of non-crystalline forms of short- and medium-range order (SRO, MRO), which may have a substantial affect on relaxation pathways and the resulting stable and metastable crystalline states. In this task area, we aim to understand the nature and development of such order along with the fundamental connections to the thermodynamic forces and mechanisms that ultimately dictate dynamical pathways involving crystallization and/or glass formation. Experiments and computer simulations have revealed SRO and MRO in glass-forming alloys, and we explore these effects in the model systems of Cu-Zr and Al-Sm. The principal objective is to build theory-based self-consistent descriptions of the relevant ordering, the critical connections to measurable thermo-kinetic properties, and the dependence on composition, temperature, and thermal history. Here, we summarize recent progress, challenges, and future directions.

Recent Progress

Crystal genes – Our experiments and simulations have shown[1] that phase selection and crystallization pathways in metallic liquids and glasses may be profoundly influenced by the presence of coincident motifs or "crystal genes." We demonstrate such crystal genes in two systems, Cu-Zr and Al-Sm, which represent strong and marginal glass formers, respectively. We

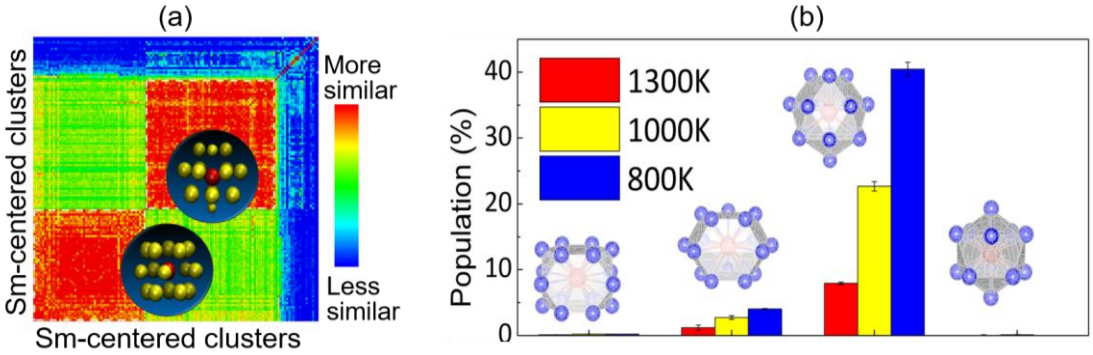

Figure 1 (a) Similarity matrix of Sm-centered clusters in GA-found Al-Sm crystals. Each element $\boldsymbol{M_{ij}}$ shows the similarity between cluster *i* and cluster *j*. Clusters with significant similarity are grouped together to represents a dominant motif. (b) Population of GA-identified motif and other typical motifs in $Al_{90}Sm_{10}$ liquids at different temperatures.

first establish dominant packing motifs in crystalline structures identified by a genetic algorithm (GA)[2,3], which is a robust and efficient method for identifying low-energy configurations in crystals. Then, we used our previously developed cluster alignment method[4] to check the popularity of the GA-identified motifs in real undercooled liquids prepared by ab initio molecular dynamics (AIMD) simulations. As an example, Fig. 1 shows the two dominant packing motifs extracted from GA-identified crystalline structures. One of these motifs also has dominant population in equilibrium or undercooled $Al_{90}Sm_{10}$ liquids.

Experimentally, $Al_{90}Sm_{10}$ glass samples can be synthesized by different techniques, such as melt spinning and magnetron sputtering. When thermally annealed, the samples prepared by different methods (e.g., liquid processing vs. sputtering) can exhibit much different devitrification behaviors, relaxing to different crystalline phases in the first devitrification step[5,6]. While the selection of these metastable structures may be promoted by the presence of "crystal gene" Sm-centered clusters (Fig. 2), which may serve to lower the nucleation barrier, we note that chemical partitioning, diffusion, and site occupancy defects are also important in the selection or these complex metastable phases during the devitrification process.

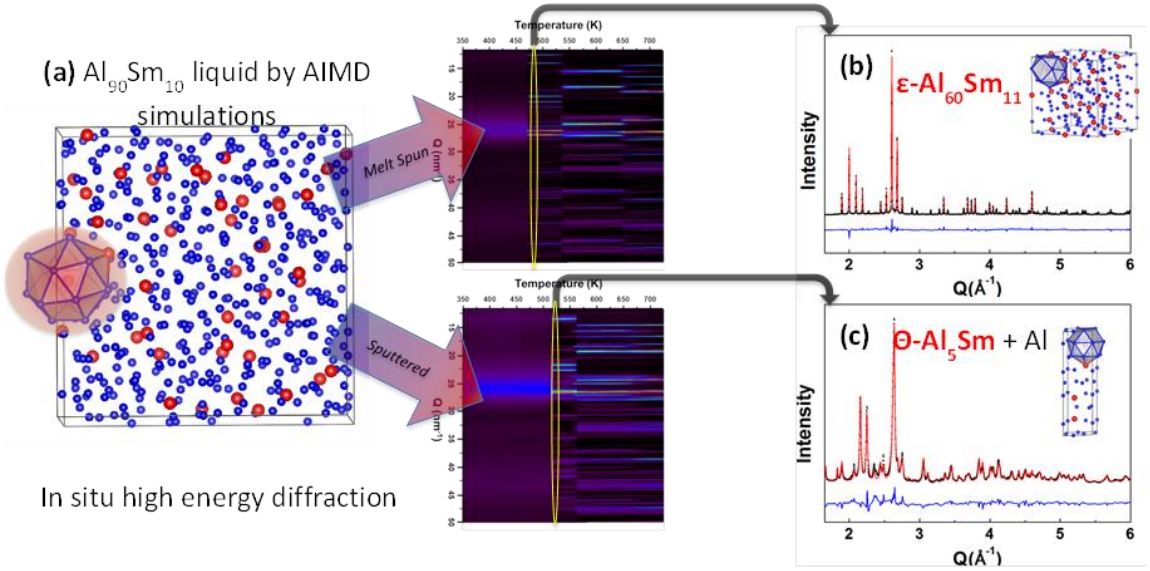

Figure 2 The common "crystal gene" in (a) undercooled liquid sample at 800K; (b) ε-$Al_{60}Sm_{11}$, which is the first crystal structure observed from devitrification of $Al_{90}Sm_{10}$ samples prepared by melt spinning; and (c) in θ-Al_5Sm, which is one of the first devitrified phases from $Al_{90}Sm_{10}$ samples prepared by magnetron sputtering. Red ball represents for Sm atom and blue for Al atom.

Medium-range order in $Al_{90}Sm_{10}$ glass – Based on the "crystal gene" that characterizes the short-range order (SRO) up to the first atomic shell, we extend our study to medium-range order (MRO) in $Al_{90}Sm_{10}$ glasses, by applying a sub-T_g annealing technique that we established to accelerate structural relaxation in glassy structures[7]. As shown in Fig. 3(a), we have achieved an effective cooling-rate of 6×10^7 K/s, which is inaccessible using conventional MD cooling

methods. Fig. 3(b) shows that the fraction of the dominant motif increases as the effective cooling rate decreases. Interestingly, as shown in Fig. 3(c), interpenetration of the local clusters characterizing the SRO is only weekly dependent on the cooling rate, which is in sharp contrast with the strong glass former $Cu_{64.5}Zr_{35.5}$, where one can see profound enhancement of interpenetration among icosahedral clusters as the cooling rate decreases [see inset of Fig. 3(c)]. This feature could be indicative of the marginal glass-forming ability of $Al_{90}Sm_{10}$[8] and may be related to other characteristic properties, such as the fragility.

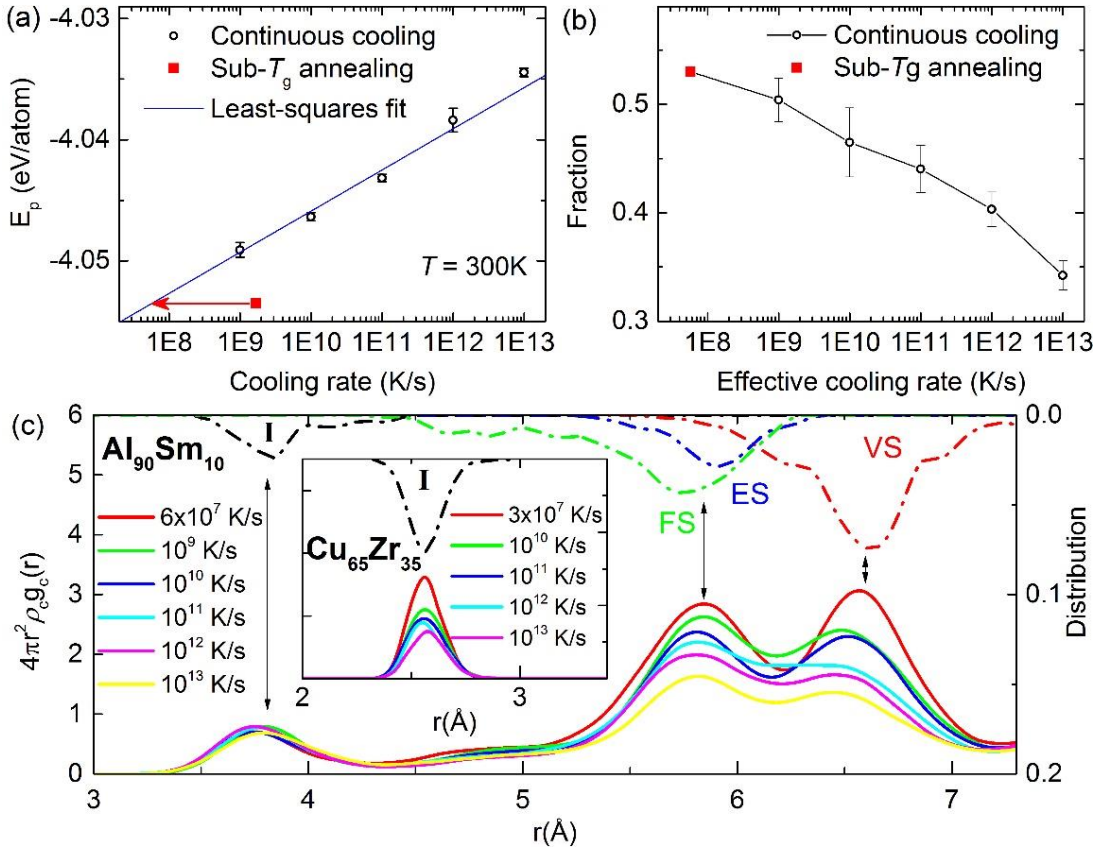

Figure 3 (a) Potential energy at 300K as a function of cooling rate. The red arrow points an effective continuous cooling rate of 6×107 K/s achieved by sub-Tg annealing. (b) The fraction of "3661" clusters as a function of effective cooling rate of the samples. The insert shows the "3661" motif. (c) The solid lines show the radial distribution function of the centers in "3661" clusters. The dashed lines show the distribution of the distance between two "3661" cluster centers adopting each type of connection, where "I" stands for interpenetration, "FS" for face sharing, "ES" for edge sharing and "VS" for vertex sharing. The insert shows the cooling rate dependence of interpenetrating connections in $Cu_{65}Zr_{35}$ metallic glass.

Future Plans

While the "crystal gene" establishes a linkage between amorphous and crystalline structures, its specific role in governing phase selection and the mechanisms of nucleation and growth is not yet fully understood. To investigate these issues, we require suitable order parameters to effectively differentiate liquid and crystal phases. Conventionally, structure-derived parameters have been used for this purpose, such as the rotation-invariant bond-orientational order parameter[9]. Due to the intrinsic thermal or chemical distortions, these parameters are sometimes ineffective in differentiating bulk liquid and crystal phases. Considering the higher level of distortion, and the existence of grain boundaries and defects, one can only expect their performance to be worse. Taking an alternative approach, we consider the major distinction between liquid and crystal to be the atomic mobility. Thus, we plan to develop a more sensitive kinetic order parameter to describe liquid and solid phases for our study of nucleation and growth. By understanding the free energy barrier, the nucleation rate, and the atomistic pathways for crystallization, we aim to predict phase selection and structure in real materials.

References

[1] Y. Sun, F. Zhang, Z. Ye, Y. Zhang, X. Fang, Z. Ding, C.-Z. Wang, M.I. Mendelev, R.T. Ott, M.J. Kramer, and K.-M. Ho, Sci. Rep. **6**, 23734 (2016).

[2] D.M. Deaven and K.M. Ho, Phys. Rev. Lett. **75**, 288 (1995).

[3] S.Q. Wu, M. Ji, C.Z. Wang, M.C. Nguyen, X. Zhao, K. Umemoto, R.M. Wentzcovitch, and K.M. Ho, J. Phys. Condens. Matter **26**, 35402 (2014).

[4] X.W. Fang, C.Z. Wang, Y.X. Yao, Z.J. Ding, and K.M. Ho, Phys. Rev. B **82**, 184204 (2010).

[5] Z. Ye, F. Zhang, Y. Sun, M.C. Nguyen, M.I. Mendelev, R.T. Ott, E.S. Park, M. Besser, M.J. Kramer, Z.-J. Ding, C.-Z. Wang, and K.-M. Ho, 22 (2015).

[6] Z. Ye, F. Zhang, Y. Sun, M.I. Mendelev, R.T. Ott, E. Park, M.F. Besser, M.J. Kramer, Z. Ding, C.-Z. Wang, and K.-M. Ho, Appl. Phys. Lett. **106**, 101903 (2015).

[7] F. Zhang, M.I. Mendelev, Y. Zhang, C.-Z. Wang, M.J. Kramer, and K.-M. Ho, Appl. Phys. Lett. **104**, 61905 (2014).

[8] Y. Zhang, F. Zhang, C.Z. Wang, M.I. Mendelev, M.J. Kramer, and K.M. Ho, Phys. Rev. B - Condens. Matter Mater. Phys. **91**, (2015).

[9] P. Steinhardt, D. Nelson, and M. Ronchetti, Phys. Rev. B **28**, 784 (1983).

Publications

1. Z. Ye, F. Zhang, Y. Sun, M. C. Nguyen, S. Zhou, L. Zhou, F. Meng, R. T. Ott, E. Park, M. F. Besser, M. J. Kramer, Z. J. Ding, M. I. Mendelev, C. Z. Wang, R. E. Napolitano, and K. M. Ho, "Structural hierarchy as a key to complex phase selection in Al-Sm, " Physical Review Materials (accepted).
2. C. Yildirim, M. Kutsal, R. T. Ott, M. F. Besser, M. J. Kramer, and Y. E. Kalay, "The Role of Amorphous Precursor in Phase Selection Hierarchy in Marginal Metallic Glasses," Materials & Design, 112, 479-484 (2016). 10.1016/j.matdes.2016.09.060.
3. F. Zhang, Y. Sun, X.D. Wang, Q.P. Cao, J.Z. Jiang, C.Z. Wang, and K.M. Ho, " Structural connection between gallium crystals and near-Tm liquids under ambient pressure, " Scripta Materialia (accepted).
4. Y. Sun, F. Zhang, Z. Ye, Z. J. Ding, M. I. Mendelev, M. J. Kramer, C. Z. Wang, and K. M. Ho, "Structural Ordering at Solid-Liquid Interfaces in Al-Sm System: A Molecular-Dynamics Study," Materials Letters, 186, 26-29 (2017). 10.1016/j.matlet.2016.07.046.
5. S. Zhou, C. Tackes, and R. Napolitano, "Enthalpy of Mixing in Al–Tb Liquid," Entropy, 19, 290 (2017). 10.3390/e19060290.
6. L. H. Xiong, X. D. Wang, Q. Yu, H. Zhang, F. Zhang, Y. Sun, Q. P. Cao, H. L. Xie, T. Q. Xiao, D. X. Zhang, C. Z. Wang, K. M. Ho, Y. Ren, and J. Z. Jiang, "Temperature-Dependent Structure Evolution in Liquid Gallium," Acta Materialia, 128, 304-312 (2017). 10.1016/j.actamat.2017.02.038.
7. Y. Zhang, R. Ashcraft, M. I. Mendelev, C. Z. Wang, and K. F. Kelton, "Experimental and Molecular Dynamics Simulation Study of Structure of Liquid and Amorphous Ni62Nb38 Alloy," Journal of Chemical Physics, 145, 204505 (2016). 10.1063/1.4968212
8. Y. X. Huang, L. Huang, C. Z. Wang, M. J. Kramer, and K. M. Ho, "Ab Initio Molecular Dynamics Simulations of Short-Range Order in Zr50Cu45Al5 and Cu50Zr45Al5 Metallic Glasses," Journal of Physics-Condensed Matter, 28, 085102 (2016). 10.1088/0953-8984/28/8/085102.
9. Y. X. Huang, L. Huang, C. Z. Wang, M. J. Kramer, and K. M. Ho, "Comparative Study of Local Atomic Structures in Zr2CuxNi1-x (x=0, 0.5, 1) Metallic Glasses," Journal of Applied Physics, 118, 195902 (2015). 10.1063/1.4935877.
10. Y. Sun, Y. Zhang, F. Zhang, Z. Ye, Z. J. Ding, C. Z. Wang, and K. M. Ho, "Cooling Rate Dependence of Structural Order in Al90Sm10 Metallic Glass," Journal of Applied Physics, 120, 015901 (2016). 10.1063/1.4955223.
11. Y. Sun, F. Zhang, Z. Ye, Y. Zhang, X. W. Fang, Z. J. Ding, C. Z. Wang, M. I. Mendelev, R. T. Ott, M. J. Kramer, and K. M. Ho, "'Crystal Genes' in Metallic Liquids and Glasses," Scientific Reports, 6, 23734 (2016). 10.1038/srep23734.

Growth of 2-d materials with tunable electronic band structures

M.C.Tringides[1,2] K.M. Ho[1,2] , M.Hupalo[1] , P. A. Thiel[1,3] , C. Z. Wang[1]

[1] Ames Laboratory, [2] Department of Physics-ISU, [3] Department of Chemistry-ISU Ames IA 50011

I. Program Scope

The goals of this FWP are the controlled growth of nanostructured materials and their use to solve important technological problems. Novel properties emerge as the nanostructure dimensions are reduced, when compared to bulk materials, because lower atom coordination, electron confinement and interface compatibility play key roles. Heterostructure formation built from the assembly of novel dissimilar materials offers the possibility to engineer new hybrid materials with tunable band structures. Utilizing our previous expertise, we plan to grow and use tunable metal nanostructures in two new directions, related to graphitic applications:(i) Studying metal growth on graphene/graphite to find kinetic conditions where the metal intercalates in graphene/graphite and generates new phases and 2-d layered structures.(ii). Use metal intercalation to grow 2-d quantum materials that can have topologically interesting electronic and spintronic properties.

II. Previous work

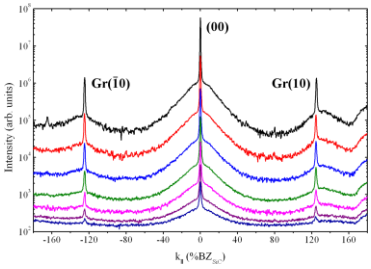

Fig. 1.SPA-LEED profiles as a function of deposited Dy amount showing that the graphene spot becomes extinct with 2ML of Dy at 110K. This shows that metal layer-by-layer growth on graphene is possible.

Metals grown on graphene have been of interest because of their potential use as metal contacts in graphene devices, for spintronics applications, and for catalysis. All applications require good understanding and control of the metal growth morphology, which in part reflects the strength of the metal-graphene bond. Also of importance is whether the interaction between graphene and metal is sufficiently strong to modify the electronic structure of graphene. Over the last two years we have continued our experimental and computational studies related to the deposition of metals on graphene and graphite. Of specific interest are the metal-graphene interactions (adsorption energies and diffusion barriers of metal adatoms) and how the grown morphology (whether layer-by-layer or 3-d) can be controlled. Our studies have identified the role of the weak metal-graphene interaction that favors 3-d growth into multi-height islands (even for very small deposited amounts) as a major challenge to be addressed experimentally. Our extensive work in this area has been presented in a well documented review article summarizing the status of the field[1].

Finding ways to wet graphene and to grow layer-by-layer is a necessary requirement for any use of graphene, since it will enable the fabrication of stable low resistance metal contacts or high selectivity spin filters. We employed the complementary techniques of SPA-LEED and STM to study the growth of Dy on graphene. We found that under kinetic limitations it is possible to fully cover graphene with a bilayer Dy film, by growing well below room temperature using, not continuous, but stepwise deposition experiments[2]. The transfer of Dy to islands which is favored thermodynamically is suppressed kinetically at the low temperatures; the stepwise deposition results in the seeding of a larger number of nucleation sites that favors the incorporation of the adatoms to complete a growing layer.

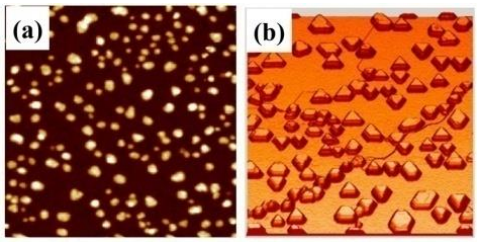

Fig. 2. (a) The nucleated island density after 0.4 ML of Dy over 100×100nm^2. (b) Dy islands grown on at 660 K with 1.36 ML within 250×240 nm^2. They have triangular shapes suggesting they are fcc(111).

Experiments on graphene that has mixed phases, pristine and intercaleted by Dy, show that nucleation is favored on the intercalated areas[3]. This can lead to novel methods to manipulate the location of the metal nanostructures on graphene. A key question is mass transport, i.e., how atoms deposited initially uniformly on graphene populate different areas, depending on whether they are intercalated or not. Using first-principles calculations, we show that graphene, with a mixture of intercalated and pristine areas, can induce a spatially alternating electric field due to the spatial variations

in electron doping. This alternating field can change normal, stochastic adatom diffusion to biased diffusion, leading to selective mass transport and nucleation, on the intercalated areas, if the charge transfer is from the metal to the carbon adatoms.

Intercalation experiments were also carried on graphite[4]. We found that 3 metals--Dy, Ru, and Cu--can be encapsulated at the graphite(0001) surface if two specific conditions are met: Defects are present in the graphite surface to act as entry portals for the deposited atoms, and the deposition temperature is well above ambient. Focusing on Dy as a prototype, we have shown that surface intercalation is much different than bulk intercalation (commonly performed at high pressure), because the intercalated metal takes the form of bulk-like Dy rafts, rather than the $(\sqrt{3}\times\sqrt{3})R30^{o}$ structure known for the bulk compound. Based on this work, it may be possible to modify the surface properties of graphite, and to spatially control those properties by patterning the entry portals with metals of interest.

Continuing earlier work on the unusual collective diffusion on Pb/Si(111) we have shown how this novel effect dramatically changes the film conductivity[5]. Using *in situ* electrical resistivity measurements and Scanning Tunneling Microscopy (STM) we show that for temperatures T>140 K the specific resistivity $\rho(\theta)$ vs coverage θ shows an unusual "hump", instead of the expected monotonic decrease with θ. This novel result correlates well with the very fast collective motion of the wetting layer, since sensing changes in the film conductivity in real time is only possible if mass transport is exceedingly fast at such low temperatures.

III. Future Plans growth of 2-d quantum materials on and under graphene/graphite.

Tuning band structures of 2-d materials Traditionally synthesis and fabrication are based on extensive and painstaking search of materials to meet certain desired properties (high electron mobility, low effective mass, finite band gap, conductivity, magnetization, band polarization, etc). Recently a new priority has emerged, to manipulate the electronic band structure of materials. so it has these desired properties. This was a major extension of the established manipulation abilities in real space to move and assemble atoms. For example many unusual electronic band structures were predicted and confirmed: graphene, 2-d van der Waals materials[6], topological insulators[7], topological superconductors[8], Weyl metals [9], Rashba systems with spin polarized bands[10], single-layer superconductors [11])). The conditions to realize the unusual properties of such pre-designed structures are very constraining, so any deviation in one of the two spaces (structure in real space or band structure in energy space) will affect the other.

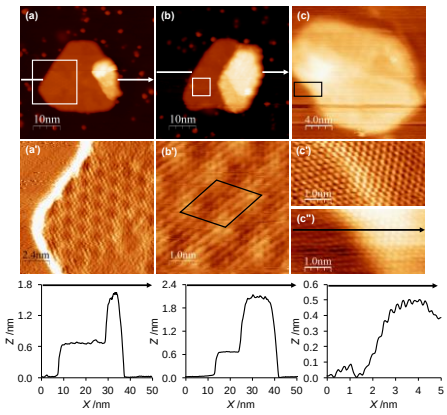

Fig. 3 Intercalated Dy islands on graphite after generating a small number of defects by sputtering. Graphene is imaged on island top with Moire pattern a result of beating of the graphene and Dy lattices.

The goal of the FWP is to use its expertize and complementary expertize in Ames lab, to grow and characterize new materials with novel, topologically protected physical and electronic properties. Reducing the dimensionality from 3-d to 2-d (i.e. growing ultrathin films) can enhance even further the related effects. The band structure manipulation is accomplished with several control parameters: composition/stoichiometry, stacking of different layered materials or interface engineering. This trend in materials discovery is expected to continue because of the increased theoretical capability to sort quickly candidate structures, to control atomistic processes and to use characterization techniques of higher resolution and acquisition speed. Recent examples of this successful strategy is the enhancement of the superconducting temperatures in ultrathin films [12, 13]. In films of topological insulators it was predicted and verified that edge states exist at the surface. The edge states are conducting with persisting currents (i.e. no channels exists to scatter into) which results in dissipation-less surface transport (while the bulk is still insulating) [14].

Truly 2-d materials of unusual uniformity can be grown with metal intercalation. This is a promising route to either use the intercalated metal to modify the graphene properties; or to optimize layer quality since graphene overgrows a step like a carpet and the metal monolayer will be an ideal

"infinite" 2-d system. In most cases the intercalation is controlled by kinetics since the metal atoms deposited on top need to move below. Because of the strong sp^2 bonds of graphene within the plane it is energetically costly for the metal atoms to diffuse through graphene. Every metal requires finding the optimal parameter 'window" of deposited amount, annealing temperature and time.

The FWP will grow intercalated quantum materials and search for ways to tune their band structure. The grown heterostructure X1-G or X1-G-X2 will consist of the intercalated metal X1 below; of graphene G; and possibly a different metal X2 on top. Such structures are novel heterostructures since they are protected and their combined electronic structures can result in interesting properties. i.e. topological insulators, Rasbha metals, 2-d electron gas in an effective magnetic field; etc, Such heterostructures posed new opportunities of synthesis/growth. They will be grown on graphene and graphite.

Intercalated metals can produce novel 2-d quantum materials and phases. For example Ca intercalation in graphene was shown to be a 2-d superconductor with T_c ~4K[14]. Pb intercalated below graphene induces magnetism to graphene because of the large Spin Orbit coupling of the Pb atoms[10]. This magnetizes graphene and produces unusually sharp Landau levels in the STS spectra. The location of the metal below, whether in contact with graphene or in deeper layers below,has different effects on the band structure and the emerging properties[16].

The Ames group has extensive experience in growing 2-d materials of unusual perfection (graphene) because the controlling barriers (for diffusion and nucleation) are first measured to select the optimal growth conditions. The bottom up approach, using 2-d materials as stacks, gives additional possibilities to realize technologically promising structures. Layered dichalcogenides by themselves or as combinations are a very promising playground for topological and Weyl materials. By combining 2-d into heterostructures, i.e., putting a non-superconducting topological material on top of a non-topological superconductor, it is possible to engineer novel topological phases. Nanostructures of a few layers thickness, have also the possibility to select by electron confinement specific electronic orbitals in the electron-electron interaction and "engineer" the preferred Hamiltonian experienced by the electrons in the layer. Considerable experience in electron confinement , especially for Pb films, will enable the group to exploit the emerging physics of the overlap between topology and confinement.

Interface effects. These artificial materials are also special because they have several interfaces that should be of the highest quality, i.e., with strongest, seamless coupling of the electrons across the interfaces. A promising area is to grow one type of 2-d material (i.e. dichalcogenides) on a different 2-d material (i. e. graphene) and this can be used as a "knob" to tune further the electronic response. These materials usually involve substrates so the physics at the interfaces (charging, doping, bonding, step density, coincidence Moire lattices, few-layer-films, instead of single laayers etc) play a more critical role in downgrading the targeted properties. Measuring thickness very precisely in 2-d materials (whether they are single or bilayer or in some cases a mixture of the two) is essential, because the band structure will be different. Attaining large domains of the grown films is important, since technically the energy dispersion is sharp only for infinite size systems. Defects and disorder should be minimized, otherwise they act as perturbations that can destroy the pre-designed band structure.

Moire patterns arising between the lattice of the 2-d material and the underlying substrate are also relevant, since they can introduce additional longer range periodicities in the potential experienced by the electrons and can modify the energy spectra. These heterostructures provide an alternative way to create essentially perfect long range patterns with "unit cells" of a few nanometers. Recent work of the group on graphene has shown similar, persisting periodicities (originating at the graphene-SiC interface) in STM, SPALEED patterns and ARPES spectra with A. Kaminki in the Complex States FWP; despite increasing graphene thickness [17]. This is very surprising since with thickness interface effects should be reduced. The team has these unique complementary capabilities to probe buried interfaces (and how they affect the graphene electron potential).

Complementary 2-d material characterization Ultrathin films will be grown epitaxially and characterized with STM and high resolution electron diffraction(SPALEED) to confirm their perfection. Once the optimal growth conditions are identified the same structures will be grown in situ and/or

transferred (after capped) to be characterized with ARPES to correlate band structure to real space structure. The films are practically in all cases metastable grown far from equilibrium. The outcome depends crucially on the growth parameters and requires efficient search to explore the phase space to select the targeted structure. The team is well experienced in identifying the atomistic processes and in measuring the key controlling parameters, so the growth outcome can match the morphology of interest. Predictive atomistic-level modeling of the kinetics will characterize film structure, including defects and roughness[18]. This modeling will be integrated with DFT calculations of the key thermodynamic and kinetic parameters. The quality of the ARPES spectra will be correlated to the quality of the morphology observed in the STM and diffraction scans.

The unusual combination of the techniques available will be the great advantage for the project and can lead to better realization of the promising structures. The need to grow structures of low dimensionality and the corresponding benefits have been sought for many years in condensed matter physics; when the bottom up growth (epitaxial) was developed it was another avenue to build 2-d systems. As conjectured in an earlier Physics Today article [17] the possibility to grow such ideal atomically uniform films , especially less than ~10 layers, will asses a truly novel regime in 2-d physics and elucidate deeper understanding of the fundamental physics. In this respect the growth of Pb/Si(111) discovered in Ames 15 years ago has initiated broad interest recently in the community and has become the benchmark over the last 5 years, used by outside groups, to confirm the laws obeyed by 2-d superconductors [19-22]. The proposed future activity on 2-d materials and the complementary characterization in real, reciprocal and energy spaces will enable such fundamental studies locally, because they crucially depend on the ability to grow morphologically ideal systems. The team has shown how the morphology of epitaxially grown nanostructures be optimized once the key atomistic barriers have been measured (diffusion barrier, cohesive energy, adatom interactions [18]).

References

1.X. Liu, et al , " *Progress in Surface Science*, **90**, 397-443 (2015)
2. D. McDougall, et al *Carbon*, **108**, 283-290 (2016)
3. P 9.X. J. Liu, et al *Nano Research*, **9**, 1434-1441 (2016)
4. Ann Lii-Rosales et al Carbon (submitted)
5. M. Jalochowski, et al *Physical Review Letters*, **116**, 086101 (2016)
6. Xu X, et al. , *Nature Physics* , 10 343 (2014)),
7.G. Bian, et al. *ACS Nano* 10, 3859 (2016),
8. S. Ichinokura et al., *ACS Nano* 10, 2761 (2016)),
9. Xu, Su-Yang et al. Nature Physics 11(9) 748 (2015)
10. F. Calleja, et al. *Nature Physics* 11 43 (2015
11. H. Nam, et al PNAS. 113 no. 38 10513–10517 (2016)
12.Gozar, A. *et al*. *Nature* 455, 782–785 (2008),
13. Jian-Feng Ge et al. , *Nature Materials* 14, 285–289 (2015)
14. Hsieh, D., et al., *New Journal of Physics*, 2010. 12: p. 125001
15. S. Ichinokura et al *ACS Nano* 2016, 10, 2761−2765
16.M. Kim et al . *Carbon* 123 93 (2017)
17. L Huang, et al *Phys. Rev. B* **96**, 035411 (2017)
18 J .W. Evans, et al. *Surf. Sci. Reports* 61 1
19. Goldman A M and Markovic N 1998 Phys. Today 51 39 11
20. Zhang T et al 2010 *Nat. Phys.* 6 104
21. Guo Y et al 2004 *Science* 306 1915
22. Brun C et al 2014 *Nat. Phys*. 10 444

Publications published by the FWP from Previous Support (FY 2015-2017)

1.Liu X.J.; Wang C.Z.; Lin H.Q.; Chang K.; Chen J.; Ho K.M. *Physical Review B* 2015 91, 035415.
2.Kwolek E.J.; Widmer R.; Groning O.; Deniz O.; Walen H.; Yuen C.D.; Huang W.Y.; Schlagel D.L.; Wallingford M.; Thiel P.A. *Inorganic Chemistry* 2015 54, 1159-1164
3.Souto-Casares J.; Chan T.L.; Chelikowsky J.R.; Ho K.M.; Wang C.Z.; Zhang S.B. *Physical Review B* 2015 92, 094103.
4. T. L. Chan, J. Souto-Casares, J. R. Chelikowsky, K. M. Ho, C. Z. Wang, S. B. Zhang, *Solid State Commun.* **217**, 43-46 (2015).

5.H. Hattab, M. Hupalo, M.T. Hershberger, M. Horn von Hoegen, and M.C. Tringides, *Surface Science* 646 50 (2016)
6.M. Jalochowski, R. Zdyb, and M. C. Tringides, *Physical Review Letters*, 116, 086101 (2016). 10.1103/PhysRevLett.116.086101
7.X. Liu, Y. Han, J. W. Evans, A. K. Engstfeld, R. J. Behm, M. C. Tringides, M. Hupalo, H.-Q. Lin, L. Huang, K.-M. Ho, D. Appy, P. A. Thiel, and C.-Z. Wang, " *Progress in Surface Science*, 90, 397-443 (2015). 10.1016/j.progsurf.2015.07.001
8.X. Liu and C.-Z. Wang, *RSC Advances*, **6**, 64595-64604 (2016)
9.X. J. Liu, C. Z. Wang, M. Hupalo, H. Q. Lin, K. M. Ho, P. A. Thiel, and M. C. Tringides, *Nano Research* 1434-1441 (2016).
10.L. L. Wang, D. D. Johnson, and M. C. Tringides *Phys RevB* 92 245405 (2015)
11.W. Zhang, W. C. Lu, H. X. Zhang, K. M. Ho, and C. Z. Wang JCMP **28**, 115001 (2016)
12.Z. J. Ye, A. Martini, P. Thiel, H. H. Lovelady, K. McLaughlin, and D. A. Rabson, *Physical Review B*, 93, 235438 (2016)
13.W. Zhang, W. C. Lu, H. X. Zhang, K. M. Ho, and C. Z. Wang, *Carbon*, **110**, 330-335 (2016)
14. X. J. Liu, C. Z. Wang, M. Hupalo, K. M. Ho, P. A. Thiel, and M. C. Tringides, *Physical Chemistry Chemical Physics*, **18**, 31238-31243 (2016). 10.1039/c6cp05639c
15.A E. J. Kwolek, H. Lei, A. Lii-Rosales, M. Wallingford, Y. Zhou, C.-Z. Wang, M. C. Tringides, J. W. Evans, and P. A. Thiel, *The Journal of Chemical Physics*, **145**, 211902 (2016)
16.D. McDougall, H. Hattab, M. T. Hershberger, M. Hupalo, M. H. von Hoegen, P. A. Thiel, and M. C. Tringides, *Carbon*, **108**, 283-290 (2016)
17.N. A. Anderson, Q. Zhang, M. Hupalo, R. A. Rosenberg, M. C. Tringides, and D.Vaknin J. Appl. Phys. 121, 014310 (2017)
18.X. J. Liu and C. Z. Wang, *JCMP* **29**, 185504 (2017)
19N. A. Anderson, Q. Zhang, M. Hupalo, R. A. Rosenbergb , J. W. Freeland , M. Tringides, D. Vaknin *Journal of Magnetism and Magnetic Materials* 435 212 (2017)
20L. Huang, Y Wu, D. Mou. M C. Tringides, M. Hupalo and A. Kamisnki *Phys. Rev. B* 96, 035411 (2017)
21M. Kim, M. C. Tringides, M. T. Hershberger, S. Chen, M. Hupalo, P. A. Thiel, C.Z. Wang, and K. M. Ho *Carbon* 123 93 (2017)
22 C. Brand, S. Muff, M. Fanciulli, H. Pfnür, M. C. Tringides, J. H. Dil, and C. Tegenkamp *Phys. Rev. B 96*, 035432 (2017)
24. A. Lii-Rosales, Y. Zhou, M. Wallingford, C.Z. Wang, M. C. Tringides, and P. A. Thiel *Physical Review Materials* 1, 026002 (2017)
25.D. Appy, M. Wallingford, D. Jing, R. Ott, M. C. Tringides, G. Richter, and P. A. Thiel JVST A 35, 061401 (2017)
26. Yong Han, A. Lii-Rosales, Y. Zhou, C.-J. Wang, M. Kim, M. C. Tringides, C.-Z. Wang, P. A. Thiel, and James W. Evans *Physical Review Materials (accepted).*

This page is intentionally blank.

University Grants' Abstracts

Electrodeposition of metals in viscoelastic liquid electrolytes

Lynden A. Archer and Donald L. Koch, School of Chemical & Bimolecular Engineering, Cornell University

Program Scope

Electrodeposition is used in manufacturing processes for creating metal, colloid, and polymer coatings on conductive substrates. The process also plays an important role in electrochemical storage technologies based on batteries, where it must be carefully managed to facilitate stable and safe operations at low operating temperatures, high rates and over many cycles of charge and discharge. In all currently used electrolytes deposition is subject to a variety of hydrodynamic and morphological instabilities at both low and high current densities, which lead to complex transport phenomena in the electrolyte and unstable deposition, including formation of ramified structures known as dendrites. These instabilities were first studied in the context of electroplating, where it was found to be remarkably difficult to achieve uniform deposition of many metals. They have received renewed interest due to the role unstable electrodeposition plays in creating metallic dendrites implicated in the failure of microcircuits and in the failure of high-energy lithium and emerging sodium-metal batteries by internal short circuits. The proposed research employs experiment, theory, and numerical approaches to understand the effect of elasticity in liquid electrolytes on the stability of electrodeposition. A related goal of the study is to develop design principles for viscoelastic liquid electrolytes that are able to stabilize electrodeposition at low and high current densities. The project is designed to evaluate the hypothesis that liquid electrolytes comprised of semidilute, entangled solutions of high molecular weight polymers (M_w > 1 x 10^6 g/mol) with high, liquid-like ion mobilities should be able to stabilize electrodeposition by multiple processes (Figure 1), including fundamental changes in convective flow produced by polymer stresses, polymer adsorbtion at and retardation of ion transport to dendrite nucleates, osmotic resistance to ion concentration at dendrite tips, and polymer drag on a bulk electrolyte. All of these effects originate from the assumption that polymer chains move more slowly than solvent molecules or ions in solution.

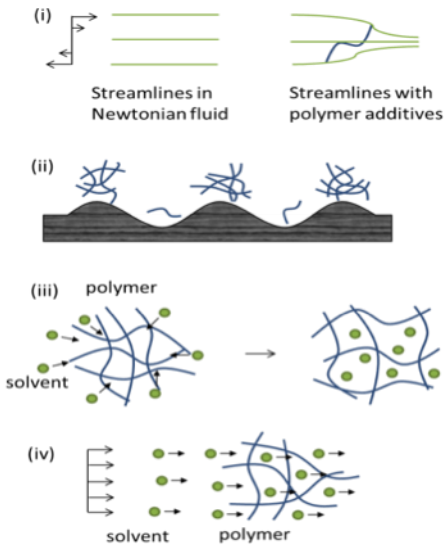

Fig. 1 Possible stabilizing mechanisms introduced by high molar mass polymer additives in a liquid electrolyte.

.

Recent Progress

1. Electroconvection drives morphology

It is commonly assumed in the literature that electroconvection is the primary driving force for morphological instabilities leading to dendrite growth. However, this relationship has never been fully established theoretically. In this component of the study, we show the very close relationship between the growth rate predicted in a linear stability analysis for a purely electroconvective (*E*) instability and a combined electroconvective and morphological (*E*+*M*) instability in a Newtonian fluid. The only difference between the two problems is that the former contains an electrode that grows due to the transport of cations to the surface, while the latter consists of a stationary electrode surface.

We performed linear stability analysis [1] of these equations and found the growth rate for the combined morphological and electroconvective instabilities can be captured by the following algebraic equations,

$$\sigma = \frac{\frac{v_m}{F} k_c J}{1 - \frac{\varepsilon V_0^2 \left(D_c + D_a\right)}{16 \eta_F D_c D_a} \frac{k^2}{\left(k + k_c\right)^2} + \frac{v_m J \left(D_c + D_a\right)}{4 D_c D_a F} \frac{2k + k_c}{\left(k + k_c\right)^2}} \tag{1}$$

$$k_c = \sqrt{k^2 + \frac{\sigma\left(D_c + D_a\right)}{2 D_c D_a}} \tag{2}$$

Whence, the purely electroconvective instability can be shown to grow at the following rate,

$$\sigma = k^2 \left[\frac{\varepsilon V_0^2}{8 \eta_F} - \sqrt{\frac{\varepsilon V_0^2 D_c D_a}{\eta_F \left(D_c + D_a\right)}} \right] \tag{3}$$

Thus, it is seen that for voltages $V_0 \le 8\sqrt{\eta_F D_c D_a / \varepsilon\left(D_c + D_a\right)}$, the growth rate for the electroconvectivity is negative for all inhomogeneity length scales, and electroconvection is stable. This observation is identical to the corresponding result obtained by Rubinstein and Zaltzman [2]. The variation of the growth rate with wavenumber of *E* and *E*+*M* instabilities is shown in Fig 2. It is apparent that the growth rates of the two instabilities are very close at all wavenumbers with a scaling of k^2, reflective of the result for the electroconvective instability. The results clearly show that electroconvective instability dominates and growth of the interface is strongly driven by hydrodynamics, with the contribution of the diffusive mechanism being negligible.

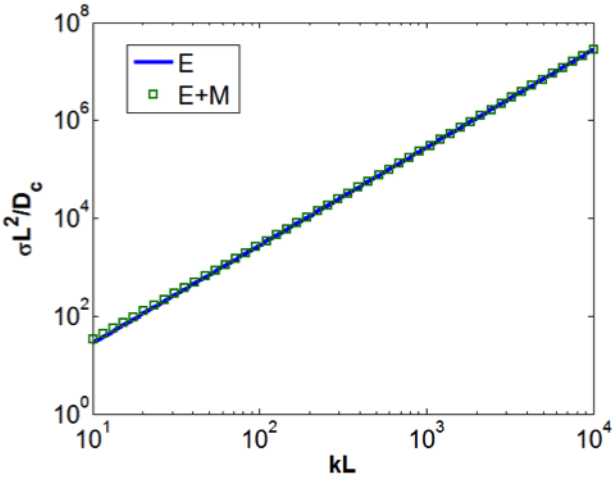

Fig. 2 Linear growth rates of the purely electroconvective (*E*) and morphological (*M*) instabilities in a Newtonian fluid.

2. Polymer Additives Suppress Electroconvection and thereby Influence Morphology

A direct consequence of the result in *Eq* (3) is that electroconvection should be stable over a range of voltages, $V_0 \leq \frac{8F}{RT}\sqrt{\eta_F D_c (1-t_c)/\varepsilon}$. This means that stable interfacial ion transport should be observed in a Newtonian liquid electrolyte over a voltage range, $\Delta V = \frac{RT}{F} V_0 - V_c$ that, for a fixed cation transference number t_c, increases as $\sqrt{\eta_F D_c}$. For simple dilute liquid electrolytes, $D_c : 1/\eta_F$, and the stable voltage range is not a function of electrolyte viscosity. The situation is different in a viscoelastic electrolyte composed of a semidilute, entangled solution of a high molecular weight neutral polymer in a high-dielectric constant liquid host. In that case ions are able to move freely in the solvent network defined by polymer chain entanglements and $D_c : 1/\eta_s$, where η_s is the solvent viscosity. This means that in the viscoelastic electrolyte, $\Delta V : \sqrt{\eta_F / \eta_s}$ and a slow-moving network of long chains would have a large stabilizing effect on electroconvection, but almost no effect on conductivity.

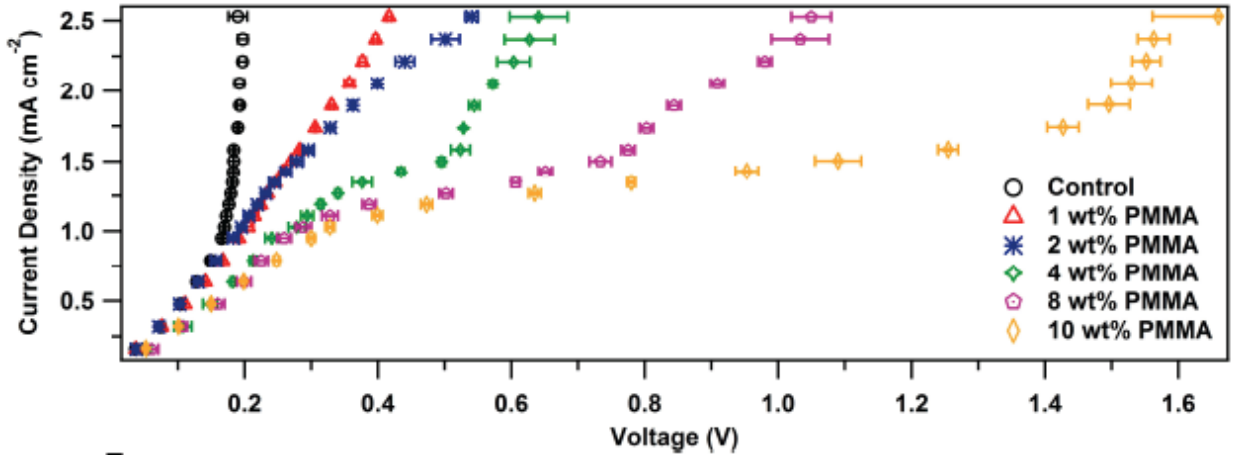

Fig. 3 Current-voltage curve for viscoelastic electrolytes as a function of polymer concentration

We tested this prediction experimentally using current-voltage (*i*-*V*) measurements in an electrochemical cell in which the voltage scan rate is maintained low, such that ion transport limits the electrodeposition rate, and the results are shown in Figure 3. To create electrolytes in which ion and momentum transport pathways are uncoupled, the study focused on semidilute solutions of high molecular weight (M_w ~ 1.5 x 10^6 g/mol, M_w/M_n = 1.1), atactic poly(methyl methacrylate) (*PMMA*) (Agilent Technologies), dissolved in a EC/PC-1M bis(trifluoromethane) sulfonimide lithium (LiTFSI) electrolyte. At low current densities, an Ohmic region is observed in electrolytes with and without PMMA and the slope of the *i*-V curve is a weak function of polymer concentration. In the control cells, the Ohmic region is immediately followed by a second regime in which current increases much faster than linear with *V*. This stands in sharp contrast to the *i*-V curve obtained upon addition of just 1wt% of the polymer to the electrolyte,

where the diffusion controlled Ohmic regime extends to voltages more than ten-times the thermal voltage (RT/F). At a PMMA concentration of 4wt% a clear plateau is observed over a range of voltages, indicative of diffusion-limited transport. At yet higher polymer concentration, the diffusion-limited transport regime extends further, becoming more than forty-times the thermal voltage at 10wt% polymer, and the high-voltage slope of the *i*-V curve is lower. These results imply that the presence of even small amounts of high molar mass polymer in the electrolyte is highly effective in reducing overlimiting conductance, known to originate from mixing effects produced by electroconvection instability.

Future Plans

Figure 4 shows how the width ΔV of the *i*-V plateau deduced from Fig. 3 varies with electrolyte viscosity. It is apparent that the results support a scaling relation of the form $\Delta V : \eta_F^{1/4}$, which is substantially weaker than expected from the linear stability analysis. We suspect that orientation of polymer chains near the interface is responsible for this weaker than predicted relationship. More direct information about the effect of electrolyte viscoelasticity on electroconvenction is required to ascertain this and to develop a broader understanding of the origin of viscoelastic stabilization. Research during the next year will study the motions of neutrally buoyant tracer particles dispersed in Newtonian and viscoelastic liquid electrolytes to characterize the effect of electrolyte elasticity on electroconvection. By performing these experiments in tandem with direct numerical simulations of various viscoelastic fluid models, we will be able to identify the polymer-scale physical phenomena that produce enhanced stability and which are responsible for the expanded i-V plateaus in Figs. 3 and 4. Finally, by directly studying how the interface evolves during electrodeposition, we will be able to assess the effect of electrolyte viscoelasticity on the combined *E* and *M* instabilities.

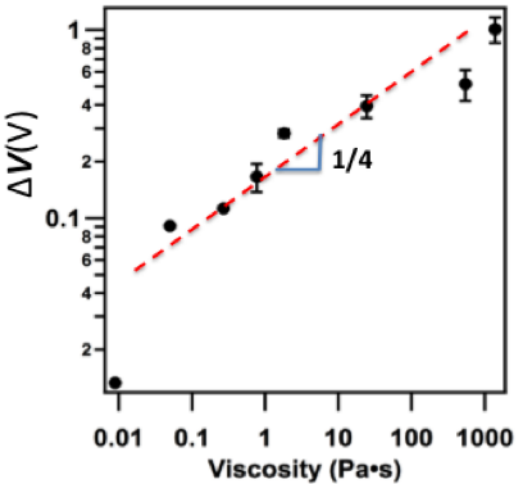

Fig. 4 Width of limiting current regime versus electrolyte viscosity. The line through the data is a power-law fit, $\Delta V : \eta_F^{1/4}$.

References

[1] Tikekar, M. D., Archer, L. A., and Koch, D. L., Stabilizing electrodeposition in elastic solid electrolytes containing immobilized anions, *Sci. Adv.*, **2 (7)**, e1600320 (2016)

[2] Rubinstein, I. & Zaltzman, B., Electro-osmotically induced convection at a perm-selective membrane, *Phys. Rev. E* **62**, 2238-2251 (2000)

Publications

[1] Wei, S., Cheng, Z., Nath, P., Tikekar, M. D., Li, G., and Archer, L. A., Stabilizing electrochemical interfaces in viscoelastic liquid electrolytes, *Submitted* (2017)

Anisotropic Template-Less Substrate-Driven Synthesis of Graphene Nanoribbons

Michael S. Arnold, Department of Materials Science and Engineering, University of Wisconsin-Madison

Program Scope

We have discovered how to drive graphene crystal growth with a giant shape anisotropy via chemical vapor deposition (CVD).[1] This anisotropy is not only fundamentally intriguing from the perspective of 2D materials crystal growth but is remarkable because it enables the direct synthesis of narrow, long, and oriented nanoribbons of graphene with smooth edges that are semiconducting. This giant anisotropy has been achieved on the surface of a Ge(001) single-crystal. Not only are the growth kinetics highly anisotropic, but the Ge(001) surface uniquely interacts with the evolving graphene crystals to facet them with atomically smooth, armchair (as opposed to zigzag) edges. The resulting long and narrow crystals are, in essence, ribbons that have uniform width from end-to-end, with a width that can be rationally tuned from 0 to 100's of nanometers by controlling the growth duration.

Nanoribbons are important materials because unlike continuous sheets of graphene, which are semimetals, nanoribbons (that have the proper types of edges and that are less than 10 nm in width) are semiconductors that can also demonstrate novel edge-derived phenomena. The synthesis of nanoribbons on Ge overcomes many of the synthetic roadblocks that have previously limited the field. However, there are still many fundamental challenges that must be addressed in order to both understand and control the synthesis.

The overarching objective of this project is to both understand and control the highly anisotropic crystal growth and nucleation of graphene and graphene nanoribbons via CVD. The activities in this project are designed to address three goals related to this overarching objective:

A. Understanding anisotropic crystal growth kinetics and armchair edge-faceting on Ge(001);
B. Determining and dictating where nanoribbon nucleation and growth occur; and,
C. Tailoring substrate composition and designing graphene templates for heterogeneous synthesis.

Recent Progress

1) Without seeds, nanoribbons stochastically nucleate at random locations at random times on Ge(001), yielding unorganized ensembles of nanoribbons with substantial width and bandgap polydispersity whereas parallel arrays of homogeneous nanoribbons are wanted for eventual technological applications. We have recently completed a study on the seeded synthesis of graphene on Ge(001). The study provides significant insight into the origins of anisotropic crystal growth phenomena on Ge(001) while enabling the seeded synthesis of organized, parallel arrays of unidirectionaly aligned nanoribbons with substantially reduced polydispersity.

The use of seeds is fundamentally interesting because it decouples nucleation and growth, controls where growth occurs, and allows graphene to grow with lattice orientations that do not spontaneously form without seeds. We have discovered that high-aspect nanoribbons can be seeded only if the armchair crystallographic orientation of the seeds (parallel to the C – C bonds) is aligned with Ge⟨110⟩. In contrast, increasing misorientation from Ge⟨110⟩ yields decreasingly anisotropic crystals (Fig. 1). Attachment-limited kinetics dictate the growth velocity of each edge (Fig. 2), in which the attachment rate depends on the angle of the edge with respect to Ge⟨110⟩ – as opposed to fast diffusion along Ge⟨110⟩. Measured growth rate data are used to generate a construction analogous to a kinetic Wulff plot that quantitatively predicts the shape of graphene crystals on Ge(001). This knowledge is employed to fabricate regularly-spaced, unidirectional arrays of nanoribbons and to significantly reduce their polydispersity. These results show that seed-initiated graphene synthesis on Ge(001) will be a viable route for creating wafer-scale arrays of narrow, semiconducting, armchair nanoribbons with rationally-controlled placement and alignment for a wide range of semiconductor technologies.

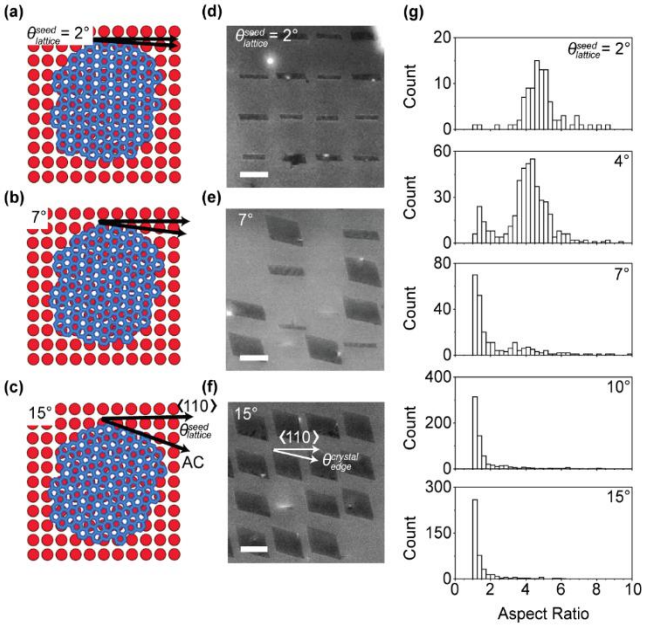

Figure 1. (a-c) Schematics of graphene seeds on Ge(001) with $\theta_{lattice}^{seed}$ of 2° (a), 7° (b), and 15° (c). Only the top layer of Ge atoms is shown. (d-f) SEM images of representative graphene crystals grown from seeds with $\theta_{lattice}^{seed}$ of 2° (d), 7° (e), and 15° (f). Scale bars are 400 nm. (g) Histograms showing the distribution of aspect ratio for ribbons grown from seeds with $\theta_{lattice}^{seed}$ = 2°, 4°, 7°, 10°, and 15°.

We have also learned that the controlled introduction of part per million O_2 into the CVD chamber during synthesis rotates the crystals anywhere from 3° to 17°; that unidirectional alignment of nanoribbons is possible on miscut Ge; and that nanoribbons with extremely high aspect ratios > 200 can be grown in a low-CH_4 regime.

2) We have elucidated the charge transport properties of sub-10 nm wide nanoribbons grown on Ge(001) for the first time and realized nanoribbons with exceptionally high on-state conductance and conductance modulation.

We have grown a polydisperse mixture of nanoribbons of width varying from ~5 to 30 nm and developed a protocol that allows the transfer of the ribbons to dielectric on silicon substrates for charge transport measurements. The measurements indicate that nanoribbons grown on Ge(001) can achieve both a high on-state conductance of 6 μS and a high on/off conductance modulation

ratio of 5×10^4 (at room temperature), favorably comparing to or exceeding the performance of nanoribbons fabricated by other methods (Fig. 3) and motivating future research into this promising approach for nanoribbon synthesis.

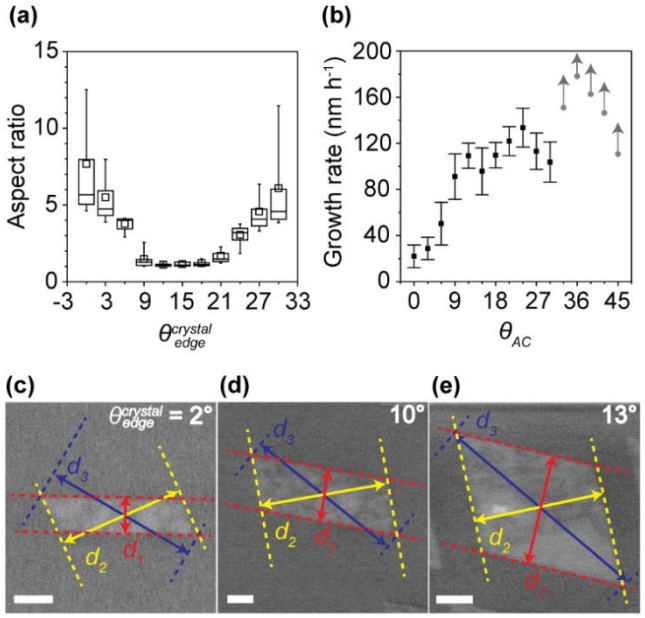

Figure 2. (a) Aspect ratio *versus* $\theta^{crystal}_{edge}$ (the misorientation between the crystal long-edge and the nearest Ge⟨110⟩ direction). (b) Growth rate *versus* the angle between the armchair direction of each edge and Ge⟨110⟩. Black data points are physical measurements, while the gray data points are lower bounds. (c-e) SEM images of representative ribbons with $\theta^{crystal}_{edge}$ = 2° (c), 10° (d), and 13° (e) in which Ge[110] and Ge[1$\bar{1}$0] are horizontal and vertical to the image. The magnitude of arrows provide growth rate data. Only a lower estimate for d_3 can be determined, because this plane does not bound the crystal. Scale bars are 100 nm.

3) We have studied the templating of block copolymers using van der Waals templates of graphene, realizing surprisingly high density multiplication factors by using self-defined nanoribbons as templates. Block copolymers are important because they are capable of self-assembling into well-ordered patterns that can be used for lithography with feature sizes below the resolution of conventional optical lithography. Supported post-doc Jacobberger has discovered and shown that block copolymers register to graphene nanoribbon templates on germanium, yielding exceptionally high density multiplication factors greater than 20, which means that block copolymers can self-assemble with feature sizes of *w*/20 when assembled on nanoribbon patterns of width *w* (Fig. 4). A perpendicular lamellar microstructure develops selectively on the graphene. The assembly and multiplication is implemented using a block copolymer previously developed by our collaborators in Paul Nealey's group at the University of Chicago. The mechanism is not yet clear but is believed to originate from the chemical contrast between the graphene and Ge surface and the smooth graphene ribbon edges.

4) We have collaborated with groups of P. Desarjdins, R. Martel, and O. Moutanabbir at Ecole Polytechnique de Montreal and the University of Montreal on the templated heteroepitaxy of InP on Ge using interlayers of graphene templates to decouple inter-layer bonding.

In these studies, InP has been grown on graphene templates via cold wall metal-organic chemical vapor deposition (MOCVD) at Montreal, resulting in InP nanowires, micrometer-scale crystals, and films with high quality graphene/InP interfaces. In some cases, the crystals are polytypic, switching over nanometer length scales between zinc-blende phase and wurtzite phases, which is uncommon in InP, affords the creation of type-II homojunctions, and will be studied in more detail in future experiments.

Future Plans

• Determine the C_xH_y hydrocarbon species building unit responsible for nanoribbon growth by performing pressure- and temperature-dependent growth kinetics measurements. Calculated energy barriers from collaborators in Manos Mavrikakis' group (UW-Madison) will be used to confirm conclusions drawn from the experimental data.

• Complete O_2 dependence experiments. We will use LEED/LEEM to understand if the crystallographic orientation of the crystals changes with increasing O_2 or if crystallographic orientation is fixed and the edge faceting of the crystals is changing.

• Implement smaller, denser arrays of seeds.

• Perform charge transport measurements on nanoribbon arrays and characterize their edge structure and crystallinity as a function of synthesis and processing approaches and parameters.

• Investigate synthesis on related technologically relevant substrates.

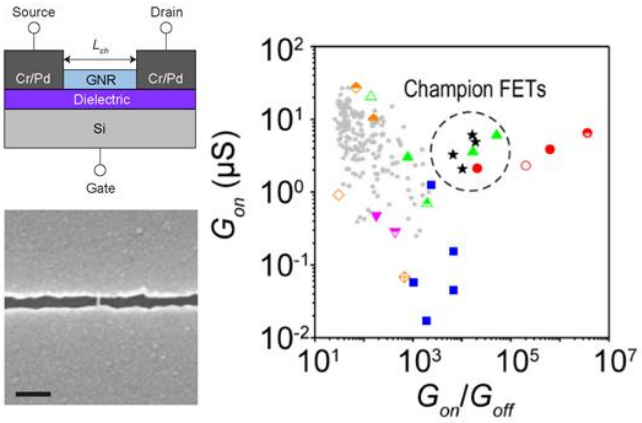

Figure 3. (Left top) Schematic of nanoribbon transport measurement architecture in which a nanoribbon channel is contacted by Cr/Pd/Au and the Si substrate serves as the back gate to modulate the nanoribbon charge density. (Left bottom) SEM image of a nanoribbon channel with apparent width of ~7 nm and L_{ch} of ~25 nm. (Right) Comparison of the on-state conductance (G_{on}) versus G_{on}/G_{off} at room temperature for nanoribbons synthesized on Ge(001) via CVD (black and gray stars) compared to those reported in literature with $G_{on}/G_{off} > 30$.

References

1. **Jacobberger RM**, Kiraly B, Fortin-Deschenes M, Levesque PL, McElhinny KM, **Brady GJ**, Rojas Delgado R, **Singha Roy S**, Mannix A, Lagally MG, Evans PG, Desjardins P, Martel R, Hersam MC, Guisinger NP, **Arnold MS,** *Direct Oriented Growth of Armchair Graphene Nanoribbons on Germanium*, NATURE COMMUNICATIONS, 6, 8006 (2015).

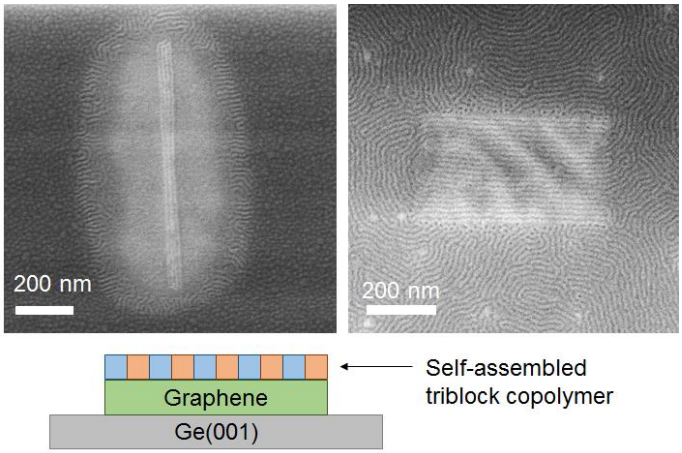

Figure 4. Templating block copolymers. The block copolymer self-assembles so that it runs parallel to the long-axis of the ribbons (top left). Density multiplication > 20 can be achieved (top right).

Publications (and Patents)

1. B. Kiraly, **R. M. Jacobberger**, A. J. Mannix, G. P. Campbell, M. J. Bedzyk, **M. S. Arnold**, M. C. Hersam, N. P. Guisinger, *Electronic and mechanical properties of graphene–germanium interfaces grown by chemical vapor deposition*. NANO LETTERS 15, 7414 (2015).

2. **M. S. Arnold**, **R. M. Jacobberger**, *Oriented bottom-up growth of armchair graphene nanoribbons on germanium*, U.S. PATENT 9287359, March 15 (2016).

3. T.-H. Chang, S. Xiong, **R. M. Jacobberger**, S. Mikael, H. S. Suh, C.-C. Liu, D. Geng, X. Wang, **M. S. Arnold**, Z. Ma, *Directed self-assembly of block copolymer films on atomically-thin graphene chemical patterns*. SCIENTIFIC REPORTS 6, 31407 (2016).

4. B. Kiraly, A. J. Mannix, **R. M. Jacobberger**, B. L. Fisher, **M. S. Arnold**, M. C. Hersam, N. P. Guisinger, *Sub-5 nm, globally aligned graphene nanoribbons on Ge (001)*. APPLIED PHYSICS LETTERS, 108, 213101 (2016).

5. K. M. McElhinny, **R. M. Jacobberger**, A. J. Zaug, **M. S. Arnold**, P. G. Evans, *Graphene-induced Ge (001) surface faceting*. SURFACE SCIENCE, 647, 90 (2016).

6. P. F. Nealey, T.-H. Chang, S. Xiong, Z. Ma, **M. S. Arnold**, **R. M. Jacobberger**, *Atomic layer chemical patterns for block copolymer assembly*, U.S. PATENT APP. 15/215,016 (2016).

7. **S. Singa Roy**, **R. M. Jacobberger**, **C. Wan**, **M. S. Arnold**, *Controlling the density of pinhole defects in monolayer graphene synthesized via chemical vapor deposition on copper*. CARBON 100, 1 (2016).

8. L. Samad, S. M. Bladow, Q. Ding, J. Zhuo, **R. M. Jacobberger**, **M. S. Arnold**, S. Jin, *Layer-controlled chemical vapor deposition growth of MoS2 vertical heterostructures via van der Waals epitaxy*. ACS NANO 10 (7), pp 7039–7046 (2016).

9. L. Zhang, **S. Singha Roy**, **N. S. Safron**, M. J. Shearer, R**. M. Jacobberger**, **V. Saraswat**, R. J. Hamers, **M. S. Arnold**, T. L. Andrew, *Orientation Control of Selected Organic Semiconductor Crystals Achieved by Monolayer Graphene Templates*. ADVANCED MATERIALS INTERFACES 3 (22), 10.1002/admi.201600621 (2016).

10. **M. S. Arnold**, **A. J. Way**, **R. M. Jacobberger**. *Seed-Mediated Growth of Patterned Graphene Nanoribbon Arrays*, U.S. PATENT 9,761,669 (2017).

11. **R. M. Jacobberger**, **M. S. Arnold**, *High Performance Charge Transport in Semiconducting Armchair Graphene Nanoribbons Grown Directly on Germanium*. ACS NANO, In Press (2017).

12. R. Rojas Delgado, **R. M. Jacobberger**, **S. Singha Roy**, V. S. Mangu, **M. S. Arnold**, F. Cavallo, M. G. Lagally, *Passivation of Germanium by Graphene*. ACS APPLIED MATERIALS & INTERFACES, 9 (20), pp 17629–17636 (2017).

13. **Saraswat V**, **Jacobberger RM**, Ostrander J, **Hummell C, Way AJ**, **Wang J**, Zanni MT, **Arnold MS,** *Invariance of water permeance through size-differentiated graphene oxide laminates*, SUBMITTED (2017).

14. Rojas Delgado R, **Jacobberger RM**, **Singha Roy S**, Mangu VS, **Arnold M**S, Cavallo F, Lagally MG, *Passivation of Germanium by Graphene*, ACS APPLIED MATERIALS & INTERFACES, 9 (20), pp 17629–17636 (2017).

15. **A. J. Way**, **R. M. Jacobberger**, **M. S. Arnold**, *Seed-Initiated Anisotropic Growth of Unidirectional Armchair Graphene Nanoribbon Arrays on Germanium*, SUBMITTED (2017).

16. F. Anwar, C. R. Carlos, **V. Saraswat**, V. S. Mangu, **M. S. Arnold**, and F. Cavallo, SUBMITTED (2017)**.**

17. Campbell GP, Kiraly B, **Jacobberger RM**, Mannix AJ, **Arnold MS**, Guisinger NP, Hersam NC, Bedzyk MJ, SUBMITTED (2017).

18. Mukherjee, Nateghi, **Jacobberger**, Bouthillier, de la Mata, Arbiol, Coenen, Cardinal, Levesque, Desjardins, Martel, **Arnold**, and Moutanabbir, SUBMITTED (2017).

Elucidating Mechanisms of Nucleation and Growth in Atomic Layer Deposition

Stacey F. Bent
sbent@stanford.edu
Department of Chemical Engineering
Stanford University, Stanford, CA 94305

Program Scope

Atomic layer deposition (ALD) is a materials synthesis technique with potential to produce the precise, nanostructured materials needed in emerging energy conversion technologies. The fundamental nucleation and growth mechanisms of ALD can impact the properties of resultant thin film materials. The major goal of the project is to discover a framework of governing principles for ALD by performing fundamental studies to elucidate molecular-level reaction mechanisms and nucleation processes using both *in situ* and *ex situ* experimental tools complemented by theory. In the project, we focus on three exemplary ALD systems – 2D transition metal dichalcogenides, ternary metal oxides, and nucleation-enhancing surfaces.

Recent Progress

Our recent results have examined the mechanisms of nucleation and growth in three primary areas: mechanisms in ternary metal oxide ALD systems; growth of 2D materials; and deposition on nucleation–enhanced surfaces. We also set up a new quartz crystal microbalance tool for *in situ* mechanistic study.

Mechanisms of ternary metal oxide ALD

Ternary metal oxides have a wide variety of applications in nanotechnology, and one of their advantages is that their properties can often be controlled by tuning the composition of the materials. ALD provides a controlled manner of synthesis for these materials, but when combining two binary ALD processes into one ternary process, many non-idealities in growth often arise. To better understand the fundamental mechanisms that can lead to these non-idealities, we investigated both the zinc-tin-oxide (ZTO) and nickel-aluminum oxide ALD systems.

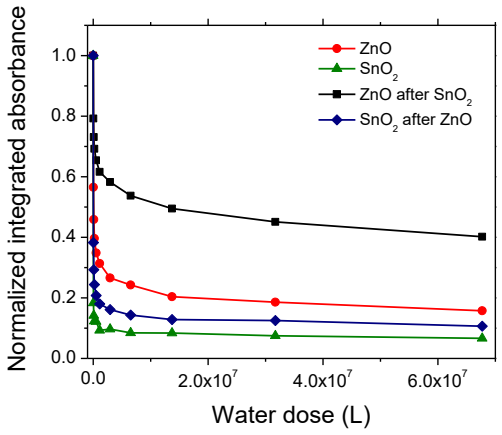

Figure 1. Integrated absorbance of C-H stretching peaks as a function of the water dose for SnO_2 ALD, ZnO ALD, the first cycle of ZnO ALD after SnO_2 ALD, and the first cycle of SnO_2 ALD after ZnO ALD at 150 ºC.

ALD of zinc-tin-oxide (ZTO). We applied *in situ* IR spectroscopy to ALD of zinc-oxide, tin-oxide, and ZTO. A major aim was to investigate the molecular basis for the nucleation delay during ALD of ZTO,

observed when ZnO ALD is carried out after SnO_2 ALD. Through gas-phase IR spectroscopy, we showed that dimethylamine, the main reaction product of the SnO_2 ALD process, is released not only during SnO_2 ALD but also when depositing ZnO after SnO_2, indicating incomplete removal of the ligands of the TDMASn precursor from the surface. *In situ* transmission IR spectroscopy performed during ALD on SiO_2 powder revealed that a significant fraction of the ligands persist during both SnO_2 and ZnO ALD. We also showed that the removal of precursor ligands by H_2O exposure is even less effective when ZnO ALD is carried out after SnO_2 ALD (Figure 1), which likely causes the previously-reported nucleation delay in ZnO ALD during the deposition of ZTO. These observations provide experimental evidence for a recently proposed cooperative mechanism, based on theoretical calculations, and may have broad implications for other ALD processes.

ALD of nickel aluminum oxide. The Ni-Al-O ternary process was studied using a nickelocene ($NiCp_2$) precursor, trimethylaluminum and ozone in a supercycle approach. Unlike the ZTO system, the growth rate was found to closely follow a linear combination of the individual steady state growth rates. However, composition of the as-deposited films was found to differ greatly from the expected rule of mixtures, with the films being nickel-deficient (see Figure 2). Synchrotron grazing incidence XRD studies performed at SSRL show that the crystallinity of nickel oxide decreases upon increasing aluminum composition, with the films becoming amorphous at a Ni-to-Al ratio of approximately 1:1. Based on the growth and composition of the as-deposited ternary films, the data suggests that aluminum oxide deposition is enhanced while nickel oxide is suppressed. This may be partially explained by the loss of crystallinity in the films, resulting in a decrease in the density of nickel. Ozone exposure and the presence of surface oxygen may also effect growth behavior.

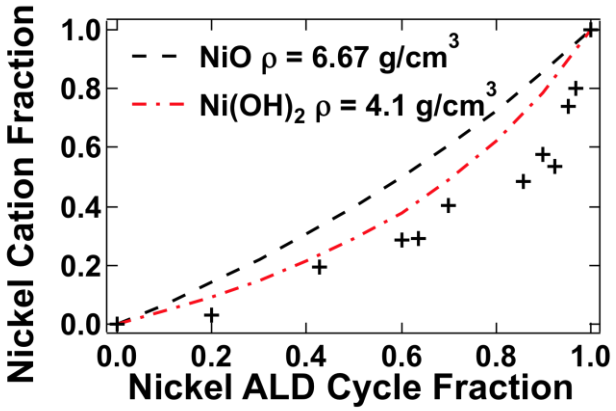

Figure 2: XPS composition of ternary ALD Ni-Al-O films as a function of nickel ALD cycle fraction.

Toward understanding nucleation of 2-D materials by ALD

We studied the processes of nucleation and growth of MoS_2 ALD using H_2S and $Mo(CO)_6$ as precursors with grazing incidence X-ray scattering (GISAXS). GISAXS data allows information about the size, shape, and geometry of the nucleating film to be extracted, and points to when the coalescence of the film occurs. Films with between 7 and 100 cycles of MoS_2 ALD growth on silicon oxide-covered Si(100) were examined *ex situ* at the Stanford Synchrotron Radiation Lightsource (SSRL). Although samples prepared with fewer than 7 cycles generated insufficient signal to model, higher numbers of cycles led to detectable scattering signal (see Figure 3). Our analysis indicates that the MoS_2 forms semi-spherical islands as it nucleates, then transitions from an island-growth regime by 100 ALD cycles.

Nucleation-Enhanced Surfaces

Achieving proper nucleation is one of the most important requirements for many applications of ALD, since the aim is frequently to deposit a continuous, conformal film, often at very small thicknesses. This research effort focuses on identifying surface pre-treatments that could enhance ALD nucleation. We also aim to better understand how the substrate surface properties affect the nucleation process in the initial stages of ALD.

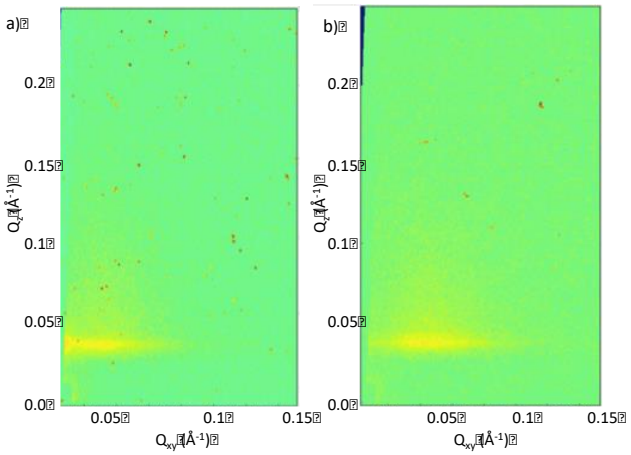

Figure 3. GISAXS data for (a) 85 ALD cycles and (b) 25 ALD cycles of MoS_2 deposited on native-oxide covered Si(100) wafers.

We identified a surface pre-treatment that enhances ALD nucleation. Initial results indicate that an NF_3 remote plasma surface pre-treatment on thermal silicon oxide surfaces improves nucleation in Pt ALD (Fig. 4). Further, our initial results show that a combination of the remote plasma treatment with exposure to air leads to a significant increase in surface hydrophilicity. The Pt ALD process is based on oxidative decomposition of the precursor ligands by dissociated O_2 adsorbed at the substrate surface. It is believed that the low abundance of these dissociated oxygen atoms in the initial stages of the ALD process leads to a nucleation delay. We postulate that the treatment provides oxygen-containing sites, facilitating nucleation and resulting in the higher growth rates of Pt. A surface reaction mechanism leading to increased surface hydroxyl groups is developed.

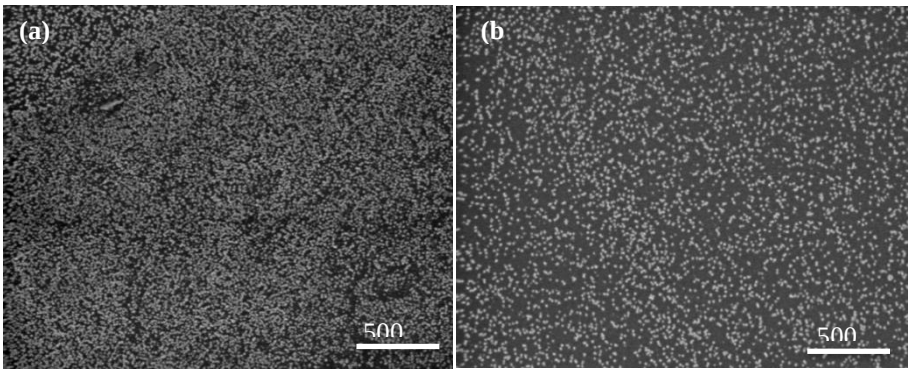

Figure 4. SEM image after 200 cycles Pt ALD on (a) SiO_2 surface treated with NF_3 remote plasma. Calculated apparent coverage is 46%. (b) untreated thermal SiO_2. Calculated apparent coverage is 19%. Scale bars represent 500 nm.

Future Plans

We plan to continue our studies of ternary metal oxide ALD. Studies will look at the interactions between precursors and the substrate, particularly the effect of ligand elimination. We will continue investigating the Ni-Al oxide system and expand to Ni-Fe-Al oxide films, a material with useful catalytic and optical properties, and will also begin studies of other ternary metal oxide systems.

We will expand our studies of nucleation behavior of MoS_2 ALD using synchrotron-based x-ray methods. We expect to extend the work to understand ALD of metals and metal oxides on the 2D materials. We will continue to develop the method of nucleation enhancement by plasma treatment and other substrate pre-treatments. The goal is to introduce a surface treatment that is largely independent of the underlying substrate and hence generalizable in ALD.

In each of these studies, we will continue to deploy and optimize our custom-built ALD systems will for use at SSRL and in our laboratory, for both *in situ* and *ex situ* XRD, x-ray scattering measurements, IR, XPS and QCM.

Publications

1. "A process for topographically-selective deposition on 3D nanostructures by ion implantation," W. H. Kim, F. S. Minaye Hashemi, A. J. M. Mackus, J. Singh, Y. Kim, D. Bobb-Semple, Y. Fan, T. Kaufman-Osborn, L. Godet, and S. F. Bent, *ACS Nano* **10** (2016) 4451–4458.

2. "Growth, intermixing and surface phase formation for zinc tin oxide nanolaminates produced by atomic layer deposition," C. Hägglund, T. Grehl, J. T. Tanskanen, Y. Yee, M. N. Mullings, A. J. M. Mackus, C. MacIsaac, B. M. Clemens, H. H. Brongersma and S. F. Bent, *J. Vac. Sci. Technol. A,* **34** (2016) 021516.

3. "Incomplete elimination of precursor ligands during atomic layer deposition of zinc-oxide, tin-oxide, and zinc-tin-oxide," A. J. M. Mackus, C. MacIsaac, W. H. Kim and S. F. Bent, *J. Chem. Phys*., 146 (2017) 052802, doi: 10.1063/1.4961459.

4. "Thermal adsorption-enhanced atomic layer etching of Si_3N_4," W. H. Kim, D. Y. Sung, S. Oh, J. Woo, S. K. Lim, H. J. Lee, and S. F. Bent, *J. Vac. Sci. Technol. A*, submitted.

In-situ Monitoring of Dynamic Phenomena during Solidification

A.J. Clarke (PI), A.W. Stokes, F.G. Coury, J.A. Jankowski (Colorado School of Mines)
D. Tourret, J.W. Gibbs, S.D. Imhoff, T.G. Holesinger, M.A. Espy, J.F. Hunter (Los Alamos National Laboratory)
K. Fezzaa, T. Sun (Advanced Photon Source, Argonne National Laboratory)
J.T. McKeown, J.D. Roehling (Lawrence Livermore National Laboratory)
J.D. Madison, T. Rodgers (Sandia National Laboratories)

Program Scope

Solidification of metallic alloys is spatially and temporally multi-scale. We use real-time imaging with electrons, x-rays, and protons at U.S. DOE National User Facilities to study metallic alloy solidification dynamics to inform, develop, and validate state-of-the-art computational models to achieve predictive capability (Fig. 1) [1-9]. Although we have primarily focused on real-time, two-dimensional (2D) and three-dimensional (3D) characterization of hierarchical solidification structures during synthesis to date, we are currently pursuing four-dimensional (4D) imaging (3D plus time) of aluminum-copper (Al-Cu) alloys during *controlled* directional solidification (e.g. Fig. 2). More recently, our focus has been on far from equilibrium processing, such as in-situ characterization of aluminum alloy microstructural evolution at the nanoscale during rapid solidification. We are also experimentally exploring the role of chemical and structural heterogeneities that develop during solidification on solid-state phase transitions in metallic alloys, with an emphasis on phase growth (diffusion- and interface-controlled) and kinetics, stability, and transition pathways. This new knowledge will lead to predictive alloy design and directed synthesis strategies to achieve mechanistic control of microstructural evolution to accelerate the discovery of new and improved materials with emergent properties.

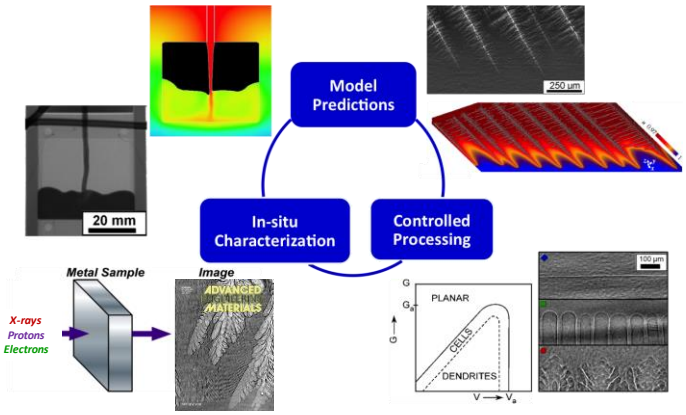

Fig. 1. Multi-scale prediction and control of metallic alloy solidification dynamics.

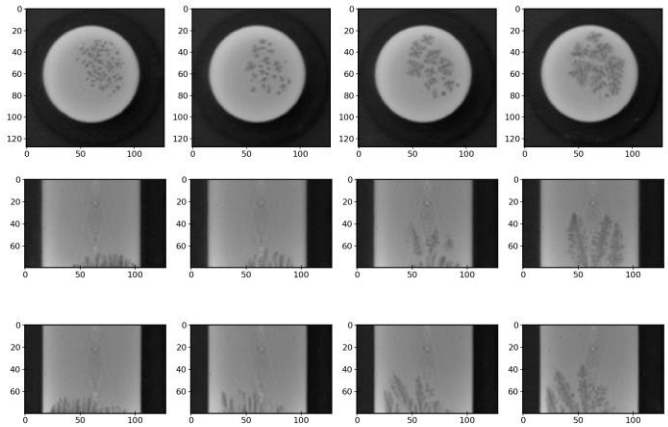

Fig. 2. Example synchrotron x-ray images obtained during a 4D microscopy experiment of controlled directional solidification of an Al-Cu alloy.

Recent Progress

Solidification theory predicts that combinations of thermal gradient (G) and solid-liquid interfacial velocity (V) dictate pattern formation and growth regime transitions [10,11]. Clarke *et al.* have recently studied microstructural selection in a dilute Al-Cu alloy by combining in-situ synchrotron x-ray imaging of 50+ controlled directional

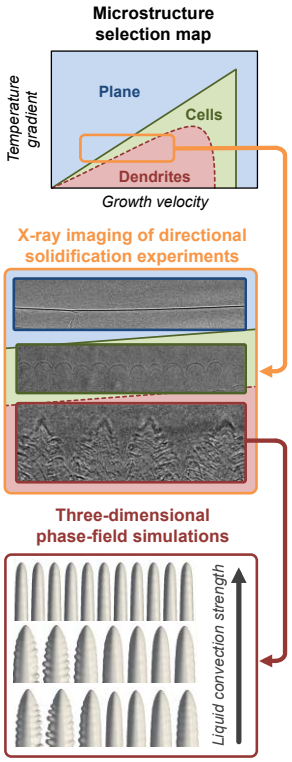

Fig. 3. (Top) A schematic microstructure selection map, (middle) example x-ray images of Al-Cu alloy solidification dynamics, (bottom) example three-dimensional phase-field simulations that elucidate the role of liquid convection on microstructure selection [4].

solidification experiments with quantitative 3D phase-field simulations (Fig. 3) [3]. We quantitatively demonstrated that the critical velocity for the planar-to cellular growth regime transition and the dependence of primary dendrite spacing upon growth velocity are only predicted by simulations if strong convection in the liquid is invoked [3]. In contrast with morphological transitions (planar-to-cellular and cellular-to-dendritic) and primary dendrite spacings, measurements and simulations of primary dendrite tip radii showed little to no dependence upon convection in the liquid, in agreement with classical theory [3]. This study reveals the importance of convection in the liquid on microstructure selection during the solidification of metallic alloys, even in constrained sample geometries thought to limit its extent [3], and the power of in-situ experiments for informing and validating computational modeling.

In addition to microscale experimental and computational studies of metallic alloy solidification dynamics, our earlier work included 2D x-ray imaging of mesoscopic structural evolution in Al-based alloys and comparisons with 2D and 3D dendritic needle network (DNN) predictions [8,9]. These studies revealed the need for 3D simulations to accurately describe the microstructural characteristics of complex, hierarchical solidification structures. More recently, we have performed 4D synchrotron x-ray microscopy of Al-Cu alloys during *controlled* directional solidification, employing the Time-Interlaced Model-Based Iterative Reconstructive (TIMBIR) methodology for improved temporal resolution of early-stage growth dynamics [12,13]. Although time-resolved reconstructions are still needed (e.g. Fig. 2), we anticipate these 4D datasets acquired under controlled solidification conditions will provide a wealth of information for future comparisons with theory and modeling.

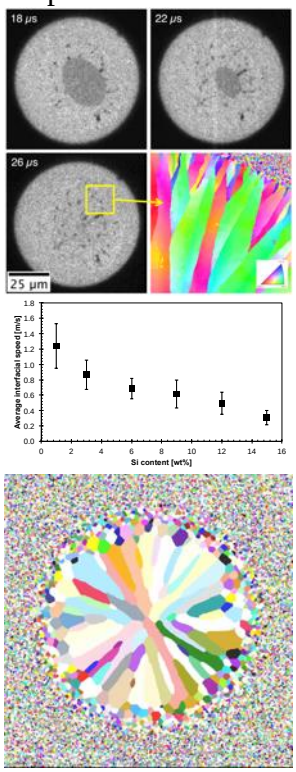

Fig. 4. (Top) DTEM of an Al-Si alloy, highlighting the solid-liquid interface location over microseconds, and some crystallographic grain orientations. (Middle) The effect of Si on solid-liquid interfacial speed and (bottom) early kMC modeling informed by our experiments.

To date, we have also used dynamic transmission electron microscopy (DTEM) and laser heating to image rapid (m/s rates) solidification and microstructural evolution at the nanoscale during far from equilibrium processing [2,14]. Example DTEM of an aluminum-silicon (Al-Si) alloy is shown in Fig. 4, along with post-mortem, high spatial resolution crystal orientation mapping performed in the transmission electron microscope (TEM) and average interfacial speeds for the different alloys examined. These results are informing complementary kinetic Monte Carlo (kMC)

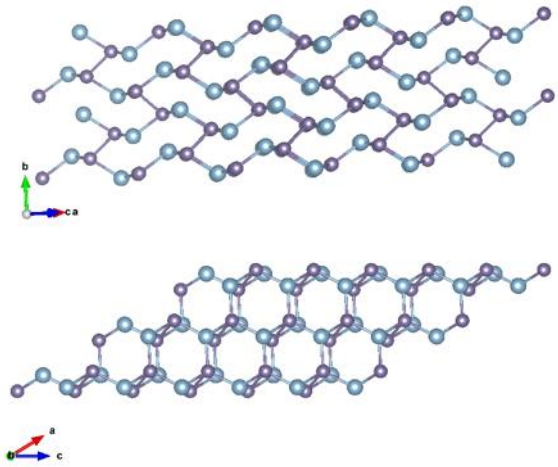

Fig. 5. (Top) Characteristic layered structure of the M-phase. (Bottom) Characteristic 6-member rings of the M-phase. Blue atoms = Al, purple atoms = Ge.

simulations (e.g. [4]) of grain structure evolution during rapid solidification (Fig. 4). These types of simulations will be particularly useful for parametric studies of melt pool sizes and shapes, heat-affected zones, grain sizes and morphologies, for example, to inform the design of synthesis conditions.

Aluminum-germanium (Al-Ge) is an important binary alloy system for studying anisotropy and entropy of fusion effects during solidification. A rich landscape of metastable phases and highly altered solubility limits has been found for these alloys [15-18], especially after far from equilibrium processing. Although rapid solidification results in the formation of metastable phases and complex microstructures, little is known about the structures of these phases or the phase transition pathways. Thus, we solved the crystal structure of the Al-Ge M-phase ($P12_1/c1$, a=6.73 A, b=5.82 A, c=8.05 A, β=32.16°), a metastable monoclinic phase commonly observed after rapid solidification, using the charge flipping algorithm Superflip with laboratory-collected powder diffraction data by spinning capillary diffraction (Fig. 5). The crystal structure has a unit cell containing 8 atoms, 4 Al and 4 Ge. The crystal structure is characterized by distorted 6-member rings, where Al atoms have a coordination number of 3 and are bonded to neighboring Ge atoms. The Ge atoms have a coordination number of 4 and form interlayer bonds. Density Functional Theory (DFT) calculations predict that the crystal structure is a semiconductor.

We have recently imaged Al-Ge alloy solidification dynamics with DTEM to watch the formation of metastable phases, phase transition pathways, and microstructural evolution. Fig. 6 shows a solidification structure composed of coarse, metastable M-phase dendrites and interdendritic eutectic consisting of the M-phase and face-centered cubic (FCC) Al. Near the melt pool edge, Ge-rich particles are

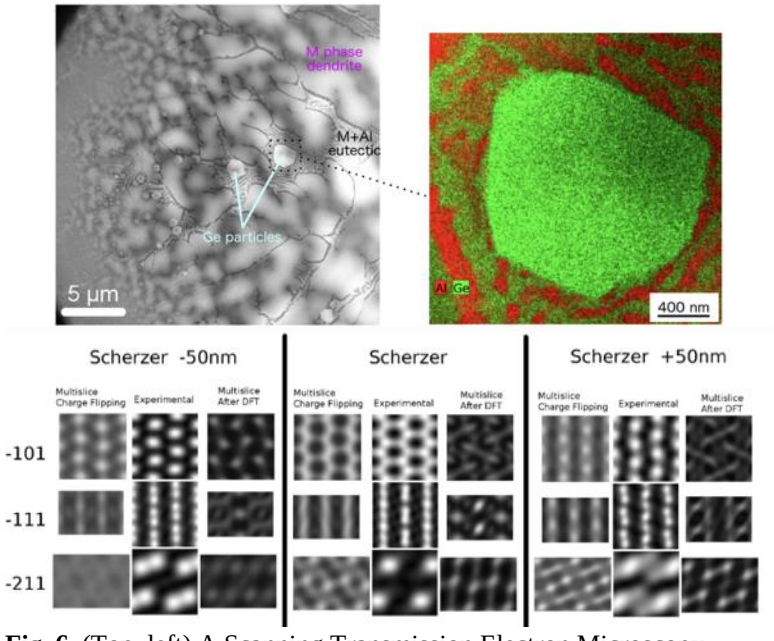

Fig. 6. (Top, left) A Scanning Transmission Electron Microscopy (STEM) High Angular Annular Dark Field (HAADF) image and (top, right) a chemical map of a Ge-rich particle and the Al+M-phase eutectic. (Bottom) HRTEM images processed with the software CRISP and M-phase simulations for three different zone axes at three different focus conditions. The two unit cells used for the M-phase simulations were obtained experimentally by charge flipping and directly by DFT.

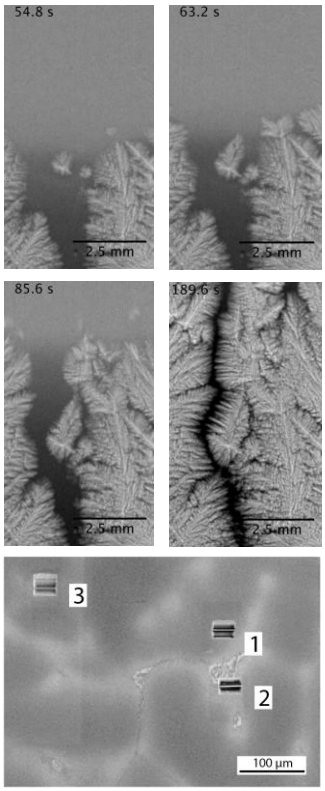

Fig. 7. High-energy x-ray imaging, highlighting Al-Ag solidification dynamics during controlled directional solidification. The resulting microsegregation that develops is shown below, along with the locations of 3 focused ion beam (FIB) lift-outs for subsequent TEM (e.g. Fig. 8).

also observed (Fig. 6). The structure of the M-phase was confirmed by High Resolution Transmission Electron Microscopy (HRTEM), image processing with the software CRISP, and simulations informed by our experimental charge flipping and DFT calculations.

We have also imaged the solidification dynamics of an aluminum-silver (Al-Ag) alloy with high-energy x-rays (Fig. 7). Significant chemical heterogeneities develop in the form of microsegragation, which impacts the subsequent solid-state phase transitions. The precipitation sequence in Al-Ag is: $\alpha_0 \rightarrow \alpha_1 +$ Guinier-Preston (GP) Zones $\rightarrow \alpha_2 + \gamma' \rightarrow \alpha_3 + \gamma$, where α_0 is the original supersaturated solution, α_1 is the composition of the matrix in equilibrium with GP zones, etc. Examples of these phases are shown in Fig. 8. We are currently imaging the solid-state phase transition *dynamics* at the nanoscale associated with the phase transition pathways that occur. We are also performing complementary post-mortem TEM and site-specific atom probe tomography to provide holistic, new insights into phase growth (diffusion- and interface-controlled) and kinetics, the formation of intermediate phases, transport/diffusion, etc.

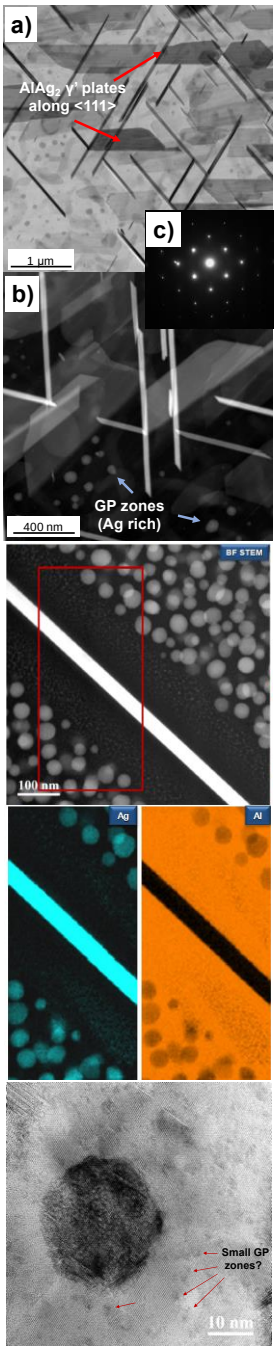

Fig. 8. Multi-scale structure and chemistry of GP zones and γ' precipitates in Al-Ag, imaged with advanced electron microscopy techniques. In-situ experiments of solid-state phase transitions are currently underway.

Future Plans

Our future plans include pursuing reconstructions of our 4D controlled directional solidification experiments on Al-Cu alloys. We will also complete our kMC/DTEM parametric study of Al-Si alloy rapid solidification dynamics. We will continue studying the metastable phases and phase transition pathways in Al-Ge alloys during beyond equilibrium processing. We will also perform in-situ imaging of solid-state phase transition dynamics in Al-Ag, which will provide mechanistic insights into phase growth. The overarching goal this project has been to fundamentally understand multiscale microstructural evolution in metallic alloys during synthesis. This new knowledge is advancing the prediction and control of interfacial (liquid-solid, solid-solid) dynamics by directed synthesis to create new and improved materials.

References

1. D. Tourret, J.C.E. Mertens, E. Lieberman, S.D. Imhoff, J.W. Gibbs, K. Henderson, K. Fezzaa, A.L. Diery, R. Lebensohn, B.M. Patterson, A.J. Clarke. “From solidification processing to microstructure to mechanical properties: a multi-scale x-ray study of an Al-12 at.% Cu alloy sample”, Metallurgical and Materials Transactions A, 2017, 48A:5529-5546.

2. J.D. Roehling, D.R. Coughlin, J.W. Gibbs, J.K. Baldwin, J.C.E. Mertens, G.H. Campbell, A.J. Clarke, J.T. McKeown. “Rapid solidification growth mode transitions in Al-Si alloys by dynamic transmission electron microscopy”, Acta Materialia, 2017, 131:22-30.

3. A.J. Clarke, D. Tourret, Y. Song, S.D. Imhoff, P.J. Gibbs, J.W. Gibbs, K. Fezzaa, A. Karma. “Microstructure selection in thin-sample directional solidification of an Al-Cu alloy: in-situ x-ray imaging and phase-field simulations”, Acta Materialia, 2017, 129:203-216.

4. M.M. Francois, A. Sun, W.E. King, N. Henson, D. Tourret, C., Bronkhorst, N.N. Carlson, C. Newman, T. Haut, J. Bakosi, J.W. Gibbs, V. Livescu, S. VanderWiel, A.J. Clarke, M. Schraad, T. Blacker, H. Lim, T. Rodgers, S. Owen, F. Abdeljawad, J. Madison, A.T. Anderson, J-L. Fattebert, R.M. Ferencz, N.E. Hodge, S.A. Khairallah, O. Walton. “Modeling of additive manufacturing processes for metals: challenges and opportunities”, Current Opinions in Solid State & Materials Science, 2017, 21:198-206.

5. D. Tourret, Y Song, AJ Clarke, A Karma. “Grain growth competition during thin-sample directional solidification of dendritic microstructures: A phase-field study”, Acta Materialia 2017, 122, 220-235.

6. D. Tourret, Y. Song, A.J. Clarke, A. Karma. “Phase-field simulation study of dendritic grain growth competition during alloy directional solidification”, Frontiers in Solidification: Symposium in Honour of Michel Rappaz, Ed. W. Kurz, J. Dantzig, A. Karma, J. Hoyt, EPFL Materials Science: Lausanne, Switzerland, 2016, pp. 35-40.

7. A.J. Clarke, D. Tourret, S.D. Imhoff, J.W. Gibbs, Y. Song, A. Karma, K. Fezzaa, pRad Team, N.N. Carlson, P.J. Gibbs, D.R. Coughlin, J.D. Roehling, J.T. McKeown, J.K. Baldwin. “Multi-scale experiments and modelling of metal alloy solidification dynamics”, Frontiers in Solidification: Symposium in Honour of Michel Rappaz, Ed. W. Kurz, J. Dantzig, A. Karma, J. Hoyt, EPFL Materials Science: Lausanne, Switzerland, 2016, pp. 77-82.

8. D. Tourret, A.J. Clarke, S.D. Imhoff, P.J. Gibbs, J.W. Gibbs, A. Karma. “Three-dimensional multiscale modeling of dendritic spacing selection during Al-Si directional solidification”, JOM, 2015, 67(8):1776-1785.

9. D. Tourret, A. Karma, A.J. Clarke, P.J. Gibbs, S.D. Imhoff. “Three-dimensional dendritic needle network model with application to Al-Cu directional solidification experiments”, Modeling of Casting, Welding and Advanced Solidification Processes (MCWASP XIV) IOP Conference Series: Materials Science and Engineering, 2015, 84:012082.

10. W. Kurz, and D.J. Fisher. Fundamentals of Solidification, Trans Tech Publications Ltd., Aedermannsdorf, Switzerland, 1992.

11. W. Kurz and D.J. Fisher. “Dendrite growth at the limit of stability: tip radius and spacing”, Acta Metallurgica 1981, 29:11-20.

12. K. Aditya Mohan, S.V. Venkatakrishnan, J.W. Gibbs, E. Begum Gulsoy, X. Xiao, M. De Graef, P.W. Voorhees, C.A. Bouman. “TIMBIR: a method for time-space reconstruction from interlaced views”, IEEE Transactions on Computational Imaging, 2015, 1(2):96-111.

13. J.W. Gibbs, K. Aditya Mohan, E.B. Guksoy, A.J. Shahani, X. Xiao, C.A. Bouman, M. DeGraef, P.W. Voorhees. “The three-dimensional morphology of growing dendrites”, Scientific Reports, 2015, 5:11824.

14. J.T. McKeown, K. Zweiacker, C. Liu, D.R. Coughlin, A.J. Clarke, J.K. Baldwin, J.W. Gibbs, J.D. Roehling, S.D. Imhoff, P.J. Gibbs, D. Tourret, J.M.K. Wiezorek, G.H. Campbell. “Time-resolved in situ measurements during rapid solidification: experimental insight for additive manufacturing”, JOM 2016, 68(3):985-999.

15. M.J. Kaufman and H.L. Fraser. “Characterization of metastable crystalline in the Al-Ge alloy system”, Acta Metallurgica, 1985, 33(2):191-203.

16. M.J. Kaufman, J.E. Cunningham Jr. and H.L. Fraser. “Metastable phase production and transformation in Al-Ge alloy films by rapid crystallization and annealing treatments”, Acta Metallurgica, 1987, 33(5):1181-1192.

17. T. Laoui and M.J. Kaufman. “Nonequilibrium behavior in the Al-Ge alloy system – insights into the metastable phase-diagram”, Metallurgical and Materials Transactions A, 1991, 22(9):2141-2152.

18. M.J. Kaufman and H.L. Fraser. “The importance of undercooling in the formation of non-equilibrium structures in the Al-Ge alloy system”, International Journal of Solidification, 1984, 1(1):27-50.

Publications (2-year list of publications SUPPORTED BY BES)

1. F.E. Merrill, J. Goett, J. Gibbs, S. Imhoff, F.G. Mariam, C.L. Morris, L. Neukirch, J. Perry, D. Poulson, R. Simpson, P. Volegov, P. Walstrom, C.H. Wilde, C. Hast, K. Jobe, T. Smith, U. Weinansa, A.J. Clarke, D. Tourret. “Transmission High Energy Electron Microscopy”, submitted to Applied Physics Letters, 2017.

2. P.J. Gibbs, E.A. Holm, S.D. Imhoff, K. Fezzaa, W.-K. Lee, A.D. Rollett, K.D. Clarke, A.J. Clarke. “X-ray imaging of recrystallization and abnormal grain growth”, submitted to Acta Materialia, 2017.

3. D. Tourret, J.C.E. Mertens, E. Lieberman, S.D. Imhoff, J.W. Gibbs, K. Henderson, K. Fezzaa, A.L. Diery, R. Lebensohn, B.M. Patterson, A.J. Clarke. “From solidification processing to microstructure to mechanical properties: a multi-scale x-ray study of an Al-12 at.% Cu alloy sample”, Metallurgical and Materials Transactions A, 2017, 48A:5529-5546.

4. J.D. Roehling, D.R. Coughlin, J.W. Gibbs, J.K. Baldwin, J.C.E. Mertens, G.H. Campbell, A.J. Clarke, J.T. McKeown. “Rapid solidification growth mode transitions in Al-Si alloys by dynamic transmission electron microscopy”, Acta Materialia, 2017, 131:22-30.

5. A.J. Clarke, D. Tourret, Y. Song, S.D. Imhoff, P.J. Gibbs, J.W. Gibbs, K. Fezzaa, A. Karma. "Microstructure selection in thin-sample directional solidification of an Al-Cu alloy: in-situ x-ray imaging and phase-field simulations", Acta Materialia, 2017, 129:203-216.

6. M.M. Francois, A. Sun, W.E. King, N. Henson, D. Tourret, C., Bronkhorst, N.N. Carlson, C. Newman, T. Haut, J. Bakosi, J.W. Gibbs, V. Livescu, S. VanderWiel, A.J. Clarke, M. Schraad, T. Blacker, H. Lim, T. Rodgers, S. Owen, F. Abdeljawad, J. Madison, A.T. Anderson, J-L. Fattebert, R.M. Ferencz, N.E. Hodge, S.A. Khairallah, O. Walton. "Modeling of additive manufacturing processes for metals: challenges and opportunities", Current Opinions in Solid State & Materials Science, 2017, 21:198-206.

7. D. Tourret, Y Song, AJ Clarke, A Karma. "Grain growth competition during thin-sample directional solidification of dendritic microstructures: A phase-field study", Acta Materialia 2017, 122, 220-235.

8. B.M. Patterson, N. L. Cordes, K. Henderson, J.C.E. Mertens, A.J. Clarke, B. Hornberger, A. Merkle, S. Etchin, A. Tkachuk, M. Leibowitz, D. Trapp, W. Qui, B. Zhang, H. Bale, X. Lu, R. Hartwell, P.J. Withers, R.S. Bradley. "In situ laboratory-based transmission x-ray microscopy and tomography of material deformation at the nanoscale", Experimental Mechanics 2016, 1-13, DOI: 10.1007/s11340-016-0197-3.

9. J.T. McKeown, K. Zweiacker, C. Liu, D.R. Coughlin, A.J. Clarke, J.K. Baldwin, J.W. Gibbs, J.D. Roehling, S.D. Imhoff, P.J. Gibbs, D. Tourret, J.M.K. Wiezorek, G.H. Campbell. "Time-resolved in situ measurements during rapid solidification: experimental insight for additive manufacturing", JOM 2016, 68(3):985-999.

10. J.W. Gibbs, D. Tourret, P.J. Gibbs, S.D. Imhoff, M.J. Gibbs, B.A. Walker, K. Fezzaa, A.J. Clarke. "In situ x-ray observations of dendritic fragmentation during directional solidification of a Sn-Bi alloy", JOM 2016, 68(1):170-177.

11. A.J. Clarke, K. D. Clarke, R.J. McCabe, C.T. Necker, P.A. Papin, R.D. Field, A.M. Kelly, T.J. Tucker, R.T. Forsyth, P.O. Dickerson, J.C. Foley, H. Swenson, R.M. Aikin, and D.E. Dombrowski. "Microstructural evolution of a uranium-10 wt.% molybdenum alloy for nuclear reactor fuels", Journal of Nuclear Materials 2015, 465:784-792.

12. D. Tourret, Y. Song, A.J. Clarke, A. Karma. "Phase-field simulation study of dendritic grain growth competition during alloy directional solidification", Frontiers in Solidification: Symposium in Honour of Michel Rappaz, Ed. W. Kurz, J. Dantzig, A. Karma, J. Hoyt, EPFL Materials Science: Lausanne, Switzerland, 2016, pp. 35-40.

13. A.J. Clarke, D. Tourret, S.D. Imhoff, J.W. Gibbs, Y. Song, A. Karma, K. Fezzaa, pRad Team, N.N. Carlson, P.J. Gibbs, D.R. Coughlin, J.D. Roehling, J.T. McKeown, J.K. Baldwin. "Multi-scale experiments and modelling of metal alloy solidification dynamics", Frontiers in Solidification: Symposium in Honour of Michel Rappaz, Ed. W. Kurz, J. Dantzig, A. Karma, J. Hoyt, EPFL Materials Science: Lausanne, Switzerland, 2016, pp. 77-82.

14. C.L. Morris, E.N. Brown, C. Agee, T. Bernert, M.A.M. Bourke, M.W. Burkett, W.T. Buttler, D.D. Byler, C.F. Chen, A.J. Clarke, J.C. Cooley, P.J. Gibbs, S.D. Imhoff, R. Jones, K.

Kwiatkowski, F.G. Mariam, F.E. Merrill, M.M. Murray, C.T. Olinger, D.M. Oro, P. Nedrow, A. Saunders, G. Terrones, F. Trouw, D. Tupa, W. Vogan, B. Winkler, Z. Wang, M.B. Zellner. "New developments in proton radiography at the Los Alamos Neutron Science Center (LANSCE)", Experimental Mechanics, 2016, 56:111-120.

15. A. Karma and D. Tourret. "Atomistic to continuum modeling of solidification microstructures", Current Opinion in Solid State and Materials Science, 2015, DOI: 10.1016/j.cossms.2015.09.001.

16. B. Hornberger, H. Bale, A. Merkle, M. Feser, W. Harris, S. Etchin, M. Leibowitz, W. Qiu, A. Tkachuk, A. Gu, R.S. Bradley, X. Lu, P.J. Withers, A. Clarke, K. Henderson, N. Cordes, B. Patterson. "X-ray microscopy for in situ characterization of 3D microstructure evolution in the laboratory", Proc. SPIE Vol. 9592 X-ray Nanoimaging: Instruments and Methods II, 2015, DOI:10.1117.12.2188728.

17. D. Roehling, A. Perron, J.-L. Fattebert, D.R. Coughlin, P.J. Gibbs, J.W. Gibbs, S.D. Imhoff, D. Tourret, J.K. Baldwin, A.J. Clarke, P.E.A. Turchi, J.T. McKeown. "Imaging the rapid solidification of metallic alloys in the TEM", Microscopy and Microanalysis, 2015, 21(S3):469-470, DOI: 10.1017/S1431927615003141.

18. D. Tourret, A.J. Clarke, S.D. Imhoff, P.J. Gibbs, J.W. Gibbs, A. Karma. "Three-dimensional multiscale modeling of dendritic spacing selection during Al-Si directional solidification", JOM, 2015, 67(8):1776-1785.

19. D. Tourret, A. Karma, A.J. Clarke, P.J. Gibbs, S.D. Imhoff. "Three-dimensional dendritic needle network model with application to Al-Cu directional solidification experiments", Modeling of Casting, Welding and Advanced Solidification Processes (MCWASP XIV) IOP Conference Series: Materials Science and Engineering, 2015, 84:012082.

20. A.J. Clarke, D. Tourret, S.D. Imhoff, P.J. Gibbs, K. Fezzaa, J.C. Cooley, W.-K. Lee, A. Deriy, B.M. Patterson, P.A. Papin, K.D. Clarke, R.D. Field, J.L. Smith. "X-ray imaging and controlled solidification of Al-Cu alloys toward creating microstructures by design", Advanced Engineering Materials, 2015, 17(4):454-459.

21. S.D. Imhoff, P.J. Gibbs, M.R. Katz, T.J. Ott Jr., B.M. Patterson, W.-K. Lee, K. Fezzaa, J.C. Cooley, A.J. Clarke. "Dynamic evolution of liquid-liquid phase separation during continuous cooling", Materials Chemistry and Physics 2015, 153:93-1023.

Stability, Structure, and Molecular Orientation in Organic Glasses Produced by Physical Vapor Deposition

Y. Qiu, D.M. Walters, J. Gomez, A. Gujral, K. Bagchi, and M.D. Ediger
Department of Chemistry
University of Wisconsin-Madison, Madison, WI 53706

Program Scope

Organic glasses with high density, low enthalpy, and remarkably high kinetic stability can be prepared by physical vapor deposition (PVD).[1] We are investigating the extent to which high kinetic stability and tailored anisotropy can coexist in the same material. These experiments build upon the recent development of a high-throughput temperature-gradient methodology to efficiently prepare and characterize organic glasses. Using materials applicable to organic electronics, we are working to further our fundamental understanding of the vapor-deposited glasses and the amorphous state by pursuing the following objectives: 1) Utilize grazing-incidence and wide-angle x-ray scattering, and optical absorption and emission, to characterize vapor-deposited glasses. 2) Find and understand general trends in the properties of glasses prepared by depositing single and multiple component systems. We seek to identify the range of anisotropic amorphous structures that can be produced by PVD and develop the mechanistic understanding needed to predict the anisotropy produced by specific deposition conditions. 3) Build upon recent work showing that PVD can produce "stable glasses" with unprecedented thermal stability by investigating the extent to which stable glass packing can also increase photochemical stability and resistance to crystallization.

Recent Progress

Significantly enhanced photostability. In light of the high kinetic stability of glasses prepared by vapor-deposition, [2] we have investigated their photostability, which is an important parameter for organic electronics that influences device efficiency and lifetimes.[3] To assess photostability, we use spectroscopic ellipsometry to measure changes in the density and molecular orientation of glassy thin films during light irradiation. Coarse-grained molecular simulations, which mimicked glass preparation and the photoreaction, were also performed. Both experiments and simulations demonstrate that photostability can be substantially increased by performing vapor-deposition at the correct substrate temperature ($T_{substrate}$).

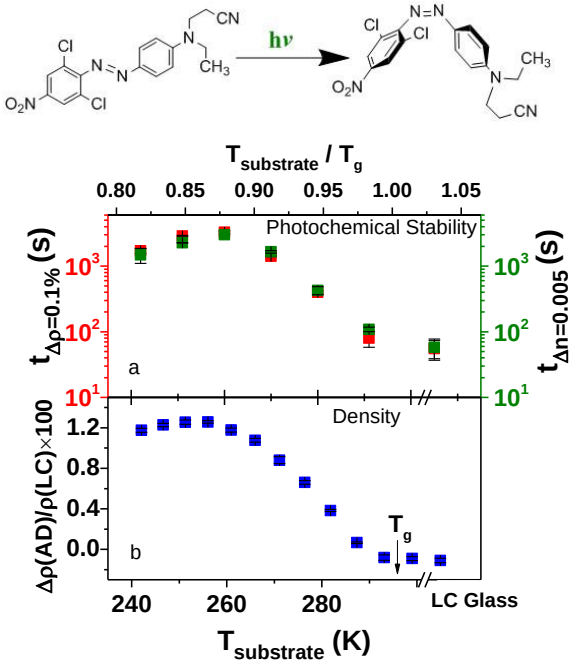

Figure 1. Photostability and density of PVD glasses of DO37 (structure shown at top), with comparison to the liquid-cooled (LC) glass. (a) Irradiation time required to achieve a 0.1% density change (red) and 0.005 birefringence change (green). (b) Density of as-deposited (AD) glasses relative to the LC glass.

Spectroscopic ellipsometry was used to characterize photostability in films of dispersed orange 37 (DO37), an azobenzene molecule that can undergo a *trans->cis* photoisomerization reaction when irradiated by light.[4] Figure 1a shows the photostability of glasses of DO37 prepared by physical vapor deposition at various $T_{substrate}$. Photostability is quantified by the irradiation time required to induce structural changes that are detected as small changes in density and birefringence. Photostabilities deduced from these two observables are highly consistent. Figure 1b shows the density for DO37 glasses vapor-deposited at different substrate temperatures. By comparing Figure 1a and 1b, it is evident that there is a strong correlation between photostability and glass density. Significantly, the higher density of the PVD glasses is associated with a 50-fold increase in photostability, which is an unprecedented large effect.

Anisotropic molecular orientation. Molecular orientation is vital to OLED device performance as it influences both light out-coupling efficiency and charge transport.[5] Our studies show the role molecular shape plays in determining molecular orientation in vapor-deposited glasses. We recently studied the molecular orientation of disk-shaped molecules commonly used in OLEDs as shown in Figure 2. Here S_z is the orientation order parameter; $S_z = 1$ indicates vertical orientation of the molecular symmetry axis and for $S_z = -0.5$ the symmetry axis lies in the plane. Three disk-shaped molecules showed a similar dependence of molecular orientation on $T_{substrate}$ and the pattern is clearly different than for the rod-shaped molecules that we studied earlier. Collaborators (Anthony and De Pablo) have performed molecular dynamics simulations on the equilibrium liquids of m-MTDATA and TCTA. These results are consistent with the surface equilibration mechanism that we introduced earlier.[2] High surface mobility during deposition allows partial equilibration towards low energy states with high kinetic stability. In this process, the bulk molecular orientation of the vapor-deposited glasses is inherited from the anisotropic surface structure of the equilibrium liquid.[6]

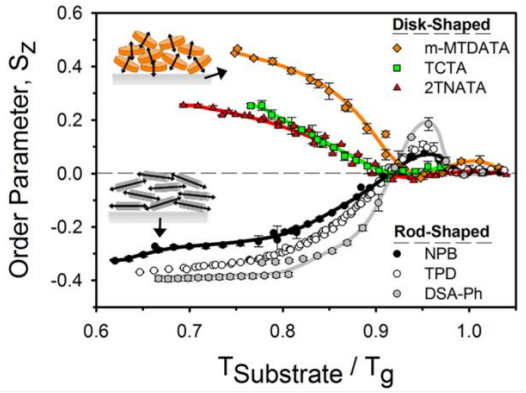

Figure 2. Orientational order parameter in vapor-deposited glasses of disc- and rod-shaped molecules as a function of substrate temperature during deposition.

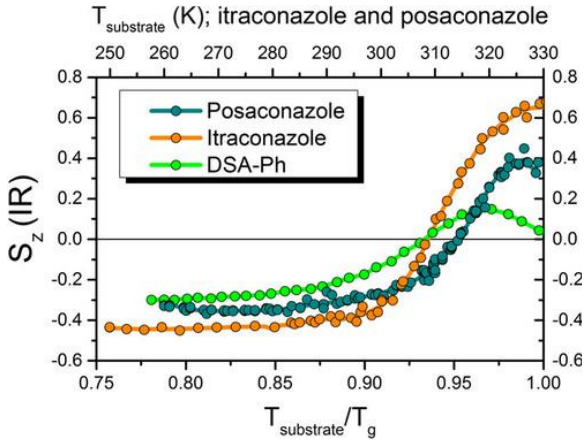

Figure 3. Molecular orientation order parameters for vapor-deposited glasses of posaconazole and two previously reported glass formers, DSA-Ph and itraconazole.

We recently vapor-deposited a rod-shaped molecule (posaconazole) for which the molecular orientation does not fit the pattern shown in Figure 2. The results shown in Figure 3 indicate substantial vertical orientation for glasses deposited just below T_g. Posaconazole has a molecular structure very similar to itraconazole. While itraconazole exhibits liquid crystalline phases, posaconazole does not. Nevertheless, the value of $S_z = 0.4$

observed for posaconazole is consistent with an aligned nematic liquid crystal! This strong vertical orientation in vapor-deposited glasses of posaconazole is consistent with the surface equilibration mechanism if molecules have a strong tendency for perpendicular molecular orientation at the free surface.[7]

The ability to create glasses with vertical molecular orientation is significant because in OFETs vertical orientation is optimal.[8] Vapor-deposited glasses of posaconazole also have enhanced thermal stability and enhanced density as compared to the liquid cooled glasses making such materials desirable from an organic electronics perspective. Moreover, broadly speaking, materials with liquid-crystalline order are promising materials for organic electronics.[9] Our studies provide a strategy for achieving liquid crystalline order in vapor-deposited glasses of molecules that do not exhibit an equilibrium liquid crystalline phase.

Anisotropic molecular packing. In addition to exhibiting anisotropic molecular orientation, vapor-deposited glasses can exhibit a tendency for molecular layering. This type of anisotropic structure cannot be detected from ellipsometry or IR dichroism, and its origin and influence on properties have remained unclear. We have performed grazing incidence wide angle x-ray scattering (GIWAXS) on vapor-deposited glasses of Alq3, a common electron transport and emitter material in OLED devices. In preliminary results shown in Figure 4, we observe a substrate temperature dependent tendency for molecular layering. We use the GIWAXS order parameter, previously used to study vapor-deposited glasses of TPD, to characterize the layering Alq3 glasses.[10] We also observe that these structurally anisotropic glasses of Alq3 are optically isotropic (i.e., no birefringence). While the tendency for molecular layering is most pronounced at lower substrate temperatures in Figure 4, it disappears at higher substrate temperature. Unpublished simulations by collaborators Jackson and de Pablo, indicate that the free surface of supercooled Alq3 exhibits a tendency for layering. Consistent with the surface equilibration mechanism described above, this layering becomes trapped in the bulk glass during deposition.

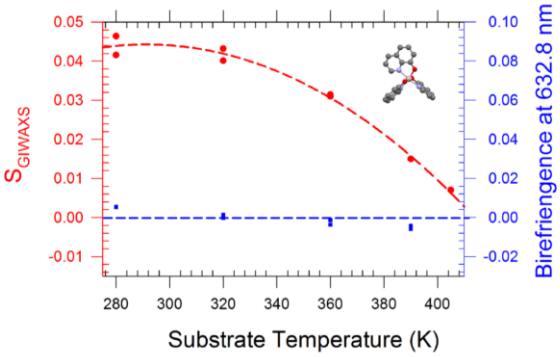

Figure 4. GIWAXS order parameter and birefringence for PVD Alq3 glasses prepared at different substrate temperatures. The GIWAXS order parameter quantifies the extent of structural anisotropy while the birefringence quantifies the tendency for preferential molecular orientation. While Alq3 glasses exhibit varying degrees of structural anisotropy, all the glasses are optically isotropic.

The tendency for molecular layering in Alq3 has so far been ignored in the literature even though a large number of devices have been made from this molecule. Previous studies have shown that Alq3 glasses deposited at different substrate temperature have different conductivities.[11] Our x-ray structural studies identifies a new structural parameter that may correlate with performance.

Future Plans

In the final 10 months of this grant period, we will: 1) Extend the photostability studies to glasses of additional organic molecules, including indomethacin. We need to test the generality of the results obtained with DO37 with different types of photoprocesses. 2) Complete our study of Alq3, integrating the experimental and simulation results. This is an important new test of the surface equilibration mechanism and opens the door to understanding the anisotropic x-ray scattering often observed in vapor-deposited glasses of organic semiconductors.

References

(1) Swallen, S. F.; Kearns, K. L.; Mapes, M. K.; Kim, Y. S.; McMahon, R. J.; Ediger, M. D.; Wu, T.; Yu, L.; Satija, S. *Science* **2007**, *315*, 353.
(2) Dalal, S. S.; Walters, D. M.; Lyubimov, I.; de Pablo, J. J.; Ediger, M. D. *Proc. Natl. Acad. Sci. USA* **2015**, *112*, 4227.
(3) Wang, Q.; Luo, Y. C.; Aziz, H. *Appl. Phys. Lett.* **2010**, *97*, 063309.
(4) Qiu, Y.; Antony, L. W.; de Pablo, J. J.; Ediger, M. D. *J. Am. Chem. Soc.* **2016**, *138*, 11282.
(5) Yokoyama, D. *J. Mater. Chem.* **2011**, *21*, 19187.
(6) Walters, D. M.; Antony, L. W.; de Pablo, J. J.; Ediger, M. D. *J. Phys. Chem. Lett.* **2017**, *8*, 3380.
(7) Gomez, J.; Gujral, A.; Huang, C. B.; Bishop, C.; Yu, L.; Ediger, M. D. *J. Chem. Phys.* **2017**, *146*, 054503.
(8) O'Neill, M.; Kelly, S. M. *Adv. Mater.* **2011**, *23*, 566.
(9) Iino, H.; Hanna, J. *Polym. J.* **2017**, *49*, 23.
(10) Gujral, A.; O'Hara, K. A.; Toney, M. F.; Chabinyc, M. L.; Ediger, M. D. *Chem. Mater.* **2015**, *27*, 3341.
(11) Chung, J. M. L., Y. Z.; Jian, Z. A.; Kuo, M. C.; Yang, C. S.; Chou, W.C.; Chiu, K. C. *Jpn. J. Appl. Phys.* **2004**, *43*, 1631.

DOE-Sponsored Research Publications (last two years):

(1) Jiang, J.; Walters, D. M.; Zhou, D.; Ediger, M. D. *Soft Matter* **2016**, *12*, 3265.
(2) Qiu, Y.; Antony, L. W.; de Pablo, J. J.; Ediger, M. D. *J. Am. Chem. Soc.* **2016**, *138*, 11282–11289
(3) Gomez, J.; Gujral, A.; Huang, C.; Bishop, C.; Yu, L.; Ediger, M. D. *J. Chem. Phys.* **2017**, *146*, 054503.
(4) Laventure, A.; Gujral, A.; Lebel, O.; Pellerin, C.; Ediger, M. D. *J. Phys. Chem. B* **2017**, *121*, 2350.
(5) Walters, D. M.; Antony, L.; de Pablo, J. J.; Ediger, M. D. *J. Phys. Chem. Lett.* **2017,** *8* (14), 3380-3386.

Program Title: Novel Synthesis of Quantum Epitaxial Heterostructures by Design

Principle Investigator: Chang-Beom Eom
Mailing Address: Room 2166 ECB, 1550 Engineering Drive, University of Wisconsin-Madison, Madison, WI 53706
E-mail: eom@engr.wisc.edu

Program Scope

Quantum materials such as topological insulators, interfacial 2D electron gas (2DEG), novel superconductors and multiferroics have been fertile ground for new discoveries, due particularly to the delicate balance between charge, spin, orbital, and lattice ordered states tuned by external parameters. Such materials can exhibit exciting emergent phenomena whose description requires new quantum mechanical models to be developed and experimentally validated. Atomic level controlled synthesis is critical for all experimental studies.

Epitaxial thin films of quantum materials are advantageous both for study of fundamental science and for development of new applications. These films can be of comparable or higher quality than available bulk single crystals, but more importantly deposition conditions can be maintained far from equilibrium, so that metastable phases (nonexistent in nature) can be obtained by epitaxial stabilization. Furthermore, growth of artificially layered superlattices, and control of film crystallographic orientation probe fundamental intrinsic properties of quantum materials such as dimensionality, anisotropy, and electronic correlations.

This program focuses on the novel synthesis of epitaxial heterostructures by controlling point defects, strain, and interfaces at the atomic level to understand the relationship between structure and emergent quantum phenomena, and to design and create unique quantum materials tuned to take advantage of the properties only possible in this unique epitaxial heterostructures. The **thrusts** of our proposed work are:

(1) *Development of **Novel Synthesis Route** for Epitaxial Thin Film Heterostructures with Controlled Point Defects.*
Modern quantum materials are very sensitive to defects, and require a new synthesis route to produce high-quality epitaxial oxide thin films and interfaces. We are developing a chemical pulsed laser deposition (CPLD) growth process that promises dramatically lower concentration of *point defects*. The higher quality epitaxial films and heterostructures remove several roadblocks that have limited the development of new science using quantum materials.

(2) ***Coupled bilayers of oxide interfacial electron and hole gases***
The 2DEG at oxide heterointerfaces has resulted in several important discoveries, however the equivalent ***hole*** gas has been elusive, primarily due to the presence of point defects and other impurities. Coexistence of both 2DEG and 2D hole gas (2DHG) in a single heterostructure allows a new quantum material based on interaction of the hole and electron gas over only a few unit cells, leading to new functionalities and emergent phenomena.

(3) ***Strain- and Interface engineered** Superconducting Heterostructures*
Quantum materials supporting interfacial superconductivity are delicately sensitive to point defects. Our new synthesis routes now allow exploration of strain- interface- and electric-field dependent superconducting properties, such as the interaction of monolayer FeSe with strain- and interface engineered $SrTiO_3$ films, the control of T_c by lattice distortion in strain-engineered pnictides thin films.

Recent Progress

1. Two-Dimensional Hole Gas at Oxide Interfaces

The discovery of two-dimensional electron gas (2DEG) at the $LaAlO_3/SrTiO_3$ interface has revealed a plethora of new properties not present in conventional semiconductor heterostructures, becoming a focal point of novel device applications. Its counterpart, two-dimensional hole gas (2DHG), has long been expected to complement 2DEG and provide versatile functionalities. However, while 2DEG has been widely observed, the 2DHG has been elusive. We demonstrate a highly-mobile 2DHG in epitaxially-grown $SrTiO_3/LaAlO_3/SrTiO_3$ heterostructures. Using electrical transport measurements and in-line electron holography charge density mapping, we provide direct evidence of 2DHG coexisting with 2DEG at complementary heterointerfaces in the same structure. First-principles calculations, coherent Bragg rod analysis, and depth-resolved cathodoluminescence spectroscopy consistently support our finding that eliminating ionic point-defects is key to realize 2DHG. The coexistence of 2DEG and 2DHG in a single oxide heterostructure provides a platform for exciting new physics of confined electron-hole systems and for developing novel applications.

We choose (001) $SrTiO_3/LaAlO_3/SrTiO_3$ (STO/LAO/STO) heterostructures to realize the 2DHG. If the STO substrate is TiO_2-terminated, *p*-type and *n*-type interfaces are expected to form at the top and the bottom of the STO/LAO/STO heterostructure, respectively, to avoid the polar catastrophe. The polar discontinuity may, however, be also resolved by the accumulation of positively-charged oxygen vacancies at the top interface. This is evident from our first-principles calculations indicating the absence of 2DHG when oxygen vacancies are formed in STO or LAO close to the top interface. This implies that, even though one can fabricate a high-quality *p*-type interface, the interface may still be electrically insulating due to the ionized oxygen vacancies. Therefore, we focus on (1) building an atomically-sharp *p*-type interface consisting of SrO/AlO_2 layers, and (2) minimizing oxygen vacancies near the *p*-type interface.

We synthesized STO/LAO thin films by pulsed laser deposition with *in-situ* RHEED on TiO_2-terminated (001) STO substrates, with the substrate interface designed to host the 2DEG, and the top STO/LAO interface to host the 2DHG. To minimize the oxygen vacancy formation, oxygen partial pressure in the chamber was kept high during the growth. The samples were also *in-situ* post annealed in oxygen ambient. The magnified atomic structure (Fig. 1a) indicates that a high-quality SrO/AlO_2 interface has been built between the top STO and LAO thin films. The Atomic-scale energy dispersive X-ray spectroscopy (EDS) elemental maps show the chemically-abrupt top interface (Fig. 1b). The electron density map determined by synchrotron X-ray surface diffraction-based coherent Bragg rod analysis (COBRA) across the top interface shows that the top interface consists of SrO and AlO_2 layers as we designed (Fig. 1c).

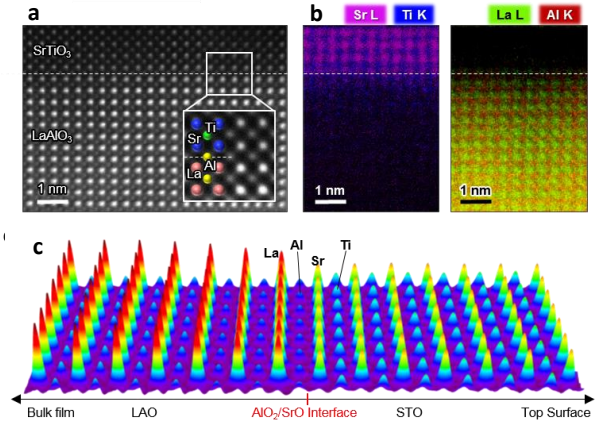

Figure 1. a, STEM images obtained at the top STO/LAO interface. **b,** EDS elemental mapping. **c,** COBRA-derived cation electron density map across the interface.

We examined the electrical transport properties of the top and the bottom interfaces in the STO/LAO/STO heterostructure. The magnetic field-dependent Hall resistance R_{xy} (H) measured at the top interface clearly shows a positive Hall coefficient, while the bottom interface shows negative. It is notable that the mobility of 2DHG is comparable and even slightly higher than the mobility of 2DEG at low temperature. The electrons are known to be strongly coupled to phonons in the LAO/STO system forming large polarons. As the result, the effective electron mass renormalizes to a larger value of 2.5 m_o. On the contrary, holes are weakly coupled to phonons, which is evident from the calculated electron-phonon coupling matrix element for the valence band maximum being seven times smaller than that at the conduction band minimum. Hence, considering the electron-phonon coupling, it is likely that the effective mass of holes is comparable or even smaller than the effective mass of electrons. This qualitatively explains the relatively large hole mobility being comparable to the electron mobility.

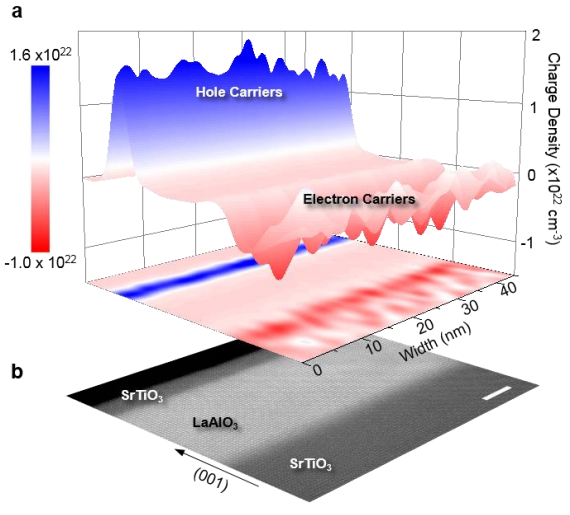

Figure 2. a, The charge density map obtained by the in-line electron holography technique. b, The STEM-ADF image of the entire STO/LAO/STO heterostructure.

Using in-line electron holography, we directly demonstrate that the 2DHG is formed at the STO/LAO interface. The in-line electron holography, using a field-emission TEM, can map the internal charge distribution by retrieving phase shift information of the transmitted electron beam. A high density of positive charges is clearly observed at the top interface, while the bottom interface showed negative charges.

The presence of holes at the top interface can be more strongly supported by verifying the lack of oxygen vacancy near the interface. To obtain more detailed information about the oxygen vacancy distribution, we performed depth-resolved cathodoluminescence spectroscopy analyses. The top STO exhibited a considerably small sign of oxygen vacancy, which is even smaller than that of bulk STO substrate. All these structural studies unambiguously show that the 2DHG was realized in oxide heterostructures containing minimal oxygen vacancy.

The coexistence of 2DEG and 2DHG in a single oxide heterostructure enables exploration of the exciting new physics of confined electron-hole systems, including long-lifetime bilayer excitons, Coulomb drag with spin-orbit coupling, bilayer electron-hole superconductivity, and Bose–Einstein condensation of excitons.

Future Plans

(1) Strain control of superconductivity in $BaFe_2As_2$ Pnictide thin film heterostructures

Control of the detailed atomic configuations in Fe-based superconductors is crucial for understanding the fundamental mechanisms of its unconventional superconductivity. For instance, structural distortion from an ideal Fe-As tetrahedron is believed to be related to the superconducting transition temperature, and can play a role in explaining the high-T_c superconductivity in Fe-based materials. Biaxial strain is a much more natural way to tune the tetrahedral geometry, accomplished in a thin-film geometry by different lattice constant substrates rather than by hydrostatic pressure in bulk system. In-plane strain in thin films can be controlled by

substrates, which provide the excellent platform for tuning the wide range of thermal and lattice mismatch between thin films and the substrates. We plan to modify superconductivity in high quality epitaxial doped and undoped $BaFe_2As_2$ pnictide thin films heterostructrues by in-plane strain induced by substrates, tuning the As-Fe-As bond angle for understanding the macroscopic quantum phenomena of pnictide superconductors. This approach enables tuning the bond angle in a single material platform. Our approach is based on biaxial strain of single crystal films controlled by various substrates with different lattice and thermal expansion mismatch.

(2) Suppression of the charge density wave in $BaBiO_3$/$BaPbO_3$ bilayers and superlattices

We will grow $BaBiO_3$ and $BaPbO_3$ bilayers and heterostructures to investigate the possibility of engineering high T_c superconducting structures. Bulk $BaBiO_3$ has a charge density wave that opens a semiconducting bandgap and exists for Bi concentrations of ~35% and higher. By growing ~4 nm $BaBiO_3$ the charge density wave is suppressed in single layers. We hope to utilize thin $BaBiO_3$ layers to suppress the charge density wave, separated by $BaPbO_3$ conducting layers, engineering a new quantum material through superlattice heteroepitaxy. In order to limit chemical intermixing, smooth surfaces are required, which we can achieve on $LaLuO_3$. If the charge density wave is a competing phase that limits T_c in bulk BPBO, this artificial suppression may enable doping to higher levels. The first superlattices have been grown and preliminary results show a cubic-like structure and superconductivity. Raman spectroscopy, terahertz spectroscopy, and synchrotron diffraction will be used to characterize the charge density wave and octahedral tilting of these superlattices as a function of temperature to explore structure-property relationships in artificial bismuthates.

Publications (which acknowledge DOE support)

1. "Polar Metals by Geometric Design", T. H. Kim, D. Puggioni, Y. Yuan, L. Xie, H. Zhou, N. Campbell, P. J. Ryan, Y. Choi, J.-W. Kim, J. R. Patzner, S. Ryu, J. P. Podkaminer, J. Irwin, Y. Ma, C. J. Fennie, M. S. Rzchowski, X. Q. Pan, V. Gopalan, J. M. Rondinelli, and C. B. Eom, *Nature,* **533**, 68 (2016)
2. "Imprint Control of $BaTiO_3$ Thin films *via* Chemically-induced Surface Polarization Pinning", H. Lee, T. H. Kim, J. J. Patzner, H. Lu, J. W. Lee, H. Zhou, W. Chang, M. K. Mahanthappa, E. Y. Tsymbal, A. Gruverman, and C. B. Eom, *Nano Letters*, **16**, 2400 (2016)
3. "Tailoring $LaAlO_3$/$SrTiO_3$ interface metallicity by oxygen surface adsorbates", Weitao Dai, Sanjay Adhikari, Andrés Camilo Garcia-Castro, Aldo H. Romero, Hyungwoo Lee, Sangwoo Ryu, Chang Beom Eom, Cheng Cen, *Nano Letters* **16**, 2739 (2016)
4. "Tunable electron-electron interactions in $LaAlO_3$/$SrTiO_3$ nanostructures" Guanglei Cheng, Michelle Tomczyk, Alexandre B. Tacla, Hyungwoo Lee, Shicheng Lu, Josh P. Veazey, Mengchen Huang, Patrick Irvin, Sangwoo Ryu, Chang-Beom Eom, Andrew Daley, David Pekker, Jeremy Levy, *Phys. Rev. X* **6**, 041042 (2016)
5. "Localized GHz frequency electrodynamic behavior of an optimally-doped $Ba(Fe_{1-x}Co_x)_2As_2$ epitaxial film" Tamin Tai, Behnood G. Ghamsari, J.H. Kang, S. Lee, C.B. Eom, Steven M. Anlage, *Physica C: Superconductivity and its Applications,* **532**, 44, (2017)
6. "Origin of the emergence of higher T_c than bulk in iron chalcogenide thin films" Sehun Seo, Jong-Hoon Kang, Myeong Jun Oh, Il-Seok Jeong, Jianyi Jiang, Genda Gu, Jung-Woo Lee, Jongmin Lee, Heesung Noh, Eric Hellstrom, Joo-Hyoung Lee, Y. J. Jo, Chang-Beom Eom, and Sanghan Lee, *submitted* to *Scientific Reports* (2017) (under revision)
7. "Two-Dimensional Hole Gas at Oxide Interfaces", H. Lee, N. Campbell, J. Lee, T. J. Asel, T. R. Paudel, H. Zhou, J. W. Lee, B. Noesges, L. J. Brillson, S. H. Oh, E. Y. Tsymbal, M. S. Rzchowski, and C. B. Eom, submitted to *Nature Materials*, (2017) (under revision)

8. “Shubnikov-de Haas-Like Quantum Oscillations in Artificial One-Dimensional $LaAlO_3/SrTiO_3$ Electron Channels”, Guanglei Cheng, Anil Annadi, Shicheng Lu, Hyungwoo Lee, Jung-Woo Lee, Mengchen Huang, Chang-Beom Eom, Patrick Irvin, Jeremy Levy, *submitted to Phys. Rev. Letts.* (2017)

Using Multi-Phase Energetic Precursor Jets to Enable New Modes of Focused Electron Beam Induced Processing (FEBIP)

Andrei G. Fedorov, G. W. Woodruff School of Mechanical Engineering, Georgia Tech

Program Scope

The current program furthers development of a family of techniques based on multiphase energetic jets for the growth of micro- and nanoscale deposits by FEBIP. A particular focus is on using nanoelectrospray to establish precursor-rich, ultra-thin liquid films in vacuum environment suitable for multi-material growth at far from equilibrium conditions. The role of electron energy on deposit nucleation in the presence of multi-phase (vacuum/liquid/solid) interfaces has been established by studying the formation of primary (desired) and secondary (parasitic) material deposition through controlled electron beam exposure of electrospray-established (ES) films. We postulate that electron beam-directed growth of deposits primarily depends by local electron energy and number density, along with the concentration of precursor molecules – both absolute and relative (e.g. preferential reaction pathways). Unique processing capabilities are advanced through experiments and models directed to understanding of the dynamics of these pathways.

Recent Progress

The goal that drives the study of the fundamental underpinnings of the NESA-FEBID process (Fig. 1) is to develop a process that enables the "direct-write" formation of pure metal and composite (metal-carbon and alloy) nanostructures of defined shape and structural stability. Underlying this goal is discovery and in-depth exploration of physical phenomena linking electron beam physics in a confined liquid domain and interfaces to liquid-phase transport and chemistry through the thermalized or "solvated" electron, a principal reactant in electrochemical reduction.

The principal objectives are to establish understanding of the roles of electron energy and interfaces on nanostructure fabrication. The two objectives are intrinsically linked, as control over local electron energy and number density involves control over interface locations and domain (precursor film) sizes. This information is accessed through quantification of reaction rates and characterization of the NESA-FEBID nanofabrication process (i.e. a detailed growth pattern description) to allow for the determination of the specific conditions under which deposits form. There are challenges to fabricating the structures necessary to answer these questions due to the complex dynamics of electrospray and film formation in vacuum. Our experiments have been carefully designed to address the process control challenges and to capture the phenomenological complexities, which enable us to begin answering the underlying questions as detailed below.

Electrospray of liquid films in vacuum is a non-equilibrium process. Using kinetic theory, a representative timescale of replacement for a typical film's solvent content is estimated to be around 100 μs, effectively concentrating the solute by a factor of ~100,000 for a typical

~10s process time. Therefore, the electrospray solution composition is amplified respectively (e.g. 10 nM solution concentration becomes 1 mM within the film) – for both intended precursors and contaminants. Trace components in liquid are respectively amplified, thus necessitating a high-purity experimental approach to the problem. The motion of the film is rapid due to quick film evaporation in vacuum. Rapid spray-driven charge transport through the film leads to unsteady charging effects when the film is rapidly evaporating and being replaced by the spray. Further, localized electron beam heating of the film can further drive evaporation and warping of the film structure. As such, the precursor ion and solvated electron concentrations are likely to be in a highly non-equilibrium state, which is a condition that is not typically found for nanomaterial synthesis through gas-phase FEBID. This is indeed a grand challenge multi-physics problem!

The process of electron beam deceleration is modeled through the PENELOPE method, a track structure method that produces electron trajectories for primary and secondary electrons. Each point in a trajectory contains electron position and energy information, and each trajectory contains information regarding its origination and termination, which is linked to generation of solvated electrons. For aqueous solutions, the secondary electrons are liberated from the water molecules via radiolysis, thermalized and are known to eventually recombine with water through a background reaction. The unstable water radicals may decompose prior to recombination in order to neutralize the resulting positive charge, resulting in byproduct formation such as hydrogen and oxygen gas. Gas formation inherently leads to film instability if it is sufficient to allow for bubble formation.

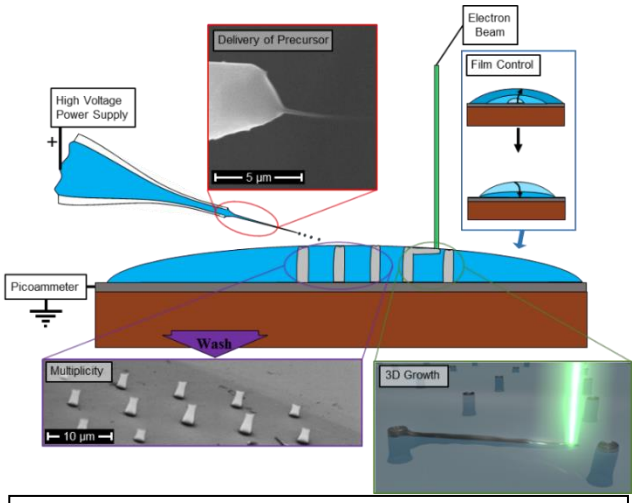

Fig. 1. Illustration of NESA-FEBID Process

Carbon co-deposition, typically found as amorphous carbon grown from the decomposition of residual hydrocarbons, is commonly the limiting factor in achieving high deposit purity and critical aspect to advancing any growth enhancement methods. Trace amounts of hydrocarbons present in the electrospray delivery and solution preparation appear to be amplified through electrospray deposition; while it is an open scientific question what is the origin of carbon deposition, it does appear that solutions with low concentrations of silver cations promote growth of deposits with high carbon content. NESA-FEBID using solutes we studied, typically a metal salt in concentrations ranging from 1 nM to ~10 mM in water, does not deposit silver at sufficiently low salt concentrations but preferentially grows carbon structures with some oxygen present.

Recent observations by us and others suggest that the bias (positive or negative) of the electrospray capillary plays a major role in determining the nature of the material observed at the

spray site. From the charge separation perspective, positive ES is the mode which would best facilitate the growth of metal deposits, as the excess charge in positive ES of a metal salt is usually an excess of metal cations. However, positive electrospray bias is found to generate nanoparticles that originate solely from the electrospray process. Regardless of the presence of the electron beam (i.e., with beam on or off), silver nanoparticles accumulate on the substrate from a positively-biased spray at higher metal salt concentrations leading to the formation of parasitic nanoparticle. Interestingly, NESA-FEBID using positive-mode electrospray of near-saturation salt solutions yields the spine-like structures made of homogeneously nucleated nanoparticles growing from the film on the substrate towards the spray capillary. These observations are consistent with literature, [1] which suggests that positively charged metal nanoparticles nucleate and grow within evaporating electrospray droplets during flight. These particles tend to self-assemble into whisker-like structures.

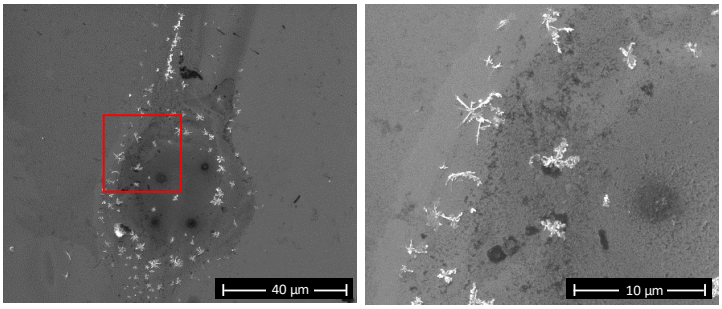

Fig. 2. NESA-FEBID via 30 keV beam irradiating a film formed from a solution of 100 µM AgNO3 in water. *Left*: Entirety of film with four beam exposures – left two exposures for 1 second, right two exposures for 3 seconds. *Right*: Magnification of highlighted region. White dendritic structures have high silver content, while dark spots are found to be carbonaceous.

Negative electrospray bias was adopted as a preferred precursor delivery mode to mitigate homogeneous growth and accumulation metal nanoparticles. It was found that the nanoparticles observed in positive ES are not present in negative ES, which is a critically important, positive result for NESA-FEBID. Regardless of the experimental conditions, due to evaporative enrichment some unreacted precursor salts remain on the substrate and are typically readily removed via soaking. Sample analysis both before and after salt removal provides unique insights: (1) pre-washed samples provide information about the film composition and environment during and at the end of the experiment; and (2) cleaned (washed) samples provide information about material that is adhered to the substrate via e-beam.

Experiments with deposit growth in negative ES have revealed several interesting unexpected features, depending on film thickness. For thick films with significant internal motion and relatively low concentration of salts in the spray solution, large size, substrate-adherent metal deposits cannot be formed. As thicker films tend to be unstable due to not only motion within the film, but fluctuations in film thickness from thick in the middle to very thin at the pinned edge, deposit formation is irregular. Thin carbon deposits are sometimes observed beneath liquid films in patterns associated with electron beam dwelling. Fig. 2 shows an example of those effects. High purity silver dendritic structures (as confirmed via EDS) are found littering the edge of the spray site, with carbonaceous material beneath spots that were exposed to an electron beam dwelled for one or three seconds. It is hypothesized that the silver

structures are formed at the liquid/vacuum interface due to an elevated secondary electron yield (and thus solvated electron generation), then move away from the beam location due to film motion, eventually settling at the outer edge of the film. A computational model used to determine the initial spatial solvated electron yield distribution shows (Fig. 3) that the generation of solvated electrons is the highest at the liquid/vacuum interface where the high-energy primary electron beam impacts the film, producing a cascade of low-energy secondary electrons. Electrons below 100 eV will only travel a few nanometers in water before being absorbed – thus, most solvated electrons thermalize near where they are generated. Consequentially, the majority of solvated electrons are produced right inside of the liquid/vacuum interface, and with their excessive presence, solid-phase silver nucleates and forms a deposit. As silver has a significantly higher secondary electron yield than water, the surface of the newly-formed silver deposits becomes a region of particularly high solvated electron concentration, driving the growth of the deposit. These deposits would grow to form large silver deposits if they were able to remain beneath the electron beam – but due to motion of thick films, they are unable to attach to the substrate. It is only in achieving thin films that these deposits will be able to grow to reach the substrate and to become eventually a beam-directed nanostructure.

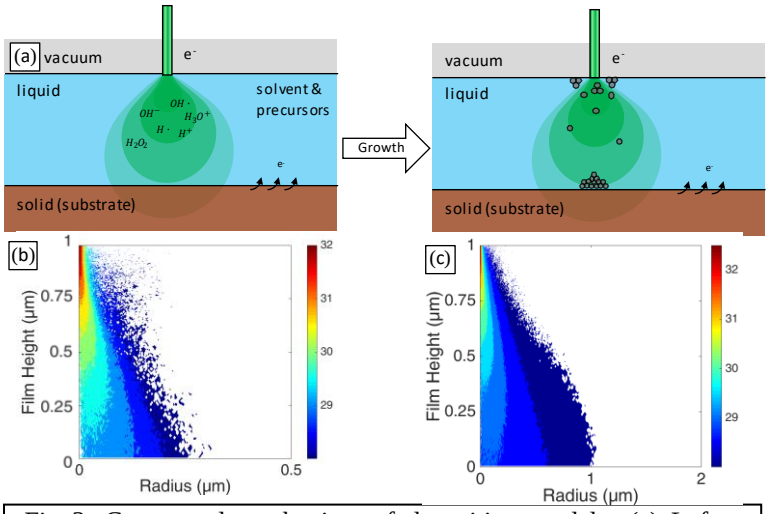

Fig 3. Conceptual mechanism of deposition model. (a) Left – Liquid film irradiated by e-beam immediate prior to growth. High energy electrons radiolize solvent, forming radicals which may participate in reactions along with the solute. Right – After solid phase nucleation and material precipitation, initial structures are formed. Generation rate (1/(m^3-s)) of solvated electrons by (b) 30 keV beam and (c) 10 keV beam impinging a 1 μm-thick water film.

Future Plans

Deposit Growth with Negative-Mode ES-Assisted Ultra-Thin Films: We hypothesize, based on the observations of silver dendritic structures present with thick films in negative ES cases, that ultra-thin ("invisible") precursor films are required for robust FEBID: (i) by minimizing electrokinetic motion within the film, and (ii) stabilizing the solid nucleation site at the liquid/ vacuum interface before it moves away from the beam and prevents a subsequent deposit growth and attachment to the substrate. We are currently in process of performing such experiments with ultra-thin films, as well as quantifying the dependence of deposition pathway on local solvated electron concentrations and secondary electron yields.

Role of Non-Equilibrium Film Conditions on Deposit Growth: Precise deposit shape definition demands the control over the extent of deviation of the state of the film from

equilibrium. We suspect that an increase in solute concentration leads to further deviation from equilibrium; exploring lower-concentration or near-equilibrium may lead to determination of the degree of non-equilibrium and the formation of smaller deposits down to the nanoscale. It is likely that high solute concentrations lead to rapid formation of deposits due to the film's non-equilibrium state (high localized precursor concentrations) – the phenomena we plan to exploit for enhanced growth.

References

1. Li, A., Luo, Q., Park, S.-J., Cooks, R. G., "Synthesis and Catalytic Reactions of Nanoparticles formed by Electrospray Ionization of Coinage Metals", *Angew. Chem. Int. Ed.*, **53**, 3147-3150 (2014).

Publications (last 2 years: 2015-2017)

1. Fisher, J., Kottke, P., Kim, S., Fedorov, A., Rapid electron beam writing of topologically complex 3D nanostructures using liquid phase precursor, *Nano Lett.*, **15**, 8385-8391 (2015).
2. Kim, S, Henry, M., and Fedorov, A., Using energized oxygen micro-jet for improved graphene etching by focused electron beam, *Appl. Phys. Lett,* **107** (23), 233102-06 (2015).
3. Kim, S, Kulkarni, D., Henry, M., Zackowski, P., Jang, S., Tsukruk, V. V. and Fedorov, A., Localized conductive patterning via focused electron beam reduction of graphene oxide, *Appl. Phys. Lett.,* **106**, 133109 (2015).
4. Kim, S, Russell, M., Henry, M., Kim, S., Naik, R., Voevodin, A. A., Jang, S., Tsukruk, V. V. and Fedorov, A., Dynamic modulation of electronic properties of graphene by localized carbon doping using Focused Electron Beam Induced Deposition, *Nanoscale,* **7**, 14946-14952 (2015).
5. Kim, S, Russell, M., Kulkarni, D., Henry, M., Kim, S., Naik, R., Voevodin, A. A., Jang, S., Tsukruk, V. V. and Fedorov, A., Activating "invisible" glue: using electron beam for enhancement of interfacial properties of graphene-metal contact, *ACS Nano,* **10**, 1042-1049 (2016).
6. Henry, M., Kim, S. and Fedorov, A., High purity tungsten nanostructures via focused electron beam induced deposition with carrier-gas assisted supersonic jet delivery of organometallic precursors, *J. Phys. Chem. C,* **120** (19), 10584–10590 (2016).
7. Henry, M. and Fedorov, A., Adaptive Direct Simulation Monte Carlo algorithm for unified continuous through molecular flow regime simulations with improved computational efficiency, *J. Computational Physics*, in review (September 2017).
8. Henry, M. and Fedorov, A., Molecular scale control of sticking probability and surface energy state using energized jets, *Science*, in preparation (October 2017).
9. Kim, S., Henry, M., M., Kim, S., Naik, R., Voevodin, A. A., Jang, S., Tsukruk, V. V., and Fedorov, A., Direct-write patterning and dynamic doping of monolayer graphene using focused electron beam induced processing, *Materials Research Society (MRS) Spring 2016 Meeting,* Phoenix, Arizona, March 28-April 1, 2016.

10. Kim, S. and Fedorov, A., FEBIP of graphene: etching/patterning, doping and contact modification, *6th FEBIP (Focused Electron Beam Induced Processing) International Workshop,* Vienna, Austria, July 5-8, 2016.
11. Henry, M., Fisher, J., Kim, S., Kottke, P. A.., and Fedorov, A., New capabilities for FEBIP using supersonic carrier-gas micro-jet and liquid nanoelectrospray for precursor delivery, *6th FEBIP (Focused Electron Beam Induced Processing) International Workshop,* Vienna, Austria, July 5-8, 2016.
12. Fedorov, A., Nanoelectrospray-Assisted Focused Electron Beam Deposition – A New Tool for Additive Nanomanufacturing. *Invited lecture at the Material Research Society (MRS) Spring 2018 Annual Meeting, Symposium on Additive Manufacturing*, Phoenix, Arizona, USA (April 2-6, 2018).

Forces, Crystallization, and Assembly in Nanoparticle Suspensions

K. A. Fichthorn, PI
Department of Chemical Engineering
The Pennsylvania State University
University Park, PA, 16802

Program Scope

Our research focuses on understanding the growth, transformations, and assembly of colloidal nanoparticles. We apply first-principles calculations based on (dispersion-corrected) density-functional theory (DFT), atomic-scale molecular dynamics (MD) simulations, and coarse-grained, meso-scale Monte Carlo (MC) simulations to several problems within this theme. We believe that our approach is appropriate and beneficial. Although first-principles calculations can be highly beneficial for understanding aspects of nanostructure formation, it is prohibitively difficult at present to simulate nanometer-sized particles in the presence of solvent (and perhaps additives) entirely from first principles. Such problems fall within the capabilities of classical MD simulations. The interatomic potentials in MD simulations can be parameterized and tested against first-principles calculations and/or experiments to ensure their suitability and this is a growing component of our research.

In classical MD, we model every atom and molecule of a colloidal suspension and obtain the force and the interaction potential between two or more colloidal nanoparticles as a function of their separation - a measurement that is beyond the reach of current experimental capabilities. We also simulate the aggregation of nanoparticles to unravel the underlying atomic-scale phenomena. We resolve thermodynamic and kinetic aspects of nanocrystal growth and how these may be influenced by solution-phase additives. Although in many cases, these phenomena can only be inferred from experiment, recent advances in real-time transmission electron microscopy (TEM) have made it possible to obtain a glimpse of nanoparticle aggregation and restructuring processes *in situ*.

Recent Progress

Thermodynamics of Nanocrystal Shapes

The solid-liquid interfacial free energy γ_{sl} is an important quantity in wetting, nucleation, and crystal growth. Since it is not always easy to measure this quantity, atomic-scale simulations have played an important role in establishing its value. Although various methods have been developed to calculate γ_{sl} with atomic-scale simulations, such calculations still remain challenging. We developed a multi-scheme thermodynamic integration method aimed at obtaining γ_{sl} using open-source MD simulation packages [1]. This method advances two aspects of its predecessor methods. First, we incorporate separate schemes to resolve difficulties when manipulating periodic boundary conditions of the

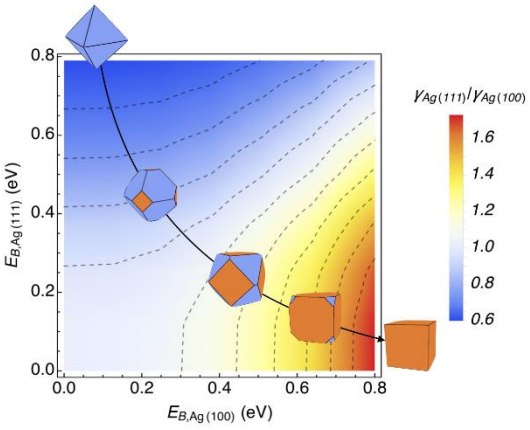

Figure 1: A map of $\gamma_{sl,Ag(111)}/\gamma_{sl,Ag(100)}$ as a function of zero-K binding energies, along with representative crystal shapes.

supercell using open-source simulation packages. Second, we introduce a numerical approximation to obtain thermodynamic integrands for complicated force fields when an analytical differentiation is not readily available.

We applied our method to resolve the thermodynamic influence of polyvinylpyrrolidone (PVP) in the shape-selective synthesis of Ag nanocrystals [2]. We find that although PVP has a preferred binding to Ag(100), its selectivity is not sufficient to induce a thermodynamic preference for {100}-faceted nanocubes, as has been observed experimentally [3,4]. This indicates that PVP promotes Ag nanocube formation kinetically rather than thermodynamically. We further quantify the thermodynamic influence of adsorbed solution-phase additives for generic molecules, by building a γ_{sl} ratio / nanocrystal shape map as a function of zero-temperature binding energies. This map is shown in Figure 1 and it can be used to gauge the efficacy of candidate additive molecules for producing targeted thermodynamic nanocrystal shapes. The results indicate that only additives with a strong facet selectivity can impart significant thermodynamic-shape change. Therefore, many of the nanocrystals observed in experiments are likely kinetic products.

Influence of Hexadecylamine on Cu Nanocrystal Shape

Hexadecylamine (HDA) and alkylamines, in general, are key molecules in the shape-selective synthesis of {100}-faceted Cu nanostructures. To resolve the origins of shape selectivity in these syntheses, we used dispersion-corrected density-functional theory to probe possible structures for adsorbed layers of HDA on Cu(100) and Cu(111) [5]. HDA forms self-assembled layers on these surfaces (see the inset of Figure 2), analogous to alkanethiols on various metal surfaces, and it binds by donating electrons in the amine group to the Cu surface atoms, consistent with experiment [6]. We find that HDA binds more strongly to Cu(100) than to Cu(111). This strong binding stems from the capability of HDA to form more densely packed layers on Cu(100), which leads to stronger HDA-tail interactions, as well as the stronger binding of the amine group to Cu(100). By drawing analogies to previous theoretical work [7], it seems likely that HDA-covered Cu nanocrystals could have kinetic shapes that primarily express {100} facets, as is seen experimentally [8].

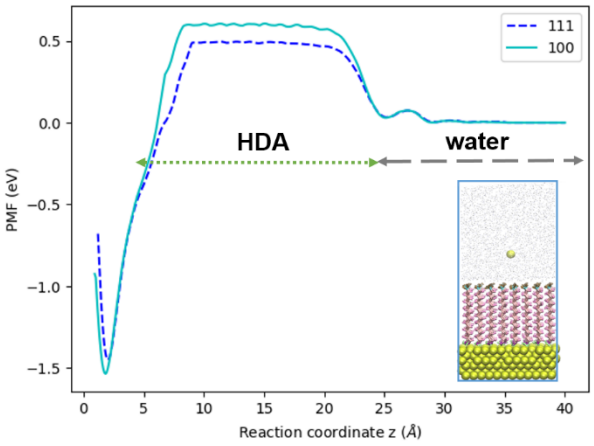

Figure 2: The PMF for a Cu atom to diffuse through HDA layers on Cu(100) and Cu(111). The inset shows a simulated self-assembled HDA layer on Cu(100), with a Cu atom in the aqueous phase above it.

To resolve the effect of HDA on nanocrystal growth, we developed a classical many-body force field to describe the interactions of HDA with Cu surfaces [9]. Our force field reproduces the DFT binding energies and configurations of self-assembled HDA layers on Cu(100) and Cu(111) at various coverages. To understand how HDA actuates {100}-faceted nanocrystals, we used umbrella-sampling MD simulations to calculate the potential of mean force (PMF) and

diffusion-coefficient profiles for Cu atom deposition onto Cu(100) and Cu(111) in aqueous solution with surface-adsorbed HDA. These profiles are shown in Figure 2. We use these profiles to calculate the mean-first passage times, as we did previously for PVP layers on Ag surfaces [7]. We find that self-assembled HDA layers can regulate the flux of Cu atoms to be greater towards Cu(111) than Cu(100). HDA's relatively weak binding to Cu(111) compared to Cu(100) leads to a lower free-energy barrier for Cu atoms to enter and diffuse through the HDA layer. The ratio of inverse mean-first passage times for the two facets is 32, which yields a cube based on the kinetic Wulff construction. The predicted kinetic Wulff shapes are in agreement with the analogous experimental system [8].

Solution-Phase Binding of PVP to Ag Surfaces: Theory and Experiment

The adsorption of solute molecules on surfaces in a liquid environment is an important phenomena in many cutting-edge applications such as nanomaterials, biosensors, and catalysis. Here, we examine the adsorption of PVP molecules on Ag surfaces in ethylene glycol solvent, with theory and experiment. We use MD simulations based on a many-body organic-metal force field [10] to calculate the PMF between PVP analog molecules and surfaces of Ag in both ethylene glycol solvent and in vacuum. In the resulting binding free energies, we see that solvent drastically decreases the binding free energy of the molecules from their vacuum values. We find that the entropy changes due to adsorption are generally negative in vacuum and their magnitude increases with molecular size. However, in solvent the entropy change is slightly positive and independent of molecular size. These results show that the liberation of adsorbed solvent molecules when a molecule binds to a solid surface can contribute more to the system's entropy change than the configurational entropy loss of the solute molecule due to adsorption. As we see in Figure 3, our calculated binding energies in solvent are consistent with those in experiment.

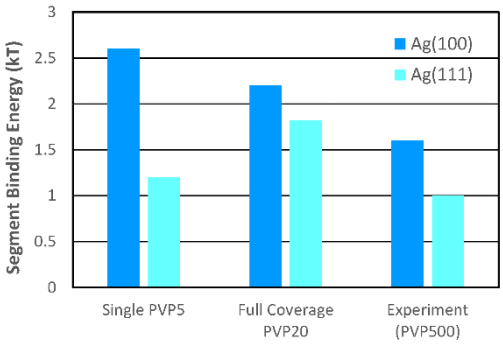

Figure 3: Calculated and experimental values for PVP binding energies on Ag(100) and Ag(111).

Future Plans

Many interesting studies are in the works. First, we are conducting an *in silico* search for effective capping molecules for Cu nanocrystals. At this point, we have extensive results with alkylamine molecules which show that matching of molecular geometry of alkylamines to the Cu surface, such that the amine groups have registry with the surface, can considerably enhance their binding to the Cu surface. Such studies will be useful in the search for optimal capping molecules for shape-selective syntheses. We conducted an *ab initio* thermodynamics study of the role of chlorine in promoting cubic Ag nanostructures and our results affirm that Cl can affect Ag surface energies enough to actuate {100}-faceted nanostructures. These studies show that, in addition to PVP, Cl can play a significant role in facilitating {100}-faceted nanostructures. Studies are underway of the oriented attachment of Ag nanoplates which show that selective plate aggregation into sheets is controlled by the density of PVP on the plate surfaces. We are studying the kinetics of fivefold-twinned Ag nanowire growth. These studies indicate that nanowire growth is dominated by the diffusion on Ag atoms on the nanowire

surfaces and that PVP plays a key role in facilitating the anisotropic structures of these wires. We look forward to an exciting year as we complete and publish this work.

References

1. X. Qi, Y. Zhou, and K. A. Fichthorn, *J. Chem. Phys.* **145**, 194108 (2016).
2. X. Qi and K. A. Fichthorn, *Nanoscale* (DOI: 10.1039/C7NR05765B)
3. X. Xia, J. Zeng, L.-K. Oetjen, and Y. Xia, *J. Am. Chem. Soc.* **134**, 1793-1801 (2012).
4. Y. Xia, Y. Xiong, B. Lim, and S. E. Skrabalak, *Angew. Chem. Int. Edit.* **48**, 60-103 (2009).
5. S.-H. Liu, T. Balankura, and K. A. Fichthorn, *Phys. Chem. Chem. Phys.* **18**, 32753-32761 (2016).
6. A. Glaria, J. Cure, K. Piettre, Y. Coppel, C.-O. Turrin, B. Chaudret, and P. Fau, *Chem.-Eur. J.* **21**, 1169-1178 (2015).
7. T. Balankura, X. Qi, Y. Zhou, and K. A. Fichthorn, *J. Chem. Phys*. **145**, 144106 (2016).
8. M. Jin, G. He, H. Zhang, J. Zeng, Z. Xie, and Y. Xia, *Angew. Chem.-Int. Edit.* **50**, 10560-10564 (2011).
9. S.-H. Liu and K. A. Fichthorn, *J. Phys. Chem. C* (DOI: 10.1021/acs.jpcc.7b07861)
10. Y. Zhou, W. A. Saidi, and K. A. Fichthorn, *J. Phys. Chem. C* **118**, 3366-3374 (2014).

Publications

1. K. A. Fichthorn, **(Invited Paper)** "Atomic-Scale Aspects of Oriented Attachment", *Chem. Eng. Science* **121**, 10-15 (2015).
2. S.-H. Liu, W. A. Saidi, Y. Zhou, and K. A. Fichthorn, "Synthesis of {111}-faceted Au Nanocrystals Mediated by Polyvinylpyrrolidone: Insights from Density-Functional Theory and Molecular Dynamics", *J. Phys. Chem. C* **119**, 11982-11990 (2015).
3. X. Qi, T. Balankura, Y. Zhou, and K. A. Fichthorn, "How structure-directing agents control nanocrystal shape: PVP-mediated growth of Ag nanocubes", *Nano Letters* **15**, 7711–7717 (2015).
4. K. A. Fichthorn, T. Balankura, and X. Qi, (Invited Paper) "Multi-Scale Theory and Simulation of Shape-Selective Nanocrystal Growth", *CrystEngComm* 18, 5410-5417 (2016).
5. T. Balankura, X. Qi, Y. Zhou, and K. A. Fichthorn, "Predicting Kinetic Nanocrystal Shapes through Multi-Scale Theory and Simulation: Polyvinylpyrrolidone-Mediated Growth of Ag Nanocrystals", *J. Chem. Phys*. 145, 144106 (2016).
6. X. Qi, Y. Zhou, and K. A. Fichthorn, "Obtaining the solid-liquid interfacial free energy via multi-scheme thermodynamic integration: Ag-ethylene glycol interfaces", *J. Chem. Phys.* 145, 194108 (2016).
7. S.-H. Liu, T. Balankura, and K. A. Fichthorn, "Self-Assembled Monolayer Structures of Hexadecylamine on Cu Surfaces: Density-Functional Theory", *Phys. Chem. Chem. Phys.* 18, 32753-32761 (2016).
8. S.-H. Liu and K. A. Fichthorn, "Interaction of Alkylamines with Cu Surfaces: A Metal-Organic Many-Body Force Field", *J. Phys. Chem. C* (DOI: 10.1021/acs.jpcc.7b07861)
9. X. Qi and K. A. Fichthorn, "The thermodynamic influence of solution-phase additives in shape-controlled nanocrystal synthesis", *Nanoscale* (DOI: 10.1039/C7NR05765B)

Nano-scale selective growth and Microstructural control of III-nitride growth

Zhen Deng, Ge Yuan, Jung Han

Department of Electrical Engineering,

Yale University, New Haven CT, 06520

Program Scope

Selective area growth (SAG) is a phenomenon in thin film deposition where the sample surface is marked by a dielectric or refractory layer such that growth takes place only in the exposed window regions. Now SAG has become a powerful and versatile method to reduce the dislocation density in heteroepitaxy. A reduction of dislocation density by a factor of 10 to 100 in SAG has been accomplished by dislocation blocking and bending. The selectivity is introduced due to the large disparities in incorporation energetics and kinetics between the mask and window region. When the opening window is pushed to nano-scale, it becomes possible to confine and control epitaxial evolution with lithographically engineered geometry with a feature size comparable to that of a single grain. An example is shown in Fig 1, where an array of deep nano-trenches is formed on a silicon wafer.

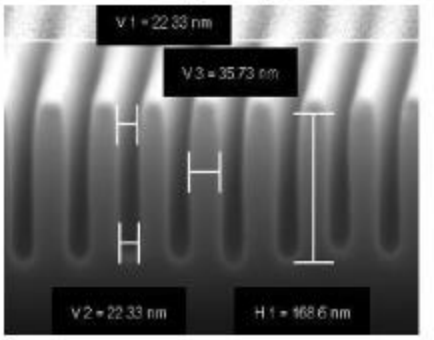

Fig 1. An example of modern Si-CMOS lithography showing an array of Si nano-trenches with a width of 22 nm and an aspect ratio of 7.5.[1]

We believe that the ability to precisely direct the vapor-phase deposition into nano-fabricated boundaries and contours will create new paradigms for III-nitride material synthesis and processing. In this program, we will focus on the nano-scale SAG of III-nitride and we wish to address fundamental questions related to synthesis science and material discovery. A fundamental hypothesis is that nano-engineered growth molds can dramatically alter the dynamics in microstructural evolution. We are particularly interested in SAG within highly asymmetric, nano-constricted geometries such as nano-trenches (illustrated in Fig 2). Two questions that will be addressed are (1) how does nanoscale constriction in one direction impact the microstructure evolution in the other orthogonal directions? Intuitively the nano-trenches would act like a "roller press" that plays an active role in "forcing out" defects in heavily-mismatched growth. There is little knowledge, however, regarding the coalescence dynamics along the lateral direction over micrometer scale. (2) How does the presence of nanoscale geometric boundaries affect the crystallographic orientation during SAG? Is it possible to influence if not direct the crystallographic orientation by the geometric shape of

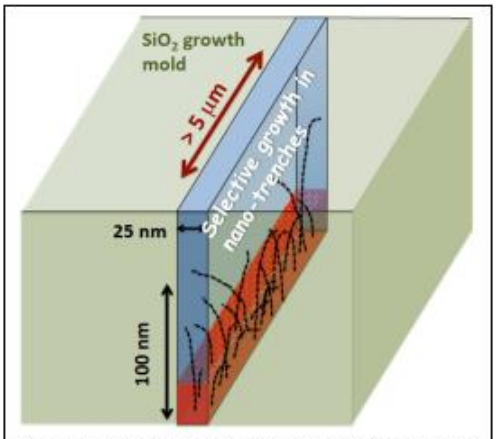

Fig 2. A schematic drawing of selective growth in a nano-trench.

the nano-trenches? This is reminiscent to the basic concept of graphoepitaxy [2,3], and we believe that SAG in a nanotrench would be a perfect test ground to understand the role of layer-dielectric interaction. InN, of which recent study has shown superior transport properties in defect free nanowires, is chosen as a case study to demonstrate the efficacy and unveil the science in nanoscale SAG. So far all the planar growth of InN has resulted in highly defective samples. However, recent works of InN nanowires provided initial evidence of truly superior transport properties in defect-free nanowires. In this project, we would like to address this intriguing and technologically important question: (3) What are the intrinsic properties of InN? Using nano-fabricated trenches with a high aspect ratio, we plan to prepare pristine InN nanosheets and address this question in a definite way.

Recent Progress

A. Nanoscale SAG of InN nanowalls

Recently, InN has attracted intensive studies in terahertz devices and high speed electronics due to its superior electron transport properties. Compared to other III-nitride materials (e.g., GaN and AlN), the epitaxial growth of InN still remains challenging. In our lab, we demonstrated the uniform and continuous InN nanowalls on GaN/Si template with nano-pattern utilizing MOCVD. The challenge in the nano-SAG of InN is related to the comparable strength in the In-N covalent bond and the In-In metallic bond. A comprehensive study of InN nano-SAG was performed. We studied the effect of various growth parameters (temperature, pressure, and V/III ratio) on the InN nanowall growth in details. With optimized growth condition, we obtained uniform and continuous nano-wall with perfect selectivity, as shown in figure a. Cross sectional TEM images of nanowall was shown here. There is no dislocation in the nanowall, which may be eliminated at the InN/GaN interface. The height of dislocation-free InN nanowall greatly exceeds the critical thickness encountered in conventional heteroepitaxy.

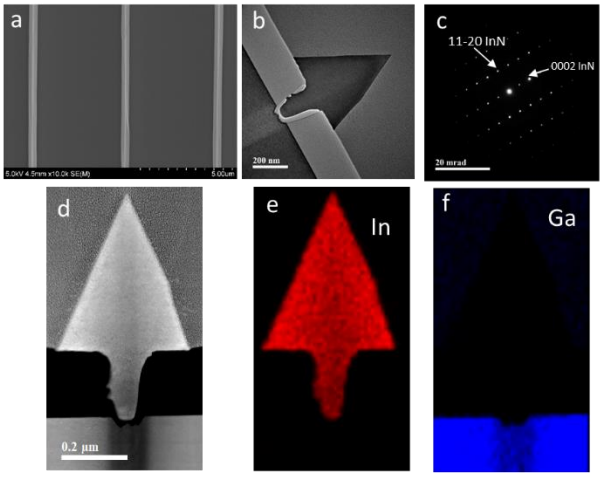

Figure 3 Demonstration of InN nanowalls by nano-SAG. (a) top-view SEM image of InN nanowalls, (b) a bright-field TEM image of a cross section, with a corresponding selected-area diffraction pattern(figure c), (d) STEM HAADF of an InN nanowall, (e-f) the EDX mapping results of In and Ga, respectively.

B. Investigation of InN-SiO2 trench wall interaction

An important vision of this BES project is to study and utilize the weak interaction between a crystalline nucleus and the SiO2 surface, which is often neglected in most of the SAG experiments, to induce a crystallographic anisotropy in the nucleation process, which can then be used as an orientation filter. The thermodynamic consideration involves the interplay and balance of four terms in Gibbs free energy of nucleation: 1) bulk energy of crystallization (phase

transition), 2) free surface energy of nucleus, 3) work of adhesion between the nucleus and the SiO2 wall, and 4) the torsional energy if any rotation happens with the nucleus. T quantify the effect of work of adhesion, we prepared a series of nano trenches with width from 50 to 500 nm (Fig 4, middle) and performed nucleation study. As the trench width decreases, we observed an unambiguous increase (Fig 4, right panel) of the nuclei density by almost six fold, from 20 to 110 μm^{-2}. We therefore conclude that the work of adhesion is sufficient to substantially lower the conventional heterogeneous, planar nucleation (the sum of items 1 and 2).

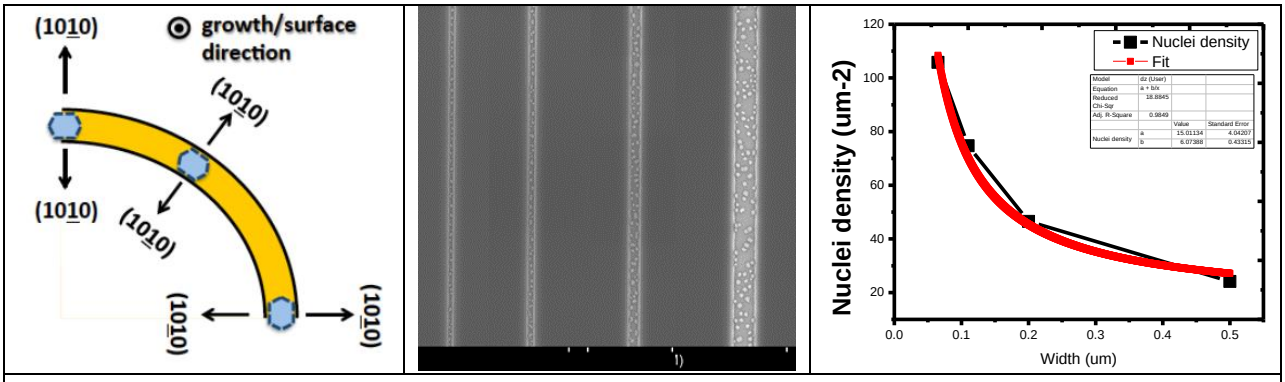

Fig 4. (Left) The vision of nanoscale crystal rotation with enhanced interaction of nuclei with nano trenches, (middle) SEM images of InN nuclei in nano-trenches with different widths from 50 to 500 nm, and (right) a plot of the measured area density of InN nuclei vs trench width, indicating a clear enhancement of nucleation rate by the work of adhesion.

C. Demonstration of orientation filtering by nano-trenches

Based on the result of Part B, we studied the effect of having the nano trenches to be misaligned from the crystallographic axis of the underlying epitaxial template, as illustrated in Fig 5 (left). The idea is that the work of adhesion will be a function of the misalignment angle (θ), with θ equals zero being the perfect alignment of SiO2 wall with the m-plane of InN, and possibility the highest work gained in the nucleation process As θ starts to increase, the work of adhesion will become less negative or even positive, thus increasing the nucleation barrier and reducing the nucleation rate. We studied a series of nano trench patterns with a width varying from 50 to 500 nm, and a misalignment angle from 0 to 30 degree. The nuclei densities are summarized in Fig 5, middle plot. Here we continue to observe the trend of an enhanced interaction as the trench width narrows. More interestingly, when we plot the nuclei density as a function of θ (Fig 5, right), we observed an interesting trend. When the trenches are relatively wide, there is little or no angular dependence (the bottom three curves). When the trench width is reduced to 65 nm, a size that starts to approach the nuclei size of 25 nm, we started to notice an unambiguous dip in nuclei density. This series of study provide a first evidence that the presence of parallel nanotrenches can introduce crystallographic anisotropy, possibly to mediate and even control the selective growth event.

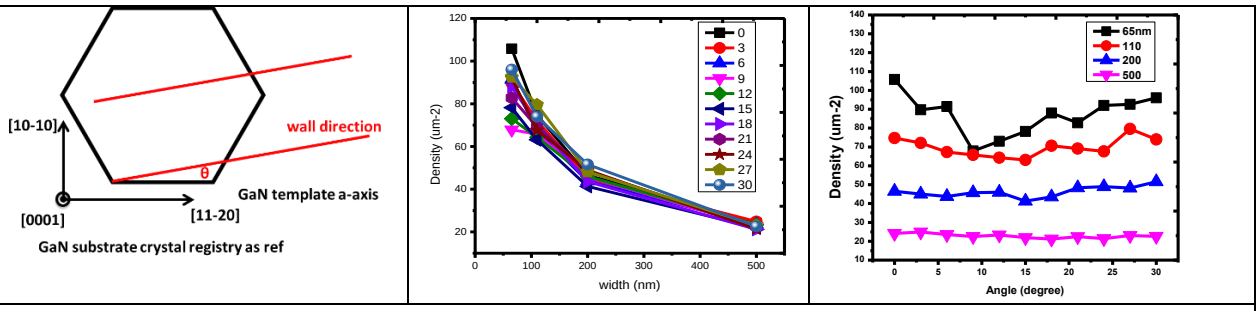

Fig 5. (Left) Schematic illustration of misalignment between nano-trenches and GaN to probe the angular dependence of the work of adhesion, (middle) summary chart of the density of InN nuclei in nano-trenches with different widths from 50 to 500 nm, and with a misalignment angle from 0 to 30°, and (right) a plot of the measured area density of InN nuclei vs the misalignment angle, with the trench width varied from 500 to 65 nm. The effect of nano-trench becomes noticeable below 65 nm.

Future Plans

- Further study of nanotrench effect, going to the angle of 30 to 60°.
- Further study of nanotrench effect, using m-axis as the reference.
- Making the nanotrench narrower (~40 nm) to enhance the work of adhesion.
- Making InN nanoscale transisters.

References

1. From Oxford Instruments Plasma Technology website http://www.oxfordinstturments.com/products/etching-depostion-and-growth/processes/etching-processes/silicon.

2. M. W. Geis, D. C. Flanders, and Henry I. Smith, "Crystallographic orientation of silicon on an amorphous substrate using an artificial surface-relief grating and laser crystallization", Appl. Phys. Lett. 35, 71 (1979).

3. D.C. Flanders, "Orientation of crystalline overlayers on amorphous substrates by artificially produced surface relief structures", MIT thesis, (1978).

DoE Sponsored Publications in the Last 2 Years

1. Ge Yuan, Sung Hyun Park, Benjamin Leung, and Jung Han, "New directions in GaN material research: thinner and smaller". SPIE, 2016.

2. Zhen Deng, Ge Yuan, Jun Li, and Jung Han, "Growth of uniform and continuous Indium nitride nanowalls by Metal-organic chemical vapor deposition". Manuscript preparation.

3. Zhen Deng, Ge Yuan, and Jung Han, "Evaluation of growth and optimization of growth parameters for InN epitaxy in nano-scale trenches on GaN template". Manuscript preparation.

4. Zhen Deng, Ge Yuan, and Jung Han, “Growth, structural and optical properties of InN nanorods prepared by nano-scale selective area metalorganic chemical vapor deposition”. Manuscript preparation.

Fabricating single crystal quantum dot solids by inkjet printing (DE-SC0018026)

Tobias Hanrath,[1] Paulette Clancy,[1] Lena Kourkoutis[2]

1 Robert Fredrick Smith School of Chemical and Biomolecular Engineering, 2Applied and Engineering Physics , Cornell University, Ithaca, New York 14853

Program Scope

This collaborative research program to develop new fabrication techniques that enable the creation of single crystal quantum dot solids (QDS) with programmable symmetry and composition. Our approach towards that goal builds on a firm foundation of preliminary results and a successful track record of previous collaborations. We will leverage access to and experience with unique *in-situ*, multi-probe characterization techniques to gain deep insights into the fundamental relationship between processing conditions and nucleation and growth of QDS. The program integrates computational modeling and experiment to gain atomic-level insights into the underlying physical phenomena governing assembly and attachment and to guide development of optimized processing methods.

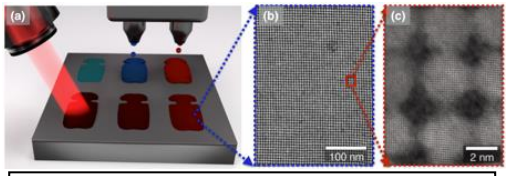

The project aims to develop new fabrication techniques that integrate (a) inkjet printing of small liquid volume and laser annealing to create (b,c) single crystal quantum dot solids.

Recent Progress

We report initial advances towards controlling the directed self-assembly and attachment in small-scale droplets formed by inkjet printing. Self-assembly of semiconductor nanocrystals into superlattice has opened up the materials library by design. Driven by the complex interplay between nanocrystal, ligands, solvent and substrate, integration of nanostructures into solid state devices needs to overcome difficulties in preserving surface stabilities of nanocrystals while maintaining the long-range order of the superstructure. Here we demonstrate the fabrication of lead sulfide nanocrystals thin films using inkjet printing. Uniform thin films with monolayer to bilayer thicknesses with periodic arrangement of nanocrystals were obtained. Adding a liquid subphase to initiate the self-assembly at fluid interface increased the range of order. Further improvements in the printing technique such as the compatibility with low viscosity ink and surface sensitive materials would advance the fabrication of single crystal nanostructured thin film.

Future Plans

Our initial studies with inkjet printed quantum dot solids have provided important new insights into the underlying parameter space in which high-fidelity structures can be formed. Our future efforts focus on extending these processing insights to ‘connect the dots’ by applying chemical treatments to initiate formation of epitaxial inter-dot connections.

References

n/a

Publications

n/a

Mechanochemical, Electrochemical, and Electromechanical Manipulation of Graphene and Carbon Nanotube Synthesis

PI: A. John Hart, Massachusetts Institute of Technology

1. Program Scope

The goal of this program is to investigate the influence of mechanical forces on the nucleation, growth, and post-synthesis manipulation of carbon nanostructures. In our past work, we developed techniques and instrumentation to study the influence of forces on carbon nanotube (CNT) growth, and in the past two years we have shifted our main focus to graphene growth as an exemplary 2D material system. The overarching goal of this combined effort is to understand how stresses at to the catalyst-carbon interface govern the nucleation and precipitation of carbon into graphene and CNTs, and how these processes may be manipulated by non-thermal means. Specifically, in the past two years, we have completed a long-term investigation of mechanically-modulated CNT growth, and studied the nucleation and growth of graphene and CNTs from metal surfaces via environmental TEM. In addition, we studied the electrochemical formation of graphitic carbon on Ni, and developed an electromechanical method to transfer graphene from metal substrates to polymers.

2. Recent Progress

2.1 Mechanical manipulation of CNT forest growth

In our previous work, we found that application of controlled compressive forces, ranging from 0.1 g to 10 g (~1.2 kPa to ~125 kPa), can cause measureable changes in the growth kinetics and the morphological development of CNT forests forest. We have since performed small-angle X-ray scattering (SAXS) characterization of these forests at the Advanced Photon Source at Argonne National Lab, allowing us to map the Hermans orientation parameter (Fig. 1a), volume fraction, and density throughout the height of the forests with 20 μm vertical resolution. Using this data and the mechanical properties of a forest as determined by a high-temperature compression test performed within our custom CVD reactor, we have developed a model of the mechanical deformation of a nominal forest under applied compression. Assuming the forest exhibits foam-like behavior [1],

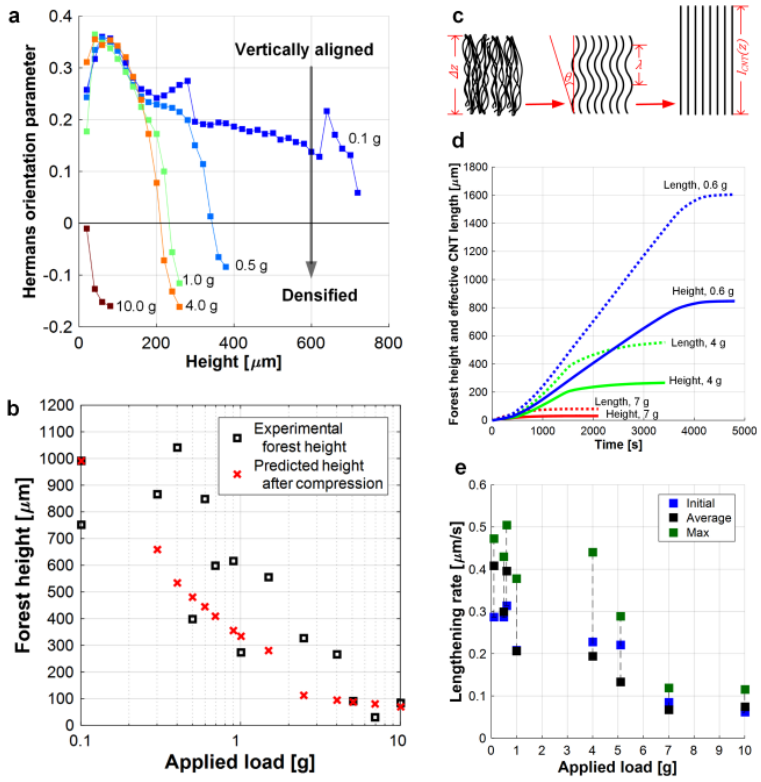

Figure 1. (a) Hermans orientation parameter from as a function of distance from the top of CNT forests (height = 0) grown under different applied loads. (b) Terminal height of forests grown under load and the predicted height of a nominal forest compressed under the same load. (c) Representative CNT geometries were used to determine (d) the average CNT length vs. growth time and (e) lengthening rates of the average CNT in forests grown under different applied loads.

we find that the predicted compressed height of a forest is similar to the termination height of the forests grown under the same load (Fig. 1b). We thus conclude that the forest collapse and termination height is a macroscale mechanical response to the applied load.

Further, we estimated the average lengthening rate of a CNT within the forest as a function of growth time. The SAXS alignment data allows us to approximate the average waviness of a CNT (assuming a sinusoidal shape as observed in SEM images) for each position in the forest, which can be then be used with our *in situ* forest height measurements to determine the length of the average CNT as a function of growth time (Fig. 1c,d). Figure 1e shows that the lengthening rate of the average CNT decreases as a function of applied load, indicating that mechanical force not only influences the morphological development of the CNTs, but also has a mechanochemical influence on the kinetics of CNT growth.

2.2 In situ transmission electron microscope studies of graphene and CNT growth

Further understanding of how the CNT and graphene growth can be tailored by carbon exposure kinetics has been obtained by environmental transmission electron microscopy (ETEM), performed as external users at Brookhaven National Lab. In our lab CNT growth reactors, we have observed a drastic increase in catalyst particle density and CNT yield due to a trace amount of carbon during annealing. We have replicated this effect in the ETEM by including 0.1 mTorr C_2H_2 with 40 mTorr H_2 during the annealing of Fe catalyst before increasing the pressure of C_2H_2 to 10 mTorr for growth, as compared to annealing in 40 mTorr H_2 without C_2H_2 but with the same growth conditions (Fig. 2a,b). However, we also observe a similar increase in density in the ETEM by annealing in NH_3 rather than H_2, and introduction of a small amount of C_2H_2 during the anneal in NH_3 actually has a detrimental effect (Fig. 2c,d). Understanding of why H_2 and low C_2H_2 exposure *or* just NH_3 exposure during annealing resulted in highest catlayst density and CNT yield is a subject of further investigation, and will involve determination of the active catalyst phase during CNT growth for each of these conditions.

We have also studied graphene growth on Ni using MEMS TEM chips, which have the capability of heating to up to 1100 ^{o}C within a few seconds while minimizing thermal drift, allowing for high resolution images and videos to be obtained at high temperature throughout the whole growth process. We used Ni-oxide nanorods that decomposed into reduced Ni particles (to serve as the catalyst for graphene growth) while heating to 650 ^{o}C in H_2. Nucleation and growth of graphene was observed with videos taken at 400 frames per second; a few frames of the video at time stamps corresponding to time after introduction of C_2H_2 into the ETEM are shown in Fig. 2e-h. The particles appear to swell and breathe as carbon diffuses throughout and eventually forms graphitic layers, as indicated with arrows in Fig. 2h, and further

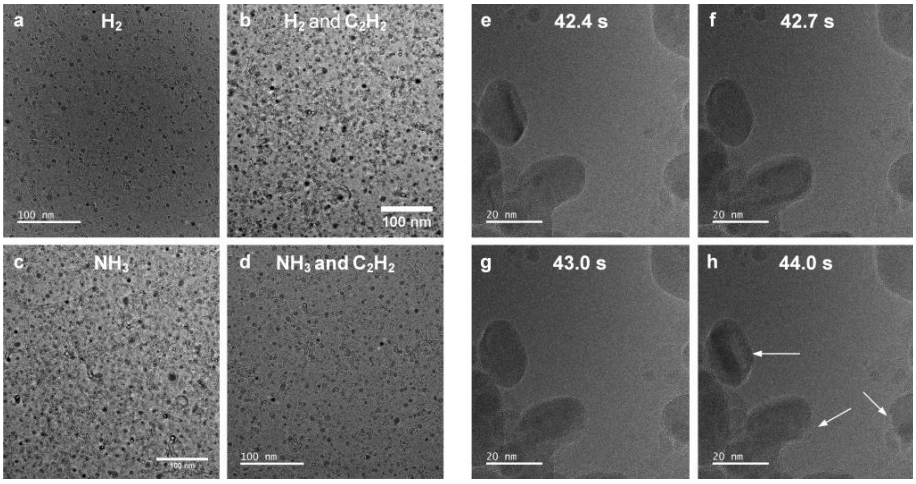

Figure 2. Images taken in an ETEM (a-d) after four CNT growths with different annealing environments, and in a time series (e-h) after introduction of C_2H_2,

investigation of this mechanism is underway.

2.3 Electro-organic chemistry for graphene synthesis

To better understand and control the mechanism of graphene synthesis, we have explored the room temperature liquid phase electrodeposition of organic compounds that undergo catalytic conversion to form graphitic materials. The synthesis procedure follows a liquid-solid mechanism, wherein the liquid carbon molecules (tetrachloromethane, tetrachloroethylene) are converted to solid graphitic carbon, catalytically assisted with a heteropolyacid such as phosphotungstic acid. The process is conducted in a 2-electrode cell with a working electrode (cathode) of Ni foil and a counter electrode (anode) of Pt mesh; Fig 3a shows the resulting synthesized carbon deposits on the Ni electrode.

Raman spectroscopy reveals a D peak (~1350 cm^{-1}) and a G peak (~1600 cm^{-1}) characteristic of carbonaceous materials (Fig 3b). A G/D value of 1.9, found from Gaussian/Lorentzian line fits of the peaks, indicates that the degree of graphitization of the material is comparable to many carbon nanomaterials such as multi-walled CNTs and graphene. SEM imaging (Fig. 3c) shows a similar morphology to other carbon nanomaterials such as a CNT forest. By using energy dispersive spectroscopy, we conclude the structures are primarily carbon, with some non-bonded chlorine contamination. TEM imaging also provides indication of the formation of graphitic layers (Fig. 3d). Additionally, Fourier-transform infrared spectroscopy (FTIR) data suggests the presence of acyl chloride materials, which would likely form as a byproduct during electrochemical deposition. Other moieties found with FTIR include alkanes, aldehyde, and some degree of aromatic alkene molecules, which are typical reaction by-products formed during the cathodic reduction of halogenated hydrocarbons.

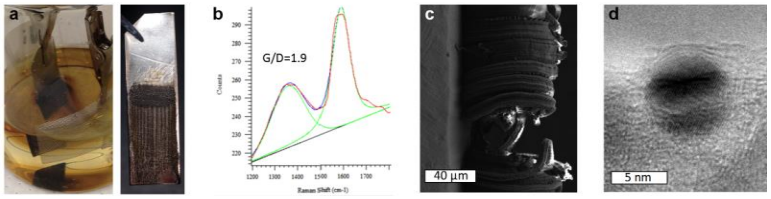

Figure 3. (a) Graphitic formation on a Ni working electrode in a 2-electrode electrochemical cell. (b) Representative Raman spectrum of the synthesized graphitic material. (c) Large-scale morphology in SEM and (d) TEM images indicating the presence of graphitic layers around a Ni particle that had formed during the cathodic reduction process.

2.4 High-speed electromechanical transfer of graphene

During the past reporting period, we developed a high-speed electromechanical transfer technique which enables direct transfer of graphene from their growth substrates (e.g. Cu foils) to dielectric substrates (e.g. polyethylene terephthalate, PET), without need of any chemical adhesives or etchant. Transfer is achieved by first oxidizing the graphene-coated Cu to weaken their adhesion, and then applying a mechanical load (~10-100 N/m), electric field (~1-1.5 kV), and elevated temperature (~100-130 °C) to establish intimate contact and provide a driving force for direct transfer. The new contact transfer process is entirely dry, not requiring any adhesives, etchants, or sacrificial transfer layers.

Process steps for the graphene transfer are illustrated in Fig. 4a. We first immersed a CVD grown monolayer of graphene on a copper foil in a hot water (40-50 ºC). This step facilitates the oxidation of copper on every surface, including the graphene/copper interface, which is known to reduce the adhesive strength between the graphene and the copper foil [2]. Then, we sequentially placed a thin PET film and the graphene/copper on top of a flat bottom conductive plate. An electromechanical contact was applied by rolling a conductive roller with a high compressive force, while the roller and the bottom plate were connected to a bias voltage. High electromechanical force is required to compromise the inherent roughness of the copper foils,

which allows uniform contact between the graphene and PET and therefore enhances their work of adhesion (Fig. 4b). After electromechanical contact, the copper foil was manually peeled off which may leave the transferred graphene layer on the PET film.

We applied mechanical force of 1-5 N which corresponds to a line contact force of 100-500 N/m for transferring one centimeter wide graphene layers and bias voltage up to 1.5 kV. In addition to electromechanical contact, an electrical heater was embedded beneath the bottom plate to elevate the temperature of PET films during the contact. Temperature above the glass transition point of polymeric films can dramatically reduce the mechanical stiffness, which is advantageous to achieve uniform contact against other surfaces. From this setup, we demonstrated transfer of a monolayer of graphene from its growth substrate to a PET film at a speed of 200 mm/s (Fig. 4d).

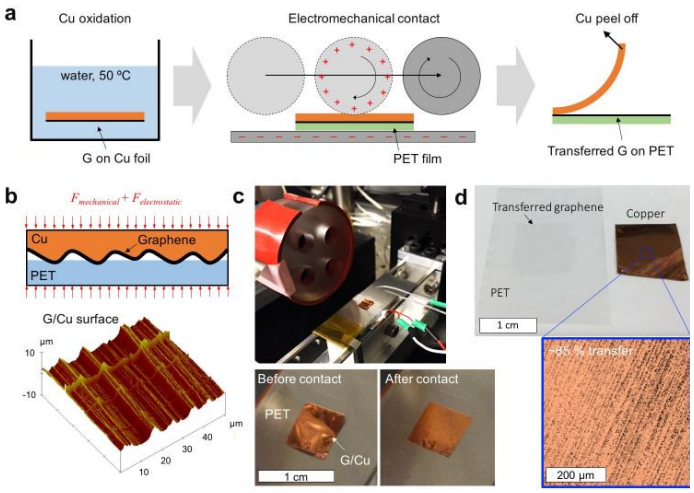

Figure 4. Electromechanical transfer of graphene: (a) schematics of process steps of electromechanical transfer of a CVD grown graphene layer from its growth substrate (a thin Cu foil) to a dielectric film (PET). (b) A schematic of interface between G/Cu and PET during electromechanical contact (not in scale) and a AFM image of a G/Cu surface. (c) Photographs of a roll-to-plate apparatus used for electromechanical transfer demonstration. Bottom left shows a G/Cu placed on top of a PET film before and after electromechanical contact. (d) A photograph of a transferred graphene layer at 100 N/m, 1.5kV, 130 °C of a preoxidized G/Cu for 2 hours. Bottom is an analyzed SEM image of the copper surface after the transfer, where amber and black colors represent the local area where the graphene has transferred and has not, respectively.

3. Future Plans

The overarching goal of the above efforts is to establish an improved processing route for uniform, large area graphene and CNT-based materials, relying on mechanical and electrochemical manipulation of the reaction process. Therefore, in the ongoing year, we plan to perform additional high-resolution TEM of graphene synthesis on Ni, and use macroscale mechanical experiments to quantify interfacial adhesion strengths both during and after synthesis. This will provide an improved fundamental understanding of how manipulation of carbon dissolution and precipitation in metals (e.g. Ni, Cu) controls the synthesis of nanostructured carbon; and how graphen may be transferred to secondary substrates for employment in practical applications. In addition, measurements of adhesion mechanics under various conditions will present guidelines for stacking of different 2D materials for device integration.

.

4. References

1. X. Liang, J. Shin, D. Magagnosc, Y. Jiang, S. Jin Park, A. John Hart, K. Turner, D. S. Gianola, and P. K. Purohit, “Compression and recovery of carbon nanotube forests described as a phase transition,” *Int. J. Solids Struct.*, vol. 123, pp. 196–209, 2017.
2. P. R. Whelan et al., Raman spectral indicators of catalyst decoupling for transfer of CVD grown 2D materials, Carbon 117, 75-81 (2017).

5. Publications (Past 2 years)

1. A.Ya'akobovitz, M. Bedewy, A. Rao, A.J. Hart. Strain Relaxation and Resonance of Carbon Nanotube Forests Under Electrostatic Loading. *Carbon,96*, 250-258, 2016. http://dx.doi.org/10.1016/j.carbon.2015.09.038.
2. M. Bedewy, B. Viswanath, E.R. Meshot, D.N. Zakharov, E.A.Stach, A.J. Hart. Measurement of the Dewetting, Nucleation, and Deactivation Kinetics of Carbon Nanotube Population Growth by Environmental Transmission Electron Microscopy. *Chemistry of Materials* (2016). http://dx.doi.org/10.1021/acs.chemmater.6b00798.
3. B. Viswanath, M. Bedewy, E.R. Meshot, S.W. Pattinson, E.S. Polsen, F. Laye, D.N. Zakharov, E. Stach, A.J. Hart. Real-Time Imaging of Self-Organization and Mechanical Competition in Carbon Nanotube Forest Growth. *ACS Nano* 2016, 10 (12), pp 11496–11504. http://dx.doi.org/ 10.1021/acsnano.6b07251
4. N. Dee, M. Bedewy, J. Beroz, A. Rao, H. Zhao, P.R. Kidambi, T. Serbowicz, E.R. Meshot, K. Teichert, B. Lee, P.K. Purohit, A.J. Hart. In Situ Mechanical Modulation of Carbon Nanotube Forest Growth. *In preparation,* 2017.
5. S. Kim, A.J. Hart. Continuous Electromechanical Transfer of 2D Materials. *In preparation*, 2017.
6. P. Kidambi, D. Mariappan, N. Dee, A. Vyatskikh, S. Zhang, R. Karnik, A.J. Hart. A scalable route to large-area graphene nanofiltration membranes by roll-to-roll chemical vapor deposition and polymer casting. *In preparation,* 2017.

A Theory of Growing Crystalline Nanorods

Hanchen Huang
Department of Mechanical and Industrial Engineering, Northeastern University

Program Scope

The long-term scope of this project has been to establish a theoretical framework of nanorod growth using physical vapor deposition (PVD). In the previous project period, we had developed an analytical theory of the smallest diameter of nanorods under idealized geometrical shadowing of nearly 90° incidence of deposition flux and complete dominance of multiple-layer surface steps [1]. Building on this achievement, in the current project period we develop theories that apply to generalized growth conditions, particularly (1) no-idealized geometrical shadowing and (2) incomplete dominance of multiple-layer surface steps. Further, we also explore possible technological impacts of the scientific discoveries.

Our theoretical development relies on a synergy with atomistic simulations and experiments. The atomistic simulations serve to reveal atomistic mechanisms for inclusion in the theoretical formulations, and also to verify the theories. The experiments serve to validate the theories, and to test designed growth of nanorods under the guidance of the theories.

Recent Progress

Among the many progresses as the publication list indicates, this report focuses on three that represent (a) the development of a theory for non-idealized geometrical shadowing [2]; (b) the exploratory development of a theory that bridges thin film growth and nanorod growth, and involves competition of multiple-layer and monolayer surface steps [3]; and (c) a metallic glue technology that derives directly from the scientific discoveries through this project [4].

First, we have considered non-idealized geometrical shadowing, for which the incidence angle of deposition flux is below 90°. As a result, the diameter L_m of nanorods explicitly depends on their separation L_S, as it should. As shown in Figure 1a, the diameter under idealized geometrical shadowing would have been l_m. In this generalized theory, L_m is linearly proportional to L_S with a proportionality constant that depends on l_m as well as incidence angle θ and z_c that characterizes the kinetic energy of incidence atoms:

$$L_m = \left(\frac{4}{\pi f}\right) L_s$$

where $f = \frac{F_e}{F} = 1 + \left[0.48\left(\frac{z_c}{l_m}\right) - 3.14\left(\frac{z_c}{l_m}\right)^3\right]\tan\theta$ and $l_m = \left(\frac{10}{\alpha^2}\ln\frac{n}{2}\frac{v_{3D}}{fF}\right)^{\frac{1}{5}}$ as derived in ref [1]. As shown in Figure 1b, the generalized theory shows that the slope of the linear dependence of L_m on L changes as the incidence angle of deposition flux changes. It is encouraging that the experimental data confirms such dependencies.

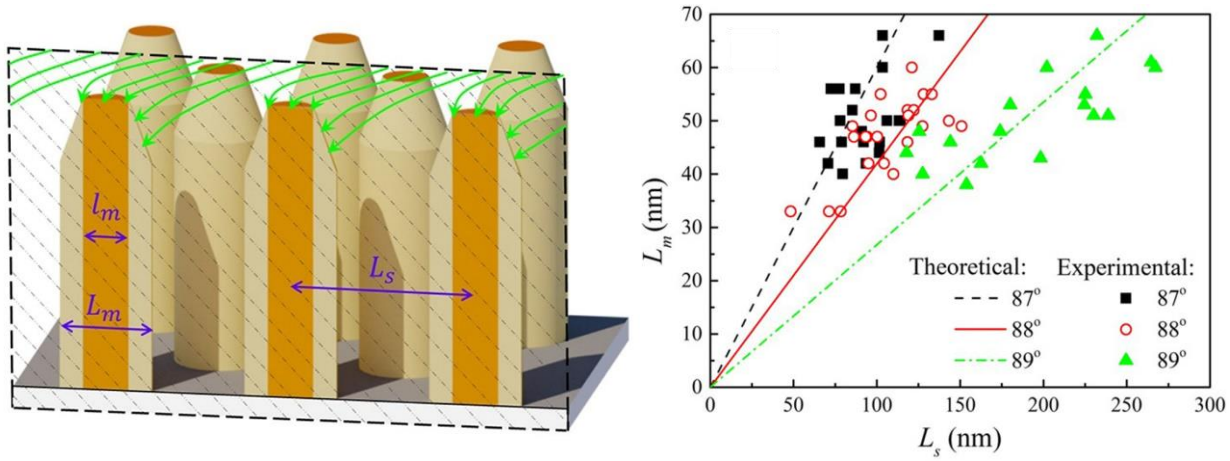

Figure 1: (a) Schematic of nanorod growth, showing atomic flux (green lines) in a vertical cross-section that cuts through the center of three nanorods in the front; and (b) comparison of experimental data with closed-form theory for nanorod diameter vs separation.

Second, having established the theory for non-idealized geometrical shadowing, we explore the transition between nanorod growth and thin film growth. Equivalently, this is also the transition from complete dominance of multiple-layer surface steps to a combination of multiple-layer and monolayer surface steps, and then to complete dominance of monolayer surface steps. For this purpose, we start from the well-established wedding cake model [5, 6] that is valid for complete dominance of monolayer surface steps. This exploratory study is in two dimensions, so as to achieve simpler theoretical formulations and clearer verifications from atomistic simulations.

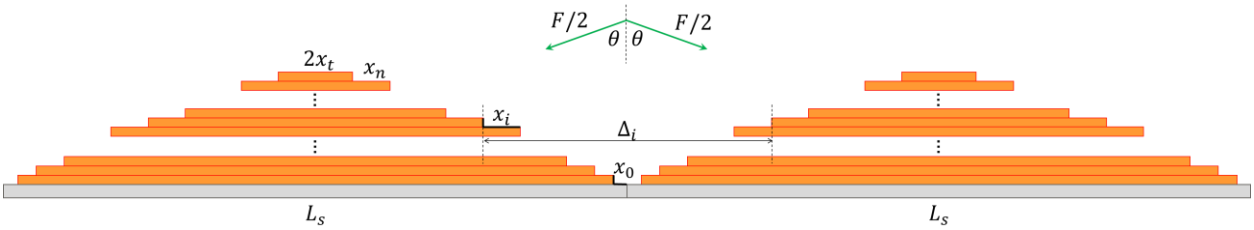

Figure 2: Schematic of array of terraces with monolayer step, showing terrace lengths x_i, with the i-th terrace and the i-th step highlighted as dark lines, and the size of the top layer $2x_t$.

As shown in Figure 2, the growing surface is initially covered with monolayer surface steps. Interestingly, as the incidence angle of deposition flux is below a critical threshold, the wedding cake model is directly applicable although it was formulated for normal incidence. However, beyond this threshold, the first transition occurs at a critical coverage Θ_I so the wedding cake model no longer applies, and the surface roughness is larger than what the wedding cake model would predict. As deposition continues, beyond another critical coverage Θ_{II} multiple-layer surface steps form, so the surface is covered by a mixture of multiple-layer and monolayer surface steps. The theoretical values of critical coverages as a function of the incidence angle are shown as solid lines in Figure 3. The accompanying atomistic simulations are conducted for each combination of coverage and incidence angle. In the upper right domain,

multiple-layer surface steps form 80% or more frequently out of 500 independent simulations for each combination of incidence angle and coverage. In the lower left domain, this probability is lower than 20% or nearly zero.

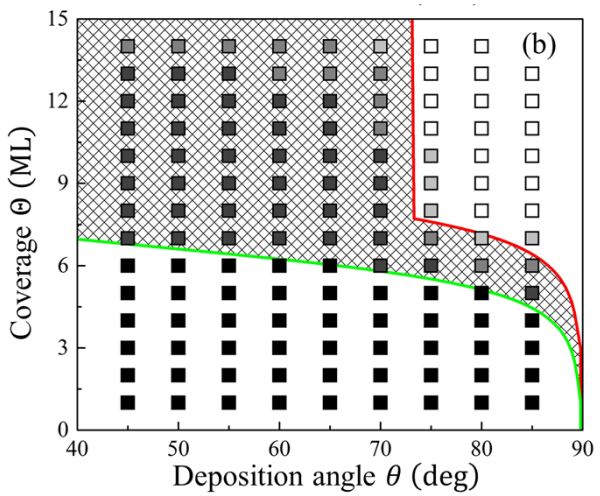

Figure 3: Phase diagram with two separatrices that divide the phase space into the lower-left domain for thin film growth governed by the wedding cake model, the upper-right domain for nanorod growth with multiple-layer surface steps, and the domain in between for thin film growth not governed by the wedding cake model; with atomistic simulation results shown as squares.

Beyond the two progresses in scientific discoveries, we have invented a metallic glue technology [4]. This technology relies on the realization of small and well-separated metallic nanorods that were achieved in the previous project period [1]. While focusing on basic energy science, this effort demonstrates that basic research can indeed impact technologies and the economy. As two sets of small and well-separated metallic nanorods are brought into contact, interpenetration occurs, and diffusion upon interpenetration then leads to sintering and formation of metallic glue. The process takes place at room temperature, under small mechanical pressure of a few mega-pascals, and in air. This technology is featured as one of "The 20 Coolest Inventions of 2016" by the Interesting Engineering magazine.

Future Plans

The first major step in the plan is to develop the theory for transition between thin film growth and nanorod growth, in three dimension; the recent exploration [3] is in two dimensions. Then, another major development is on a theory for nanorod growth with a combination of monolayer and multiple-layer surface steps that compete. Both developments will be in synergy with atomistic simulations and experiments, as in the past.

References

1. X. B. Niu, S. P. Stagon, Hanchen Huang*, J. K. Baldwin, and A. Misra, "Smallest Metallic Nanorods Using Physical Vapor Deposition", **Physical Review Letters** *110*, 136102 (2013).
2. F. Du, P. R. Elliott, and Hanchen Huang*, "Generalized Theory of Smallest Diameter of Nanorods", **Physical Review Materials** *1*, 33401 (2017).

3. F. Du and Hanchen Huang*, "Theory of Transition from Thin Film Growth to Nanorod Growth", **Surface Science** (2017) being finalized for submission.
4. S. P. Stagon, A. Knapp, P. R. Elliott, and Hanchen Huang*, "Metallic Glue for Ambient Environments Making Strides", **Advanced Materials & Processes** *174*, 22 (2016).
5. J. Tersoff, A. W. Denier van der Gon, and R. M. Tromp, "Critical Island Size for Layer-by-Layer Growth", **Physical Review Letters** *72*, 266 (1994).
6. J. Krug, "Four Lectures on the Physics of Crystal Growth", **Physica A** *313*, 47 (2002).

Publications

1. L. W. Ma, Z. J. Zhang, and Hanchen Huang*, "Design of Ag Nanorod for Sensitivity and Thermal Stability of Surface-enhanced Raman Scattering", **Nanotechnology** *28*, 405602 (2017).
2. Shuai Shao, Amit Misra, Hanchen Huang, and Jian Wang, "Micro-scale Modeling of Interface-dominated Mechanical Behavior", **Journal of Materials Science** (2017) invited review with minor revisions requested.
3. F. Du, P. R. Elliott, and Hanchen Huang*, "Generalized Theory of Smallest Diameter of Nanorods", **Physical Review Materials** *1*, 33401 (2017).
4. H. J. Chu, Hanchen Huang, and J. Wang, "Clustering on Magnesium Surfaces – Formation and Diffusion Energies", **Scientific Reports** *7*, 5167 (2017).
5. Z. Y. Li and Hanchen Huang*, "Synergy to Discovery and Innovation – Growth of Nanorods", **Theoretical and Applied Mechanics Letters** *6*, 249-252 (2016).
6. F. Du and Hanchen Huang*, "Closed-form Theory of Nuclei Separation on Highly Anisotropic Surfaces", **Applied Surface Science** *390*, 107-110 (2016).
7. Q. Peng, W. Ji, J. Lian, F. Gao, S. M. Peng, Hanchen Huang, and S. De, "A First-principles Study of the Avalanche Pressure of Alpha Zirconium", **RSC Advances** *6*, 72551-72558 (2016).
8. S. P. Stagon, A. Knapp, P. R. Elliott, and Hanchen Huang*, "Metallic Glue for Ambient Environments Making Strides", **Advanced Materials & Processes** *174,* 22-25 (2016).

Single crystal growth via solid→solid transformation (SCGST) of glass

PI: Himanshu Jain and Co-PI: Volkmar Dierolf, Lehigh University, Bethlehem, PA USA

Program Scope

Efficient ways of harnessing, generating, conserving, and storing energy require single crystals in specific composition, size, shape and form. Many highly promising applications remain unrealized because of the unavailability of complex materials in single crystal form with superior properties. The critical obstacle to the development of these new crystals is that they cannot be grown using existing methods due to incongruent melting, decomposition upon heating to high temperature or phase transformation upon cooling. Previously, we devised multiple strategies based on localized laser heating to address this generic challenge, and introduced a new paradigm of single crystal growth via solid→solid transformation (SCGST) of glass [1]. The proof-of-concept to produce 0D, 1D and 2D single crystal architectures was demonstrated using Sb_2S_3 and SbSI as model systems. We discovered that often the lattice of resulting crystals appears to rotate smoothly, resulting in a new class of solids, termed rotating lattice single (RLS) crystals with characteristic rate of rotation that may be secured hopefully by controlling various growth conditions.

A phenomenological, working model has been proposed to explain the origin of lattice rotation, which needs verification. Further, key features and impact of SCGST and lattice rotation on properties remain unexplored/unexplained. To overcome this deficiency and to advance the distinctive attributes of such metastructures in practical applications, we have formulated four complementary working hypotheses: (A) SCGST is a widely applicable phenomenon, and not limited to congruently crystallizing glass compositions. (B) Rotation of lattice within RLS crystal represents dynamic equilibrium between the stresses arising from densification during SCGST and structural relaxation in the surrounding glass. (C) Although nucleation of crystal within the glass matrix is a random process, it should be possible to control the orientation of nuclei, hence of the desired crystal, by polarization or intensity profile of the laser. (D) SCGST imposes unique boundary conditions that allow the synthesis of single crystal architecture, which is otherwise very difficult or impossible to fabricate. To validate them a set of crucial questions is identified about the optimum processing conditions for SCGST; the fabrication and characteristics of RLS crystals; the control of the orientation of initial seed for growing single crystal; and the growth of preferred phases. In response to these questions and hypotheses, our goal is to investigate SCGST phenomenon and lattice rotation characteristics using three model glass systems that are selected for their special physico-chemical characteristics and compositional simplicity. The resulting information about the glass, the RLS crystal and the interfacial region in relation to local temperature and composition will help establish a comprehensive understanding suitable for guiding the fabrication of single crystal architecture of novel compositions and properties, which would not be feasible by the existing methods.

Recent Progress

During the current report period we have focused on Hypotheses (A) and (B) in relation to the discoveries of SCGST and RLS crystal reported previously. The progress made in support of these hypotheses is summarized next:

(a) Effect of incongruency of glass and crystal compositions on SCGST

Having demonstrated SCGST in congruently crystallizing Sb_2S_3 glass to single crystal lines of the same composition by CW laser, we investigated the same phenomenon in off stoichiometric $16SbI_3$–$84Sb_2S_3$ glass wherein the addition of SbI_3 enhances glass-forming ability significantly. The composition of single crystal in this case remained the same i.e. Sb_2S_3, so that crystallization required expulsion of I and Sb at the growth front by diffusion. A priori it was not clear if it would be possible to fabricate single crystal architecture under such dynamic condition of interdiffusion and validate Hypothesis (A). Note that even the fabrication of a single crystal straight line involves forming a seed dot first, and then extend it into line by moving the sample relative to laser. Clearly, the growth conditions would vary remarkably during the formation of initial hemispherical dot shaped seed, the desired line and the region of transition from dot to line. The results showed that indeed it was possible to fabricate single crystal dot and extend it to line of unlimited length in the new composition as well as in stoichiometric Sb_2S_3 glass. However, in approximately half the experiments we observed formation of extraneous grains abruptly within the dot → line transition region N, as seen in Fig. 1. Note that the lattice of these grains is not randomly oriented, but closely aligned to that of the grain that ultimately wins the competition and grows as single crystal beyond the transition region.

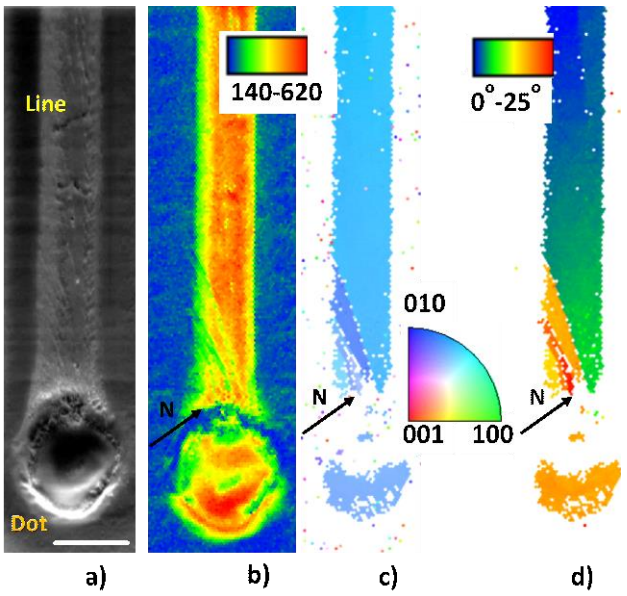

Fig. 1. Formation Sb_2S_3 single crystal line starting with a dot on the surface of $16SbI_3$–$84Sb_2S_3$ glass: (a) SEM image, (b) image quality (IQ), (c) colored inverse pole figure (IPF) map with reference vector normal to sample surface (ND), and (d) crystal orientation deviation (COD) map. The crystal dot was created by slowly ramping in 5s the laser power density from 0 to 90 μW/μm^2 and then constant power exposure for 60s. It was then transformed to a crystal line by moving the laser spot at 20 μm/s in nitrogen environment. Scale bar is 5 μm.

We recall that no extraneous grains formed within the dot → line transition region in the case of congruently crystallizing Sb_2S_3 glass, which itself had much higher propensity to devitrify upon cooling from melt. We explain qualitatively the formation of observed extraneous grains in Fig. 1 as a consequence of competition between nucleation and growth of Sb_2S_3 single crystal during laser-induced solid-state transformation of $16SbI_3$–$84Sb_2S_3$ glass vis-à-vis congruent crystallization of Sb_2S_3 glass. This difference in propensity for introducing such 'defects' arises from the difference in their glass-forming ability. For the case of relatively stable non-stoichiometric glass, additional nucleation around the initially formed single crystal dot becomes viable, as the growth rate is negligible. Subsequently, these nuclei form unwanted grains as the growth front extends to form the line. A comparison of laser crystallization of just these two glasses suggests the following guideline: To avoid the appearance of undesirable grains, the addition of glass former should be sufficient to facilitate the formation of glass of otherwise non-glass-forming component. However, the addition of too much glass former could help form unwanted grains in the vicinity of laser-irradiated region. In addition, once a stable

seed has formed, we should move the laser rapidly and not allow any further laser heating which would only introduce additional nuclei. Thus, we can minimize the possibility of unwanted nucleation in the '*challenge'* zone of transition from dot to line too. A detailed description of this analysis is under review for publication in J. Non-cryst. Solids [2].

(b) Fundamental nature of lattice rotation within laser-fabricated RLS crystal

Initially RLS crystals of unlimited length were made as straight lines on the surface of Sb-S-I glasses [3]. The lattice of such crystals rotates linearly at a constant rate of Θ°/μm about an axis that is parallel to surface but normal to the direction of laser displacement; no rotation is observed across the width of crystal line. Typical value of Θ varies from 0 to 1.0°/μm, depending on the direction of crystal growth relative to the orientation of starting seed. From these observations, it became clear that anisotropy of crystal growth rate influences the magnitude of Θ. In fact, a complete description of lattice rotation requires the knowledge of Θ and the axis of rotation. Then a fundamental question arises: what happens to these two parameters as the direction of laser scanning is changed to fabricate complex single crystal architecture? We addressed this question by comparing lattice rotation within 2D structures formed by two protocols as described in Fig. 2: First, a 1D RLS crystal line is formed by scanning the laser beam in *x*-direction. The orientation of lattice, θ, as defined by the angle between the direction of the normal to surface lattice plane at the beginning of the line and the same plane at the position of interest, varies with *x*. Experimentally, for a straight line θ_x varies linearly with *x*, which is the direction of laser displacement as well as the crystal growth [3]. After the first RLS crystal line is fabricated to desired length, the next line must be formed, using the first line as the seed, by some small laser displacement and crystal growth in the *y*-direction, and then scanning the laser in *–x* direction. If the lattice rotates within the small segment along *y*-direction and then rotates during the growth in *–x* direction, there will be a mismatch in the value of θ_y for the same value of *x* in the preceding and newly forming lines, and the two lines will join with constant θ_y misorientation. On the other hand, if the new line grows from the preceding line at an angle to scanning direction, as the laser moves along *–x*-direction, there would appear an additional *y*-component of lattice rotation between the lines. When assessing these different possibilities, a crucial question arises: will the orientation of the lattice be determined by the direction of heat gradient (which will be predominantly along *x* direction) or the direction of crystal growth (which can have a component along *y*-direction)? Of course, if the rate of lattice rotation Θ (= θ °/μm) is different in *x* and *–x* directions, there could still be a seam between the lines and/or the nature of lattice rotation would become complex.

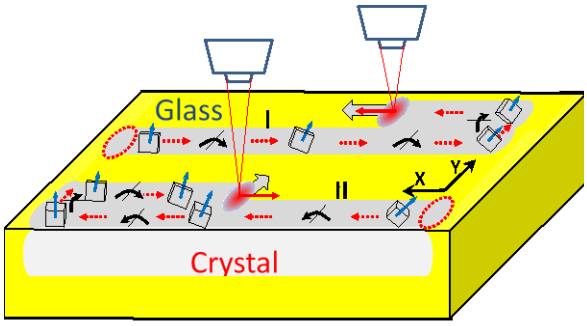

Fig. 2. Two different protocols, I and II, for fabricating 2D crystal. The black parallelepipeds and lines (and arrows) indicate the orientation of the unit cell of crystal lattice, and the axis (and direction) of lattice rotation locally.

For the investigated Sb_2S_3 crystal pattern on the surface of $16SbI_3$–$84Sb_2S_3$ glass, the value of Θ depends on the direction of laser movement relative to initial lattice orientation. Therefore, an appropriate choice of initial seed orientation and direction of scanning can help minimize the rate of lattice rotation, for example, down to 5^o for a 2D pattern of 50x50 μm^2 size [4]. All lines of 2D patterns created by either protocols demonstrate strongly correlated rotation,

which is set by the rotation of the first line. The pole figure (PF) and inverse pole figure (IPF) maps from the analysis of μSXRD Laue patterns show that the rotation within all lines have a component that parallels those in an isolated RLS crystal line. In addition, there is also an orthogonal component of rotation, which depends on the extent of overlap between successive lines, and can be different for the two protocols. The overall message of all the observations on crystals fabricated by CW laser on glass surface is that: whereas the magnitude of lattice rotation is determined by the crystallographic direction of crystal growth relative to the orientation of starting seed, the axis of lattice rotation is given the intersection of growth front with the sample surface – the latter can be controlled by laser beam profile (see Fig. 3).

(c) Control of the orientation of nucleated dot seed

In view of the crucial role of the orientation of initially formed seed on subsequent lattice rotation, we attempted to establish the possibility of oriented crystal nucleation, which is generally expected to be a random process under stationary laser. We investigated the formation of Sb_2S_3 single crystal on the surface of $63Sb_2S_3$–$37SbI_3$ and Sb_2S_3 glasses. Further, we used a spatial light modulator (SLM) to design beam profile with desired intensity distribution on the sample surface. The intensity of the laser was chosen such that the temperature in the crystal growth region remained below the melting temperature of the glass, so that each single crystal grew with solid→solid transformation of glass. From EBSD analysis, we found that indeed Sb_2S_3 single crystals formed with preferential orientation of their crystallographic <001> direction parallel to the surface of glass and to the polarization of laser light, but the degree of orientation alignment was variable. A comparison of results obtained with super bandgap (wavelength, λ = 520 nm) and sub bandgap (λ = 639 nm) laser indicated that confinement close to surface and polarization fields were the most important factor for determining the nucleus orientation, while the gradient of temperature and associated gradient of chalcogenide composition were much less effective for controlling the orientation of nuclei.

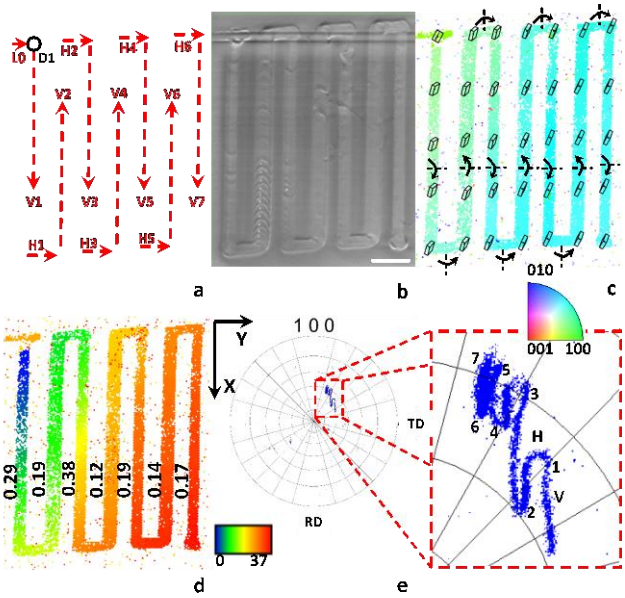

Fig. 3. The 2D single crystal pattern created using rastering protocol with 7 μm step on the surface of $16SbI_3$–$84Sb_2S_3$ glass. The previously laser-induced line L0 was used as seed for growth. Pattern was created as a raster by moving the laser spot with scanning speed 20 μm/s in nitrogen environment. Scale bar = 10 μm. (a) Plan-view, (b) SEM image, (c) orientation inverse pole figure (IPF) map with reference vectors along surface normal, (d) crystal orientation deviation map relative to the crystal orientation at beginning of the initial line (V1), and (e) pole figure map and its enlarged version of the crystal architecture. The arrows in (a) indicate the direction of laser motion relative to sample and arrows on IPF map (c) describe the axis and direction of the lattice cell rotations. Numbers in (d) indicate average rotation rate (in degrees/μm) for writing the lines, and the labels on (e) indicate the points which correspond to the lines of the crystal architecture.

Future Plans

We plan to pursue four types of experiments: (a) As noted above, the lattice of single crystal line formed on the surface of glass undergoes gradual rotation to accommodate the density mismatch between the glass and crystal. Our current explanation of lattice rotation assumes the presence of randomly distributed dislocations and tilt dislocation walls (small angle grain boundaries) whose burgers vectors add up to produce lattice rotation. We propose to verify this critical assumption of lattice rotation through direct observation of such defects using transmission electron microscopy. (b) We have just initiated investigating the basic nature of SCGST that includes 'lattice rotation' using in situ observation of Sb_2S_3 crystals by μSXRD at ALS/ LBNL using X-ray beam both as pump and probe. It will help us observe the transformation of glass to single crystal in real time, which in principle can occur by classic nucleation and growth, or recently proposed particle attachment mechanisms [5]. (c) We will further probe the possibility of controlling the orientation of seed by combining the effect of surface orientation, laser polarization and temperature gradient. (d) We will continue the verification of Hypothesis (B) by extending the studies of SCGST to As-Ge-Se glass system, as proposed.

References

[1] D. Savytskii, B. Knorr, V. Dierolf, H. Jain, Demonstration of single crystal growth via solid-solid transformation of a glass, *Sci. Reports* 6 (2016) 23324, https://doi.org10.1038/srep23324.
[2] D. Savytskii, V. Dierolf, N. Tamura, H. Jain, 'Fabrication of single crystal architecture in glass: transition from dot to line', *J. Non-cryst. Solids*, under review, 2017.
[3] D. Savytskii, H. Jain, N. Tamura, V. Dierolf, Rotating lattice single crystal architecture on the surface of glass, *Sci. Reports* 6 (2016) 36449, https://doi.org/10.1038/srep36449.
[4] D. Savytskii, H. Jain, C. Au-Yeung, V. Dierolf, N. Tamura, Laser fabrication of 2D rotating-lattice single crystal, *Cryst. Growth Des.* 17 (2017) 1735, https://doi.org/10.1021/acs.cgd.6b01709.
[5] J. J. De Yoreo et al., Crystallization by particle attachment in synthetic, biogenic, and geologic environments, *Science*, 31 Jul 2015:Vol. 349, 6247, aaa6760. DOI: 10.1126/science.aaa6760

Publications

Since submission of previous progress report, three papers were published and one is under review at present. They are listed as References [1-4].

Presentations at conferences

1. (Invited Talk) D. Savytskii, V. Dierolf and H. Jain, Single crystal growth from glass via solid-solid transformation, Materials Science & Technology 2016, Salt Lake City, UT, 2016 Oct.
2. (Invited poster) D. Savytskii, V. Dierolf, H. Jain, "A Solid State Process for Fabricating Single Crystal from Glass", Corning Glass Summit, June 1-3, 2016, Corning, NY.
3. (Invited Talk) D. Savytskii, K.Veenhuizen, S. McAnany, B. Aitken, D. Nolan, V. Dierolf, H. Jain, "Single crystal architecture in glass (SCAG): new active metamaterials for photonics, Ann. Meet. MRS, Boston
4. (Invited Talk) D. Savytskii, A. Stone, K. Veerhuizen, S. McAnany, C. Au-Yeung, V. Dierolf, H. Jain, "Single crystal architecture in glass (SCAG): A new frontier of glass applications", Int'l Conf. Advances in Glass Science and Technology (ICAGST-2017), Jan 23-25, Kolkata, India.

5. (Invited Talk) D. Savytskii, K. Veenhuizen, C. Au-Yeung, S. McAnany, B. Aitken, D. Nolan, V. Dierolf, H. Jain, "Single crystal architecture in glass (SCAG): A new frontier of glass applications", XI Brazilian Symp. Glass & Related Materials, July 13-16, 2017, Curitiba, Brazil
6. (Invited Talk) D. Savytskii, C. Au-Yeung, K. Veenhuizen, V. Dierolf, H. Jain, "Engineering the lattice of single crystal grown in glass", 12th Int'l Symposium on Crystallization in Glasses and Liquids", Sep. 10-13, Segovia, Spain.
7. (Am Ceram Soc. Varshneya Award Lecture) H. Jain, "Pathways of glass→crystal transformation", 12th Pacific Rim Conference on Ceramic and Glass Technology, May 21 - 27, 2017, Waikoloa, HI.
8. (Invited Talk) K. Veenhuizen, C. Au-Yueng, S. McAnany, B. Aitken, D. Nolan, D. Savytskii, H. Jain, V. Dierolf, "Single crystal growth by laser-induced solid-solid conversion: Concepts and Applications", 12th Pacific Rim Conference on Ceramic and Glass Technology, May 21 - 27, 2017, Waikoloa, HI.
9. (Invited Talk) D. Savytskii, K. Veenhuizen, S. McAnany, B. Aitken, D. Nolan, V. Dierolf, H. Jain, "Single crystal architecture in glass (SCAG): new active metamaterials for photonics", 41st International Conference and Expo on Advanced Ceramics and Composites, Daytona Beach, Jan 22-27, 2017.
10. D. Savytskii, V. Dierolf and H. Jain, Conversion of glass to single crystal via solid-solid transformation, Society of Glass Technology Centenary Conference & European Society of Glass, Sheffield, UK, Sep 4-8, 2016.
11. D. Savytskyy, V. Dierolf, H. Jain, "Laser-induced oriented Sb_2S_3 single crystal dots on the surface of Sb-S-I glasses using spatial light modulator", Am. Ceram Soc. Ann. Meet. May 22-26, 2016 in Madison, WI.
12. (Invited Talk) K. Veenhuizen, C. Au-Yueng, S. McAnany,, D. Savytskii, H Jain**,** V. Dierolf, **"**Single crystal growth by laser-induced solid-solid conversion: Concepts and Applications", Workshop on Electromag. Effects in Materials Synth., Carnegie Mellon Univ., June 5,6, 2017.

Investigating structure-property relationship in correlated transition-metal compounds

Rongying Jin (rjin@lsu.edu)

Department of Physics & Astronomy, Louisiana State University, Baton Rouge, LA 70803

Research Scope

This project is designed to discover, grow, and characterize crystalline materials that are formed under high temperatures and/or high pressure. The objective is to uncover mechanisms and hidden correlations in materials that are metastable under ambient conditions. The team consists of a postdoctoral fellow (Dr. Lingyi Xing), a graduate student (Mr. Roshan Nepal), a visiting scholar (Dr. Hong Chang), and the PI. We collaborate with Drs. Jiaqiang Yan and Brian Sales at Oak Ridge National Laboratory (ORNL) on high-pressure floating-zone growth, and with Dr. Yimei Zhu at Brookhaven National Laboratory (BNL) on Lorentz force microscopy (LFM). This spearheads a unique opportunity to train young scientists, co-advised by experts at both LSU and National Laboratories, who will be essential for expanding materials research with ability to grow crystals, characterize their properties, and design new materials.

The main scientific focus of this project is to understand the role of coupling between the important degrees of freedom in complex materials and its impact on the structure-property relationship. Therefore, we investigate their structural, magnetic, electronic, and thermal properties. In particular, magnetic properties are studied through several approaches including magnetization, LFM, and neutron scattering measurements.

Recent Progress

The Ruddensen-Popper (RP) ruthenate family $Sr_{n+1}Ru_nO_{3n+1}$ (n = integer) is a prototype system that exhibits strong coupling between charge, lattice, spin, and orbital degrees of freedom. Especially, the subtle distortion of octahedron (Fig. 1(c)), the building block of the PR series, can dramatically change the physical properties of the system. When n > 1, the system is structurally stabilized with octahedral rotation. The rotation angle Φ tends to increase with increasing n, the number of octahedral layers in the stack. We previously found that the substitution of Ru by smaller Mn reduces $(Ru/Mn)O_6$ octahedral rotation angle with $\Phi \sim 0$ at $x \sim 0.2$ in the double-layered (n = 2) $Sr_3(Ru_{1-x}Mn_x)_2O_7$ (Fig. 1(a)) [1]. Correspondingly, the long-range antiferromagnetic ordering disappears. To elucidate the structure-property

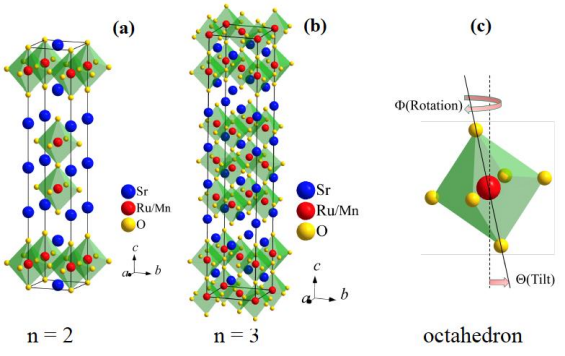

Fig 1. Crystal structure of $Sr_{n+1}(Ru/Mn)_nO_{3n+1}$: (a) n = 2, (b) n = 3, and (c) octahedron with distortion.

relationship in this series, single crystalline samples are necessary, which require high-temperature and high-pressure crystal growth environment. With the access of high-pressure optical furnace at ORNL, we have successfully grown (1) $Sr_3(Ru_{1-x}Mn_x)_2O_7$ single crystals with $x \sim 0.25$, and (2) triple-layered (n = 3) $Sr_4(Ru_{1-x}Mn_x)_3O_{10}$ single crystals with $x \leq 0.42$. Upon Mn doping in $Sr_4(Ru_{1-x}Mn_x)_3O_{10}$, the rotational distortion of $(Ru/Mn)O_6$ is quickly suppressed, and the ground state changes from a ferromagnetic metal for $x = 0$ to a ferromagnetic insulator for $x = 0.42$. This suggests that Mn doping enhances electron-electron correlation, resulting Mott-type insulation [2].

Another material system under investigation is spinel $FeMn_2O_4$, which can only be stabilized by quenching from high temperature to 77 K (liquid nitrogen). Figure 2(a) shows large single crystalline $FeMn_2O_4$ grown in a floating-zone furnace under high temperature and high pressure. Both X-ray and neutron diffraction measurements indicate that the crystal grows along the [111] direction. Through magnetization, specific heat, electrical and thermal transport, neutron scattering, and X-ray photoelectron spectroscopy measurements, we have identified, for the first time, three phase transitions. As shown in Figure 2(b), there is one structural transition from cubic at high temperatures to tetragonal below $T_s \sim 595$ K, one magnetic transition at $T_{FI-1} \sim 373$ K from high-temperature paramagnetism (PM) to collinear ferrimagnetism (FI), and the other magnetic transition at $T_{FI-2} \sim 50$ K from high-temperature collinear FI to non-collinear FI. Of particularly interesting is its thermal property. As a crystalline material, the thermal conductivity is considerably low in a wide temperature range (Figure 2(c)). Through the analysis of low temperature data, we find that thermal conductivity exhibits $T^{3/2}$ dependence (Figure 2(d)), indicating solely ferrimagnetic contribution. Thus, $FeMn_2O_4$ may be regarded as a phonon-glass system, with negligible phonon contribution to thermal conduction [3]. In addition, the geometric frustration inherent in the spinel structure results in significant magnetic frustration, leading to non-collinear ferrimagnetic grand state [3,4].

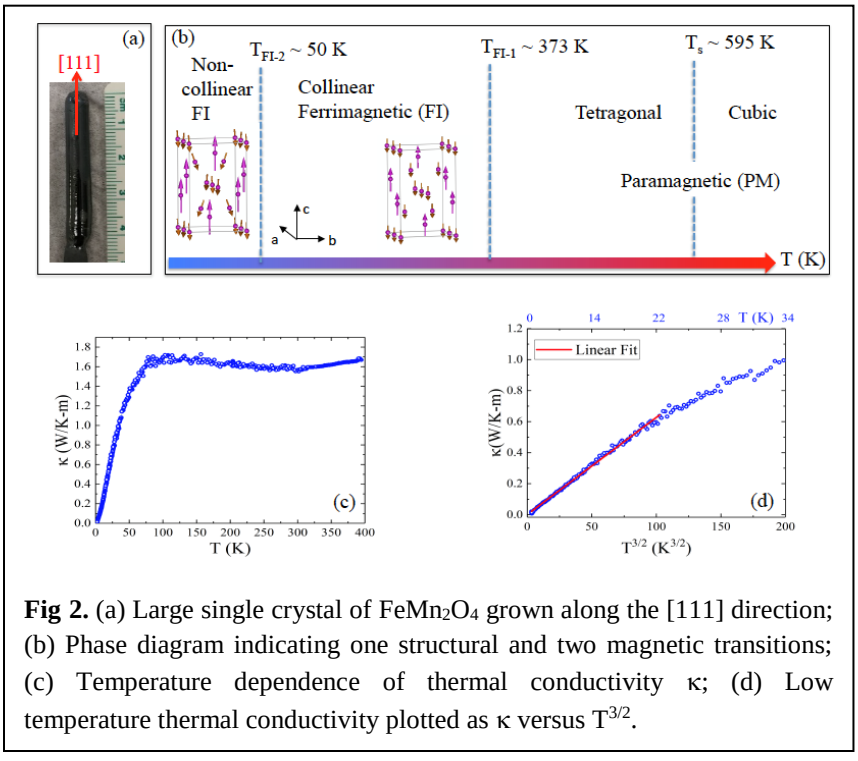

Fig 2. (a) Large single crystal of $FeMn_2O_4$ grown along the [111] direction; (b) Phase diagram indicating one structural and two magnetic transitions; (c) Temperature dependence of thermal conductivity κ; (d) Low temperature thermal conductivity plotted as κ versus $T^{3/2}$.

Future Plans

Our future plans involve both the continued study of these materials, as well as to identify new materials for investigation, with a focus on novel properties. This includes the following tasks.

- Complete the phase diagram of $Sr_3(Ru_{1-x}Mn_x)_2O_7$, so to identify the key parameter(s) that control material properties.
- Measure magnetic properties of $Sr_4(Ru_{1-x}Mn_x)_3O_{10}$ and $FeMn_2O_4$ using Lorentz force microscopy at BNL to investigate the evolution of magnetic domains with temperature. This will allow us to elucidate magnetic interactions in the nanoscale.
- Explore ferroelectric properties in spinel materials such as FeT_2O_4 (T = Mn, V).
- Investigate new material systems such as $TaSe_3$ and IrMnX (X = Sn, Sb) to explore the relationship between magnetism, superconductivity, and topological properties.

References

[1] B. Hu, G. T. McCandless, V. O. Garlea, S. Stadler, J. Y. Chan, E. W. Plummer, R. Jin Phys. Rev. B **84**, 174411 (2011).
[2] L. Xing, X. Gui, W. Xie, H. Cao, J. Yan, B. C. Sales, R. Jin (to be submitted).
[3] R. Nepal, Q. Zhang, S. Dai, W. Tian, S. Nagler, R. Jin (submitted).
[4] Q. Zhang, R. Nepal, W. Tian, S. Nagler, R. Jin (to be submitted).

Publications

[1] R. Nepal, Q. Zhang, S. Dai, W. Tian, S. Nagler, R. Jin, "Structural and magnetic transitions in spinel $FeMn_2O_4$ single crystals" (under review).
[2] S. Nie, L. Gustin, L. Xing, R. Jin, W. Xie, Z. Wang, F. B. Prinz, "Topological phases in the superconductor $TaSe_3$" (under review).
[3] L. Gustin, L. Xing, M. T. Pan, R. Jin, W. Xie, "Electron counts, structural stability, and magnetism in $BaCuSn_2$-type YM_xGe_2 (M = Cr, Mn, Fe, Co, and Ni)" (under review).

Group IV Nanomembranes and Sheets: New Synthesis, Alloys, and Composites

Max G. Lagally and Mark A Eriksson, University of Wisconsin-Madison, Madison WI 53705

Program Scope

Our research effort focusses on the synthesis and characterization of Group IV single-crystal nanomembranes (NMs) and sheets, as well as combination and composites of semiconductor nanomembranes. It is by now well established that single-crystal semiconductor sheets represent a platform for entirely new science and technology, and it is amazing how the early work to establish this platform has expanded in terms of different materials, approaches, and applications. In addition to synthetic methods, modifications of electronic and optical properties brought about by strain engineering, thinness, and heterostructure formation have been major foci of work in this field. Our work in Group IV-based nanomembranes and sheets involves Si, Ge, SiGe alloys, graphene, and graphene in combination with these and other materials. The platform of single-crystal semiconductor sheets offers the choice of nano-size in one, two, or three dimensions, as well as the formation of structures with mixed dimensions, but the true advantage is working at the nanoscale in one dimension, while the other two dimensions are at the mesoscale or macroscale. The platform is extendable to other materials and a range of structures and functions, using the materials processing approaches we have developed, as long as a material exists that is differentially etchable so it can act as a release layer. Doing so expands the range of accessible growth substrate lattice parameters and thus the potential for growing new alloy NMs. We are currently using binary and ternary III-V alloys as growth substrates and release layers for making Ge NMs and new SiGe alloys with high Ge concentration. The latter are potentially useful for novel Group IV light sources.

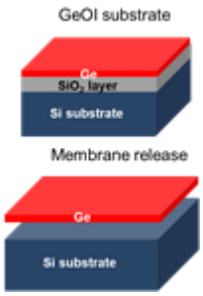

Fig. 1. Schematic diagram of simple GeNM fabrication.

We are combining the growth and transfer of graphene with these Group IV NMs to make novel composites that may have unique electrical and thermal transport properties, and are making such measurements.

Recent Progress

We have perfected a release and transfer protocol for NMs grown on III-V substrates that allows in principle wafer size release of NMs without etch holes, see Fig. 2 for a schematic diagram. We have made GaAs NMs, Ge NMs, and most recently high-Ge-content SiGe alloy NMs. The latter is in principle a new material, as the NM can be grown

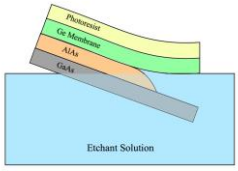

Fig. 2. Schematic diagram of release procedure.

dislocation-free by keeping the thickness below the kinetic critical thickness before release, and subsequently continuing the growth on the now *elastically* relaxed crystalline structure. We have previously shown this process for low-Ge-content SiGe alloys. [1] Using now a different substrate and release layer, in which we can adjust the lattice constant, we can grow Si/Ge NMs of any composition, and use these as seed crystals for thicker alloy crystals. A patent application has been filed.

Along with the Arnold Group at UW-Madison, we have been investigating aspects of the combination of graphene on Ge. We have shown that graphene "properly grown" by CVD on Ge passivates Ge, with no sign of oxidation after several months.[2] To investigate non-complete passivation under non-ideal growth conditions we are measuring pinhole and defect densities in the graphene. We want to establish a quantitative relationship between defects in grown graphene and resistance to oxidation. A manuscript is in preparation.

To follow on earlier charge transport measurements for graphene on Ge, [3] we are attempting to grow graphene on Ge NMs. That involves some challenges, but progress is being made. There are also challenges in interpreting Hall effect measurements on these structures.

To support Arnold's efforts on growth of graphene ribbons on Ge, we are preparing samples with specific large miscut.

We have built our own graphene CVD system to take the pressure off existing systems. It is successfully growing graphene. We are using it partly for some rather farther-out work, for example growing graphene on metals as a protection against plasma wall interactions in etchers, sputter systems, or research reactors for fusion reactors. [4]

Future Plans

Described above are several efforts in progress. We will continue those. Additionally we are refurbishing our low-energy electron microscope to aid in a project in making step-free Si mesas and growing strained-Si 2DEGs n them. The idea is that steps influence strongly the valley splitting in Si-based qubit formation in quantum information processing. Our group supplies the strained-Si 2DEGs for significant portion of the world effort in Si-based quantum information processing research. Valley splitting is an unresolved problem and our effort will at least shed light on this issue and the relative importance of steps.

Only alluded to above is another effort we are involved in, namely thermal transport across interfaces. As interfaces in heterostructures tend to be more thermally resistive than the materials themselves, thermal transport in multilayer heterostructures can strongly influence performance in communications devices, light emitters, light converters, and computation devices. After redesigning the electronics after our first efforts, [5] we have undertaken as an exercise a problem in III-V heterostructures with significant technological application. This is almost complete. Next is a Ge/graphene/Ge/…. heterostructure, with nonepitaxial interfaces.

References

[1] “Defect-Free Single-Crystal SiGe: A New Material from Nanomembrane Strain Engineering”, D. M. Paskiewicz, B. Tanto, D. E. Savage, and M.G. Lagally, ACS Nano 5, 5814 (2011); “Nanomembrane-based Materials for Group IV Semiconductor Quantum Electronics”, D. M. Paskiewicz, D.E. Savage, M.V. Hole, P.G. Evans, and M.G. Lagally, Nature Scientific Reports 4, 04218 (2014).

[2] “Passivation of germanium by graphene”, R. Rojas Delgado, R.M. Jacobberger, S.S. Roy, V.S. Mangu, M.S. Arnold, F. Cavallo, and M.G. Lagally, ACS Applied Materials and Interfaces 9, 17629–17636 (2017) DOI: 10.1021/acsami.7b03889.

[3] “Exceptional Charge Transport Properties of Graphene on Germanium”, F. Cavallo, R. Rojas Delgado, M.M. Kelly, H. Xing, J.R. Sánchez Pérez, D.P. Schroeder, M. A. Eriksson, and M.G. Lagally, ACS Nano 8, 10237-10245 (2014).

[4] “Implantation of 30 keV Helium into Graphene-Coated Tungsten”, M.X. Navarro, R. R. Delgado, M. G. Lagally, G.L. Kulcinski & J.F. Santarius, Fusion Science and Technology 7, xxx (2017).

[5] “Thermal Resistance of Transferred Silicon Nanomembrane Interfaces”, D. P. Schroeder, Z. Aksamija, A. Rath, P. M. Voyles, M. G. Lagally, and M. A. Eriksson, Phys. Rev. Letters 115, 256101 (2015).

Publications (both partially and principally supported by BES)

458.“Characterization of a gate-defined double quantum dot in a Si/SiGe nanomembrane”, T. J. Knapp, R.T. Mohr, Yize Li, B. Thorgrimsson, R.H. Foote, Xian Wu, D.R. Ward, D.E. Savage, M.G. Lagally, Mark Friesen, S.N. Coppersmith, and M.A. Eriksson, IOP Nano-technology 27, 154002 (2016).

459. “Synchrotron x-ray thermal diffuse scattering probes for phonons in Si/SiGe/Si trilayer nanomembranes”, K.M. McElhinny, G. Gopalakrishnan, D.E. Savage, D.A. Czaplewski, M.G. Lagally, M.V. Holt, and P.G. Evans, MRS Advances 2016.352, pp 1 - 6 (2016) DOI: 10.1557/adv.2016.352

461. “Extrinsic Stress-Induced Nanoscale Disorder in Si Quantum Electronic Devices”, J.K. Park, Y.J. Ahn, J.A. Tilka, K.C. Sampson, D.E. Savage, J.R. Prance, C.B. Simmons, M.G. Lagally, S.N. Coppersmith, M.A. Eriksson, M.V. Holt, and P.G. Evans, APL Materials 4, 066102 (2016).

462. “Combining Experiment and Optical Simulation in Coherent X-ray Nanobeam Characterization of Si/SiGe Semiconductor Heterostructures”, J.A. Tilka, J. Park, Y. Ahn, A. Pateras,

K.C. Sampson, D.E. Savage, J.R. Prance, C.B. Simmons, S.N. Coppersmith, M.A. Eriksson, M.G. Lagally, M. V. Holt, and P.G. Evans, J. Appl. Phys. 120, 015304 (2016).

464. "Gate fidelity and coherence of an electron spin in a Si/SiGe quantum dot with micro-magnet", E. Kawakami, T. Jullien, P. Scarlino, D. R. Ward, D. E. Savage, M. G. Lagally, V. V. Dobrovitski, Mark Friesen, S. N. Coppersmith, M. A. Eriksson, and L. M. K. Vandersypen, PNAS 113, 11738 (2016).

466. "State-conditional coherent charge qubit oscillations in a Si/SiGe quadruple quantum dot", D. R. Ward, Dohun Kim, D. E. Savage, M. G. Lagally, R. H. Foote, Mark Friesen, S. N. Coppersmith, and Mark A. Eriksson, npj Quantum Information 2, 16032 (2016).

467. "Capturing Structural Dynamics in Crystalline Silicon Using Chirped Electrons from a Laser Wakefield Accelerator", Z.-H He, B. Beaurepaire, J.A. Nees, G. Gall´e, S.A. Scott, J.R. Sanchez Perez, M.G. Lagally, K. Krushelnick, A.G.R. Thomas, and J. Faure, Scientific Reports 6, article No 36224 (2016).

468. "Dressed photon-orbital states in a quantum dot: Intervalley spin resonance", P. Scarlino, E. Kawakami, T. Jullien, D.R. Ward, D.E. Savage, M.G. Lagally, Mark Friesen, S.N. Coppersmith, M.A. Eriksson, and L.M.K. Vandersypen, Physical Review B 95, 165429 (2017).

469. "Passivation of germanium by graphene", R. Rojas Delgado, R.M. Jacobberger, S.S. Roy, V.S. Mangu, M.S. Arnold, F. Cavallo, and M.G. Lagally, ACS Applied Materials and Interfaces 9, 17629–17636 (2017) DOI: 10.1021/acsami.7b03889

470. "Extending the coherence of a quantum dot hybrid qubit", B. Thorgrimsson, D. Kim, Y.-C.Yang, L.W. Smith, C.B. Simmons, D.R. Ward, R.H. Foote, J. Corrigan, D.E. Savage, M.G. Lagally, M. Friesen, S.N. Coppersmith, and M.A. Eriksson, npj Quantum Information 3, Article number: 32 (2017); doi:10.1038/s41534-017-0034-2

471. "Effects of charge noise on a pulse-gated singlet-triplet S – T_ qubit", Zhenyi Qi, X. Wu, D. R. Ward, J. R. Prance, Dohun Kim, John King Gamble, R. T. Mohr, Zhan Shi, D. E. Savage, M. G. Lagally, M. A. Eriksson, Mark Friesen, S. N. Coppersmith, and M. G. Vavilov, Phys Rev. B 96, 115305 (2017).

472. "Implantation of 30 keV Helium into Graphene-Coated Tungsten", M.X. Navarro, R. R. Delgado, M. G. Lagally, G.L. Kulcinski, and J.F. Santarius, Fusion Science and Technology 7, xxx (2017)

476. "Charge Transport in H-Terminated Si(001) Nanomembranes", Weina Peng, Marziyeh Zamiri, S.A. Scott, Francesca Cavallo, James Endres, Irena Knezevic, Mark A. Eriksson, and Max G. Lagally, Phys. Rev. Applied submitted.

Formation of Dirac and Topological States on Semiconductor Surface and Strain Engineering

Feng Liu
University of Utah

Program Scope

This project encompasses a comprehensive study of physical mechanisms that lead to formation of exotic quantum electronic states on semiconductor surfaces and explores a novel approach of strain engineering of such states. It covers four correlated research topics: (1) Mechanistic study of epitaxial growth of an overlayer of Dirac and topological states on semiconductor surfaces, which is atomically bonded but electronic isolated from the underlying substrates. (2) Self-assembled growth of topological states arising from non-conventional lattice symmetry in semiconductor surfaces. (3) Strain engineering of topological surface/edge states and topological nanomechanical architecture. (4) Nanostructured topological materials. The common theme of the proposed research is to understand a new class of "surface-based" 2D Dirac and topological materials chemically supported (i.e., non Van der Waals type) on a substrate. The theoretical studies will be done in collaboration with experiments including Prof. Lagally funded by the DOE-BES "Materials Synthesis and Processing" program.

We will employ a multiscale approach, combining several state-of-the-art theoretical and computational techniques, ranging from first-principles density-functional-theory (DFT) electronic structure calculations to semi-empirical tight-binding (TB) model Hamiltonian analyses and calculations and to classical molecular dynamics (MD) simulations. Specifically, surface equilibrium structure and associated energetics will be calculated by DFT and MD methods. Electronic band structure will be studied using both DFT and TB methods with the TB parameters fit to the DFT band structures in supercells of slab geometry to represent a surface. Band topology will be revealed by analyzing the bulk (thin film) Bloch wavefunctions and the topological surface (edge) states using DFT and TB bands and iterative Green's function and Wannier function method. In addition, DFT as well as classical MD simulations will be carried out to directly simulate topological nanomechanical architectures resulted from the strain induced bending of thin films to study strain engineered topological states and spin manipulation.

Our studies will significantly improve our fundamental understanding of physical origins of surface-based Dirac and topological states in solid material systems, in terms of lattice geometry, spin-orbit coupling (SOC), orbital composition and surface/interface interactions. It will open up a new route towards realizing topological quantum phases in a new class of surface-based 2D materials. It will foster a new field of research by taking the effect of stress/strain to new territories on topological order of materials, beyond strain engineering of self-assembled nanostructures and of electronic properties that we have studied in the past decade within the

DOE-BES program. We believe many of our theoretical findings will provide useful guidance for future experimental efforts in growing surface-based 2D materials as we propose, realizing novel topological phases, strain engineering of topological states and spin texture, and nanostructured topological materials. These studies have also technological impact on advancing electronic and optoelectronic materials for energy applications, to fulfill the mission of Department of Energy.

Recent Progress

During the last two years, we have published twenty-six journal papers fully or partially supported by this DOE grant, including one Nature Materials, two PRL, one Nature Communications, one Advanced Materials, three Nano Lett and one ACS Nano papers. Three postdoctoral research associates and two graduate students have been fully or partially supported by this DOE project. The PI gave fourteen invited talks at national/international conferences, and twenty-three departmental colloquium/seminar presentations. Below is a brief summary of four topics of research achievements pertaining to this project:

(a) Topological edge states in a high-temperature superconductor FeSe/SrTiO3(001) film[1].

Superconducting and topological states are two most intriguing quantum phenomena in solid materials. The entanglement of these two states, the topological superconducting state, will give rise to even more exotic quantum phenomena. While many materials are found to be either a superconductor or a topological insulator, it is very rare that both states exist in one material. Recently, we demonstrated by first-principles theory as well as scanning tunneling spectroscopy and angle-resolved photoemission spectroscopy experiments that the recently discovered 'two-dimensional (2D) superconductor' of single-layer FeSe also exhibits 1D topological edge states within an energy gap of ~40meV at the M point below the Fermi level. It is the first 2D material that supports both superconducting and topological states.[1,2] Our finding will provoke an exciting opportunity to study 2D topological superconductors through the proximity effect, which may help advance our fundamental understanding of physical properties associated with the topological superconducting state, such as Majorana fermions. It will pave the way to building novel quantum and spintronics devices by interfacing a superconductor with a topological insulator through a p-n junction (see Fig. 1) since n- and p-type FeSe is respectively a superconductor and

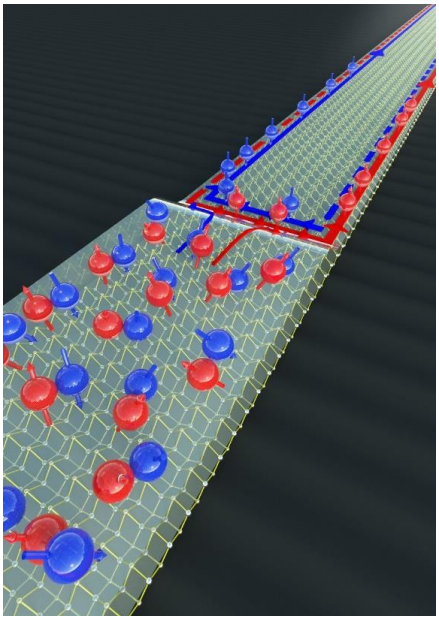

Fig. 1. Schematic illustration of a superconductor-topological insulator P-N junction in doped FeSe/SrTiO3, showing the electron doped superconducting bulk states on one side (low left) and the hole doped topological edge states on the other side (top right).

topological insulator. This work was published last year as one of the "cover" articles in Nature Materials[1], commented by Nature Materials News & Views column[2] and covered by news media.

(b) Quantum Spin Hall Phase in 2D Trigonal Lattice[3]

The quantum spin Hall (QSH) phase is an exotic phenomena in the condensed-matter physics. Recently, we show that a minimal basis of three orbitals (s, px, py) is required to produce a QSH phase via nearest-neighbor hopping in a two-dimensional trigonal lattice.[3] Tight-binding model analyses and calculations show that the QSH phase arises from an spin-orbit coupling (SOC) induced s-p band inversion or p-p band gap opening at Brillouin zone center (Γ point), whose topological phase diagram is mapped out in the parameter space of orbital energy and SOC. Remarkably, based on first-principles calculations, this exact model of QSH phase is shown to be realizable in an experimental system of Au/GaAs(111) surface (see Fig. 2) with an SOC gap of ~73 meV, facilitating the possible room-temperature measurement. Our results significantly extend the search for substrate supported QSH materials to new lattice and orbital types.

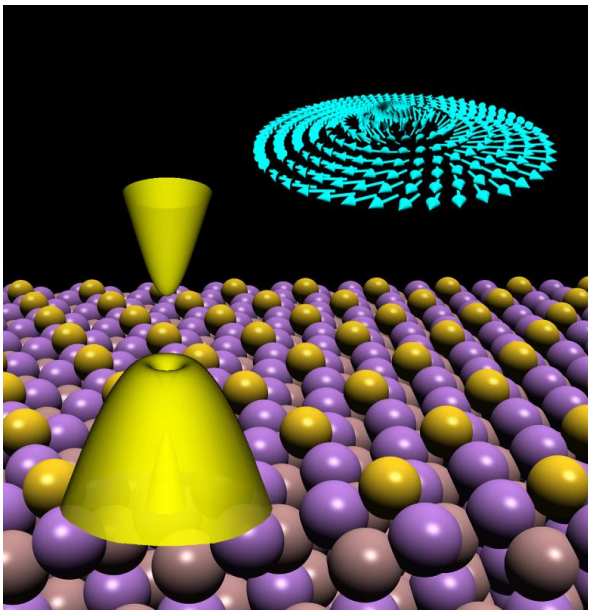

Fig. 2. Schematic illustration of a topological insulating state [3D band structure (middle left) and spin texture of topological edge state(top right)] form with a trigonal lattice of Au overlayer on GaAs(111) surface (bottom).

(c) Bending strain engineering in quantum spin hall system for controlling spin currents[4,5].

Quantum spin Hall system can exhibit exotic spin transport phenomena, mediated by its topological edge states. Recently we demonstrated a new concept of bending strain engineering as an effective means to tune the spin transport properties of a quantum spin Hall system.[4,5] We show that bending strain can be used to control the spin orientation of counter-propagating edge states of a quantum spin system to generate a non-zero spin current. This physics mechanism can be applied to effectively tune the spin current and pure spin current decoupled from charge current in a quantum spin Hall system by control of its bending curvature. Furthermore, the curved quantum spin Hall system can be achieved by the concept of topological nanomechanical architecture in a controllable way, as demonstrated by the material example of Bi/Cl/Si(111) nanofilm[4] and As-graphane[5] (see Fig. 3) This concept of bending strain engineering of spins via topological nanomechanical architecture affords a promising route towards the realization of topological nano-mechanospintronics..

Future Plans

We plan to expand our current studies in the following areas:

(a) Search for new inorganic and organic topological materials
(b) Explore different epitaxial growth routes towards formation of topological quantum phases on semiconductor surfaces
(c) Extend efforts in strained engineered topological materials
(d) Continue exploring a new research direction in "topological nanomechanical architecture"
(e) Exploring topological phases in nanostructured materials, such as nanotube arrays
(f) Continue the efforts of experimental collaborations.

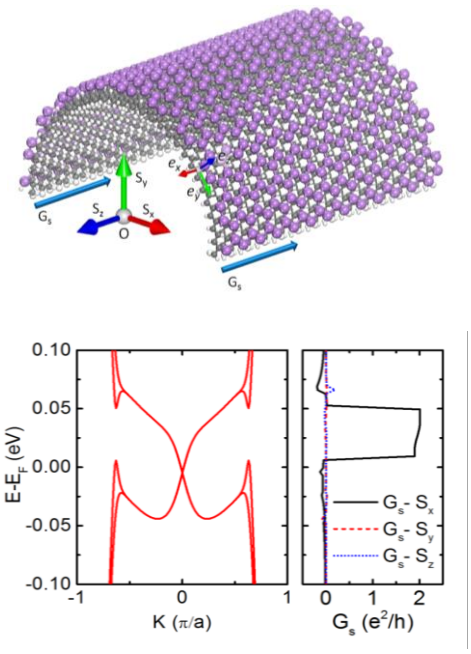

Fig. 3. Up: A self-bent As-graphane, a curved 2D topological insulator. Lower left: Band structure of the bent As-graphane;; lower right: Edge spin conductance.

References

1. "Topological Edge States in High-Temperature Superconductor FeSe/SrTiO3(001) Film", Z. F. Wang, H. Zhang, D. Liu, C. liu, C. Tang, C. Song, Y. Zhong, J. Peng, F. Li, C. Nie, L, Wang, X. J. Zhou, X, Ma, Q. K. Xue and Feng Liu, *Nature Mat.*, **15**, 968 (2016).
2. "Topological Insulators and Superconductivity: The integrity of Two Sides", W.-F. Tsai and H. Lin, *Nature Mat.*, **15**, 927 (2016).
3. "Quantum spin Hall phase in 2D trigonal lattice", Z. F. Wang, Kyung-Hwan Jin & Feng Liu, *Nature Commun*. **7**, 12746 (2016).
4. "Bending strain engineering in quantum spin hall system for controlling spin currents", B. Huang, K.-H. Jin, B. Cui, F. Zhai, J. Mei and Feng Liu, *Nature Commun*. **8**, 15850 (2017).
5. "Quantum Spin Hall Effect and Tunable Spin Transport in As-Graphane", L. Zhang, F. Zhai, K-H Jin, B. Cui, B. Huang, Z. Zhang, J. Lu and Feng Liu. *Nano Lett*. **17**, 4359 (2017).

Publications

1. “Topological Edge States in High-Temperature Superconductor FeSe/SrTiO3(001) Film”, Z. F. Wang, H. Zhang, D. Liu, C. liu, C. Tang, C. Song, Y. Zhong, J. Peng, F. Li, C. Nie, L, Wang, X. J. Zhou, X, Ma, Q. K. Xue and Feng Liu, Nature Mat., 15, 968 (2016).
2. “Quantum spin Hall phase in 2D trigonal lattice”, Z. F. Wang, Kyung-Hwan Jin & Feng Liu, Nature Commun. 7, 12746 (2016).
3. “Direction-Controlled Light-Driven Movement of Microribbons”, Y. Zhang, C. Peng, B. Cui, Z. Wang, X. Pang, R. Ma, Feng Liu, Y. Che, J. Zhao, Adv. Mat., 28, 8538 (2016).
4. "Large-Gap Quantum Spin Hall State in MXenes: d-Band Topological Order in a Triangular Lattice", C. Si, K.-H. Jin, J. Zhou, Z. Sun, and Feng Liu. Nano Lett. 16, 6584 (2016).
5. “Strain engineering of graphene: a review”, C. Si, Z. Sun and Feng Liu, Nanoscale, 8, 3207 (2016).
6. "Effect of Chlorine Substitution on Lattice Distortion and Ferroelectricity of CH3NH3PbI3", W. L. Yan, G. H. Lu and Feng Liu, J. Phys. Chem. C 120, 17972 (2016).
7. “Graphene processing using electron beam assisted metal deposition and masked chemical vapor deposition growth”, A. Merrell and Feng Liu, J. Vac. Sci. Technol. B 34, 4 (2016).
8. “Interface Orbital Engineering of Large-gap Topological States: Decorating Gold on a Si(111) Surface, B. Huang, K. Jin, H. L. Zhuang, L. Zhang, and Feng Liu, Phys. Rev. B 93, 115117 (2016).
9. “Thickness dependence of surface energy and contact angle of water droplets on ultrathin MoS2 films”, Y. Guo, Z. Wang, L. Zhang, Xiao. Shen and Feng Liu, Phys. Chem. Chem. Phys., 18, 14449 (2016).
10. “Electronic structure evolution of single bilayer Bi(111) film on 3D topological insulator Bi2SexTe3-x surfaces”, T. Lei, K. Jin, N. Zhang, J. Zhao, C. Liu, W. Li, J. Wang, R. Wu, H. Qian, Feng Liu and K. Ibrahim, J. Phys.: Condens. Matter. 28, 255501 (2016).
11. “Electrophobic Interaction Induced Impurity Clustering in Metals”, H.-B. Zhou, J.-L. Wang, W. Jiang, J. A. Aguiar, G.-H. Lu1, and Feng Liu, Acta Materialia, 119, 1 (2016).
12. “Formation of Ideal Rashba States on Layered Semiconductor Surfaces Steered by Strain Engineering”, W. Ming, Z.F. Wang, M. Zhou, M. Yoon, and Feng Liu, Nano Lett., 16, 404 (2016).
13. "Formaiton of a quantum spin Hall state on a Ge(111) surface", P. Li, M. Zhou, L. Zhang, Y. Guo and Feng Liu, Nanotechnology, 27, 095703 (2016).
14. “Tunable Topological States in Electron-Doped HTT-Pt”, X. Zhang, Z. Wang, M. Zhao, Feng Liu, Phys. Rev. B, 93, 165401 (2016).
15. “Structural, electronic, and magnetic properties of tris(8-hydroxyquinoline)iron(III) molecules and their magnetic coupling with ferromagnetic surface: first-principles study”, J. Phys.: Condens. Matter 28, 176004 (2016).
16. “Intrinsic Two-Dimensional Organic Topological Insulators in Metal-Dicyanoanthracene Lattices”, L. Z. Zhang, Z. F. Wang, B. Huang, B. Cui, Zhiming Wang, S. X. Du, H.-J. Gao, and Feng Liu, Nano Lett., 16, 2072 (2016).
17. “Engineering electronic structure of a 2D topological insulator Bi(111) bilayer on Sb nanofilms by quantum confinement effect", G. Bian, Z.F. Wang, X. Wang, C. Xu, S. Xu, T. Miller, M. Hasan, Feng Liu, T.-C. Chiang, ACS Nano, 10, 3859 (20016).

18. “Bis(aminothiolato)nickel nanosheet as a redox switch for conductivity and an electrocatalyst for the hydrogen evolution reaction”, X. Sun, K. Wu, R. Sakamoto, T. Kusamoto, H. Maeda, X. Ni, W. Jiang, Feng Liu, S. Sasaki, H. Masunage and H. Nishihara. Chem. Sci., 2017, DOI: 10.1039/C7SC02688A.
19. “Multivalency-Driven Formation of Te-Based Monolayer Materials: A Combined First-Principles and Experimental study”, Z. Zhu, X. Cai, S. Yi, J. Chen, Y. Dai C. Niu, Z. Guo, M. Xie, Feng Liu, J. Cho, Y. Jia and Z. Zhang. Phys. Rev. Lett. 119, 106101 (2017).
20. “Theoretical Discovery of a Superconducting Two-Dimensional Metal−Organic Framework”, X. Zhang, Y. Zhou, B. Cui, M. Zhao and Feng Liu. Nano Lett. DOI: 10.1021/acs.nanolett.7b02795 (2017).
21. “Topological nodal-line semimetal in nonsymmorphic Cmce-phase Ag2S”, H. Huang, K-H Jin and Feng Liu. Phys. Rev. B 96, 115106 (2017).
22. “Atomically Abrupt Topological p−n Junction”, S. Kim, K-H Jin, B. Kho, B. Park Feng Liu J. Kim, H. Yeom. ACS Nano, DOI: 10.1021/acsnano.7b03880 (2017).
23. “ Creation of half-metallic f-orbital Dirac fermion with superlight elements in orbital-designed molecular lattice”, B. Cui, B. Huang, C. Li, X. Zhang, K-H Jin, L. Zhang, W. Jiang, D. Liu, and Feng Liu. Phys. Rev. B 96, 085134 (2017).
24. “Spin fluctuation induced linear magnetoresistance in ultrathin superconducting FeSe films”, Q. Wang, W. Zhang, W. Chen, Y. Xing, Y. Sun, Z. Wang, J. Mei, Z. Wang, L. Wang, X. Ma, Feng Liu, Q. Xue and J. Wang. 2D Mater. 4, 034004 (2017).
25. “Tuning interfacial spin filters from metallic to resistive within a single organic semiconductor family”, J. Wang, A. Deloach, W. Jiang, C. M. Papa, M. Myahkostupov, F. N. Castellano, Feng Liu and D. B. Dougherty. Phys. Rev. B, 95, 241410(R) (2017).
26. “Quantum Spin Hall Effect and Tunable Spin Transport in As-Graphane”, L. Zhang, F. Zhai, K-H Jin, B. Cui, B. Huang, Z. Zhang, J. Lu and Feng Liu. Nano Lett, 17, 4359 (2017).
27. “Bending strain engineering in quantum spin hall system for controlling spin currents”, B. Huang, K-H Jin, B. Cui, F. Zhai, J. Mei and Feng Liu. Nature Commun. 8, 15850 (2017) .
28. “π conjugation in the epitaxial Si(111)-(√3×√3) surface: Unconventional “bamboo hat” bonding geometry for Si”, W. Jiang, Z. Liu, M. Zhou, X. Ni and Feng Liu. Phys. Rev. B, 95, 241405(R) (2017).
29. “Tensile strained gray tin: Dirac semimetal for observing negative magnetoresistance with Shubnikov–de Haas oscillations”, H. Huang and Feng Liu. Phys. Rev. B, 95, 201101(R) (2017).
30. “Computational design of two-dimensional topological materials”, Z. F. Wang, K-H Jin and Feng Liu. WIREs Comput Mol Sci 2017. doi: 10.1002/wcms.1304.

Quasiepitaxial Growth of Organic-Organic Charge Transfer Complexes

Richard R. Lunt
Johansen Crosby Endowed Associate Professor
Department of Chemical Engineering and Materials Science, Department of Physics
Michigan State University, East Lansing, MI, 48824

Program Scope:

(1) The presence of excitons in organic semiconductors at room temperature distinguish them from traditional semiconductors, providing exceptional opportunities for manipulating energy in a range of structures from light emitting diodes, lasers, transparent photovoltaics, and optical switches, and have already shown superior performance in the light emitting diode (LED) field. However, control over crystalline order, orientation, and defect formation are crucial to the fabrication and optimization of these excitonic organic electronics. There have been few examples of preserved-ordering during multilayer crystalline organic growth despite the keen interest in the novel physics afforded by crystalline organic semiconductors. Accordingly, there is a wealth of opportunities for this unexplored regime of organic crystalline growth phenomena. The overarching goal of this project is to understand and explore bottom-up vapor-deposition routes to the growth of large-area organic crystalline films with controlled thickness, doping, and defect concentration. Looking ahead, the integration of pure metals in these systems often hinders the ability to maintain organic crystalline ordering grown from the bottom up. To solve this challenge, we have turned to organic charge transfer complexes, where it has recently been shown that organic molecules can demonstrate metallic conduction in both the bulk and at laminated crystalline interfaces. Indeed, there are a range of exciting properties that have been demonstrated including high metallic conductivities, high electron mobilities, non-centrosymmetric symmetry, Peierls transitions, and ultra-small bandgap formation. These properties make charge-transfer complexes enticing for a variety of applications. Thus, understanding the impact of growth ordering, orientation, and coupling of ordered quasiepitaxial (QE) charge-transfer multilayers is a key next step to making organic QE electronics a reality and enabling new organic electronic functionality.

(2) In parallel, we have begun investigating routes to the epitaxial growth of another promising class of materials, halide perovskites. The growth of epitaxial semiconductors and oxides has long since revolutionized the electronics and optics fields, and continues to be exploited to uncover new physics stemming from quantum interactions. While the recent emergence of halide perovskites offer exciting new opportunities for a range of thin-film electronics, the principles of epitaxy have yet to be applied to this new class of materials and the full potential of these materials is still not yet known. Therefore, by exploiting this epitaxial growth to demonstrate quantum wells of a halide-perovskite system, it can ultimately unlock new routes to push halide perovskites to their full potential.

Recent Progress

A) *Homoepitaxial Growth of Metal Halide Crystals:* On the route to understanding organic quasiepitaxy, we have taken steps to understand the homo-epitaxial growth of metal halide crystals to provide better control over the surface quality, step density, lattice constant (via alloying), and terrace width which can play a significant role in the subsequent organic growth. We report the homoepitaxial growth of metal halide on single crystals investigated with *in situ* reflection high-energy electron diffraction (RHEED) and ex situ atomic force microscopy (AFM). Epitaxial growth of NaCl on NaCl (001) is explored as a function of temperature and growth rate, which provides the first detailed report of RHEED oscillations for metal halide growth. Layer-by-layer growth is observed at room temperature accompanied by clear RHEED oscillations while the growth mode transitions to an island (3D) mode at low temperature. At higher temperatures (>100°C), RHEED oscillations and AFM data indicate a transition to a step-flow growth mode (Fig.1a-b). To show the importance of such metal

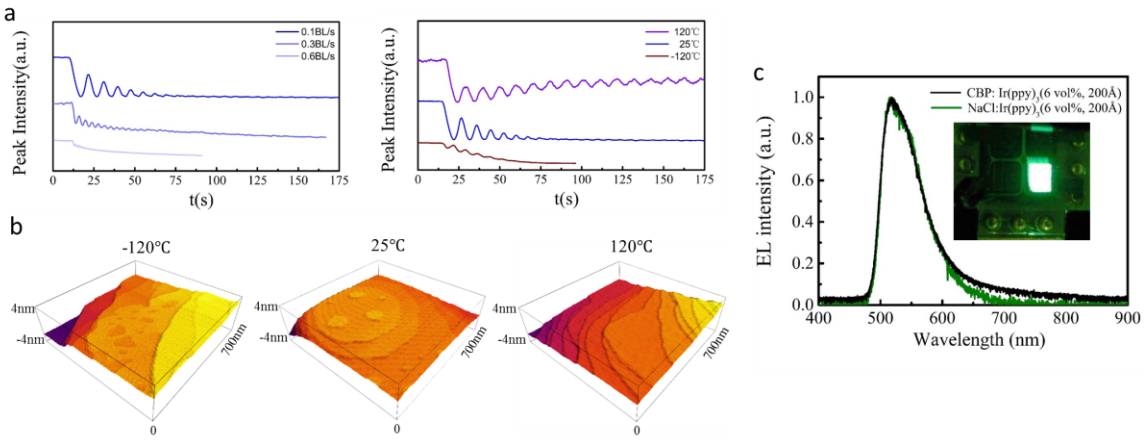

Figure 1. Above: Room temperature growths as a function of growth rate: (left); fixed rate growths of 0.1BL/s as a function of growth temperature (right). (b) AFM images for homoepitaxial growth as a function of growth temperature. (c) Electroluminescence (EL) spectrum of the conventional CBP:Ir(ppy)$_3$ and NaCl:Ir(ppy)$_3$ devices. (Inset) Photo of the NaCl:Ir(ppy)$_3$ device showing green emission at room temperature.[3]

halide growth, green organic light-emitting diodes (OLEDs) are demonstrated using a doped NaCl film with a phosphorescent emitter as the emissive layer (Fig.1c). This work demonstrates the ability to perform in situ and non-destructive RHEED monitoring even on insulating substrates and enables greater control over the surface properties for a range of organic quasiepitaxial and epitaxial halide perovskite optoelectronic applications.

B) *Homoepitaxial Growth of Organic Crystals:* In addition to the cavity melt growth method we previously demonstrated to produce large area organic crystal substrate, we have utilized high temperature vapor methods to grow DPA crystals with lateral length up to 1.5 cm. These crystals have subsequently been utilized as growth substrates for homo-epitaxial and hetero-quasiepitaxial organic crystalline growth. XRD patterns show a single orientation (Fig.2a) that is confirmed by cross-polarized optical imaging (Fig.2b). Rotation dependence of RHEED patterns and the emergence of Kikuchi patterns that vary along different azimuthal angles further demonstrate the single-crystalline nature (Fig.2c). Growth mode phase diagrams for DPA homoepitaxy have been mapped and we have found a transition from stepflow growth at moderate temperatures to 2D growth modes at high deposition rate and 3D growth at low temperature (Fig.2d). These trends are more reminiscent of traditional semiconductor growth, but in contrast to previous organic quasiepitaxial growth trends.

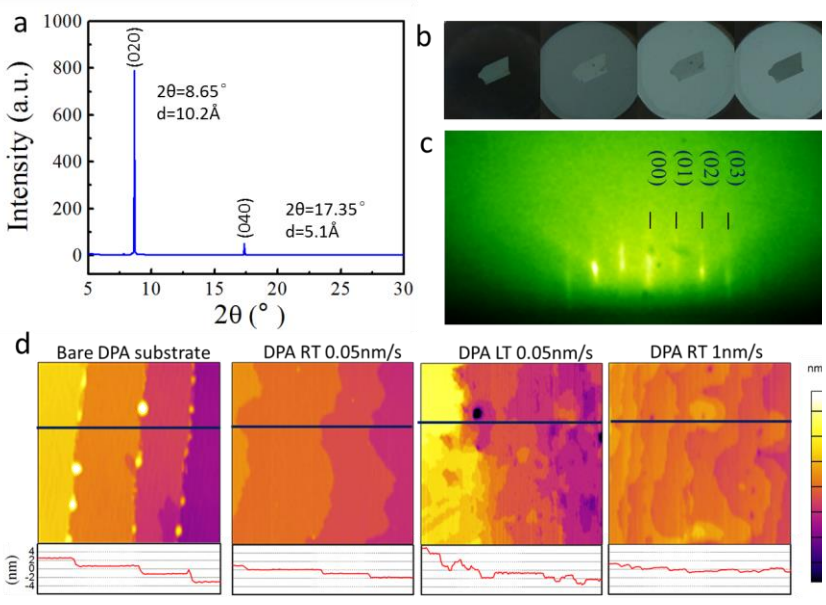

Figure 2. (a) X-ray diffraction and (b) polarized images of DPA single-crystal substrates. (c) Rotation dependence of RHEED patterns. (d) AFM images and line scan of bare DPA substrate; homoepitaxial growth at room temperature; low temperature, and high rate.

C) *Molecular Dynamics (MD) Simulation of Surface Diffusion* Understanding factors that govern molecular diffusion are key for gaining insight and control over quasiepitaxial growth modes. For hetero-quasiepitaxial systems, higher surface diffusion would help increase the ordering of each layer during the multilayer growth. To explore this effect, molecular dynamics (MD) simulation are performed on single crystals substrates for a series of small organic molecules including four linear molecules and their non-linear analogs. The effect of molecular shape, weight and conjugation on surface diffusion behaviors have been studied. In general we find higher diffusivities with decreasing length/width (*L/W)* ratio, but also higher activation energies suggesting that the diffusion barrier is reduced for a greater contact area of conjugated orbitals (Fig.3). We surprisingly find that larger *L/W* can promote diffusion along the crystalline direction of the substrate indicated by longer fractional times along these trajectories.

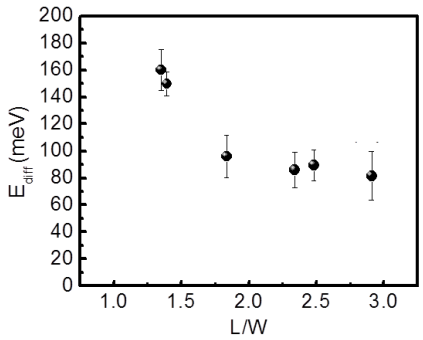

Figure 3. Activation energy as a function of *L/W* ratio. Each point represents simulations of 5-6 temperatures with an average of ~30 simulations for each temperature.

D) *Quasi-epitaxial Growth of Charge Transfer Salts:* Crystal growth conditions for organic charge transfer molecules play an even stronger role that neutral organic molecular crystals. We have demonstrated sustained alternating quasi-epitaxial layers of two organic semiconductors 1,4,5,8-naphthalene-tetracarboxylic-dianhydride (NTCDA), and dibenzotetrathiafulvalene-tetracyanoquinodimethane (DB-TCNQ) grown on single crystal substrates via vapor phase deposition. Both in-plane and out-of-plane ordering are preserved for each subsequent layer under optimized growth conditions despite the vastly differing lattice constants and lattice symmetries (Fig.4). Other potential starting layers such as tetrathiafulvalene 7,7,8,8-tetracyanoquinodimethane (TTF-TCNQ) and TCNQ have been investigated using in situ diffraction. Both materials show single crystalline like growth on KBr suggested by the rotation dependence of RHEED patterns. Paired growth of TCNQ/TTF and TCNQ/DPA have also been studied and show viable crystalline growth across the multilayer structure (Fig.4). Electronic properties of these multilayer quasiepitaxial films will be explored in the future work.

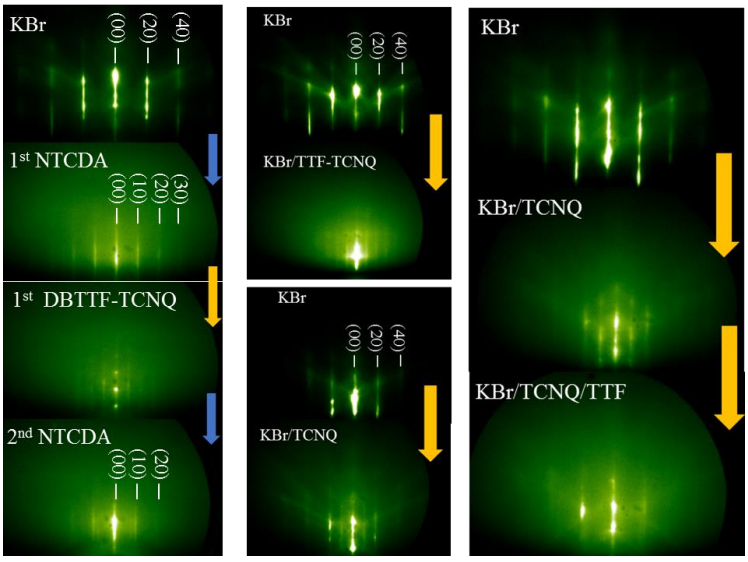

Figure 4. *In situ* RHEED patterns of alternating NTCDA/DBTTF-TCNQ growth on single crystal substrates. Ordering for over 2 pairs has been achieved with this combination, where there is a close surface energy matching of the LESs. (middle) RHEED patterns of TTF-TCNQ and TCNQ growth. (right) RHEED patterns of alternating TCNQ/TTF and TCNQ/DPA growth

E) *Single-Domain Epitaxy of Halide Perovskites:* While there has been significant research into the epitaxial growth of oxide perovskites, single-domain epitaxy has yet to be explored for halide perovskites. This has likely been hindered in large part due to a number of challenges associated with

the epitaxial growth of perovskites on dissimilar single crystal substrates including matching of lattice constants, lattice symmetry, coordination, wettability, thermal expansion differences, and bonding character (ionic versus covalent). Here, we demonstrate a route to the epitaxial growth of halide perovskites by reactive vapor phase deposition onto lattice matched single crystal substrates with congruent ionic interactions. RHEED patterns captured during the epitaxial growth of the halide perovskite at room temperature are shown in Fig. 5 along with rotation dependent patterns. We also show the emergence of two epitaxial phases of cesium tin bromide ($CsSnBr_3$ and $CsSn_2Br_5$) with vastly differing lattice constants and bandgaps based on stoichiometry control (not shown). The larger lattice of $CsSn_2Br_5$ is accommodated via the rotation of crystal planes relative to the metal halide substrates. The lattice misfit between the ionic epitaxial film and the substrate is precisely tuned by applying a pseudomorphic buffer layer of alloyed alkali metal halide salts based on the homoepitaxial growth of metal halides demonstrated above (in A), and an epitaxial lift-off method has been demonstrated for further device fabrication. The dominant performance of devices fabricated with epitaxial films confirms that the high crystallinity and low defect density are beneficial for halide perovskite optoelectronic applications. We further exploit the epitaxial growth of $CsSnBr_3$ to demonstrate multilayer epitaxial quantum wells of a halide perovskite with barrier layers of either NaCl or stroichiometrically-controlled $CsSn_2Br_5$. From these QW structures we extract a Bohr radius for $CsSnBr_3$ of 5.6 nm from photoluminescence data as a function of well width (Fig. 6). These initial demonstrations will likely spark the exploration of a range of epitaxial halide perovskites and quantum wells, and also lead to new emerging phenomena in halide perovskites.

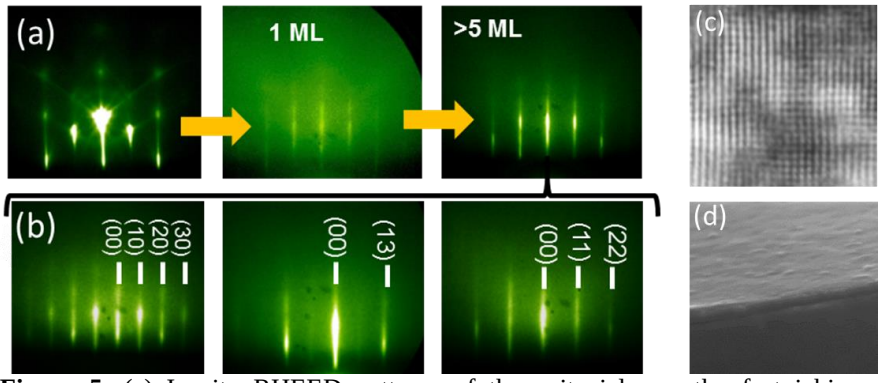

Figure 5. (a) In situ RHEED patterns of the epitaxial growth of stoichiometric $CsSnBr_3$ on NaCl(001).; (b) Rotation dependent RHEED patterns of the cubic epitaxial phase. Cross-section (c) TEM and (d) SEM of epitaxial $CsSnBr_3$ on NaCl.[5]

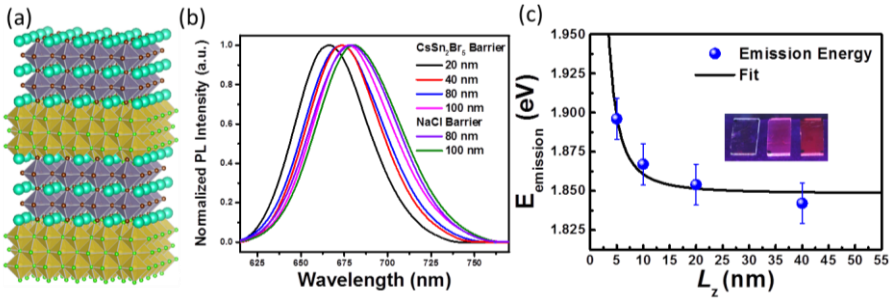

Figure 6. (a) Illustration of the grown metal-halide/halide-perovskite quantum well structure. (b) PL spectra of the quantum wells with varying well width fabricated with $CsSn_2Br_5$ or NaCl epitaxial barriers; (c) QW emission energies with varying well width. Inset: samples illuminated under UV light (left to right, bare crystal, quantum well (40 nm), and quantum well (~100 nm).[5]

Future Plans

(1) Charge-transfer molecule pairing will explore combinations of predicted surface-energy matching and mismatching combinations to understand the impact of additional charge transfer interactions. We will use and develop methods for both congruent evaporation from bulk reacted powders and reactive co-deposition from individual molecule sources and study these growth dynamics using real-time in-situ crystalline growth monitoring that we have unlocked in our current project. Subsequently, we will correlate charger transfer interactions and layer arrangement on optoelectronic properties. (2) For the

halide perovskites, we plan to further investigate the epitaxial pairing of other lead-free halide perovskites and explore their application in optoelectronics devices.

DoE Sponsored Publications in the Last Two Years

1. P. Kuttipillai, Y. Zhao, C. J. Traverse, B. G. Levine, R. R. Lunt, "Phosphorescent Nanocluster Light Emitting Diodes", *Advanced Materials,* 2015. (**Front Cover**)
2. P. Chen and R. R. Lunt, "Organic Step Edge Driven Heteroquasiepitaxial Growth of Organic Multilayer Films", *Advanced Materials Interfaces,* 2016. (**Front Cover**)
3. P. Chen, P. S. Kuttipillai, L. Wang, and R. R. Lunt," Homoepitaxial Growth of Metal Halide Crystals Investigated by Reflection High-Energy Electron Diffraction", *Scientific Reports,* 2016.
4. L. Wang, D. Moghe, S. Hafezian, P. Chen, et al. "Alkali Metal Halide Salts as Interface Additives to Fabricate Hysteresis-Free Hybrid Perovskite-Based Photovoltaic Devices", *ACS Applied Materials & Interfaces,* 2016.
5. L. Wang*, P. Chen*, N. Thongprong, M.Young, P. S. Kuttipillai, K. Sun, P. M. Duxbury, R. R. Lunt, "Unlocking the Single-Domain Epitaxy of Halide Perovskites", *Advanced Materials Interfaces,* 2017. (**Inside Front Cover**)
6. Patent: "Method For Fabricating Epitaxial Halide Perovskite Films And Devices", U.S. Provisional Patent, 2017
7. P. Chen, A. Guest, R. Lunt, "Molecular Dynamics of Organic Surface Diffusion on Crystals". *In Prep.,* 2017.
8. P. Chen, R. Lunt, "Homoepitaxial Growth of Organic Crystals Investigated by Reflection High-Energy Electron Diffraction" *In Prep.,* 2017.

Novel exotic properties of two-dimensional atomic crystals of layered ternary transition metal chalcogenides

Zhiqiang Mao and Jiang Wei
Department of Physics and Engineering Physics, Tulane University,
New Orleans, LA 70118

Program Scope

Individual atomically-thin layer of transition metal dichalcogenides (TMDCs) such as MoS_2 and WS_2 has attracted widespread attentions [1-3]. Their distinct properties, such as large direct band gaps and high photoresponsibility, have tremendous potential for applications in nanoelectronics and optoelectronics. Given the fascinating properties of 2D *binary* TMDCs, the PIs are particularly interested in studying whether 2D atomically-thin semiconductors can be realized in layered *ternary* transition metal chalcogenides (TTMCs). The distinct properties of 2D TMDCs are attributed to the combined effects of quantum confinement, localized *d*-bands, spin-orbital coupling (SOC), and inversion symmetry breaking. In layered TTMCs, these parameters can have greater tunability. Therefore, 2D atomic crystals of TTMCs can reasonably be expected to exhibit distinctive properties. There are many layered, semiconducting layered TTMCs which allow combinations of 3*d* and 4*d*/5*d*/Sb/Bi, such as Cu_2MX_4 (M=W/Mo; X=S/Se) [4-7], $Mn(Sb/Bi)_2S_4$ [8-10], (M and $Ta_2(Pd/Pt/Ni)_3Se_8$ [11,12]. Many of these materials have optical bandgaps in the visible range and their layered structures may allow accessibility of 2D atomic crystals. One major objective of this research project is to discover novel 2D TTMC materials with distinct and useful properties as well as establish the synthesis science of for the proposed TTMCs. The research work of this project includes bulk single crystal growth and characterization of TTMCs, preparation of 2D atomic crystals of TTMCs, nanoscale transport measurements, and the search for exotic properties on 2D TTMCs using field effect.

Recent Progress

The PIs have made significant progresses in the proposed research. We synthesized a wide range of layered TTMCs and demonstrated accessibility of 2D atomically thin layers for many of them, including $Ta_2(Pd/Pt)_3Se_8$, $FeTe_{1-x}Se_x$, $MnPS_3$, $CrSiTe_3$, ZrSiM(M=S, Se, Te) *etc*. From transport measurements, we have found several material systems exhibit novel emergent phenomena/controllable functional properties in 2D thin layers or 1D nanowires. The following is a summary of our major achievements:

a) **Inhomogeneous superconductivity probed in 2D atomic crystals of $Fe(Te_{1-x}Se_x)$**

$Fe(Te_{1-x}Se_x)$ has been used a model system to investigate the superconducting pairing mechanism of Fe-based superconductors due to its simple structure. The PI Mao group previously performed extensive studies on the interplay between magnetism and superconductivity in $Fe(Te_{1-x}Se_x)$ [13]. One unresolved issue with this system is that although bulk measurements suggest inhomogeneous superconductivity, this has never directly probed in experiments. We have recently addressed this issue through transport measurements on $Fe(Te_{1-x}Se_x)$ nano-crystals with various thickness (Fig. 1c). We have found that with decreasing the thickness, the superconducting transition is gradually suppressed and eventually disappears at a critical thickness around 12nm as shown in Fig. 1c-d. When the thickness of nanoflake is approaching 12nm, *i.e*. the characteristic size of superconducting islands, the conducting path of

supper current is disconnected and a nonmetallic behavior dominates the transport at the full range of temperature. This experiment directly demonstrates the nano-scale inhomogeneity of superconductivity in $Fe(Te_{1-x}Se_x)$, which not only provides important clues to the understanding of superconducting pairing mechanism of this material system, but also lays a solid foundation for us to seek high-T_c superconductivity on FeSe atomic crystals using field effect. This work has been published in ACS Nano [14]. Moreover, we recently discovered a very interesting switching behavior in the *I-V* characteristics due to Joule heating in the $Fe(Te_{1-x}Se_x)$ nano-structure.

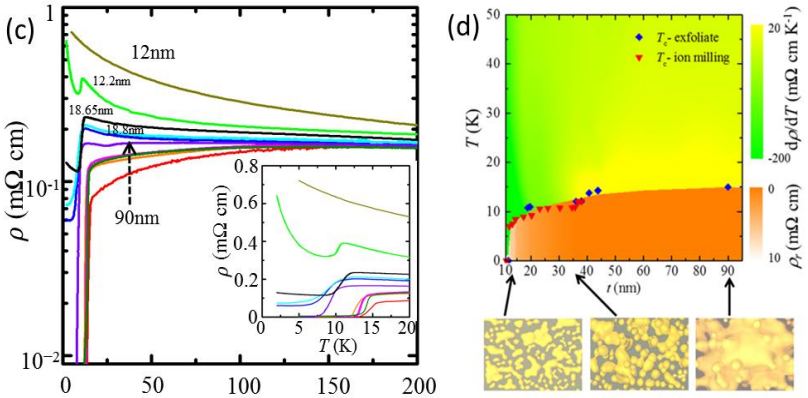

Fig.1. (c) Temperature dependences of resistivity for the $Fe(Te_{0.5}Se_{0.5})$ nano-flakes with various thicknesses . Inset: magnified resistivity data at low temperature (< 20K). (d) Phase diagram of the thickness dependence of superconducting and normal state properties. Bottom graphs show how superconducting domain evolves with sample thickness [14].

b) **Ultrastable semiconducting nanowires of $Ta_2(Pd/Pt)_3Se_8$**

We have succeeded in growing single crystals of two ternary quasi-one-dimensional (1D) van der Waals materials-$Ta_2(Pt/Pd)_3Se_8$ using chemical vapor transport (CVT) method (Fig.2a and 2b) and found these crystals can be easily exfoliated to nono-wires (Fig.2c). The crystal structure of this material (Fig. 2a) is comprised of chain-like $Ta_2(Pt/Pd)_3Se_8$ molecular ribbons. The interchain bonding energy is as small as 0.34eV, while intrachain bonding is about 5.4eV [15]. Such weak interchain-bonding enables easy mechanical exfoliation. Fig. 2c shows a TEM image of a $Ta_2Pd_3Se_8$ nano-wire consisting of a few molecular ribbons. The band structure calculations (in collaboration with Sorokin) show this material is an indirect band gap semiconductor with a gap magnitude of 0.5eV in bulk form, but a direct band gap semiconductor with a gap of 0.7-1eV in nano-wire form. Our transport measurements indeed verify its semiconducting behavior.

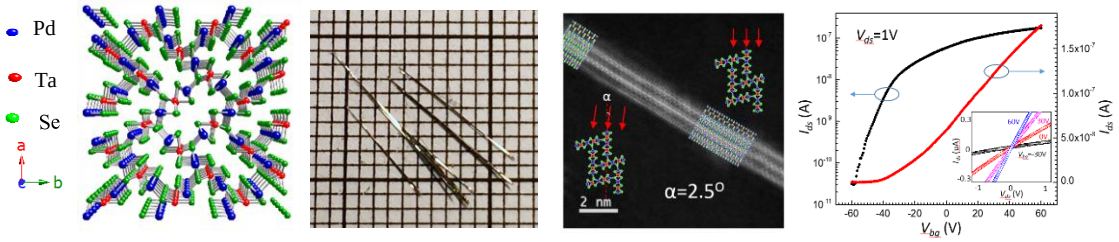

Fig.2: a) Crystal structure of $Ta_2Pd_3Se_8$. b) An optical image of $Ta_2Pd_3Se_8$ single crystals grown using the CVT method. c) A TEM image of a $Ta_2Pd_3Se_8$ nano-wire. d) Current-voltage characteristic of the field effect test structure based on $Ta_2Pd_3Se_8$ nano-wire, showing transistor performance [15].

We have also demonstrated the transistor performances of $Ta_2(Pt/Pd)_3Se_8$ nano-wires, with the current on/off ratio of 10^4 and the transport mobility of 75 $cm^2/V{\cdot}S$ (Fig. 2d) [15]. We also found $Ta_2Pd_3Se_8$ is a *n*-type semiconductor, while $Ta_2Pt_3Se_8$ is *p*-type semiconductor. Another remarkable property of $Ta_2(Pt/Pd)_3Se_8$ nano-wires is that they are ultrastable in air, without any surface oxidation layer (Fig.2c). This work (which is recently published in Nano Letter [15])

offer a new platform for exploring potential applications of semiconducting nano wires and novel 1D physics. Very recently, we have also developed a new liquid exfoliation method to synthesize $Ta_2(Pt/Pd)_3Se_8$ nanowires, which is capable of scaling up for mass production.

c) **Discovery of topological nodal-line semimetals ZrSiSe and ZrSiTe**

The recent discoveries of topological semimetals, including Dirac semimetals, Weyl semimetals and nodal line semimetals, have attracted enormous interests due to their distinct exotic properties such as high mobility and large magnetoresistance. We have recently found the first experimental evidence of new nodal line semimetals ZrSiSe and ZrSiTe from de Haas–van Alphen (dHvA) quantum oscillations measurements (Fig. 3d-e) [16]. Although ZrSiSe and ZrSiTe share similar layered structure with the reported nodal line semimetal ZrSiS (Fig. 3a) [17], their interlayer bounding energy is much smaller than that of ZrSiS, which enables the accessibility of atomically thin 2D layers through microexfoliation (Fig.3c). These results establish the first platform to explore exotic properties of topological nodal-line fermions in low dimensions. This work has been published in *Phys. Rev. Lett*. (Editor's Suggestion)[16]. We also performed the first systematic dHvA oscillation studies on ZrSiS and found its nodal line state is highly anisotropic and characterized by surprisingly strong Zeeman splitting at low magnetic fields, implying enhanced electronic correlation of Dirac fermions induced by the increased Landau level degeneracy (Hu *et al., Phys. Rev. B, 2017, Editor's suggestion*) [18]. Additionally, we have also performed quantum oscillation studies on the isostructural compounds ZrGe(S/Se/Te) and found the Ge square net lattices in these compounds also generate nodal line Dirac cone states (Hu *et al., Phys. Rev. B,2017*) [19].

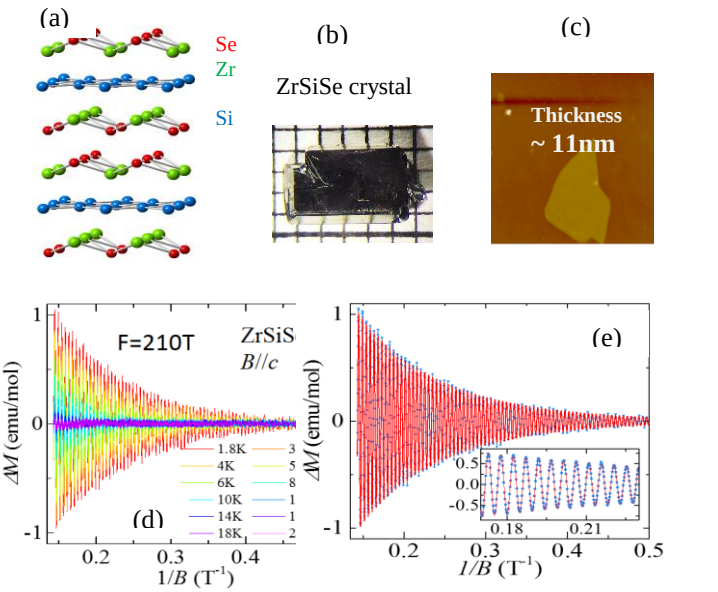

Fig. 3: (a) Crystal structure of ZrSi(Se/Te). (b) An optical image of ZrSiSe crystal. (c) An optical image of ZrSiSe nano-flake. (d) de Haas–van Alphen (dHvA) oscillations probed on ZrSiSe. (e) The fit (red curve) of dHvA oscillations by the Lifshitz-Kosevich (LK) formula, from which evidence of Dirac fermions have been found [16].

Future Plans

2D TTMC semiconductors: We will continue to explore the TTMC candidate materials proposed in the original proposal. More specifically, we will synthesize and characterize those candidate TTMCs which have not been studied in Years 1 and 2, including $Mn(Bi/Sb)_2S_4$, $FeSb_2Se_4$, $MnBi_4S_7$ and $FeBi_4S_7$. As discussed in the original proposal, we will grow single crystals of these materials and characterize electronic and magnetic properties. If some of them turn out to be magnetic semiconductors, we will explore their properties on nano-scale.

2D $Fe_{1+y}(Te_{1-x}Se_x)$: We have demonstrated the nano-scale inhomogeneous superconductivity in $Fe_{1+y}(Te_{1-x}Se_x)$ in Year 1. Recently, we observed unusual dynamic behavior in magnetotransport

associated with inhomogeneous superconductivity on nano-scale transport measurements. In Year 3, we plan to conduct more systematic studies on this using the nano-crystals with various thicknesses to understand its origin. The other sub-goal is to seek high-temperature superconductivity using field effect.

Dimensionality confinement effect of electron-phonon interactions in 2D materials: Another sub-direction the PIs plan to pursue in Year 3 is to investigate the dimensionality confinement effect on electron-phonon interaction. We previously studied this issue using quantum transport properties of Nb_3SiTe_6 nano-crystals [20] and found strong evidence for the long-predicted suppression of *e-ph* interaction caused by the crossover of phonon spectrum from 3D to 2D. We plan to extend this study to other layered materials, such as β-$K_2Bi_8Se_{13}$, to establish the universality of such dimensionality confinement effect on *e-ph* interactions. We have already obtained some preliminary results and plan to complete it in Year 3.

References

[1] Q.H. Wang *et al*., Nat. Nano. **7**, 699 (2012).
[2] M. Chhowalla *et al.*, Nat. Chem. **5**, 263 (2013).
[3] S. Butler *et al.*, ACS Nano **7**, 2898 (2013).
[4] P.D. Tran *et al.*, Energy & Environmental Science **5**, 8912 (2012).
[5] D. Jing, M. Liu, Q. Chen, and L. Guo, International Journal of Hydrogen Energy **35**, 8521 (2010).
[6] C. J. Crossland, P. J. Hickey, and J. S. O. Evans, Journal of Materials Chemistry **15**, 3452 (2005).
[7] H. Liang and L. Guo, International Journal of Hydrogen Energy **35**, 7104 (2010).
[8] S. Lee, E. Fischer, J. Czerniak, and N. Nagasundaram, J. Alloy. Comp. **197**, 1 (1993).
[9] A. Pfitzner and D. Kurowski, Zeitschrift für Kristallographie - Crystalline Materials **215**, 373 (2000).
[10] D. Kurowski, Ph.D thesis, Universität Regensburg, 2003.
[11] D. A. Keszler and J. A. Ibers, J. Solid State Chem. **52**, 73 (1984).
[12] D. A. Keszler, J. A. Ibers, S. Maoyu, and L. Jiaxi, J. Solid State Chem. **57**, 68 (1985).
[13] T.J. Liu *et al*., Nat Mater **9**, 718 (2010).
[14] C. Yue, J. Hu, X. Liu, A. M. Sanchez, Z. Mao, and J. Wei, ACS Nano **10**, 429 (2016).
[15] X. Liu, J. Liu, L. Y. Antipina, J. Hu, C. Yue, A. M. Sanchez, P. B. Sorokin, Z. Mao, and J. Wei, Nano Lett. **16**, 6188 (2016).
[16] J. Hu, Z. Tang, J. Liu, X. Liu, Y. Zhu, D. Graf, K. Myhro, S. Tran, C. N. Lau, J. Wei, and Z. Mao, Phys. Rev. Lett **117**, 016602 (2016).
[17] L.M. Schoop *et al*., Nat. Commun. **7**, 11696 (2016).
[18] J. Hu, Z. Tang, J. Liu, Y. Zhu, J. Wei, and Z. Mao, Phys. Rev. B **96**, 045127 (2017).
[19] J. Hu, Y. L. Zhu, D. Graf, Z. J. Tang, J. Y. Liu, and Z. Q. Mao, Phys. Rev. B **95**, 205134 (2017).
[20] J. Hu *et al.*, Nature Physics **11**, 471 (2015).

List of Publications in Year 1 and 2

[1] *Quantum oscillation studies of topological semimetal candidate ZrGeM (M = S, Se, Te),* J. Hu, Y.L. Zhu, D. Graf, Z.J. Tang, J.Y. Liu, and Z.Q. Mao ***Phys. Rev. B 95, 205134 (2017)***

[2] *Nearly massless Dirac fermions and strong Zeeman splitting in nodal-line semimetal ZrSiS probed by de Haas-van Alphen quantum oscillations*, Jin Hu, Zhijie Tang, Jinyu Liu, Yanglin Zhu, Jiang Wei and Zhiqiang Mao, ***Phys. Rev. B 96, 045127 (2017) (Editor's suggestion).***

[3] *Wafer-scale synthesis of monolayer and few-layer MoS2 via thermal vapor sulfurication,* John Robertson, Xue Liu, Chunlei Yue, Matthew Escarra and Jiang Wei, ***2D Materials 4, 045007 (2017)***

[4] *Evidence of Topological Nodal-Line Fermions in ZrSiSe and ZrSiTe,* Jin Hu, Zhijie Tang, Jinyu Liu, Xue Liu, Yanglin Zhu, David Graf, Kevin Myhro, Son Tran, Chun Ning Lau, Jiang Wei, and Zhiqiang Mao ***Phys. Rev. Lett. 117, 016602 (2016) (Editor's suggestion).***

[5] *Direct fabrication of functional ultra single-crystal nanowires quasi-one-dimensional van der Waal crystals*. Xue Liu, Jinyu Liu, Liubov Antipina, Jin Hu, Chunlei Yue, Ana Sanchez, Pavel Sorokin, Zhiqiang Mao, Jiang Wei, ***Nano Letters 16, 6188 (2016).***

[6] *Nano-scale inhomogeneous Superconductivity in Fe(Te1-xSex) probed by nano structure transport, Chunlei Yue, Jin Hu, Xue Liu, Zhiqiang Mao, and Jiang Wei*, ***ACS Nano 10, 429 (2016).***

[7] *Reorientation of the bicollinear antiferromagnetic structure at the surface of Fe1+yTe bulk and thin films,* Torben H¨anke,Udai Raj Singh, Lasse Cornils, Sujit Manna, Anand Kamlapure, Martin Bremholm, Ellen Marie Jensen Hedegaard, Bo Brummerstedt Iversen, Philip Hofmann, Jin Hu, Jens Wiebe, Zhiqiang Mao and Roland Wiesendanger, ***Nature Communications 8, 13939 (2016).***

[8] *Observation of Fermi arc and its connection with bulk states in the candidate type-II Weyl semimetal WTe2,* Chenlu Wang, Yan Zhang, Jianwei Huang, Simin Nie, Guodong Liu, Aiji Liang, Yuxiao Zhang, Bing Shen, Jing Liu, Cheng Hu, Ying Ding, Defa Liu, Yong Hu, Shaolong He, Lin Zhao, Li Yu, Jin Hu, Jiang Wei, Zhiqiang Mao, Youguo Shi, Xiaowen Jia, Fengfeng Zhang, Shenjin Zhang, Feng Yang, Zhimin Wang, Qinjun Peng, Hongming Weng, Xi Dai, Zhong Fang, Zuyan Xu, Chuangtian Chen, and X. J. Zhou, ***Phys. Rev. B 94, 241119 ® (2016).***

[9] *Resistivity of Weyl semimetals NbP and TaP under pressure,* M. Einaga, K. Shimizu, J. Hu, Z. Q. Mao, A. Politano, ***Phys. Status Solidi, published online 2017,* DOI: 10.1002/pssr.201700182**

[10] *Absorption edges of black phosphorus: A comparative analysis,* G. Nicotra, A. Politano, A.M. Mio, I. Deretzis, J. Hu, Z.Q. Mao, J. Wei, A. La Magna, and C. Spinella, ***Phys. Status Solidi B 253 2509(2016).***

[11] *Environmental instability and degradation of single and few-layer nanosheets in ambient conditions*, F. Ye, J. Lee, J. Hu, Z.Q. Mao, J. Wei and X.L. Feng, ***Small 12, 5802 (2016).***

[12] *Unusually strong lateral interaction in the CO overlayer in phosphorene-based systems,*

A. Politano, M.S. Vitiello, L. Viti, J. Hu, Z.Q. Mao, J. Wei, G. Chiarello and D. W. Boukhvalov, ***Nano Research 9, 2598 (2016).***

[13] *Single- and Few-layer WTe_2 suspended nanostructures: Raman signatures and nanomechanical resonances*, Jaesung Lee, Fan Ye, Zenghui Wang, Rui Yang, Jin Hu, Zhiqiang Mao, Jiang Wei, Philip X. L. Feng, ***Nanoscale 8, 7854 (2016)***

Thermochemistry of Oxides with Electrochemical and Energy Applications
DE-FG02-03ER46053

Alexandra Navrotsky
Peter A Rock Thermochemistry Laboratory and NEAT ORU
University of California Davis
Davis, CA 95616

Program Scope

The major objectives of this program are: (a) to advance and use unique calorimetric capabilities to determine the energetics of materials relevant to energy applications, with an emphasis on new materials, and (b) to understand, in terms of both macroscopic energetics and microscopic structure and bonding, the interplay of defect chemistry, oxidation-reduction and size effects at the nanoscale in determining the properties of functional oxide materials and of new classes of non-oxide materials. Recent developments have generated great excitement in organic-inorganic hybrid materials such as the alkylammonium lead halide perovskites. Our current work has emphasized fluorite-based solid electrolytes, perovskites and lithium battery materials. The systematic trends seen enable a more holistic view of the relation of thermodynamics to materials discovery and synthesis.

The presentation at this year's PI meeting emphasizes the thermodynamic stability of hybrid perovskite materials. There is intense interest in the utilization of hybrid perovskites for energy applications ranging from solar energy to water splitting to catalysis. Yet their synthesis and persistence in use often appears limited by various decomposition reactions. Some of these appear to involve water, oxygen and light, and strategies have been developed to minimize these reactions by optimizing morphology and coatings. However, it is necessary to know their intrinsic thermodynamic stability defined by possible decomposition reactions to other products of the same overall composition in order to understand their long-term behavior. Thermochemical measurements thus offer a framework for determining and predicting the feasibility of the synthesis and potential applications of new hybrid materials.

Recent Progress

Using solution calorimetry we have shown that tetramethylammonium lead iodide is intrinsically unstable with respect to disproportionation to its binary components, lead iodide and tetramethyl ammonium iodide. (Nagabhushana et al. 2016) The bromide form is marginally stable and the chloride form somewhat more so. As in inorganic perovskites, thermodynamic stability increases as the tolerance factor approaches unity, providing a strategy for the synthesis of more stable perovskites. We have also investigated two series of transition-metal-containing hybrid perovskites that are possible multiferroic materials. They show greater stability than the lead halide materials (Nagabhushana et al. 2015, 2017).

Future Plans

We are investigating certain Ruddelsten Popper phases based on tetramethylammonium lead iodide. We are continuing work on Li battery cathode materials.

References

"Thermochemistry of Multiferroic Organic-Inorganic Hybrid Perovskites $[(CH_3)_2NH_2][M(HCOO)_3]$ (M = Mn, Co, Ni and Zn)" G. P. Nagabhushana, R. Shivaramaiah, A. Navrotsky, *J. Amer. Chem. Soc.*, 137, 10351-10356 (2015)

"Direct Calorimetric Verification of Thermodynamic Instability of Lead Halide Perovskites" G. P. Nagabhushana, R. Shivaramaiah, A. Navrotsky, *Proc. Natl. Acad. Sci. USA*, 113, 7717-7721 (2016)

"Thermochemistry of Simplest Metal Organic Frameworks: Formates $[M(HCOO)_2] \cdot xH_2O$ (M = Li, Mg, Mn, Co, Ni, and Zn)" G. P. Nagabhushana, R. Shivaramaiah, A. Navrotsky, *J. Chem. Therm.*, In Press (2017)

Publications 2016—17

"Thermodynamic Properties of Polymorphs of Fluorosulfate Based Cathode Materials with Exchangeable Potassium Ions" R. Shivaramaiah, L. Lander, G.P. Nagabhushana, G. Rousse, J.-M. Tarascon, A. Navrotsky, *ChemPhysChem*, 17, 3365-3368 (2016)

"Thermodynamic Stability of Transition Metal Substituted $LiMn_{2-x}M_xO_4$ (M = Cr, Fe, Co, and Ni) Spinels" C. Lai, J. Chen, J. Knight, A. Manthiram, A. Navrotsky, *Phys. Chem. Chem. Phys.*, 17, 1973-1978 (2016)

"Effect of Synthesis Atmosphere on the Proton Conductivity of Y-Doped Barium Zirconate Solid Electrolytes" M. D. Goncalves, P. S. Maram, A. Navrotsky, and R. Muccillo, *Ceram. Intl.*, 42, 13689-13696 (2016).

"A Correlation between Formation Enthalpy and Ionic Conductivity in Perovskite-Structured $Li_{3x}La_{0.67-x}TiO_3$ Solid Lithium Ion Conductors" X. Guo, P. S. Maram. A. Navrotsky; *J. Matl. Chem A*, 5 12951-12957 (2017)

"Direct Calorimetric Verification of Thermodynamic Instability of Lead Halide Perovskites" G. P. Nagabhushana, R. Shivaramaiah, A. Navrotsky, *Proc. Natl. Acad. Sci. USA*, 113, 7717-7721 (2016)

"Thermochemistry of Simplest Metal Organic Frameworks: Formates $[M(HCOO)_2] \cdot xH_2O$ (M = Li, Mg, Mn, Co, Ni, and Zn)" G. P. Nagabhushana, R. Shivaramaiah, A. Navrotsky, *J. Chem. Therm.*, In Press (2017)

"Formation and Dehydration Enthalpy of Potassium Hexaniobate" S. K. Sahu, L. A. Boatner, A. Navrotsky, *J. Am. Ceram. Soc.*, 100, 304-311 (2017)

"Combined Experimental and Computational Investigation of Thermodynamics and Phase Equilibria in the $CaO\text{-}TiO_2$ System" W. Gong, L. Wu, A. Navrotsky; *J. Am Ceram Soc.* Submitted (2017)

"Energetics at the Nanoscale: Impacts for Geochemistry, the Environment, and Materials" A. Navrotsky, *MRS Bull.*, 41, 139-145 (2016)

"Energetics at the Nanoscale: Impacts for Geochemistry, the Environment, and Materials" A. Navrotsky, *MRS Bull.*, 41, 139-145 (2016)

"Hot Matters – Experimental Methods for High-Temperature Property Measurement" A. Navrotsky and S. V. Ushakov, *Am. Ceram. Soc. Bull.*, 96, 22-28 (2017).

"Thermodynamic Stability of Transition Metal Substituted $Mn_{2-x}M_xO_4$()M = Cr, Fe, Cop and Ni) Spinels", C. Lai, M.S. Thesis 2016

Synthesis and characterization of topological semimetals and unconventional superconductors

Ni Ni

University of California, Los Angeles, Los Angeles, CA

Program Scope

Modern research of condensed matters devotes in understanding how properties of complex solids are determined by their structural and electronic degrees of freedom. Despite of the complicity in real materials where competing orders often exist, significant progress has been driven by the discovery of new materials with emergent ground states. Of particular interests are the superconductors near the edge of structural/magnetic instabilities and materials with non-trivial topology. The discovery and characterization of materials of the former type can advance our understanding of high Tc superconductivity significantly while bulk materials with nontrivial topology provide a new platform to study the low energy excitations through band engineering. The objective of this research is to discover materials that lie at the edge of structural/magnetic instability and to explore topological semimetals with exotic low energy excitations using solid state reaction and crystal-growth methods, and to characterize them and examine their structure-property relations through thermodynamic, transport, X-ray, and neutron measurements.

Recent Progress

1. We have discovered that $Ca_{0.73}La_{0.27}FeAs_2$, is the "parent" compound of the 112 superconducting family [1]. The breaking of C_4 rotational symmetry even at room temperature makes it unique among all FPS. We first unravel a monoclinic to triclinic phase transition at 58 K, and a paramagnetic to stripe antiferromagnetic (AFM) phase transition at 54 K, below which spins order 45° away from the stripe direction. Furthermore, in addition to the central-hole and corner-electron Fermi pockets usually appearing in Fe pnictide superconductors, angle-resolved photoemission (ARPES) measurements resolve a Fermiology where an extra electron pocket of mainly As chain character exists at the Brillouin zone edge, suggesting the active role of the metallic spacer layers.

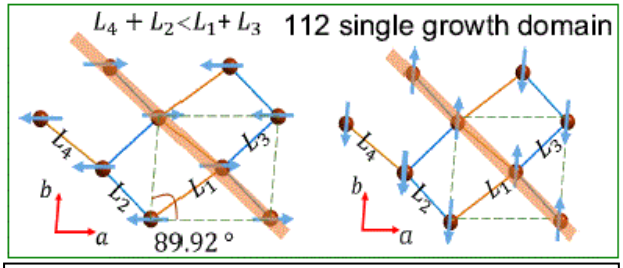

Figure 1: Magnetic structure of $Ca_{0.73}La_{0.27}FeAs_2$.

2. Topological semimetals are characterized by protected crossings between conduction and valence bands. These materials have recently attracted significant interest because of the deep connections to high-energy physics, the novel topological surface states, and the unusual transport phenomena. While Dirac and Weyl semimetals have been extensively studied, the nodal-line semimetal remains largely unexplored due to the lack of an ideal material platform.

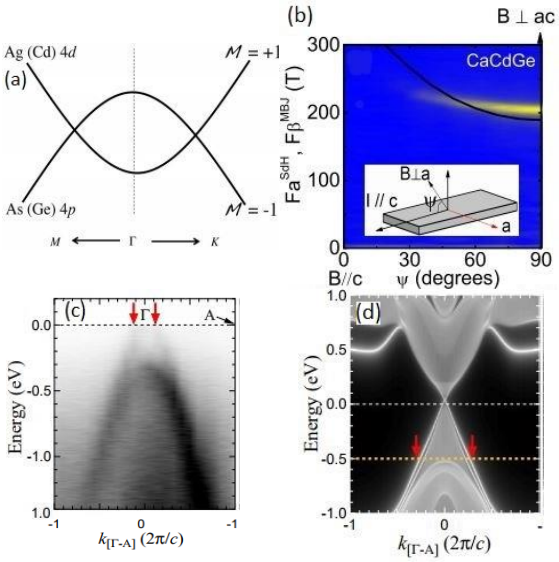

Figure 2: (a) The illustration of the band structure near the Fermi level for CaAgAs/CaCdGe. (b) The SdH QO data for CaCdGe. (c) ARPES and (d) DFT band dispersion along Γ-A directions of CaAgAs. Red arrow points to the surface states.

We found that CaAgAs and CaCdGe provide an ideal platform to perform comparative studies because the theoretical calculation shows that they feature the same topological nodal line except that CaCdGe has a more complicated Fermiology with irrelevant Fermi pockets (Fig. 2(a)-(b)).

As a result of the electron-hole compensation, the magnetoresistance of our CaCdGe sample is more than 100 times larger than that of CaAgAs. Furthermore, ARPES observed a metallic, linear, non-kz-dispersive surface band that coincides with the high-binding-energy part of the theoretical topological surface state, proving the topological nontriviality of the system (Fig. 2(c)-(d)).

3. Dirac cones have been proposed and observed in non-magnetic materials, including Cd_3As_2 and Na_3Bi. By breaking inversion either symmetry or time-reversal symmetry, Dirac point can be split into pairs of weyl points. To break the time-reversal symmetry, we can either apply an external magnetic field or we can use the spontaneous magnetic moment inside the material. For the latter case, the correlation of spontaneous magnetism and Weyl fermions has been studied in the 112 compound and half-heusler compound GdPtBi. Recently, orthorhombic CuMnAs has been proposed to be a magnetic material where Dirac point is robust to the combination of inversion and time-reversal symmetry breaking, providing a system to study the interplay of AFM and Dirac fermions. We first determined the magnetic structure of the orthorhombic $Cu_{0.95}MnAs$ and $Cu_{0.98}Mn_{0.96}As$ single crystals (Fig. 3(a)-(b)). While $Cu_{0.95}MnAs$ is a commensurate antiferromagnet (C-AFM) below 360 K with a propagation vector of k = 0, $Cu_{0.98}Mn_{0.96}As$ undergoes a second-order paramagnetic to incommensurate antiferromagnetic (IC-AFM) phase transition at 320 K with k = (0.1,0,0), followed by a second-order IC-AFM to C-AFM

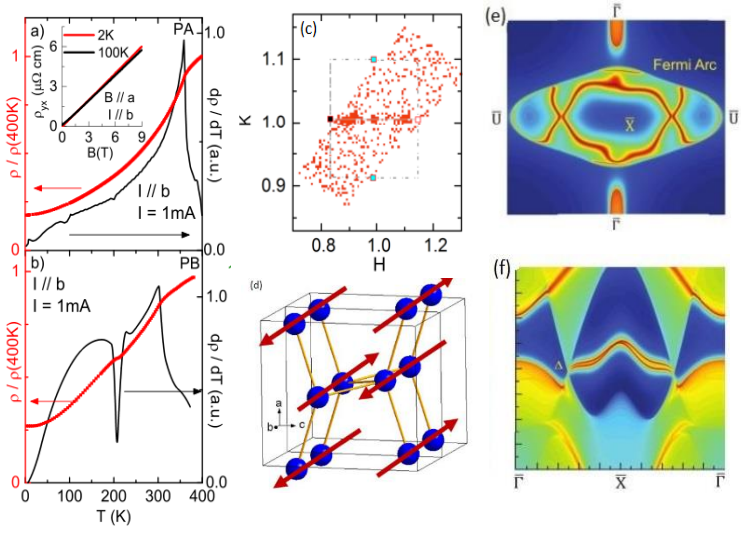

Figure 3: (a) (b)The R and derivative vs. T (c): A cut of the neutron scattering of $Cu_{0.98}Mn_{0.96}As$. (d) The magnetic structure in the C-AFM state. (e) The Fermi surface contour on the (010) surface at the Fermi level. (f) The corresponding electronic spectra along kz=0.

phase transition at 230 K (Fig. 3 (c)). In the C-AFM state, the Mn spins order parallel to the b-axis but antiparallel to their nearest-neighbors with the easy axis along the b axis (Fig. 3(d)). This magnetic order breaks R_y gliding and S_{2z} rotational symmetries, the two crucial for symmetry analysis, resulting in finite band gaps at the crossing point and the disappearance of the massless topological fermions. However, the spin-polarized surface states and signature induced by non-trivial topology still can be observed in this system (Fig. 3 (e)-(f)), which makes orthorhombic CuMnAs promising in antiferromagnetic spintronics.

4. We first mapped out the angular-dependent Shubnikov–de Haas (SdH) of weak topological insulator $NbAs_2$. Combined with the first-principles calculations, we reveal four types of Fermi-surface pockets, as shown in Fig. 4. Negative longitudinal magnetoresistance is observed which may be linked to novel topological states in this material, although systematic study is necessary to ascertain its origin.

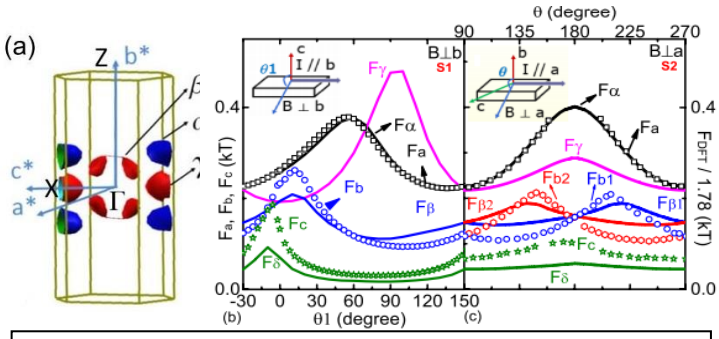

Figure 4: (a) The calculated band structure of $NbAs_2$. (b) (c) The angular dependence of oscillation frequencies. Solid line is the theoretical value.

5. We have provided high quality of superconducting and topological single crystals to various groups for further investigation, including Weyl semimetal TaAs, type II weyl semimetal $TaIrTe_4$, CaAgAs, $BaFe_2(As_{1-x}P_x)_2$, etc. This has led to the understanding of the role of Fermi arcs in the transport of TaAs by STM [1], the testing of a single-spin quantum sensor [2], the discovery of Weyl Points and Topological Nodal Lines in $TaIrTe_4$ [3], the discovery of surface state in CaAgAs [4], etc.

Future Plans

We will continue our exploration and investigation on topological materials and materials with structural/magnetic instabilities.

1. Along the direction of nonmagnetic and magnetic topological semimetals, especially topological superconductors, we will keep our exploration and focus on arsenides and chalcogenides.

2. Along the direction of superconductors near the edge of structural and magnetic instabilities: (a) Our on-going study on the AAg_4As_2 (A=Sr, Eu) has revealed the existence of charge-density-wave instability. While quantum oscillation has been observed in the $SrAg_4As_2$, the $EuAg_4As_2$ shows helical magnetic structure and very interesting behavior of the magnetoresistance, providing a platform to investigate how magnetism affects transport. We will tune their ground state through chemical doping/external pressure.

(b)The recent discovery of increased T_c in KFe_2As_2 under high pressure up to 20 Gpa has been argued to be due to the enhanced superconducting pairing in collapsed tetragonal FeAs phase. On the other hand, the collapsed tetragonal phase has been believed and proved to be harmful for spin fluctuation and thus superconductivity in $CaFe_2As_2$. Therefore, it is important to clarify the relation between superconductivity in collapsed tetragonal phase. The $Na_{1-x}La_xFe_2As_2$ system has the potential to be a chemical-doping analog of the pressure-induced KFe_2As_2. We will grow single crystals and do systematic study of this series.

References

1. Hiroyuki Inoue, et.al, *Quasiparticle interference of the Fermi arcs and surface-bulk connectivity of a Weyl semimetal*, *Science*, **351**, 1184 (2016)
2. Matthew Pelliccione, et.al, *Scanned Probe Imaging of Nanoscale Magnetism at Cryogenic Temperatures with a Single-Spin Quantum Sensor, Nature Nanotechnology*, 11, 700 (2016)
3. Xiaoqing Zhou, Qihang Liu, QuanSheng Wu, Tom Nummy, Haoxiang Li, Justin Griffith, Stephen Parham, Justin Waugh,Eve Emmanouilidou, Bing Shen, Oleg V. Yazyev, Ni Ni, Daniel Dessau, *Coexistence of Tunable Weyl Points and Topological Nodal Lines in Ternary Transition-Metal Telluride TaIrTe4, Arxiv: 1709.10245 (2017), submit to PRL.*
4.Xiao-Bo Wang, Xiao-Ming Ma, Eve Emmanouilidou, Bing Shen, Chia-Hsiu Hsu, Chun-Sheng Zhou, Yi Zuo, Rong-Rong Song, Su-Yang Xu, Gan Wang, Li Huang, Ni Ni, Chang Liu, *Topological surface electronic states in candidate nodal-line semimetal CaAgAs*, Arxiv: 1708.06484 (2017), *submit to PRB.*

Publications

1.Eve Emmanouilidou, Huibo Cao, Peizhe Tang, Xin Gui, Chaowei Hu, Bing Shen, Junyi Wu, Shou-Cheng Zhang, Weiwei Xie, Ni Ni, *Magnetic order induces symmetry breaking in the single crystalline orthorhombic CuMnAs semimetal*, Arxiv: 1708.09340 (2017), *submit to PRL.*
2. Matthew Pelliccione, Alec Jenkins, Preeti Ovartchaiyapong, Christopher Reetz, Eve Emmanuelidu, Ni Ni and Ania C. Bleszynski Jayich, *Scanned Probe Imaging of Nanoscale Magnetism at Cryogenic Temperatures with a Single-Spin Quantum Sensor, Nature Nanotechnology*, 11, 700 (2016)
3. Shan Jiang, Chang Liu, Huibo Cao, Turan Birol, Jared M. Allred, Wei Tian, Lian Liu, Kyuil Cho, Matthew M. Krogstad, Jie Ma, Keith Taddei, Makariy A. Tanatar, Ruslan prozorov, Stephan Rosenkranz, Yasutomo J. Uemura, Gabriel Kotliar and Ni Ni, *Structural and magnetic phase transitions in Ca0.73La0.27FeAs2 with electron-overdoped FeAs layers, Phys. Rev. B* **93**, 054522(2016)
4.Hiroyuki Inoue, András Gyenis, Zhijun Wang, Jian Li, Seong Woo Oh, Shan Jiang, Ni Ni, B. Andrei Bernevig and Ali Yazdani, *Quasiparticle interference of the Fermi arcs and surface-bulk connectivity of a Weyl semimetal*, *Science*, **351**, 1184 (2016)
5.J. W. Harter, H. Chu, S. Jiang, N. Ni, and D. Hsieh, *Nonlinear and time-resolved optical study of the 112-type iron-based superconductor parent Ca1−xLaxFeAs2 across its structural phase transition, Phys. Rev. B* **93**, 104506(2016)

6.Bing Shen, Xiaoyu Deng, Gabriel Kotliar, and Ni Ni, Fermi surface topology and negative longitudinal magnetoresistance observed in NbAs2 semimetal, *Phys. Rev. B* **93**, 195119(2016)
7.Andras Gyenis, Hiroyuki Inoue, Sangjun Jeon, Brian B. Zhou, Benjamin E. Feldman, Zhijun Wang, Jian Li, Shan Jiang,Quinn D. Gibson, Satya K. Kushwaha, Jason W. Krizan, Ni Ni, Robert J. Cava, B. Andrei Bernevig, Ali Yazdani, *Imaging electronic states on topological semimetals using scanning tunneling microscopy*, *New J. Phys. 18, 105003 (2016)*
8.Eve Emmanouilidou, Bing Shen, Xiaoyu Deng, Tay-Rong Chang, Aoshuang Shi, Gabriel Kotliar, Su-Yang Xu, and Ni Ni, *Magnetotransport properties of the single-crystalline nodal-line semimetal candidates CaTX (T=Ag, Cd; X=As, Ge)*, *Phys. Rev. B* **95**, 245113(2017)
9.Xiao-Bo Wang, Xiao-Ming Ma, Eve Emmanouilidou, Bing Shen, Chia-Hsiu Hsu, Chun-Sheng Zhou, Yi Zuo, Rong-Rong Song, Su-Yang Xu, Gan Wang, Li Huang, Ni Ni, Chang Liu, *Topological surface electronic states in candidate nodal-line semimetal CaAgAs*, Arxiv: 1708.06484 (2017)*, submit to PRB.*
10. Xiaoqing Zhou, Qihang Liu, QuanSheng Wu, Tom Nummy, Haoxiang Li, Justin Griffith, Stephen Parham, Justin Waugh,Eve Emmanouilidou, Bing Shen, Oleg V. Yazyev, Ni Ni, Daniel Dessau, *Coexistence of Tunable Weyl Points and Topological Nodal Lines in Ternary Transition-Metal Telluride TaIrTe4, Arxiv: 1709.10245 (2017), submit to PRL.*

Fundamentals of Spark-Plasma Sintering: Rapid and Ultra-Rapid Materials Consolidation and Joining

PI: Prof. E. Olevsky, San Diego State University

Program Scope

The main project idea is the analysis of the spark plasma sintering (SPS – Fig. 1) physical basis at multiple scales specifically exploring the role of electric current in the acceleration of mass transport and with an emphasis on ultra-rapid materials consolidation and joining. Thereby the project specifically addresses the following issues: (I) The development of a new constitutive model for spark-plasma sintering, taking into account the role of electric current in the acceleration of mass transport. (II) The development of a comprehensive multi-scale SPS modeling framework incorporating the elaborated SPS-specific constitutive model. (III) The development of a new Flash Hot Pressing (Flash SPS) processing technique. (IV) Exploring SPS capabilities for joining (including direct seamless bonding) of ceramic and metallic materials.

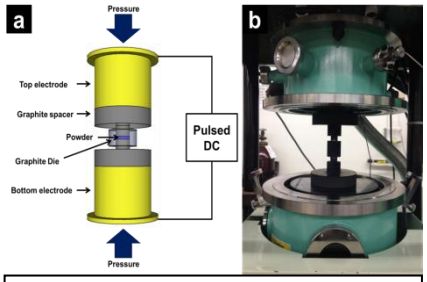

Fig. 1 (a) Schematic representation of SPS process, (b) SPS tooling before an experiment.

Recent Progress

A new flash (ultra-rapid) spark plasma sintering method applicable to various materials systems, regardless of their electrical resistivity, is developed (Fig. 2). A number of powders ranging from metals to electrically insulative ceramics have been successfully densified resulting in homogeneous microstructures within sintering times of 8-35 s [1]. A finite element simulation reveals that the developed method, providing an extraordinary fast and homogeneous heating concentrated in the sample's volume and punches, is applicable to all the different samples tested (Fig. 3). The utilized uniquely controllable flash phenomenon is enabled by the combination of the electric current concentration around the sample and the confinement of the heat generated in this area by the lateral thermal contact resistance. The presented new method allows: extending flash sintering to nearly all materials, controlling sample shape by an added graphite die, and an energy efficient mass production of

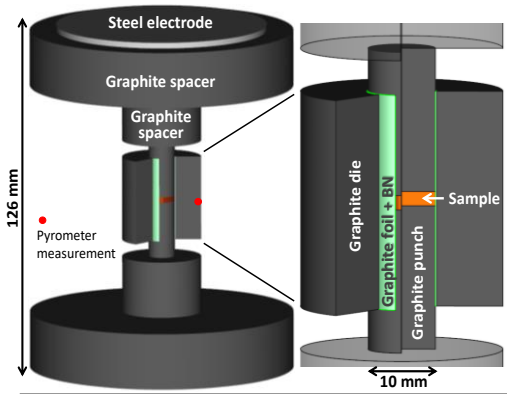

Fig. 2 The lateral graphite foil is coated with a boron nitride spray to electrically insulate the die and concentrate the electric current on the sample)

small and intermediate size objects. This approach represents also a potential venue for future investigations of flash sintering of complex shapes.

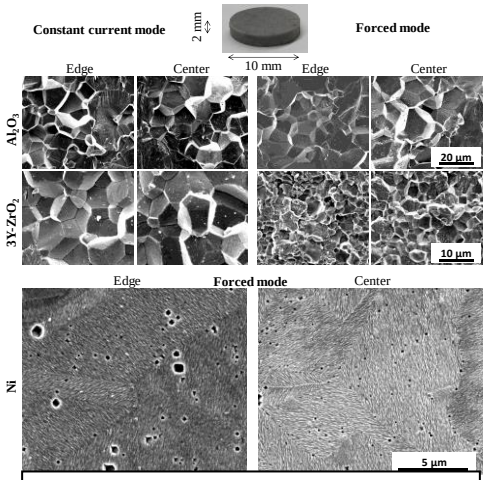

Fig. 3 SEM images in the centers and edges of nickel, zirconia and alumina samples for constant and forced current modes.

The densification mechanism of conductive powders is revealed by comparing the electric current-assisted spark plasma sintering (SPS) of ZrN powder with conventional hot pressing (HP) carried out with the same powder and under the same pressure and temperature [2]. For the first time, by taking into account the explicit influence of the electric current effect on the SPS densification mechanism, the constitutive equations describing the electric current-assisted hot pressing of powders are developed. The densification mechanism of ZrN is determined by the inverse regression of the new SPS constitutive equations and by utilizing the experimental results on ZrN powder consolidation with and without the participation of the electric current effect.

A new and straightforward method of the identification of porosity-dependent sintering constitutive parameters adaptable to a regular spark-plasma sintering device is proposed [3]. Compared to classical creep mechanism studies, this comprehensive experimental approach can reveal the in situ porous structure morphology influence on the sintering process.

Theoretical studies on the densification kinetics of the new spark plasma sinter-forging (SPS-forging) consolidation technique and of the regular SPS have been carried out based on the continuum theory of sintering [4]. Both modeling and verifying experimental results indicate that the loading modes play important roles in the densification efficiency of SPS of porous ZrC specimens. Compared to regular SPS, SPS-forging is shown to be able to enhance the densification more significantly during later sintering stages. The derived analytical constitutive equations are utilised to evaluate the high-temperature creep parameters of ZrC under SPS conditions. SPS-forging and regular SPS setups are combined to form a new SPS hybrid loading mode with the purpose of reducing shape irregularity in the SPS-forged specimens. Loading control is imposed to secure the geometry as well as the densification of ZrC specimens during hybrid SPS process.

The stability of the proportional–integral–derivative (PID) control of temperature in the spark plasma sintering (SPS) process was investigated [5]. The PID regulations of this process are tested for different SPS tooling dimensions, physical parameters conditions, and areas of temperature control. It is shown that the PID regulation quality strongly depends on the heating time lag between the area of heat generation and the area of the temperature control. Tooling temperature rate maps are studied to reveal potential areas for highly efficient PID control. The

convergence of the model and experiment indicates that even with non-optimal initial PID coefficients, it is possible to reduce the temperature regulation inaccuracy by positioning the temperature control location in highly responsive areas revealed by the finite-element calculations of the temperature spatial distribution.

Spark plasma sintering has been successfully used to produce all-solid-state lithium-ion batteries (ASSLibs). Both regular and functionally graded electrodes are implemented into novel three-layer and five-layer battery designs together with solid-state composite electrolyte. Scanning electron microscopy reveals that the functionally graded structure can eliminate the delamination effect at the electrode–electrolyte interface and, therefore, retains better performance [6].

Spark plasma sintering is adopted to fabricate transparent AlON ceramics, using a bimodal c-AlON powder synthesized by the carbothermal reduction and nitridation method [7].

Porous Ti5Al2.5Fe alloy was successfully fabricated using the spark plasma sintering technique. The compressive strength of the porous samples was found to be mainly dependent on sintering temperature, and the porous compacts exhibiting good biocompatibility properties [8].

Future Plans

In accord with the proposed plan, the following activities will be carried out:

1. The continuation of the development of new constitutive models of SPS taking into account nonthermal SPS specific factors.

2. The continuation of the development of the SPS multiscale modeling framework.

3. Modeling and experimentation on net-shape and energy efficient Flash SPS technique.

4. Continuation of modeling and experimentation on seamless SPS joining.

References

1. C. Manière, G. Lee, and E.A. Olevsky, All-materials-inclusive flash spark plasma sintering, Nature Sci. Rep. (2017) – under review.
2. G. Lee, E. A. Olevsky, C. Manière, A. Maximenko, O. Izhvanov, C. Back, J. McKittrick, Effect of electric current on the densification behavior of conductive powders consolidated by spark plasma sintering, Acta Mater. (2017) – under review.
3. C. Manière and E.A. Olevsky, Porosity dependence of powder compaction constitutive parameters: Determination based on spark plasma sintering tests, Scripta Mater., 141, 62-66 (2017).
4. X. Wei, A.L. Maximenko, C. Back, O. Izhvanov, and E.A. Olevsky, Effects of loading modes on densification efficiency of spark plasma sintering: sample study of zirconium carbide consolidation, Phil. Mag. Lett., 97, 265-272 (2017).

5. C. Manière, G. Lee, and E.A. Olevsky, Proportional integral derivative, modeling and ways of stabilization for the spark plasma sintering process, Results in Physics, 7, 1494-1497 (2017).
6. X. Wei, J. Rechtin, and E.A. Olevsky, The fabrication of all-solid-state lithium-ion batteries via spark plasma sintering, Metals, 7 (9), 372-381 (2017); [Feature Article].
7. Y. Shan, X. Wei, X. Sun, J. Xu, Q. Qin, and E.A. Olevsky, Highly infrared transparent spark plasma sintered AlON ceramics, J. Mater. Research, 32, 3279-3285 (2017).
8. R. Yamanoglu, N. Gulsoy, E.A. Olevsky, H.O. Gulsoy, Production of porous Ti5Al2.5Fe alloy via pressureless spark plasma sintering, J. Alloys Comp., 680, 654-658 (2016).

Publications

1. C. Manière, G. Lee, and E.A. Olevsky, All-materials-inclusive flash spark plasma sintering, Nature Sci. Rep. (2017) – under review.
2. G. Lee, E. A. Olevsky, C. Manière, A. Maximenko, O. Izhvanov, C. Back, J. McKittrick, Effect of electric current on the densification behavior of conductive powders consolidated by spark plasma sintering, Acta Mater. (2017) – under review.
3. C. Manière and E.A. Olevsky, Porosity dependence of powder compaction constitutive parameters: Determination based on spark plasma sintering tests, Scripta Mater., 141, 62-66 (2017).
4. X. Wei, J. Rechtin, and E.A. Olevsky, The fabrication of all-solid-state lithium-ion batteries via spark plasma sintering, Metals, 7 (9), 372-381 (2017); [Feature Article].
5. X. Wei, A.L. Maximenko, C. Back, O. Izhvanov, and E.A. Olevsky, Effects of loading modes on densification efficiency of spark plasma sintering: sample study of zirconium carbide consolidation, Phil. Mag. Lett., 97, 265-272 (2017).
6. Y. Shan, X. Wei, X. Sun, J. Xu, Q. Qin, and E.A. Olevsky, Highly infrared transparent spark plasma sintered AlON ceramics, J. Mater. Research, 32, 3279-3285 (2017).
7. C. Manière, G. Lee, and E.A. Olevsky, Proportional integral derivative, modeling and ways of stabilization for the spark plasma sintering process, Results in Physics, 7, 1494-1497 (2017).
8. D. Giuntini and E. A. Olevsky, Sintering stress of nonlinear viscous materials, J. Am. Ceram. Soc., 99, 3520–3524 (2016).
9. R. Yamanoglu, N. Gulsoy, E.A. Olevsky, H.O. Gulsoy, Production of porous Ti5Al2.5Fe alloy via pressureless spark plasma sintering, J. Alloys Comp., 680, 654-658 (2016).
10. E.A. Olevsky, S.M. Rolfing, A.L. Maximenko, Flash (ultra-rapid) spark-plasma sintering of silicon carbide, Nature Sci. Rep., 6, 33408 (2016).
11. G. Lee, J. McKittrick, E. Ivanov, E.A. Olevsky, Densification mechanism and mechanical properties of tungsten powder consolidated by spark plasma sintering, Int. J. Refr. Met. Hard Mater., 61, 22-29 (2016)

12. X Wei, C Back, O Izhvanov, CD Haines, EA Olevsky, Zirconium carbide produced by spark plasma sintering and hot pressing: densification kinetics, grain growth, and thermal properties, Materials, 9, 577 (2016)
13. D. Giuntini, J. Raethel, M. Herrmann, A. Michaelis, C.D. Haines, E.A. Olevsky, Spark plasma sintering novel tooling design: temperature uniformization during consolidation of silicon nitride powder, J. Ceram. Soc. Jap., 124, 403-414 (2016)
14. G. Cui, X. Wei, E.A. Olevsky, R.M. German, J. Chen, The manufacturing of high porosity iron with an ultra-fine microstructure via free pressureless spark plasma sintering, Materials, 9, 495 (2016)
15. E.S. Dvilis, O.L. Khasanov, V.N. Gulbin, M.S. Petyukevich, A.O. Khasanov, E.A. Olevsky, Spark plasma sintering of aluminum-magnesium-matrix composites with boron carbide and tungsten nano-powder inclusions: Modeling and experimentation, JOM, 68, 908-919 (2016)

Enhanced Thermoelectric Performance in Hierarchical Nanostructured Semiconductors

- **Dr. Pierre Ferdinand Poudeu; Materials Science and Engineering, University of Michigan**
- **Dr. Ctirad Uher; Department of Physics, University of Michigan**
- **Dr. Anton Van der Ven; Materials Department, University of California Santa-Barbara**

Program Scope

This project exploits (1) the facile co-crystallization of the half-Heusler (HH) and full-Heusler (FH) structures, (2) the high coherency and stability of the HH/FH interfaces, and (3) the solid-state inter-conversion between HH and FH structures through local atomic diffusion, to investigate, for selected compositions of the HH and FH phases, the effect of size, dimensionality, dispersion and volume fraction of FH nanostructures on the electronic, phonon and magnetic behavior of the resulting HH/FH nanocomposites. Our goal is to identify and control key material and growth parameters governing phase formation, microstructural evolution, and to understand the mechanism by which these changes of the internal structure modify the material's performance. To elucidate the mechanism by which the FH nanostructures regulate electronic charge transport and induce ferromagnetism within non-magnetic and magnetic semiconducting HH matrices, suitable series of HH/0D-FH and HH/2D-FH nanocomposites will be fabricated using synthesis conditions suggested by theoretical calculations of the formation energy and stability of various FH phases (varying M) in HH matrices with known chemical composition. The structure of the HH/FH interfaces (size, chemical composition, volume fraction and dispersion) will be investigated along with the evaluation of the electronic (carrier density, mobility, thermopower, electrical conductivity, effective mass), thermal and magnetic (susceptibility, magnetization etc.) properties of the resulting HH/FH nanocomposites.

Recent Progress

During the past two years of this research program, we elucidate the origin of phase separation in Half Heusler (HH) with composition TNi(Co)Sn(Sb) (T = Ti, Zr, Hf) matrix using first principles calculation of pseudo-binary and ternary phase diagram between various HH compositions. We found that all compositions within this systems form a uniform mixture at temperatures above 900 K but phase separate upon cooling below this temperature due to stress and strains arising from the large degree of variation in the size of transition metal atoms such as Ti, Zr and Hf.[1] The observed low critical temperature of 850 K challenges the prevailing interpretation that the microstructure in HH composites is created by an intrinsic phase separation mechanism, such as spinodal decomposition. Calculated migration barriers for Ti, Zr, and Hf atoms show that Ti-rich and Ti-poor grains may be nonequilibrium states that are kinetically trapped after solidification. In addition, we further elucidate the effect of full Heusler nanostructures on the carrier and thermal transports within HH matrix, highlighting the importance of the energy distribution of impurity states on the electronic transport of the overall composites. Using half-Heusler/full-Heusler (HH/FH) nanocomposites with general compositions $Zr_{0.25}Hf_{0.75}Ni_{1+x}Sn_{1-y}Sb_y$ as example, we found that the behavior of extrinsic carriers at the HH/FH interfaces strongly depends on the doping level (y value) as well as the energy levels occupied by impurity states in the samples. For example, it was found that carrier

filtering at HH/FH interfaces is negligible in composites with high doping level where donor states originating from Sb dopant dominate electronic conduction. However, we observed a drastic decrease in the effective carrier density upon introduction of HH/FH interfaces for the mechanically alloyed $Ti_{0.25}Zr_{0.25}Hf_{0.5}NiFe_xSn_{0.975}Sb_{0.025}$ samples where donor states from unintentional Fe impurities contribute the largest fraction of conduction electrons.[2] To further probe the effect of Fe incorporation on the structure and functional properties of HH/FH nanocomposites, we have synthesized several polycrystalline samples with compositions $Ti_{0.25}Zr_{0.25}Hf_{0.5}NiFe_xSn_{0.975}Sb_{0.025}$ by solid-state reaction of the elements followed by uniaxial hot pressing. We found that a greater solubility between Ti, Zr and Hf based half Heusler phases is promoted by the incorporation of 5 mol% Fe, whereas increasing the Fe content facilitates the phase separation. Scanning electron microscopy composition mapping indicate that the added excess elemental Fe (x) preferentially incorporates into the Ti-rich phase, whereas Ni, Sn and Sb are uniformly distributed in both Ti-rich and Ti-poor phases.[3]

In addition, we have also expanded our effort of carrier engineering through nanostructuring to Earth abundant material systems. First, we developed an energy efficient approach for the fabrication and characterization of a wide range of technologically important earth-abundant copper-metal-chalcogenide, $Cu(M^{n+})_{3/n}Q_2$ (Q = Se, Te) materials using a synergistic iterative combination of predictive theory and innovative synthesis strategies.[4,5] We apply this novel synthesis and materials design concept to the fabrication of Indium stabilized Cu_2Se nanocomposites with large figure of merit exceeding 2.6 at 800K. More importantly, we demonstrate that the incorporation of hierarchical $CuInSe_2$ nanostructures within the Cu_2Se matrix helps stabilize Cu diffusivity at high temperature and under large current density paving the way for large-scale deployment of Cu_2Se-based materials in commercial thermoelectric devices.[6]

1) Origins of phase separation in thermoelectric (Ti,Zr,Hf)NiSn half-Heusler alloys from first principles

A high thermoelectric performance has been achieved in half-Heusler alloys of composition *M*NiSn (*M* = Ti, Zr, Hf). The enhanced properties are attributed to the formation of microscale Ti-rich and Ti-poor grains. The mechanism of phase separation remains unclear, as the composition and microstructure of the grains are highly dependent upon synthesis conditions. In this work we use first principles density functional theory, combined with the cluster expansion method to calculate a thermodynamic phase diagram of the full pseudo-ternary $(Hf_{1-x-y}Zr_xTi_y)NiSn$ system. The results show that ZrNiSn and HfNiSn are fully miscible at all temperatures, and that a miscibility gap between (Zr,Hf)NiSn and TiNiSn exists at temperatures below 850 K (Figure 1).

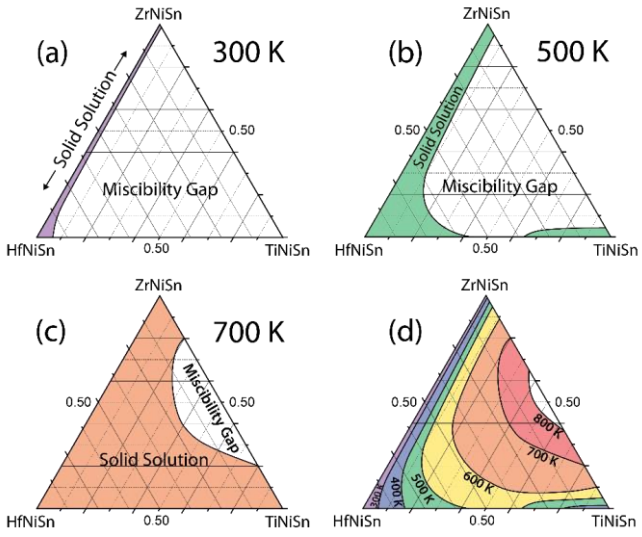

Figure 1. Pseudo-ternary $(Hf_{1-x-y}Zr_xTi_y)NiSn$ phase diagrams were calculated at 300 K **(a)**, 500 K **(b)**, 700 K **(c)**. The solid solution region is shown in color, and the miscibility gap region is shown in white. As the temperature increases, the miscibility gap shrinks, and completely disappears above 900 K. Part **(d)** shows a summary of phase boundaries calculated from 300 to 800 K.

For temperatures above 850 K, a solid solution is found to minimize the free energy. The low critical temperature of 850 K challenges the prevailing interpretation that the microstructure is created by an intrinsic phase separation mechanism, such as spinodal decomposition. Calculated migration barriers for Ti, Zr, and Hf atoms show that Ti-rich and Ti-poor grains may be non-equilibrium states that are kinetically trapped after solidification. The calculated phase diagram combined with low diffusion rates predict that Ti-rich and Ti-poor grains are created during solidification and are then kinetically trapped at lower temperatures. The low diffusion rates of *M* atoms provides new ways of controlling the phase separation via synthesis techniques and provides new routes to obtaining higher thermoelectric efficiency in HH alloys. Results of this work are reported in a manuscript published in *Journal of Materials Chemistry A*.[1]

2) Distribution of impurity states and charge transport in $Zr_{0.25}Hf_{0.75}Ni_{1+x}Sn_{1-y}Sb_y$ nanocomposites

Energy filtering of charge carriers in a semiconducting matrix using atomically coherent nanostructures can lead to a significant improvement of the thermoelectric figure of merit of the resulting composite. In this work, several half-Heusler/full-Heusler (HH/FH) nanocomposites with general compositions $Zr_{0.25}Hf_{0.75}Ni_{1+x}Sn_{1-y}Sb_y$ ($0 \leq x \leq 0.15$ and $y = 0.005$, 0.01 and 0.025) were synthesized in order to investigate the behavior of extrinsic carriers at the HH/FH interfaces. Electronic transport data showed that energy filtering of carriers at the HH/FH interfaces in $Zr_{0.25}Hf_{0.75}Ni_{1+x}Sn_{1-y}Sb_y$ samples strongly depends on the doping level (y value) as well as the energy levels occupied by impurity states in the samples (Figure 2). For example, it was found that carrier filtering at HH/FH interfaces is negligible in $Zr_{0.25}Hf_{0.75}Ni_{1+x}Sn_{1-y}Sb_y$ (y = 0.01 and 0.025) composites where donor states originating from Sb dopant dominate electronic conduction. However, we observed a drastic decrease in the effective carrier density upon introduction of HH/FH interfaces for the mechanically alloyed $Zr_{0.25}Hf_{0.75}Ni_{1+x}Sn_{0.995}Sb_{0.005}$ samples where donor states from unintentional Fe impurities contribute the largest fraction of conduction electrons. This work demonstrates the ability to synergistically integrate the concepts of doping and energy filtering through nanostructuring for the optimization of electronic transport in semiconductors. Results of this work are reported in a manuscript published in *Journal of Solid State Chemistry*. [2]

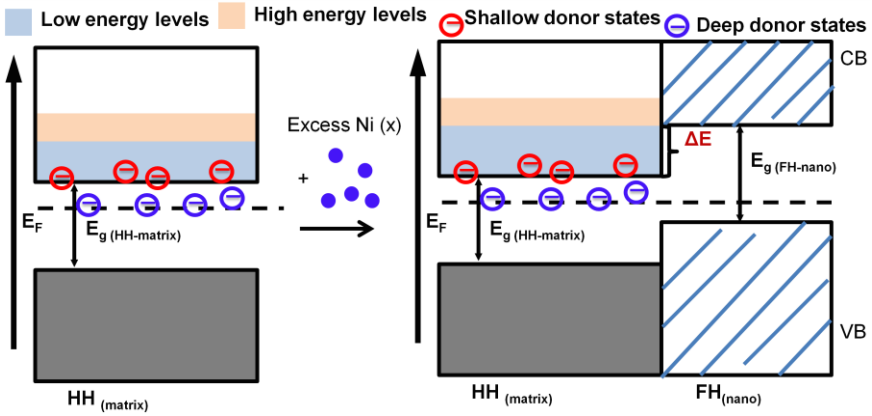

Figure 2: Formation of the potential energy (ΔE) at the interface between HH and FH phases and the distribution of donor states within the HH matrix upon addition of excess elemental Ni.

3) Iron-mediated phase segregation enables high Tc ferromagnetism and enhanced thermoelectric performance in $Ti_{0.25}Zr_{0.25}Hf_{0.5}(Ni,Fe_x)Sn_{0.975}Sb_{0.025}$ half-Heusler alloys

To investigate the effect of magnetic impurity on the thermoelectric properties of $Ti_{0.25}Zr_{0.25}Hf_{0.5}NiSn_{0.975}Sb_{0.025}$ half-Heusler alloys, several polycrystalline samples with compositions $Ti_{0.25}Zr_{0.25}Hf_{0.5}NiFe_xSn_{0.975}Sb_{0.025}$ were prepared by solid-state reaction of the elements followed by uniaxial hot pressing. X-ray powder diffraction of the synthesized materials suggests the formation of multiple phases with half-Heusler structure. Careful analysis using electron microscopy revealed the coexistence of Ti-rich and Ti-poor phases. Interestingly, the fraction as well as the average size of Ti-rich phase increase with increasing Fe content (x values) for sample with x >5 mole % Fe. The composition with x = 5 mole% Fe ($Ti_{0.25}Zr_{0.25}Hf_{0.5}(Ni,Fe_{0.05})Sn_{0.975}Sb_{0.025}$) exhibits smaller particle size as well as smaller population density of the Ti-rich phase compared to the Fe-free composition. This suggests a greater solubility between Ti, Zr and Hf based half Heusler phases upon incorporation of 5 mol% Fe, whereas increasing the Fe content facilitates the phase separation. Scanning electron microscopy composition mapping indicate that the added excess elemental Fe (x) preferentially incorporates into the Ti-rich phase (Figure 3), whereas Ni, Sn and Sb are uniformly distributed in both Ti-rich and Ti-poor phases. Magnetic susceptibility data revealed a ferromagnetic-like behavior for the sample containing 5% Fe with Curie transition temperature of 650 K, while paramagnetism was observed in samples with higher Fe content (Figure 4). Surprisingly, Hall effect measurement reveals a decrease in the carrier density of Fe-containing samples with the largest drop (over 60%) observed for the sample with 5% Fe (from 80 x 10^{19} cm^{-3} for x = 0 to 30 x 10^{19} cm^{-3} for x = 0.05). Careful analysis of the temperature dependence of carrier density and susceptibility curves indicate a sharp increase in carrier density at the temperature of magnetic transition from ferromagnetic to paramagnetic behavior suggesting that large decrease of carrier density is associated with the localization of free carrier by the

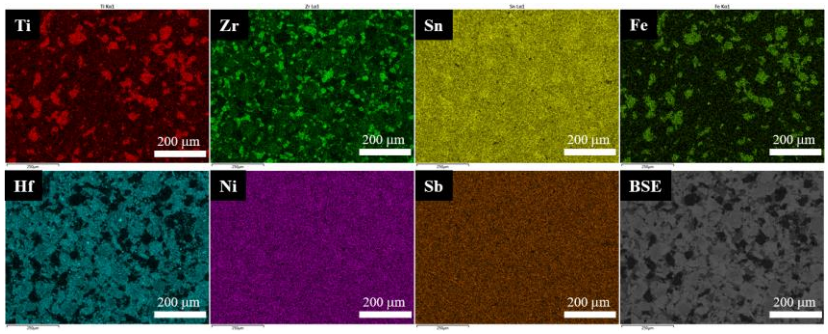

Figure 3: Elements mapping by energy dispersive spectrum (EDS) of $Ti_{0.25}Zr_{0.25}Hf_{0.5}(Ni,Fe_{0.1})Sn_{0.975}Sb_{0.025}$ sample demonstrating phase separation into Ti-rich and Ti-poor phases, and Fe preferential distribution in Ti-rich phases.

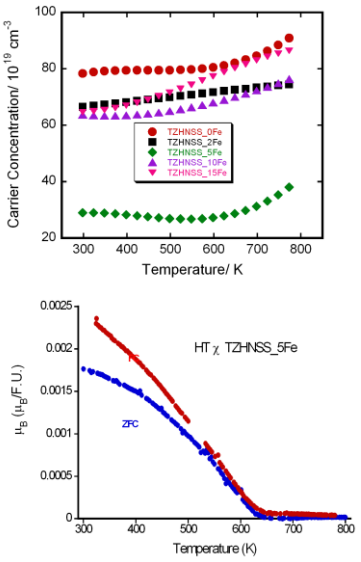

Figure 4: Temperature dependent carrier density of $Ti_{0.25}Zr_{0.25}Hf_{0.5}(Ni,Fe_x)Sn_{0.975}Sb_{0.025}$ sample demonstrating phase separation into (above) and magnetic susceptibility data for sample with x = 0.05 (below).

magnetic impurities in the sample. A manuscript reporting results of this work is in working progress.[3]

4) Partial indium solubility induces chemical stability and colossal thermoelectric figure of merit in Cu_2Se

High thermoelectric figure of merit, *ZT~2.1* at 1000 K, have been reported in $Cu_{2-x}Se$-based materials. However, their deployments in operational devices have been hampered by chemical instability and low average ZT (ZT_{ave}) values. In this work, we demonstrate improved chemical stability and a record high ZT_{ave} ~ 1.5 over a broad temperature range (T≤850 K) in $Cu_2Se/CuInSe_2$ nanocomposites, with ZT values ranging from 0.6 at 450 K to an unprecedentedly large value of 2.6 at 850 K for the sample with 1 mol% In. This remarkable performance is attributed to the localization of Cu^+ ions induced by the incorporation of In into the Cu_2Se lattice, which simultaneously boost the electrical conductivity and reduce the thermal conductivity of the nanocomposites. These findings pave the way for large-scale utilization of Cu_2Se-based materials in thermoelectric generators. Results of this work are reported in a manuscript published in Energy and Environmental Science. [6]

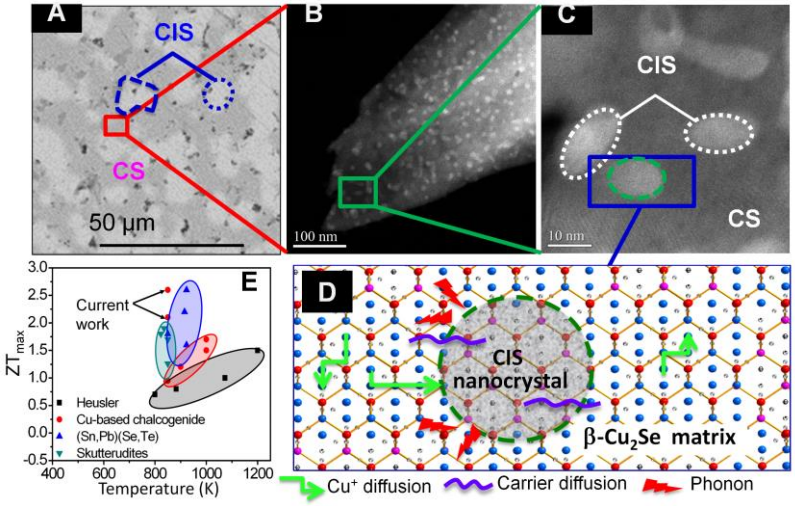

Figure 5: (A–C) Hierarchical microstructure of Cu_2Se(CS)/$CuInSe_2$(CIS) composites showing the size dispersion (atomic to micro scale) of CIS phase. Schematic D shows the interface interactions of phonons, carriers, and Cu^+ ions with a $CuInSe_2$ particle. (E) Comparison of ZT_{max} for state-of-the-art materials.

Future Plans

We will expand our efforts towards the development of high efficiency Earth abundant thermoelectric materials by exploiting the concepts of templating solid-state transformation initiated in the current program. We will focus our work on copper-metal-chalcogenides (CMCs). These materials have emerged as technologically significant device materials owing to their structural diversity and compositional flexibility, which enables the engineering of the functional properties (photovoltaic, thermoelectric, optoelectronic) through manipulations of the stoichiometry, chemical composition, and distribution of metal atoms in the chalcogenides crystal lattice. Unfortunately, research efforts until recently have largely focused on the optimization of single functionality of individual CMC for specific application. However, careful structural analysis of published CMCs compounds suggests that they are structurally related by the face centered cubic (fcc) packing of the chalcogenides (Q) sublattice. The difference in

atomic ordering of metal atoms within various CMCs ensures phase separation instead of solid solution between various CMCs while the similarity in the packing of Q^{2-} ions promotes coherency or semicoherency at their interfaces. Building on these structural and chemical principles, the future plan will focus on exploiting the structural relationship between known copper-metal-chalcogenides (CMCs) with dissimilar properties, such as Cu_2Se; CuAgSe; Cu_4TiSe_4; $CuInSe_2$; $Cu_2ZnSnSe_4$, etc. in order to create "Hierarchical hybrid multifunctional materials". This will enable exploration of exciting new physical phenomena that may result from the non-equilibrium matrix/inclusion interfaces arising from the close proximity of very different chemistries in both (a) bulk composites (0D) and (b) thin-film superstructure (2D) architectures.

References

1 Page, A., Van der Ven, A., Poudeu, P. F. P. & Uher, C. Origins of phase separation in thermoelectric (Ti, Zr, Hf) NiSn half-Heusler alloys from first principles. *J Mater Chem A* **4**, 13949-13956 (2016).

2 Liu, Y. F. *et al.* Distribution of impurity states and charge transport in $Zr_{0.25}Hf_{0.75}Ni_{1+x}Sn_{1-y}Sb_y$ nanocomposites. *J Solid State Chem* **234**, 72-86 (2016).

3 Lu, R., Lopez, J., Uher, C. & Poudeu, P. F. P. Iron-mediated phase segregation enables high Tc ferromagnetism and enhanced thermoelectric performance in $Ti_{0.25}Zr_{0.25}Hf_{0.5}(Ni,Fe_x)Sn_{0.975}Sb_{0.025}$ half-Heusler alloys *in preparation* (2017).

4 Olvera, A., Sahoo, P., Tarczynski, S. & Poudeu, P. F. P. Topochemical Solid-State Reactivity: Redox-Induced Direct Structural Transformation from $CuSe_2$ to $CuInSe_2$. *Chem Mater* **27**, 7179-7186 (2015).

5 Moroz, N. A., Olvera, A., Willis, G. M. & Poudeu, P. F. P. Rapid direct conversion of $Cu_{2-x}Se$ to CuAgSe nanoplatelets via ion exchange reactions at room temperature. *Nanoscale* **7**, 9452-9456 (2015).

6 Olvera, A. A. *et al.* Partial indium solubility induces chemical stability and colossal thermoelectric figure of merit in Cu_2Se. *Energ Environ Sci* **10**, 1668-1676 (2017).

Publications (2015-2017)

A) Journal articles

1) Alan Olvera, Nicholas A. Moroz, Pranati Sahoo, Pan Ren, Trevor P. Bailey, Alexander A. Page, Ctirad Uher and Pierre F.P. Poudeu, Partial indium solubility induces chemical stability and colossal thermoelectric figure of merit in Cu_2Se"
Energy & Environmental Science, **2017**, 10, 1668 – 1676.

2) Erica M. Chen, Stanislav S. Stoyko, Jennifer A. Aitken and Pierre F. P. Poudeu, Tuning the optical, electronic and thermal properties of $Cu_3NbS_{4-x}Se_x$ through chemical substitution, *Inorg. Chem. Front*., **2017**, 4, 1493-1500.

3) Joseph Casamento, Juan Lopez, Nicholas Moroz, Alan Olvera, Honore Djieutedjeu, and Pierre F. P Poudeu, Crystal structure and thermoelectric properties of the ^{7,7}L lillianite homologue, $Pb_6Bi_2Se_9$**,** *Inorg. Chem.* **2017**, 56, 261–268.

4) Erica M. Chen, Logan Williams, Alan Olvera, Cheng Zhang, Mingfei Zhang, Guangsha Shi, John T. Heron, Liang Qi, L. Jay Guo, Emmanouil Kioupakis, and Pierre F. P. Poudeu,

Sustainable p-type copper selenide solar material with ultra-large absorption coefficient, **2017**, submitted.

5) N A Moroz, J S Lopez, H Djieutedjeu, K G S Ranmohotti, N J Takas, P F P Poudeu, Indium preferential distribution enables electronic engineering of magnetism in $FeSb_{2-x}In_xSe_4$ p-type high-Tc ferromagnetic semiconductors, *Chem. Mater*. **2016**, 28, 8570–8579.

6) Trevor P. Bailey, Si Hui, Hongyao Xie, Alan Olvera, Pierre F. P. Poudeu, Xinfeng Tang and Ctirad Uher*, Enhanced ZT and attempts to chemically stabilize Cu_2Se via Sn doping, J. *Mater. Chem. A* **2016**, 4, 17225.

7) Yuanfeng Liu, Julien P.A. Makongo, Alexander Page, Pranati Sahoo, Ctirad Uher, Kevin Stokes, Pierre F.P. Poudeu*, Distribution of impurity states and charge transport in $Zr_{0.25}Hf_{0.75}Ni_{1+x}Sn_{1-y}Sb_y$ nanocomposites, *Journal of Solid State Chemistry*, **2016**, 234, 72 – 86.

8) Alexander Page, Anton Van der Ven, P.F.P. Poudeu, Ctirad Uher, Origins of phase separation in thermoelectric (Ti, Zr, Hf)NiSn half-Heusler alloys from first principles, J. *Mater. Chem. A* **2016**, 4, 13949.

9) Alexander Page, P.F.P. Poudeu, Ctirad Uher, A first-principles approach to half-Heusler thermoelectrics: Accelerated prediction and understanding of material properties, J Materiomics **2016**, 2, 104-113.

10) Alan Olvera, Pranati Sahoo, Stephanie Tarczynski, and Pierre F.P. Poudeu*, Topochemical Solid-State Reactivity: Redox-Induced Direct Structural Transformation from $CuSe_2$ to $CuInSe_2$, *Chem. Mater*. **2015**, 27, 7179 − 7186.

B) Book Chapter

1) Pierre F.P. Poudeu*, Ruiming Lu, Yuanfeng Liu, Pranati Sahoo, Alexander Page and Ctirad Uher, *Advances in nanostructured half-Heusler alloys for thermoelectric applications, in* Materials Aspect of Thermoelectricity, Ed. Ctirad uher, Taylor and Francis, 2016, 237 – 288.

C) PhD thesis

1) Dr. Yuanfeng Liu: "*Synthesis, Characterization and Thermoelectric Properties of Nanostructured Half-Heusler Alloys" PhD Materials Science and Engineering*, UM, April 2015

2) Dr. Nicholas Moroz: "*Engineered Transition Metal Chalcogenides for Photovoltaic, Thermoelectric, and Magnetic Applications*" PhD Materials Science and Engineering, UM, December 2016

3) Dr. Erica Chen: "*Synthesis and Characterization of Novel Transition Metal Chalcogenide Phases for Energy Storage, Energy Conversion and Optoelectronics*" PhD Materials Science and Engineering, UM, April 2017

4) Dr. Alexander Page: "*Half-Heusler Alloys as Promising Thermoelectric Materials*"; PhD Physics, UM, May 2017

5) Dr. Alan Olvera; "*Thermoelectric behavior of low thermal conductivity Cu-based and IV-V chalcogenide materials"* PhD Materials Science and Engineering, UM, September 2017

Using Crystallization to Control Filler Dispersion and Vice Versa in Polymer Nanocomposites

Linda S. Schadler, Materials Science and Engineering Department, Rensselaer Polytechnic Institute, Troy, NY

Sanat Kumar, Chemical Engineering Department, Columbia University, New York, NY

Brian C. Benicewicz, Chemistry and Biochemistry Department, University of South Carolina, Columbia, SC

Program Scope

The goals of this proposal are to: 1) hierarchically organize spherical nanoparticles (NPs) into unique morphologies by controlling the ratio of filler diffusivity / matrix crystallization rate, and 2) organize NPs in the matrix melt as a mechanism to control the crystalline morphology of the semicrystalline matrix. We will tailor the filler / matrix compatibility using surface ligands with carefully controlled graft density and molecular weight. This will allow us to answer key fundamental questions about crystallization and filler organization in nanocomposites, and to optimize the mechanical and dielectric properties of these engineering polymers.

Recent Progress

Building on our work in silica / polyethylene oxide in which we were able to organize the nanoparticles by controlling the crystallization rate, we have been turning our focus to polyethylene. Using a short chain modifier (C18) on both 15nm and 50nm nanoparticles, we have preliminarily demonstrated similar structures to that observed in the PEO under slow cooling rates (Figure 1). In addition, we have created dye doped silica nanoparticles (60nm) that we can use to get an initial indication of ordering (or not) as a function of cooling rate (Figure 2).

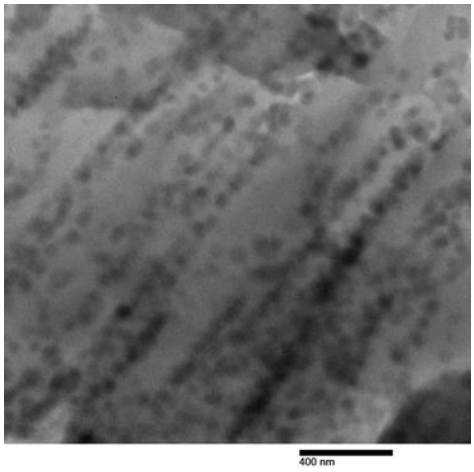

Figure 1. Preliminary result for 50nm / polyethylene composite, isothermal crystallization

Critical to the project is the development of chemistries to graft olefin chains onto the nanoparticles to both compatibilize the particles and control their diffusion rate compared to the rate of crystallization (goal 1), and to organize them in the melt state to control the resulting crystalline morphology (goal 2). We have recently demonstrated that we create well-defined PE chains on nanoparticles using a controlled polymerization technique, and form high mw polymers using this process.

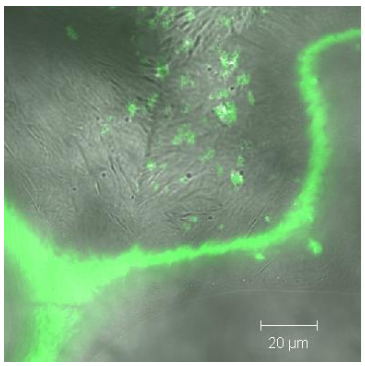

Isothermal Crystallized at 55°C

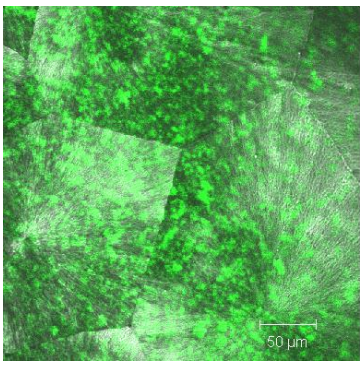

Quenched to RT

Figure 2. A slow cooled composite and quenched composite with dye doped nanoparticles showing the role of crystallization in either trapping the particles the spherulite or pushing them to the boundaries

Future Plans

Going forward we will continue to use two new handles: the isothermal crystallization rate of a polymer host, G, and NP diffusivity, to dramatically vary nanoparticle spatial organization. In the case where the NPs are miscible with the polymer above its melting point, they remain spatially well-dispersed when the polymer is crystallized at a rate that is fast relative to NP diffusion. In contrast, monolayer-thick NP sheets with intersheet spacing of (10-100nm) form in slowly crystallized samples. There is also ordering of the NPs at the larger interfibrillar scale. Importantly, the relative fraction of engulfed, interlamellar and interfibrillar NPs is determined by G. Further, the modulus of these materials increases by a factor of 2-3 due to the organization state of the NPs, while leaving fracture toughness unaffected. We propose to take these ideas, which were developed for the case of polyethyleneoxide, and critically study their applicability to commercially important polymers, i.e., polyethylene and isotactic-polypropylene, through an integrated suite of experimental and theoretical tools.

We will also exploit our ability to tailor the NP / matrix compatibility to organize fillers in the melt (e.g., the formation of string, sheets), which can be used to manipulate the matrix nucleation and crystal growth phenomena. We expect an interesting interplay between these two assembly processes, i.e., polymer crystallization driven NP organization vs. NP self-assembly driven by surfactancy. We propose to combine experiments and theory to study these hypotheses, and divide our proposed work into a series of tasks. Specifically, we shall: (i) synthesize surface functionalized NPs to control their self-assembly in the melt, (ii) study their assembly into nanostructures in the melt (primarily using electron microscopy and small and ultrasmall angle neutron and x-ray scattering), (iii) focus on how these assemblies can be manipulated under the action of polymer crystallization to achieve our overarching goal of creating semicrystalline polymer nanocomposites with optimized thermomechanical and electrical properties, (iv) model the development of both the NP organization and the crystalline morphology using coarse-grained computer simulations to understand the fundamental physical phenomena controlling this behavior.

Publications: Funding Started September, 2017

USING INTERFACES TO CREATE STRONGLY-COUPLED MAGNETIC-FERROELECTRICS

Darrell G. Schlom[1], Craig J. Fennie[2], David A. Muller[2]

[1]Department of Material Science and Engineering, Cornell University, Ithaca, New York 14853

[2]School of Applied and Engineering Physics, Cornell University, Ithaca, New York 14853

Program Scope

This project has two research objectives, both of which relate to the better understanding of a new class of $A_{n+1}B_nO_{3n+1}$ Ruddlesden-Popper phases possessing a ferroic instability. Our first-principles calculations indicate that the ferroelectric vs. antiferroelectric alignment of neighboring polar slabs in $Sr_{n+1}Ti_nO_{3n+1}$ is nearly energetically degenerate.[1] The first research objective of our project is to **manipulate control parameters to create novel functionalities in a new family of ferroics**. The near degeneracy between ferroelectric vs. antiferroelectric alignment of neighboring polar slabs in $Sr_{n+1}Ti_nO_{3n+1}$[1] begs the question of whether relaxor ferroelectricity can be created and systematically studied in this system without the chemical disorder[2,3] or free surfaces[4] that are present in all known relaxor ferroelectrics. Our studies will go beyond strained $Sr_{n+1}Ti_nO_{3n+1}$ by considering the site-specific incorporation of species that lead to ferroelectric instabilities without strain, e.g., the introduction of calcium, barium, and lead into this general family to form ordered $(Ca,Sr,Ba,Pb)_{n+1}Ti_nO_{3n+1}$ phases. These hypothetical phases containing calcium, barium, and lead are metastable. Nonetheless, we have already demonstrated that one such phase, $BaSr_2Ti_2O_7$, can be grown by MBE,[5] making it likely that we will be able to synthesize these novel phases. Intriguingly, our first-principles calculations reveal a nearly isotropic in-plane polarization of Pb_2TiO_4 under appropriate biaxial strain (about 0.7%).[6] This unusual energetic landscape is tantalizing in that it might give rise to an electrical analog of ferromagnetic resonance. Guided by theory, we will explore this and other unusual physical properties of these ordered $(Ca,Sr,Ba,Pb)_{n+1}Ti_nO_{3n+1}$ phases. Our second research objective is to **better understand the role of defects in these structures**. The extremely low dielectric losses exhibited by the strained $Sr_{n+1}Ti_nO_{3n+1}$ phases that we have studied to date lead us to *hypothesize* that these Ruddlesden-Popper structures contain fewer point defects than their perovskite analogs.[7] But is this true? We will assess this through experiments on ordered $(Ca,Sr,Ba,Pb)_{n+1}Ti_nO_{3n+1}$ films vs. their perovskite analogs, $SrTiO_3$, $BaTiO_3$, and $PbTiO_3$ analyzed by scanning transmission electron microscopy (STEM) utilizing a new mixed-mode pixel array detector capable of imaging polarity, strain fields, and contrast and dechanneling from vacancies and interstitials. We will also study the defects by positron annihilation spectroscopy, phonon spectroscopy, and the frequency dependence of dielectric loss (especially in the GHz frequency regime). Theory is an integral part of interpreting these experiments.

Recent Progress

The Ruddlesden-Popper superlattice series, $A_{n+1}B_nO_{3n+1}$ or equivalently $(ABO_3)_nAO$, has been identified as a defect mitigating structure via a proposed mechanism in which the $(AO)_2$ layer accommodates the local non-stoichiometry of the crystal by changing its extent (growing or shrinking of the $(AO)_2$ layer) in the structure. The accommodation of the $(AO)_2$ layers allows the perovskite $(ABO_3)_n$ sections of the material to remain stoichiometric. In the strained $(SrTiO_3)_nSrO$ thin film phase we recently demonstrated record tunable dielectric performance at gigahertz (mmWave) frequencies,[7] a region where point defects significantly contribute to dielectric loss. In contrast, the parent phase commonly used for frequency tunable microwave circuit elements, $Ba_xSr_{1-x}TiO_3$, experiences large attenuation at gigahertz frequencies arising from dielectric loss related to point defects. We use oxide molecular-beam epitaxy as a controlled way to fabricate materials relevant to the next generation of thin-film, mmWave tunable dielectrics via precise atomic layering and epitaxial strain. In this work we use molecular-beam epitaxy to grow related Ruddlesden-Popper phases containing $Ba_xSr_{1-x}TiO_3$, specifically $(SrTiO_3)_n(BaTiO_3)_mSrO$ shown in Figure 1, in hopes of accommodating point defects by the $(SrO)_2$ faults, allowing the rest of the dielectric material to remain stoichiometric.

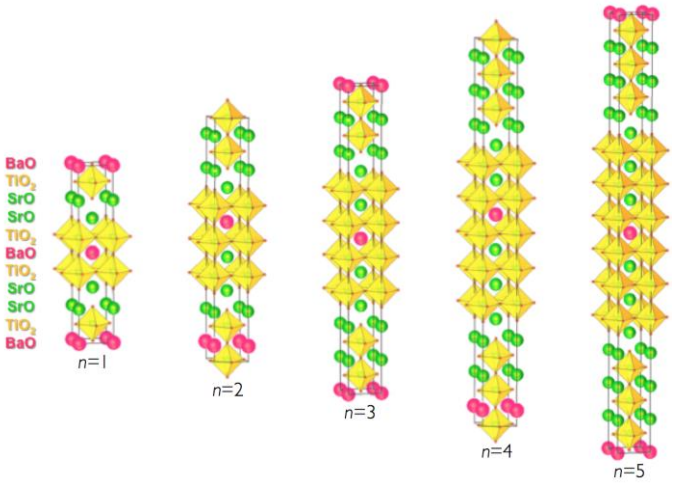

Figure 1. Schematic of the unit cell crystal structure of $(SrTiO_3)_n(BaTiO_3)_mSrO$ Ruddlesden-Popper phases for m=1, n=1-5.

An advantage of these Ba-containing Ruddlesden-Popper phases is lower epitaxial strain due to $BaTiO_3$'s smaller lattice mismatch with the (110) $DyScO_3$ substrate, which allows for thicker films without the loss of the desired low-temperature ferroelectric instability. The first five members of this Ruddlesden-Popper homologous series (n = 1- 5) have been grown on (110) $DyScO_3$ using molecular-beam epitaxy and characterized by x-ray diffraction. We use density functional theory to predict and understand the ferroelectric properties of these films. In-plane measurements of the dielectric constant have been made as a function of temperature and frequency in the gigahertz frequency regime. We use scanning transmission electron microscopy (STEM) and electron energy loss spectroscopy (EELS) to identify barium and $(SrO)_2$ fault placement, and find high quality films with 1-3 atomic layers of barium interdiffusion, despite the metastability of these atomically engineered structures.

Future Plans

As a follow-up to our $(LuFeO_3)_m$ / $(LuFe_2O_4)_1$ multiferroic work, we will investigate alternate formulations following this general design methodology. Follow-on structures to $(LuFeO_3)_m$ / $(LuFe_2O_4)_1$ were not part of our renewal proposal, however, our recent success has generated many follow-up questions about the inner workings of this new interface material. For example, what is the switching mechanism that enables deterministic switching of magnetization using an electric field[8] in $(LuFeO_3)_9$ / $(LuFe_2O_4)_1$ superlattices? Do superior manifestations of this design methodology remain to be discovered? Our goal is to better understand the fundamentals of this phenomena and the synthesis science involved in identifying and making higher temperature manifestations of this new kind of magnetoelectric multiferroic. Although not part of the scope of our renewal proposal, we now consider this area to be very exciting. We therefore plan to work on structures beyond $(LuFeO_3)_m$ / $(LuFe_2O_4)_1$ in the coming year and will reduce our effort on some of the systems described in our proposal. Intel Corporation has also expressed interest in device applications that build on this new family of magnetoelectric multiferroics, provided its Curie temperature T_C can be raised. As described in the next paragraph, we have some ideas on how to raise T_C.

$(LuFeO_3)_m$ / $(LuFe_2O_4)_1$ superlattices consist of a ferrimagnetic layer ($LuFe_2O_4$) in intimate atomic contact with a geometric ferroelectric layer ($LuFeO_3$). From theory we have established that T_C is enhanced by increasing the puckering of the geometric ferroelectric layer.[8] $LuFeO_3$ has the greatest puckering of all *RE*FeO_3 materials, so we shall attempt to make $ScFeO_3$ films that are isostructural with the $LuFeO_3$ films we have been growing. $ScFeO_3$ is a metastable polymorph (with the $YMnO_3$ structure) and we will use epitaxial stabilization in our attempts to create it. We will also investigate alternatives to the $LuFe_2O_4$ ferrimagnetic layer including *RE*Fe_2O_4 with other rare-earth atoms, $ScFe_2O_4$, and higher temperature ferrimagnets like $BaFe_{12}O_{19}$, Fe_3O_4, and $NiFe_2O_4$. Our goal is to start with a higher-temperature ferrimagnet, impose a structural distortion by placing it in atomic proximity with a highly puckered geometric ferroelectric, and exploit the decrease in the frustration of the rumpled system to increase its magnetic transition temperature. As in all of our work, theory is an integral part of guiding and interpreting our experiments.

References

1 T. Birol, N.A. Benedek, and C.J. Fennie, "Interface Control of Emergent Ferroic Order in Ruddlesden-Popper $Sr_{n+1}Ti_nO_{3n+1}$," *Phys. Rev. Lett.* **107** (2011) 257602.

2 L.E. Cross, "Relaxor Ferroelectrics," *Ferroelectrics* **76** (1987) 241–267.

3 A.A. Bokov and Z.G. Ye, "Recent Progress in Relaxor Ferroelectrics with Perovskite Structure," *J. Mater. Sci.* **41** (2006) 31–52.

4 B. Meyer and D. Vanderbilt, "*Ab Initio* Study of $BaTiO_3$ and $PbTiO_3$ Surfaces in External Electric Fields," *Phys. Rev. B* **63** (2001) 205426.

5 D.G. Schlom, J.H. Haeni, C.D. Theis, W. Tian, X.Q. Pan, G.W. Brown, and M.E. Hawley, "The Importance of *in situ* Monitors in the Preparation of Layered Oxide Heterostructures by

Reactive MBE," *Recent Developments in Oxide and Metal Epitaxy—Theory and Experiment* edited by M. Yeadon, S. Chiang, R.F.C. Farrow, J.W. Evans, and O. Auciello, Vol. 619 (Materials Research Society, Warrendale, 2000), pp. 105–114.

[6] C. Fennie and K. Rabe, "First-Principles Investigation of Ferroelectricity in Epitaxially Strained Pb_2TiO_4," *Phys. Rev. B* **71** (2005) 100102.

[7] C.H. Lee, N.D. Orloff, T. Birol, Y. Zhu, V. Goian, E. Rocas, R. Haislmaier, E. Vlahos, J.A. Mundy, L.F. Kourkoutis, Y. Nie, M.D. Biegalski, J. Zhang, M. Bernhagen, N.A. Benedek, Y. Kim, J.D. Brock, R. Uecker, X.X. Xi, V. Gopalan, D. Nuzhnyy, S. Kamba, D.A. Muller, I. Takeuchi, J.C. Booth, C.J. Fennie, and D.G. Schlom, "Exploiting Dimensionality and Defect Mitigation to Create Tunable Microwave Dielectrics," *Nature* **502** (2013) 532–536.

[8] J.A. Mundy, C.M. Brooks, M.E. Holtz, J.A. Moyer, H. Das, A.F. Rébola, J.T. Heron, J.D. Clarkson, S.M. Disseler, Z. Liu, A. Farhan, R. Held, R. Hovden, E. Padgett, Q. Mao, H. Paik, R. Misra, L.F. Kourkoutis, E. Arenholz, A. Scholl, J.A. Borchers, W.D. Ratcliff, R. Ramesh, C.J. Fennie, P. Schiffer, D.A. Muller, and D.G. Schlom, "Atomically Engineered Ferroic Layers Yield a Room-Temperature Magnetoelectric Multiferroic," *Nature* **537** (2016) 523–527.

Publications

1. N.F. Quackenbush, H. Paik, M.J. Wahila, S. Sallis, M.E. Holtz, X. Huang, A. Ganose, B.J. Morgan, D.O. Scanlon, Y. Gu, F. Xue, L.Q. Chen, G.E. Sterbinsky, C. Schlueter, T.-L. Lee, J.C. Woicik, J.-H. Guo, J.D. Brock, **D.A. Muller**, D.A. Arena, **D.G. Schlom**, and L.F.J. Piper, "Stability of the M2 Phase of Vanadium Dioxide Induced by Coherent Epitaxial Strain," *Physical Review B* **94** (2016) 085105.
2. L. Li, J. Britson, J.R. Jokisaari, Y. Zhang, C. Adamo, A. Melville, **D.G. Schlom**, L.Q. Chen, and X.Q. Pan, "Giant Resistive Switching via Control of Ferroelectric Charged Domain Walls," *Advanced Materials* **28** (2016) 6574–6580.
3. J.A. Mundy, C.M. Brooks, M.E. Holtz, J.A. Moyer, H. Das, A.F. Rébola, J.T. Heron, J.D. Clarkson, S.M. Disseler, Z. Liu, A. Farhan, R. Held, R. Hovden, E. Padgett, Q. Mao, H. Paik, R. Misra, L.F. Kourkoutis, E. Arenholz, A. Scholl, J.A. Borchers, W.D. Ratcliff, R. Ramesh, **C.J. Fennie**, P. Schiffer, **D.A. Muller**, and **D.G. Schlom**, "Atomically Engineered Ferroic Layers Yield a Room-Temperature Magnetoelectric Multiferroic," *Nature* **537** (2016) 523–527.
4. M.E. Holtz, J.A. Mundy, C.S. Chang, J.A. Moyer, C.M. Brooks, H. Das, A.F. Rebola, R. Hovden, E. Padgett, C.J. Fennie, P. Schiffer, D. Meier, **D.G. Schlom**, and **D.A. Muller**, "Imaging Local Polarization and Domain Boundaries with Picometer-Precision Scanning Transmission Electron Microscopy," *Microscopy and Microanalysis* **22** (2016) 898–899.
5. W. Wang, J.A. Mundy, C.M. Brooks, J.A. Moyer, M.E. Holtz, **D.A. Muller**, **D.G. Schlom**, and W. Wu, "Visualizing Weak Ferromagnetic Domains in Multiferroic Hexagonal Ferrite Thin Film," *Physical Review B* **95** (2017) 134443.

6. J.A. Mundy, J. Schaab, Y. Kumagai, A. Cano, M. Stengel, I.P. Krug, D.M. Gottlob, H. Doğanay, M.E. Holtz, R. Held, Z. Yan, E. Bourret, C.M. Schneider, **D.G. Schlom**, **D.A. Muller**, R. Ramesh, N.A. Spaldin, and D. Meier, "Functional Electronic Inversion Layers at Ferroelectric Domain Walls," *Nature Materials* **16** (2017) 622–627.
7. N.F. Quackenbush, H. Paik, M.E. Holtz, M.J. Wahila, J.A. Moyer, S. Barthel, T.O. Wehling, D.A. Arena, J.C. Woicik, **D.A. Muller**, **D.G. Schlom**, and L.F.J. Piper, "Reducing Orbital Occupancy in VO_2 Suppresses Mott Physics while Peierls Distortions Persist," *Physical Review B* **96** (2017) 081103.
8. L. Xie, L.Z. Li, C.A. Heikes, Y. Zhang, Z.J. Hong, P. Gao, C.T. Nelson, F. Xue, E. Kioupakis, L.Q. Chen, **D.G. Schlom**, P. Wang, and X.Q. Pan, "Giant Ferroelectric Polarization in Ultrathin Ferroelectrics via Boundary-Condition Engineering," *Advanced Materials* **29** (2017) 1701475.

In Situ Thermodynamics and Kinetics of Mixed-Valence Inorganic Crystal Formation

Daniel P. Shoemaker, Materials Science and Engineering Department and Materials Research Laboratory, University of Illinois at Urbana-Champaign

Program Scope

The major goals of this project are to investigate rapid in situ materials discovery and kinetics, and understand how to interface the process with combinatorial computational methods. Our project is demonstrating that the paths we take to make new materials can be made many times faster, and more hypothetical materials can be experimentally screened when we can watch reactions in real-time.

At the heart of our project is the ability to conduct materials synthesis with in-situ diffraction in-house, as a method of screening for new materials and understanding the kinetic barriers to compound formation. We began with trial systems in the Fe—Si—S and Fe—S systems to uncover routes to octahedral iron semiconductors. Metathesis and redox behaviors of these compounds are the next target, along with a focus on new phases and mechanisms that appeared in initial systems. Throughout the project, opportunities to interface enthalpy calculations and known kinetic data are crucial to leveraging our data for more efficient synthesis.

Recent Progress

Our first model system to examine the mechanisms of chalcogenide formation and kinetics was the olivine semiconductor Fe_2SiS_4. We commissioned an in-situ oven-type capillary furnace on our Mo-tube X-ray diffractometer and optimized its performance to collect refinable patterns within 20 minutes. Rietveld-built reaction maps of the chemical synthesis process (Figure 1) revealed key events controlling solid-state crystal formation: metal sulfidation kinetics, transition through an FeS_2 invariant point, and accompanying onset

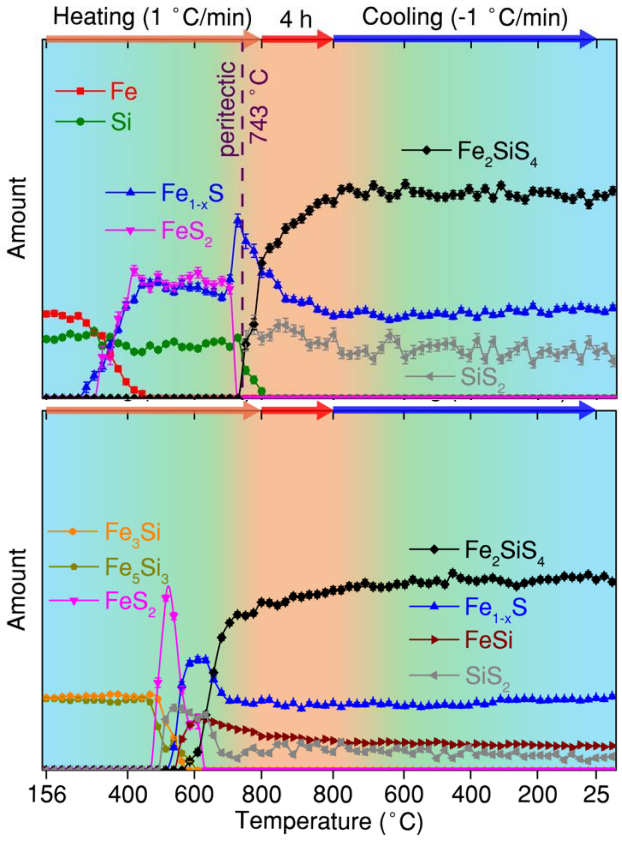

Figure 1. In-situ XRD reaction maps of Fe_2SiS_4 synthesis from elements (top) and sulfidation of intermetallics (bottom). These data reveal that Si sulfidation is the primary kinetic barrier, and peritectic decomposition of FeS_2 incites the elemental reaction. Both processes are avoided when an intermetallic precursor is used.

of ternary formation.

From the Fe—Si—S reaction map it was clear that Si sulfidation kinetics controlled the fate of the product. The formation of the target ternary from elements occurred at the spontaneous decomposition of FeS_2 at 743°C, which released superheated S liquid. [1] In this case, the kinetic barrier to Fe_2SiS_4 crystal formation (persistence of elemental Si) was overcome by the high chemical potential of superheated S.

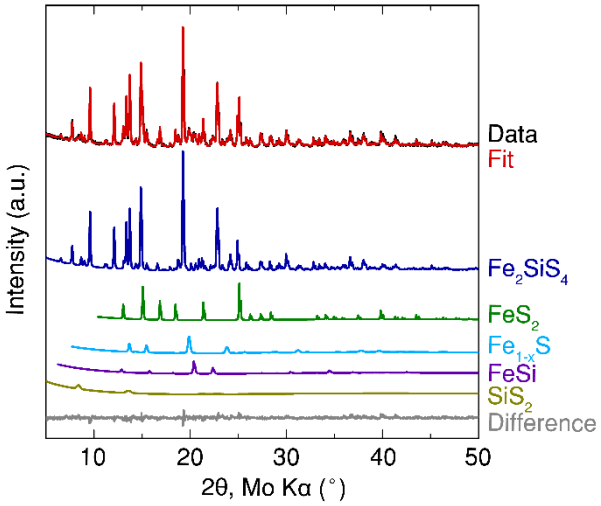

Figure 2. Rietveld refinement of the reaction product resulting from intermetallic sulfidation (Fe_3Si + Fe_5Si_3 + S) at low temperature (550°C). Iron silicide intermetallics sulfidation can easily form Fe_2SiS_4 crystals at temperatures where Fe and Si elemental sulfidation is kinetically prohibited.

With knowledge of this model reaction in hand, two new goals arose: (1) identify mechanisms to synthesize Fe—Si—S at lower temperature, and (2) use related kinetic information to aid the discovery of new materials. To address topic (1), we identified that the best approach in forming Fe_2SiS_4 crystals at low temperatures is the sulfidation of iron silicide intermetallics, with a product shown in Figure 2. This is despite the reaction being less thermodynamically downhill than the reaction of the elements.

To address point (2), a wealth of published corrosion literature confirms that the enhanced sulfidation rate of iron silicide intermetallics benefits from the defect-enhanced diffusion of iron sulfides. [2] Our scanning electron microscopy confirmed that the microstructures resulting from silicide sulfidation consisted of intimate mixing of iron sulfides and silicon sulfides with very small particle sizes, reminiscent of metal dealloying. [3] A lower-temperature reaction space is opened by incorporating the “slow” reactant, Si, in a pre-reacted intermetallic. It follows that other materials with similarly slow reaction kinetics should be rich with unexplored phase space for compound discovery, which we discuss here subsequently. These findings on the kinetic effects of Fe—Si—S crystal formation were recently published in the Emerging Investigators issue of *Journal of Materials Chemistry C.*

The second thrust of our in-situ work is a focus on metathesis reactions. We have machined a flow furnace for our in-house diffractometer that permits monitoring and control of gas flow and temperature. [4] This furnace allows us to investigate reactions at temperatures up to 900°C and switch between two process gases. The first material accommodated in our furnace was FeS_2, which has been claimed to be fully stoichiometric in some studies, and have up to 12.5% intrinsic S vacancies in others. [5,6]

We approached the valence stability of FeS_2 in two ways. First, we synthesized bulk FeS_2 with a range of nominal stoichiometries. Our analysis of X-ray diffraction data form the Advanced Photon Source beamline 11-BM is the highest-resolution study of pyrite to date. Samples with a stoichiometry of FeS_x, where $1.8 \leq x \leq 2.25$, showed a deviation in lattice parameter of only 0.000035 Å, which is smaller than any previous reports. Refined occupancies give at least 99% S filling on its sites, and no evidence of vacancies. The small deviation in lattice parameter did not depend on the sulfur content—rather, we observed the formation of Fe_7S_8 for sulfur-deficient and elemental S_8 for sulfur-rich samples. This uniformity among samples does not prove that pyrite is a line compound—in such a case it would have to be robust to chemical pressure at elevated temperature.

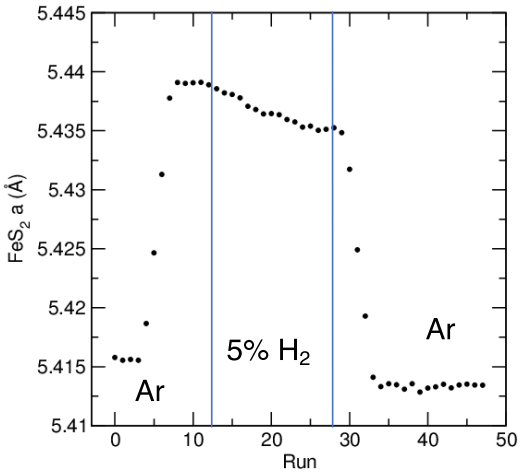

Figure 3. In-situ Rietveld-refined lattice parameters of sulfur-rich FeS_2 show a clear contraction in the lattice upon reduction with H_2, accompanied by formation of Fe_7S_8. No such variation in a is seen in direct synthesis samples with nominally S-poor stoichiometry.

For in situ reactions in 5% H_2 in Ar at 300°C, FeS_2 decomposed into Fe_7S_8 rather than forming a large homogeneity range of FeS_{2-x}. Again, line compound behavior was possible but not confirmed. However, at 400°C, the pyrite lattice parameter shows a clear contraction during the H_2-flow reduction regime. This decrease in lattice parameter *a* is shown in Figure 4. MgO was added as a "spike" standard to ensure that any sample displacement or drift was corrected. It follows that pyrite, for an autogeneous sulfur vapor pressure during synthesis, has a very narrow range of stoichiometry, but even a modest reducing agent can induce sulfur vacancies. Likewise, elevating the chemical potential of sulfur can likely tailor defects toward a more stoichiometric phase. This work is in the final stages of preparation for publication.

Future Plans

We will conduct exploratory synthesis in the complex Ba—Fe—S system, which is a far richer phase space than Fe—Si—S, with opportunities to create a molten flux. In the Fe—Si—S system, the importance of superheated peritectic liquid, and the kinetic engineering using intermetallics sulfidation were shown to play important roles in affecting the crystal growth. These two factors are now under investigation using other peritectically-decomposing compounds (*e.g.* MnS_2, CuS) and metals with known slow sulfidation kinetics (*e.g.* Zn, Ti, Cr).

Branching into more diverse synthetic reactions is a key focus of this project. Recently, we have demonstrated the synthesis of mixed-valence Cu_4O_3, a spin-½ 3D-kagome antiferromagnet, from a nitrate solution in ethanol and dimethylformamide (DMF) and began to map the reaction by ex-situ techniques. [7] However the mechanisms of this reaction are unclear.

We have conducted proof-of-concept experiments on POWGEN at the Spallation Neutron Source (SNS) to demonstrate the sensitivity of the instrument to small amounts of powder (100 mg!) in large-diameter solvothermal reactions, shown without background subtraction for a 1 hour collection in Figure 4. Our ultimate goal is to expand these efforts to an in-situ study of quantitative conversion of a hydroxide-nitrate precursor into Cu_4O_3.

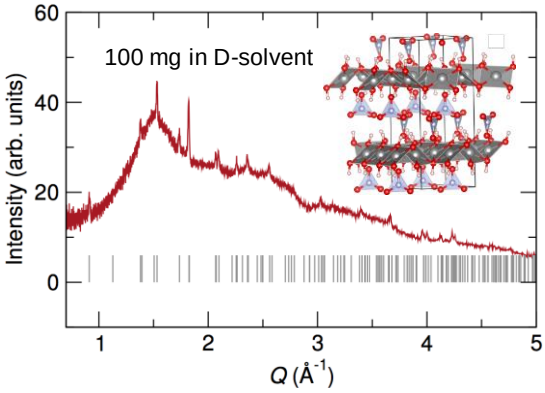

Figure 4. Solvothermal reaction trials in POWGEN at the SNS reveal easily-identifiable patterns for $Cu_2(NO)_3(OH)_3$ in only 100 mg in a deuterated ethanol-DMF solvent, shown here with the background solvent signal included.

In parallel, we have discovered new phases in the Fe—Ga—S, Na—Zn—S, Na—Zn—Se, and K—Sn—O systems that merit further investigation. The latter may be a fertile phase space for *p*-type transparent conducting oxide hosts, provided the new compounds can be stabilized with Sn^{2+}. We have obtained numerous new compounds from reactions in air and from metathesis routes. Structure solution from powder diffraction data is a key step in identifying these complex phases, such as $K_2Sn_3O_7$.

References

1. P. Waldner, and A. D. Pelton. Thermodynamic Modeling of the Fe-S System. *J. Phase Equilib. Diffus.*, 26 (1): 23-28, 2004.
2. S. Mrowec. On the defect structure and diffusion kinetics in transition metal sulphides and oxides. *React. Solids.*, 5 (4): 241-268, 1988.
3. J. Snyder, K. Livi, and J. Erlebacher. Dealloying Silver/Gold Alloys in Neutral Silver Nitrate Solution: Porosity Evolution, Surface Composition, and Surface Oxides. *J. Electrochem. Soc.*, 155 (8): C464-C473, 2008.
4. P. J. Chupas, K. W. Chapman, C. Kurtz, J. C. Hanson, P. L. Lee, and C. P. Grey. A versatile sample-environment cell for non-ambient x-ray scattering experiments. *J. Appl. Cryst.*, 41(4):822–824, 2008.
5. J. Luck, A. Hartmann, and S. Fiechter. Stoichiometry and impurity concentration in synthetically grown iron pyrite crystals and their constituents. *Fresenius Z. Anal. Chem.*, 334:441-446, 1989.
6. M. Birkholz, S. Fiechter, A. Hartmann, and H. Tributsch. Sulfur deficiency in iron pyrite (FeS_{2-x}) and its consequences for band-structure models. *Phys. Rev. B.*, 43(14):11926-11936, 1991.
7. Z. Jiang, S. Tian, S. Lai, R. McAuliffe, S. P. Rogers, M. Shim, and D. P. Shoemaker. Capturing phase evolution during solvothermal synthesis of metastable Cu_4O_3. *Chem. Mater.* 28(9): 3080-3089, 2016.

Publications

Z. Jiang, A. Ramanathan, D. P. Shoemaker. In situ Identification of Kinetic Factors that Expedite Inorganic Crystal Formation and Discovery. *J. Mater. Chem. C.* **5** 5709-5717 (2017)

R. D. McAuliffe, D. P. Shoemaker. Flexible stoichiometry in bulk pyrite FeS_2 as viewed by in-situ and high-resolution X-ray diffraction. *(in preparation)*

Exploring and Embracing Heterogeneity in Atomically Thin Energy Materials

Peter Sutter, Dept. of Electrical & Computer Engineering, University of Nebraska-Lincoln, Lincoln, NE 68588 (psutter@unl.edu); Eli Sutter, Dept. of Mechanical & Materials Engineering, University of Nebraska-Lincoln, Lincoln, NE 68588 (esutter@unl.edu)

Program Scope

Atomically thin semiconductors offer extraordinary opportunities for the manipulation of charge carriers, many-body optical excitations, and non-charge based quantum numbers. Confinement and reduced dielectric screening in the 2D limit give rise to large characteristic energies so that many-body and quantum effects dominate even at room temperature. At scales above the diffraction limit, optical excitations in these materials have been investigated intensely. Much less understood are effects that arise locally in heterogeneous materials, either near naturally occurring defects, impurities, edges and grain boundaries, or as a result of intentional alloying and interface formation. Addressing such systems experimentally involves significant challenges: *Understanding atomistic growth mechanisms*, so that high-quality materials or systems with specific "imperfections" and controlled interfaces can be realized; and *detecting local excitations* at scales that match the relevant (nanometer) length scales in heterogeneous materials. In this research program, we address these challenges by using novel platforms – including low-energy electron microscopy (LEEM) and closed-cell transmission electron microscopy (TEM) – for quantitative *in-situ* microscopy of the growth of 2D materials and heterostructures, combined with local spectroscopic measurements of quasiparticles excited at the nanometer-scale using cathodoluminescence in scanning transmission electron microscopy (STEM-CL). Experiments are guided and analyzed *via* computations of the structure, chemistry, and excitation spectra. The program focuses on three distinct classes of materials: (i) Graphene-hexagonal boron nitride alloys, interesting for realizing tunable bandgaps and novel excitonic effects; (ii) transition metal dichalcogenides and heterostructures, for which optically excited quasiparticles at defects and their manipulation near interfaces are being investigated; and (iii) group IV chalcogenides, a largely unexplored family of 2D materials promising for energy conversion processes.

Recent Progress

Our recent work has focused on group IV (Ge, Sn) chalcogenides, a class of earth-abundant 2D and layered materials with interesting fundamental properties and promise for energy conversion applications. SnS_2, for example, has shown high charge carrier mobility,[1] solution-phase sensing,[2] novel mechanisms for Li^+ uptake and release[3] and an electronic structure suitable for photoelectrochemical water splitting. The monochalcogenides SnS(e) and GeS(e), structural analogues of black phosphorus, have anisotropic lattice, thermal, electrical and optoelectronic properties. SnS is considered as an absorber for thin film photovoltaics, and SnSe

has shown record high thermoelectric figure of merit. SnS(e) and GeS(e) are predicted to be semiconducting multiferroics with coupled ferroelectricity/ferroelasticity in the 2D limit and antiferroelectric/ferroelastic behavior in the bulk.

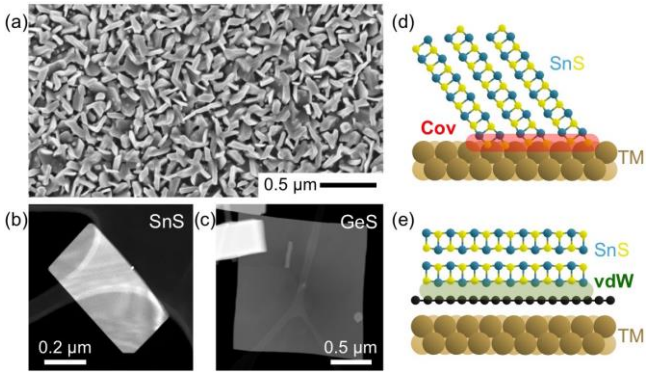

Figure 1: Challenges in group IV monochalcogenide growth. (a) SEM image of SnS on metal support. **(b)**, **(c)** High-quality metal-seeded SnS and GeS nanoflakes. **(d)** Slanted nucleation and growth due to covalent edge-substrate interaction. **(e)** Aligned layered growth on van der Waals substrates.

The controlled synthesis of few-layer and 2D group IV monochalcogenides, required to explore and pursue the unique properties of these materials, is a major challenge. On dielectric substrates (e.g., SiO_2) nucleation tends to be very sparse whereas metal supports, used for example in photovoltaics, favor the growth of slanted, randomly oriented thick plates (Fig. 1 (a)-(c)). We hypothesized that this undesirable growth mode is caused by a covalent interaction of edges of the initial nuclei with the support (Fig. 1 (d)), and that ordered growth of layered crystals aligned with the substrate surface may be achievable on atomically smooth, inert van der Waals substrates (Fig. 1 (e)).

To test this hypothesis, we carried out extensive real-time microscopy experiments focusing on SnS growth on different substrates.[4] Fig. 2 shows results obtained by LEEM during SnS growth on large-domain monolayer graphene/Ru(0001) (prepared *in-situ*, see Fig. 2 (a)). Surprisingly, SnS growth on graphene is delayed and is preceded by a growth stage in which Sn intercalation at the graphene-Ru interface leads to the growth of a few-layer Sn film beneath graphene (Fig. 2 (b)). This finding implies that dissociative adsorption of SnS releases Sn *via* graphene defects to the interface while S mostly desorbs. Additional work showed that the interfacial Sn layer can be converted to Sn-oxide, which may allow electrical gating of the graphene. Only after

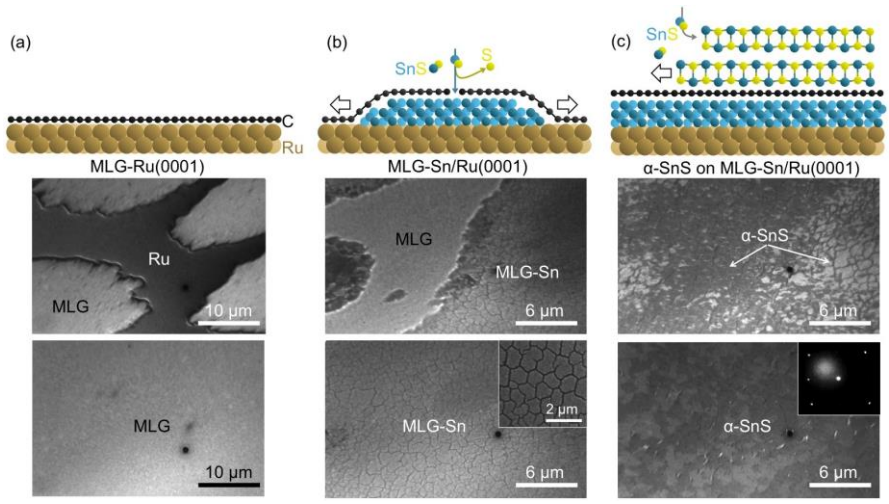

Figure 2: *In-situ* microscopy of SnS growth on graphene/Ru(0001). (a) Growth of large-domain graphene (MLG) on Ru(0001). **(b)** Dissociative adsorption of SnS and Sn growth at the MLG-Ru interface. Inset: Wrinkle network on the decoupled graphene. **(c)** Nucleation and growth of layered α-SnS on graphene. Inset: LEED of µm-scale single-crystalline SnS grains.

growth of a uniform interfacial Sn layer, SnS growth sets in on the graphene surface. LEEM and diffraction provide evidence for edge-flow growth of large, single crystalline few-layer SnS grains with basal plane parallel to the van der Waals substrate. These results open new avenues for studying the fundamental nucleation and growth mechanisms of layered and 2D materials as well as heterostructures, and establish a groundbreaking new approach for obtaining high-quality films for exploring the unique properties of anisotropic group IV chalcogenides as well as for applications, e.g., in solar energy conversion.

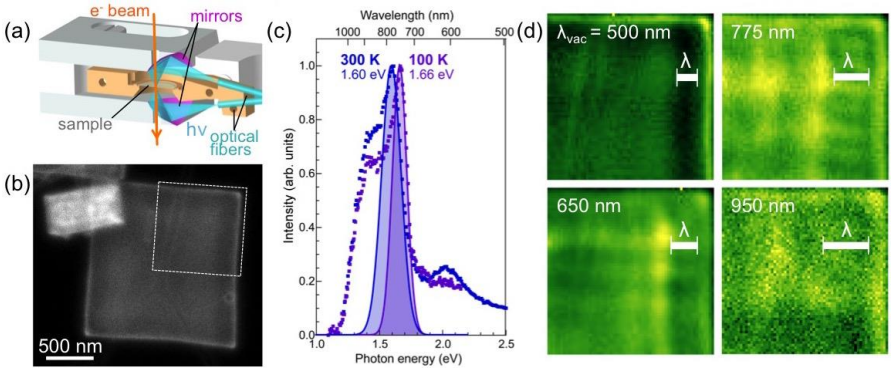

Figure 3: Nanometer-scale luminescence spectroscopy of 2D and layered semiconductors. (a) Light collection system in STEM-CL. **(b)** Panchromatic CL map of a GeS nanoplate. **(c)** Integral spectra over the entire GeS plate. **(d)** Interference for different (vacuum) wavelengths (λ_{vac}) in the segment of GeS plate outlined in (b). Bars indicate the wavelength λ inside the GeS crystal.

The optoelectronic properties of group IV chalcogenide semiconductors have been investigated using our unique nanospectroscopy approach based on STEM-CL (Fig. 3 (a)) that allows correlating the locally excited luminescence with the atomic-scale structure and chemistry. Using such measurements combined with *ab-initio* calculations performed by our collaborators in Finland and Germany, we identified key (excitonic) luminescence signatures accompanying the transformation of SnS_2 into SnS by electron-beam driven generation of sulfur vacancies.[5] In a separate study, we explored light emission and propagation in GeS nanoplates with sizes near the diffraction limit.[6] Direct gap GeS nanoplates behave as *luminescent nanoresonators* whose overall far-field light output is strongly dependent on the location of excitation within the plate due to interference enabled by efficient surface reflection (Fig. 3 (b)-(d)), making them interesting for tuning light-matter interactions in layered crystals.

Future Plans

In future work we will strive for a fundamental understanding of the synthesis of group IV chalcogenides with the goals of (i) achieving controlled 2D materials that exhibit predicted properties, e.g., ferroelectricity/elasticity; and (ii) combining different materials (e.g., SnS, GeS) in monolayer heterostructures with unexplored optoelectronic characteristics. We will use our unique *in-situ* electron microscopy and CL spectroscopy methods on lateral graphene-BN heterostructures and ternary C-B-N phases to investigate to establish possible tunable bandgaps and novel exciton and quantum emitter physics in this family of honeycomb monolayers.

2D transition metal dichalcogenides (TMDs), which received widespread attention due to their unique many-body physics, represent an ideal system for realizing the overarching goals of

this program: A fundamental understanding of the ways in which defects, edges, or judiciously placed interfaces affect the interactions between light and many-body excitations, and its translation into robust materials platforms that harness imperfections for new functionality in energy conversion or computing. To enable this thrust, we have established synthesis protocols for high-quality TMDs and are now extending them to 2D heterostructures (Fig. 4). Open questions in materials synthesis will be addressed by real-time microscopy, both *via* LEEM and in novel *Nanoreactors*, closed reaction cells for *in-situ* TEM of 2D chalcogenide growth with atomic-scale resolution at ambient S/Se pressures. STEM-CL spectroscopy correlated with the local structure and composition identified by analytical TEM will be used to establish the effects of defects on the optoelectronic properties, and to measure key characteristics of excitons in heterogeneous materials. Heterostructures will be used to probe interface physics in 2D, e.g., the possibility of creating indirect excitons at lateral interfaces that may give rise to condensate many-body states or allow manipulation of neutral quasiparticles to direct energy and information flows at the nanoscale.

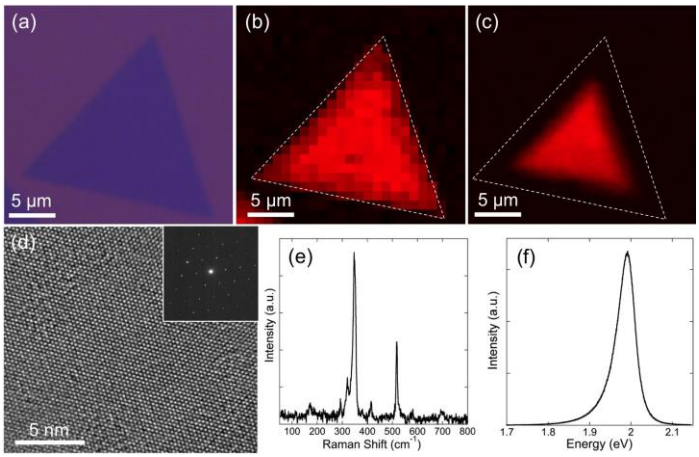

Figure 4: Growth and light-matter interactions of TMDs. (a)-(c) Optical micrograph (a), Raman map (b), and photoluminescence (PL) map (c) of a 2D WS_2 crystal. **(d)** High-resolution TEM and electron diffraction of transferred WS_2. **(e)** Raman spectrum, **(f)** PL spectrum of 2D WS_2.

References

[1] Y. Huang, E. Sutter, P. Sutter, et al., *Tin Disulfide – An Emerging Layered Metal Dichalcogenide Semiconductor: Materials Properties and Device Characteristics*, ACS Nano **8**, 10743 (2014).

[2] Y. Huang, E. Sutter, and P. Sutter, *Layered semiconductor devices with water top-gates: High on-off ratio field-effect transistors and aqueous sensors*, submitted (2017).

[3] P. Gao, Y. Huang, P. Sutter, et al., *High-Resolution Tracking Asymmetric Lithium Insertion and Extraction and Local Structure Ordering in SnS_2*, Nano Lett. **16**, 5582 (2016).

[4] P. Sutter and E. Sutter, *Growth of High-Quality Layered Tin Sulfide on Atomically Smooth Van der Waals Substrates,* in preparation.

[5] P. Sutter, H.-P. Komsa, A.V. Krasheninnikov, Y. Huang, and E. Sutter, *Defect generation during structural transformations of layered tin dichalcogenides*, submitted (2017).

[6] P. Sutter, Y. Li, C. Argyropoulos, and E. Sutter, *High-Resolution Optical Spectroscopy of GeS Nanoresonators*, in preparation.

Publications (Since Start of the Program, 09/01/2016)

1. Y. Huang, J. Qiao, K. He, S. Bliznakov, E. Sutter, X. Chen, D. Luo, F. Meng, D. Su, J. Decker, W. Ji, R.S. Ruoff, and P. Sutter, *Interaction of Black Phosphorus with Oxygen and Water*, Chemistry of Materials **28**, 8330 (2016).
2. B. Maughan, P. Zahl, P. Sutter, and O.L.A. Monti, *Ensemble Control of Kondo Screening in Molecular Adsorbates*, Journal of Physical Chemistry Letters **8**, 1837 (2017).
3. X. Zhao, J. Kotakoski, J.C. Meyer, E. Sutter, P. Sutter, A. Krasheninnikov, U. Kaiser, and W. Zhou, *Engineering and Modifying 2D Materials by Electron Beams*, Invited Review Article, MRS Bulletin **42**, 667 (2017).
4. H. Qin, X. Chen, J. Li, P. Sutter, and G. Zhou, *Atomic-Step Induced Local Non-Equilibrium Effects on Surface Oxidation*, Journal of Physical Chemistry C (in press).
5. Y. Huang, E. Sutter, and P. Sutter, *Layered Semiconductor Devices with Water Top-Gates: High On-Off Ratio Field-Effect Transistors and Aqueous Sensors*, submitted (2017).
6. B. Maughan, P. Zahl, P. Sutter and O. L. A. Monti, *Configuration-Specific Electronic Structure of Strongly Interacting Interfaces: TiOPc on Cu(110)*, submitted (2017).
7. P. Sutter, H.-P. Komsa, A.V. Krasheninnikov, Y. Huang, and E. Sutter, *Defect Generation During Structural Transformations of Layered Tin Dichalcogenides*, submitted (2017).
8. P. Sutter and E. Sutter, *Growth of High-Quality Layered Tin Sulfide on Atomically Smooth Van der Waals Substrates*, in preparation.
9. P. Sutter, Y. Li, C. Argyropoulos, and E. Sutter, *High-Resolution Optical Spectroscopy of GeS Nanoresonators*, in preparation.

Producing Ordered, Transparent, and Flexible Substrates for Electronics by Epitaxial Lift-off of Electrodeposited Single-crystal Gold Foils

Jay A. Switzer

Department of Chemistry & Materials Research Center

Missouri University of Science and Technology

Rolla, MO 65409-1170

jswitzer@mst.edu

Program Scope

Single-crystal Si is the bedrock of semiconductor devices due to the high crystalline perfection that minimizes electron-hole recombination, and the dense SiO_x native oxide, which minimizes surface states. However, the brittle nature of bulk Si precludes its use in flexible electronic devices such as wearable solar cells, sensors, and flexible displays.[1-5] To expand the palette of electronic materials beyond planar Si, an inexpensive source of highly ordered material is needed that can serve as an inert substrate for the epitaxial growth of grain boundary-free semiconductors, photonic materials, and superconductors. In our lab, we have studied the epitaxial electrodeposition of metal oxide thin films onto single-crystal substrates for several years. We have recently shown that wafer-size transparent and flexible single-crystal foils of Au for flexible electronics can be produced by a simple and inexpensive lift-off procedure using single-crystal Si(111) as the template for electrochemical epitaxial growth.[6]

Recent Progress

Here, we demonstrate a procedure for epitaxial lift-off of wafer-size flexible and transparent foils of single-crystal Au(111) using Si(111) as a template. Lateral electrochemical undergrowth of a sacrificial SiO_x layer was achieved by photoelectrochemically oxidizing n-Si(111) under light irradiation. The processing scheme is shown in Fig. 1. Cu_2O as an inorganic semiconductor was epitaxially electrodeposited onto the Au foils, which showed a more ideal diode quality factor of 1.6 (where n=1 is ideal) than the value of 3.1 observed for a polycrystalline deposit. ZnO nanowires electrodeposited epitaxially on a Au foil showed flexibility with the nanowires intact up to 500 bending cycles. A 28 nm Au foil with a sheet resistance of 7 Ω sq^{-1} showed only a 4% increase in resistance after 4000 bending cycles. A flexible organic light-emitting diode based on tris(bipyridyl)ruthenium(II) was spin-coated on a foil to exploit the transmittance and flexibility of the gold foil. The simple epitaxial lift-off procedure produces single-crystal Au foils that offer the order of traditional semiconductors such as Si wafers without the constraint of a rigid substrate.

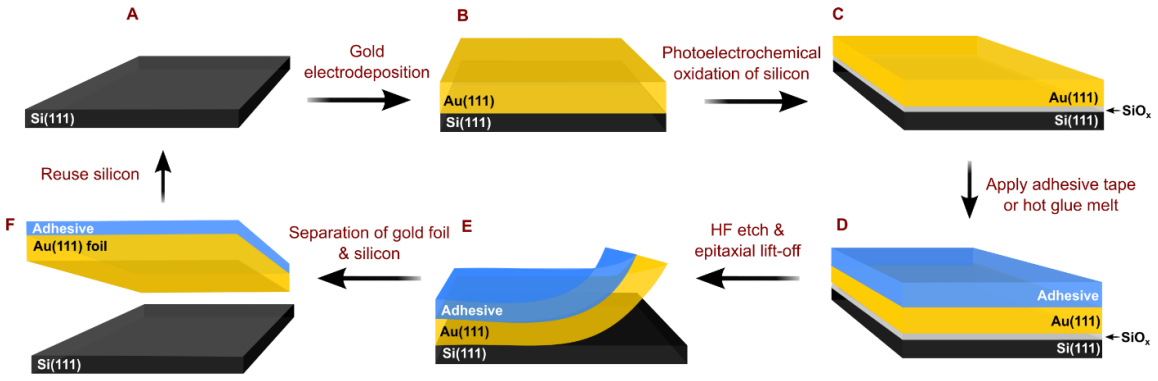

Fig. 1. Schematic for epitaxial lift-off of single-crystal Au foils from single-crystal Si.

Future Plans

1. Epitaxial electrodeposition of other metals such as Cu, Ag, and Pt onto single-crystal Si(hkl), and the lift-off of single-crystal metal foils.

2. Spin-coating epitaxial films such as PbI_2 and methylammonium lead iodide perovskite onto single-crystal Au foils.

3. Epitaxial electrodeposition of hard materials such as Cu_2O onto soft substrates using self-assembled monolayers (SAMs) of cysteine on Au(111) foils as the soft-matter substrates.

4. Enantiospecific epitaxial crystallization of chiral compounds on surfaces (such as Au(643)) that lack mirror or glide plane symmetry. The Au(643) will be produced by electrodepositing epitaxial Au onto Si(643).

References

1. B. D. Gates, Flexible electronics. *Science* **323**, 1566-1567 (2009).

2. Kenry, J. C. Yeo, C. T. Lim, Emerging flexible and wearable physical sensing platforms for healthcare and biomedical applications. *Microsystems & Nanoengineering* **2**, 16043 (2016).

3. D. Akinwande, N. Petrone, J. Hone, Two-dimensional flexible nanoelectronics. *Nat. Commun.* **5**, 5678 (2014).

4. J. A. Rogers, T. Someya, Y. Huang, Materials and mechanics for stretchable electronics. *Science* **327**, 1603-1607 (2010).

5. W. Gao, S. Emaminejad, H. Y. Y. Nyein, S. Challa, K. Chen, A. Peck, H. M. Fahad, H. Ota, H. Shiraki, D. Kiriya, D.-H. Lien, G. A. Brooks, R. W. Davis, A. Javey, Fully

integrated wearable sensor arrays for multiplexed in situ perspiration analysis. *Nature* **529**, 509-514 (2016).

6. N. K. Mahenderkar, Q. Chen, Y.–C. Liu, A. R. Duchild, S. Hofheins, E. Chason, and J. A. Switzer, "Epitaxial lift-off of electrodeposited single-crystal gold foils for flexible electronics," *Science* **355**, 1203-1206 (2017).

Publications over last two years resulting from work supported by the DOE project

1. S. Yazdanparast, J. A. Koza, and J. A. Switzer, "Copper nanofilament formation during unipolar resistance switching of electrodeposited cuprous oxide," *Chem. Mater.* **27**, 5974-5981 (2015).

2. J. C. Hill, A. T. Landers, and J. A. Switzer, "An electrodeposited inhomogeneous metal-insulator-semiconductor junction for efficient photoelectrochemical water oxidation," *Nature Materials* **14**, 1150-1155 (2015). Featured in Editors' Highlights in *Science*, **350**, 54 (2015). Featured as a Science Highlight on DOE BES webpage (June 9, 2016), https://science.energy.gov/bes/highlights/2016/bes-2016-06-v/.

3. J. C. Hill, J. A. Koza, and J. A. Switzer, "Electrodeposition of epitaxial lead iodide and conversion to textured methylammonium lead iodide perovskite," *ACS Applied Materials and Interfaces* **7**, 26012-26016 (2015).

4. J. A. Koza, J. C. Hill, A. C. Demster, and J. A. Switzer, "Epitaxial electrodeposition of methylammonium lead iodide perovskites," *Chem. Mater.* **28**, 399-405 (2016).

5. J. A. Switzer, J. C. Hill, N. K. Mahenderkar, and Y.-C. Liu, "Nanometer-Thick Gold on Silicon as a Proxy for Single-Crystal Gold for the Electrodeposition of Epitaxial Cuprous Oxide Thin Films," *ACS Applied Materials and Interfaces*, **8**, 15828-15837 (2016).

6. C. M. Hull, J. A. Koza, and J. A. Switzer, "Electrodeposition of Epitaxial $Co(OH)_2$ and Conversion to Epitaxial CoOOH and Co_3O_4," *J. Mater. Res.* **31**, 3324-3331 (2016).

7. Z. He, J. A. Koza, Y.-C. Liu, Q. Chen, and J. A. Switzer, "Room-temperature electrochemical reduction of epitaxial Bi_2O_3 films to epitaxial Bi films," *RSC Advances* **16**, 96832-96836 (2016).

8. N. K. Mahenderkar, Q. Chen, Y.–C. Liu, A. R. Duchild, S. Hofheins, E. Chason, and J. A. Switzer, "Epitaxial lift-off of electrodeposited single-crystal gold foils for flexible electronics," *Science* **355**, 1203-1206 (2017). Reviewed in *MRS Bulletin* (July 18, 2017) https://www.cambridge.org/core/journals/mrs-bulletin/news/au-foil-substrates-developed-for-flexible-electronics. Featured as a Science Highlight on DOE BES webpage (June 23, 2017), https://science.energy.gov/bes/highlights/2017/bes-2017-06-m/.

THE DYNAMICS OF COMPLEX TWO-PHASE MIXTURES DURING COARSENING: FROM DENDRITIC TO BICONTINUOUS MIXTURES

K. Thornton[2] and P.W. Voorhees[1]

[1]Department of Materials Science and Engineering, Northwestern University, Evanston IL
[2]Department of Materials Science and Engineering, University of Michigan, Ann Arbor MI

Program Scope

Dendrites frequently form during solidification into an undercooled melt. In systems with nearly isotropic interfacial energy, these dendrites possess secondary and sometimes even tertiary arms. In systems with anisotropic interfacial energy, the growth shapes can be highly crystallographic and thus of very different morphology from those in systems with isotropic interfacial energy. The resulting two-phase mixtures are topologically and morphologically complex with spatially varying mean and Gaussian curvatures. These solid-liquid mixtures are one example from a large class of morphologically and topologically complex structures found in nature that undergo coarsening. Included in this class are the bicontinuous two-phase mixtures produced following spinodal decomposition and those in nanoporous gold. Understanding the coarsening process in all of these systems requires theory, simulation, and experiments that capture their three-dimensional topology and morphology. Given the complicated morphology and topology of these systems it is not surprising that our understanding of this process is in its infancy.

A combined theoretical and experimental program is being carried out to examine the nature of the coarsening process in these highly complex, solid-liquid microstructures. The experiments will examine the time-dependent evolution of the structures in three dimensions in situ through X-ray microtomography. The results of these experiments will provide insights into the coarsening process that will guide the development of theory, serve as a test of phase field simulations and the theory, and provide initial conditions for the simulations. The results of large-scale simulations of coarsening in bicontinuous mixtures with both isotropic and highly anisotropic interfacial energy will be used to develop a theory of coarsening in these systems as well as to elucidate the importance of spatially varying curvatures, complicated topology, highly anisotropic interfacial energy, and interfacial kinetics on coarsening in solid-liquid mixtures. Through these experiments and theory, we aim to develop a comprehensive description of coarsening in complex and technologically important microstructures.

Recent Progress

The main goal of this project is to develop a general theory of coarsening of complex microstructures. To this end, we investigated coarsening of microstructures following spinodal decomposition with equal mobility between the phases [1]. Specifically, we have identified the correlations between the interfacial velocity and interfacial morphologies and used these correlations to predict the morphological evolution. Three simulated structures with varying volume fractions, two bicontinuous and one nonbicontinuous, were generated using the Cahn-Hilliard equation. We found general correlations between interfacial velocity and mean curvature, as well as between interfacial velocity and the surface Laplacian of mean curvature. Furthermore, we found that, for a population of interfaces with the same principle curvatures, the

probability of finding a patch of interface with a given normal velocity is described well by a Gaussian distribution, independent of the principal curvature values and the volume fractions of the structures. We also found that average interfacial velocity is described by a polynomial of mean curvature and the mean curvature.

In addition to the values of the interfacial mean and Gaussian curvature in the system, the spatial distribution of curvatures can be important in setting the coarsening dynamics. This is particularly the case then the coarsening process occurs by long-range diffusion, such as following spinodal decomposition. In order to quantify the long-range diffusional interactions and the interfacial curvatures that play a role in setting the dynamics of coarsening, we have determined the two-point correlation functions for interfacial velocities and interfacial curvatures during coarsening of a spinodally decomposed structure. Unlike standard two-point correlations of bulk phases, these are correlations of *interfacial* quantities. Thus, these correlations provide a much more direct connection to the coarsening process. The analysis shows that correlations are very short ranged, on a distance that is less than $1.5S_V^{-1}$ where S_V^{-1} is the inverse of the surface area per volume, and for longer distances the curvatures are randomly distributed. The correlations of the velocities are similarly short ranged. Thus, for distances that are much larger than the microstructural scale, or the surface area per volume, the velocity of an interface at a given point is uncorrelated with the velocities of the surrounding interfaces.

The dynamics of coarsening in solid-liquid mixtures, and the development of microstructure following solidification have been investigated using time-resolved x-ray tomography. These experiments involve the analysis of large, 1TB, sized datasets and draw upon the computational tools developed under this program. Without the sustained support needed to develop these tools, the analysis could not have been performed. This research led to new insights into the mechanisms responsible for the growth of faceted eutectics [3], and those responsible for the morphological evolution of faceted Si particles in a liquid phase [4-5]. The work on coarsening of faceted Si particles illustrates the importance of crystallographic defects, such as twins, in setting the morphology of these particles. The presence of these twin defects leads to a slow disappearance of the facets on the interfaces the Si particles with the liquid, and thus to the development of a much more isotropic structure. The datasets that have been used in this research have been shared with the community using the Materials Data Facility. In particular, the datasets have received digital document identifiers (DOI's) and are thus citable in a similar fashion to publications. In addition, the data is discoverable by others and freely available.

To gain further understanding of coarsening in a wider variety of systems, we have also examined systems with phases having different mobilities. Large-scale simulations of coarsening in bicontinuous systems were conducted, and the kinetics and the morphologies of these systems were characterized. We examined coarsening behavior for systems with $V_f = 50\%$ and ratios of mobilities between 1 and 10^{-3}. We found self-similar coarsening and a $t^{1/3}$ power law at late times. The self-similar interfacial shape distributions (ISDs) are found to depend on the mobility. The ISDs show wider distributions with a larger difference in mobilities. An example of the microstructural morphologies and the corresponding ISDs is compared to the uniform mobility case in Figure 1. The kinetics of coarsening in our simulations appear to be consistent with what would be expected from the effective diffusivity of a comparable bicontinuous structure.

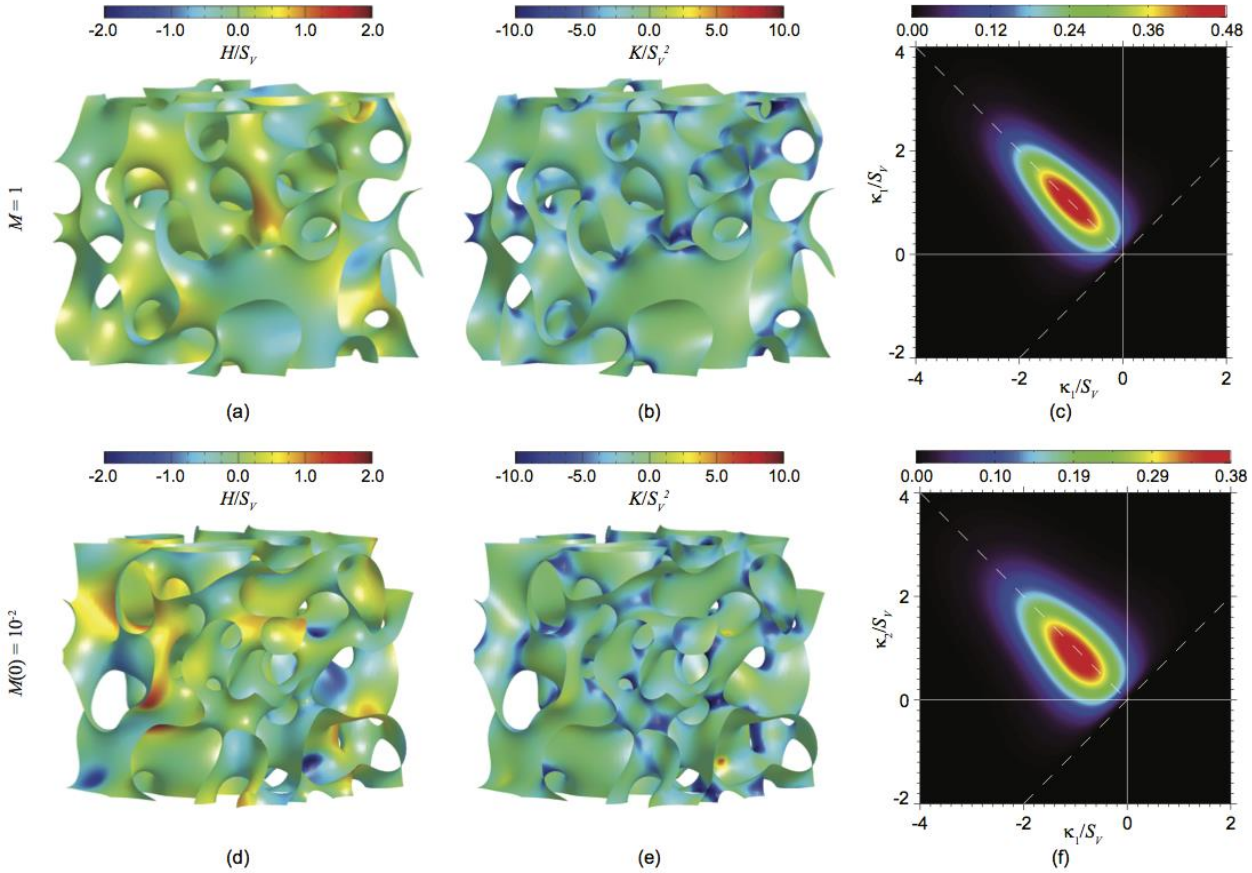

Figure 1. Self-similar structures from simulations with uniform mobility ((a), (b), and (c)) and dissimilar mobilities ((d), (e), and (f)). Subfigures (a), (b), (d), and (e) show the $c = 0.5$ isosurface in subdomains of volume $(7S_V^{-1})^3$, colored by scaled mean curvature H/S_V in (a) and (d), and by scaled Gaussian curvature K/S_V^2 in (b) and (e). Subfigures (c) and (f) are ISDs for the entire uniform mobility and dissimilar mobilities structures, respectively.

Most recently, we have begun examining the self-similar structures resulting from surface diffusion. The preliminary results suggest that the morphologies, as characterized by the ISD, remain similar to the bulk diffusion case, potentially indicating that the change in the ISD resulting from dissimilar mobilities is due to the broken symmetry in these cases. We also have initial results that shed light on the effect of topological singularities, in which we compare the coarsening kinetics, as well as morphological and topological evolution, when allowing/prohibiting pinching events.

Future Plans

On the basis of these results, in the future we plan to:

- Develop a coarse-grained kinetics model based on effective diffusivity for systems with dissimilar mobilities. If successful, such model will be able to predict the evolution of the characteristic length scale when the effective diffusivity of the microstructure is known without computationally expensive calculations.
- Perform large-scale simulations of coarsening via surface diffusion, and examine the development of morphology and topology of the resulting bicontinuous structures. This

will enable us to compare our simulations to the experimental results in nanoporous gold, and thus shed light on the mechanisms responsible for the morphological development of these important structures.

- Elucidate the role of topological singularities on coarsening dynamics. We shall examine how the length scale associated with pinching affects the kinetics of coarsening and resulting morphology and topology. This is important because such a length scale may depend on the material system as well as its microstructure.
- Examine the effects of simultaneous solidification and coarsening on the development of the morphology and topology of solid-liquid mixtures. This will be done using 4D X-ray tomography of the coarsening and solidification process in Al-Cu alloys. The data has been acquired, and we are in the process of analyzing the results.

References

[1] C.-L. Park, J.W. Gibbs, P.W. Voorhees, K. Thornton, *Coarsening of complex microstructures following spinodal decomposition*, Acta Materialia, **132**, 13-24 (2017).

[2] Y. Sun, K. Thornton and P.W. Voorhees, *Predicting interfacial dynamics during coarsening by local and non-local interfacial morphologies,* under preparation.

[3] A.J. Shahani, X. Xiao, P.W. Voorhees *The mechanism of eutectic growth in highly anisotropic materials*, Nature Comm., 12953 (2016).

[4] A.J. Shahani, E.B. Gulsoy, V.J. Roussochatzakis, J.W. Gibbs, J.L. Fife, P.W. Voorhees, *The dynamics of coarsening in highly anisotropic systems: Si particles in Al–Si liquids*, Acta Materialia, **97**, 325-337 (2015).

[5] A.J. Shahani, E.B. Gulsoy, S.O Poulsen, X. Xiao, P.W. Voorhees. *Twin-mediated crystal growth: an enigma resolved*. Scientific Reports. 2016;6:28651. doi:10.1038/srep28651.

Publications

Papers:

Y. Sun, K. Thornton and P.W. Voorhees, *Predicting interfacial dynamics during coarsening by local and non-local interfacial morphologies,* under preparation.

W.B. Andrews, P.W. Voorhees, K. Thornton, *Effects of dissimilar mobilities on coarsening in two-phase systems,* under preparation

J.W. Gibbs, C-L. Park, Y. Sun, K. Thornton and P.W. Voorhees, *Quantifying diffusional interactions during diffusion-limited two-phase evolution,* under preparation.

C.-L. Park, J.W. Gibbs, P.W. Voorhees, K. Thornton, *Coarsening of complex microstructures following spinodal decomposition*, Acta Materialia, **132**, 13-24 (2017).

A.J. Shahani, E.B. Gulsoy, V.J. Roussochatzakis, J.W. Gibbs, J.L. Fife, P.W. Voorhees, *The dynamics of coarsening in highly anisotropic systems: Si particles in Al–Si liquids*, Acta Materialia, **97**, 325-337 (2015).

C.-L. Park, P.W. Voorhees, K. Thornton, *Evolution of interfacial curvatures of a bicontinuous structure generated via nonconserved dynamics,* Acta Materialia, **90**, 82-193 (2015).

A.J. Shahani, X. Xiao, P.W. Voorhees *The mechanism of eutectic growth in highly anisotropic materials*, Nature Comm., 12953 (2016).

A.J. Shahani, E.B. Gulsoy, S.O Poulsen, X. Xiao, P.W. Voorhees. *Twin-mediated crystal growth: an enigma resolved*. Scientific Reports. 2016;6:28651. doi:10.1038/srep28651.

Datasets:

A.J. Shahani, E.B. Gulsoy, S.O Poulsen, X. Xiao, P.W. Voorhees. *Twin-mediated crystal growth: an enigma resolved*. 2016, http://dx.doi.org/doi:10.18126/M2301J.

A.J. Shahani, X. Xiao, P.W. Voorhees *The mechanism of eutectic growth in highly anisotropic materials*, 2016, http://dx.doi.org/doi:10.18126/M26P4H.

J.W. Gibbs, P.W. Voorhees, J.L. Fife, *Liquid-solid Metallic Mixture Coarsening Data - 35% Solid*, 2016, http://dx.doi.org/doi:10.18126/M2059C.

J.W. Gibbs, P.W. Voorhees, J.L. Fife, *Liquid-solid Metallic Mixture Coarsening Data* - 28% *Solid*, 2016, http://dx.doi.org/doi:10.18126/M27P4T.

J.W. Gibbs, P.W. Voorhees, J.L. Fife, *Liquid-solid Metallic Mixture Coarsening Data* - 80% *Solid* 2016, http://dx.doi.org/doi:10.18126/M23W2W.

J.W. Gibbs, P.W. Voorhees, J.L. Fife, *Liquid-solid Metallic Mixture Coarsening Data* - 55% *Solid*, 2016, http://dx.doi.org/doi:10.18126/M2VC7F.

Mapping the synthetic routes for 2-dimensional materials: bridging *micro* and *macro*

Boris I. Yakobson | Rice University, Houston, TX 77005 | 713-348-3572 | biy@rice.edu

Program Scope

Following the excitement of graphene discoveries, the research in the 2D-materials "beyond graphene" is broad and deep worldwide. Broad is the scope of research, expanded to at least a dozen of very different chemically yet all promising compositions: white graphene (h-BN), transition metal dichalcogenides (TMD or MX_2, by stoichiometry), phosphorene (2D P), silicene (Si), stanine (Sn), MAXenes, most recently borophene (2D B), and more. Deep is the type of fundamental questions being asked, from optoelectronic and catalysis to morphology and defects, and ultimately to understanding the synthetic principles and guidance through the quantitative models of growth. The latter, along with often needed additional processing (e.g., liftoff-transfer or stacking of the synthesized layers) is in the focus of this project. The scope of theoretical exploration is intentionally diverse across the materials: discovering the regularities in one case can be transferrable to others, while revealing the differences further adds valuable insight, leading to basic science across the material family. The quest for 2D materials raises a number of compelling questions about the ways of making such layers. The exfoliation from natural bulk precursors (if such exist, like in the cases of graphite→graphene, black phosphorus→phosphorene) is not scalable. On the other hand, their synthesis through chemical vapor deposition involves complex gas-solid chemistry, which may work empirically, yet its theoretical understanding and sentient design remain in infancy. This is the direction we have embarked to explore.

Besides the specific material choices, the key questions project seeks to answer are: (I) What is the energy balance between the growing material intrinsic bonding versus its interaction with the substrate, how it can favor 2D against competing nucleation into 3D-crystal? This issue can be central for Si or B while almost irrelevant for graphene or h-BN where 2D is essentially the ground state. (II) What are the elementary reactions at the edge of 2D islands defining the speed of this edge expansion? (III) How these speeds depend on crystallographic directions? (IV) Accordingly, what must be the equilibrium or kinetically-controlled shapes? These are very important questions, not only from basic science point of view but also for all practical use, since the shape and mutual orientations of the islands determine the quality of the final material, and the morphology of the grain boundaries (critical for mechanical, optical, electronic properties, or catalytic activity of the product). While putting effort into already available 2D materials, we further focus on a bigger question: (V) Can one, by the proper choice of substrate-catalyst, or with a capping layer, entice almost any desired material to nucleate and grow into 2D-form, rather than its ground 3D-bulk phase? The controlling knob here is the interaction with the

substrate, which must be strong enough to favor the 2D, yet not too strong/prohibitive for its subsequent separation (liftoff) from the substrate into truly stand-alone layer. This balance is the key to success, as we have demonstrated for 2D boron. This is a challenging goal, but we build on our strength and the known advances with 2D GaN, Si and B, showing that (V) is feasible. Although the questions (I-V) are overarching across materials, we select the examples of different chemistries and different degree of 'maturity': (i) graphene (Gr), (ii) hexagonal boron nitride (h-BN), (iii) borophene (2D B), (iv) phosphorene (2D P), and (v) transition-metal dichalcogenides—TMD or MX2 monolayers. We also keep an eye on what we group as "emergent or exotic" materials.

The benefits from this project are in both conceptual basic theory of 2D materials synthesis, with impact on entire field, and in advancing production of known and discovery of not yet existing materials, for applications in catalysis, electronics, energy systems, optics and information technology.

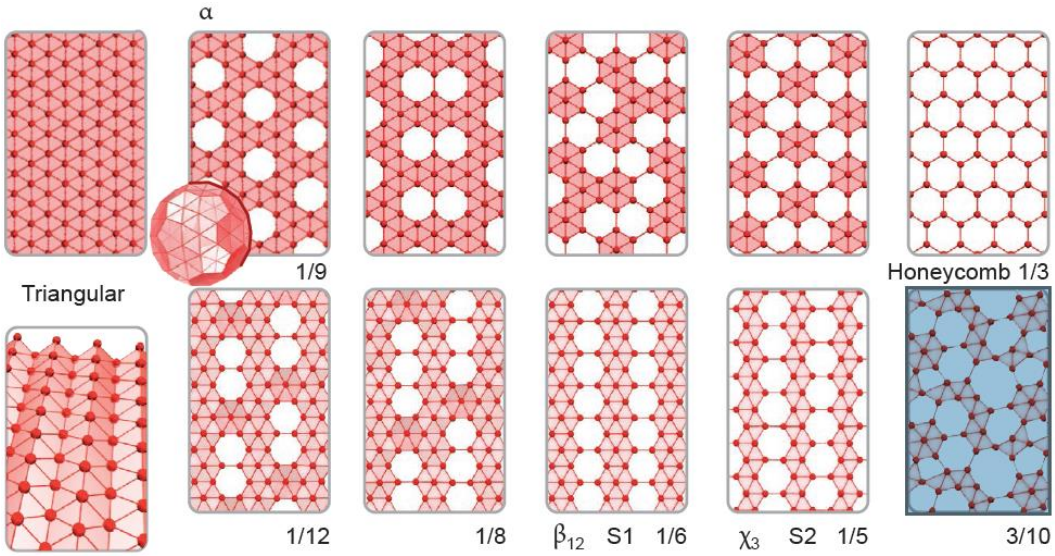

Fig. 1 Structures of polymorphic boron sheets [7]. The β_{12} and χ_3 are observed in experiments.

Recent Progress

And indeed, our line of theoretical studies has culminated recently in experimental discovery of 2D boron [i] and even identification of some predicted phases grown on Ag(111) surface, Fig. 1 [7]. Further progress critically depends on separating boron layer from metallic substrates (Ag, Au, Cu) or growing it in insulating surfaces, to permit probing its intriguing properties (plasmons, superconductivity) and also obtain less ambiguous atomic resolution images. We currently develop theoretical models for boron nucleation on nonmetals.

Among several lines of activity, we focus on two most recent examples: one is atomic scale exploration of MoS_2 growth [ii] while another is phenomenological approach to "evolutionary selection" for mono-crystallinity in 2D synthesis [iii].

Monolayer molybdenum disulphide (MoS_2) is a semiconductor with potential to revolutionize electronic and photonic devices. Chemical vapor deposition (CVD) is the most desirable scalable method for its mass production. If the CVD growth mechanism is better understood, the high quality rapid growth process can be achieved. We perform systematic DFT calculations along with AIMD simulations to identify the atomic-level mechanisms of MoS_2.growth. Traditionally, solid MoO_3 and gaseous S_2 are the *macro*-precursors in the CVD; recently, alkali metal halides, such as NaCl or KI, has been added as promoters. We find that in both cases, a simple MoS_4 molecule (Fig. 2-I) must form to serve as the building block—*molecular* precursor—for the 2D MoS_2. From the detailed reaction pathways of traditional CVD growth, the rate determining step is breakup of the ring structure of gaseous MoO_3 in the form of $(MoO_3)_3$ and then shedding a Mo_1-containing molecule from the resulting chain (Fig. 2-TS3). In contrast, salt-assisted CVD growth circumvents this high energy barrier through the formation of Mo_1-containing gaseous precursors due to the reaction between the salts and MoO_3 at early stage. Our work unravels the atomic-level growth mechanisms of monolayer MoS_2 and, by determination of *micro*-precursors, should enable the use of *nanoreactor* diagram [iv] for predicting the growth kinetics and crystal morphology. The advantage of using gaseous molecular precursors could also be applied for other transition metal dichalcogenides.

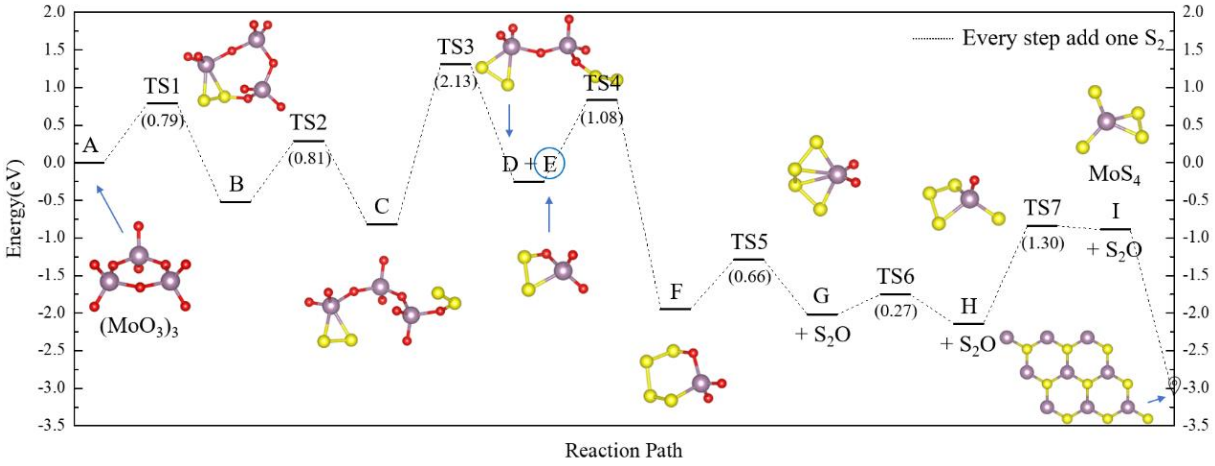

Fig. 1. Proposed reaction pathways of MoS_4 formation from $(MoO_3)_3$ molecule.

To explore macroscopic growth of 2D polycrystal, and determine the ways of deriving large single crystals, we developed a code that tracks the crystal grain shapes in time. Multiple grains merge during growth and eventually evolve into a convex polygon, usually terminated by slowest edges (ZZ for graphene), in accord to kinetic Wulff construction. When grains with identical orientation meet, they form concave corners, but rapidly become a single grain with a convex front. Grains of different orientations develop complex network of grain boundaries (GB) in areas of dense nucleation, ultimately resulting in long range GBs radiating outward. A particularly important case, relevant to practical manufacturing, is revealed from this system when growth is confined within a strip of substrate, with nucleation limited to one narrow side of it: growing material, after expanding to the full width of the strip, ends up with a single dominant growth direction - along the length of the substrate. Preliminary results indicate that all the grains

intersect and compete with each other, following "evolutionary selection" as put forward in earlier work by van der Drift. Only the grains that have their orientation of the fastest moving vertex along the growth direction dominate and eliminate other grains on the way. (Grain coarsening over time is ~$t^{0.5}$.) Based on this result, one expects developing only one grain, well aligned with the growth direction, Fig. 3. However, additional factors can still prevent or disrupt this transition to single crystal growth. For example, growth under continuous (secondary) nucleation, specifically unique to 2D growth in contrast to 3D, can hinder the selection of the fastest growing crystal. This is currently being investigated in order to describe specific criteria under which single crystal growth is achievable and how fast it can be. These results support the possibility of obtaining very large single crystal of 2D materials [v] such as graphene and transition metal dichalcogenides, which opens a door to fully realize their potential for applications.

Fig. 2. Demonstration of evolutionary selection of grains, and transition from polycrystalline growth towards monocrystalline growth [iii].

Future Plans

We intend to explore thoroughly the energetics and nucleation processes of boron on various substrate in order to guide 2D-boron synthesis on insulators or inert weakly-bonding substrates (ideally, graphene, h-BN, SiO_2). This line of work is well under way but requires broad computational search to be performed. Another core direction is to identify, for various empirically feasible CVD cases, what are true micro, molecular precursors (like C or C_2 in case of graphene); this is crucial for building first-principles based predictive growth models, like the *nanoreactor* diagrams. It is also important as providing quantitative input into larger scale phenomenology, like phase field modeling of growth or the interface tracking approach, which is much faster alternative for simulating engineering scale 2D syntheses.

References

[i] "Synthesis of borophenes: Anisotropic, two-dimensional boron polymorphs", A. Mannix, X.-F. Zhou, B. Kiraly, J. Wood, D. Alducin, B. Myers, X. Liu, B. Fisher, U. Santiago J. Guest, M. Yacaman, A. Ponce, A. Oganov, M. Hersam, N. Guisinger, ***Science***, **350**, 1513 (2015).
[ii] J. Lei, Y. Xie, B.I. Yakobson, work in progress.
[iii] N. Gupta, K. Bets, B.I. Yakobson, et al., work in progress.
[iv] "Equilibrium at the edge and atomistic mechanisms of graphene growth", V.I. Artyukhov, Y. Liu, and B.I. Yakobson, ***Proc. Natl. Acad. Sci.***, **109**, 15136 (2012).
[v] I. Vlassiouk, S. Smirnov, et al., work in progress.

Publications (DE-SC0001479, DE-SC0012547)

1. "Tilt grain boundary topology induced by substrate topography", H Yu, N. Gupta, Zh. Hu, K. Wang, B.R. Srijanto, K. Xiao, D.B. Geohegan, and B.I. Yakobson, **ACS Nano**, **11**, 8612–8618, DOI: 10.1021/acsnano.7b03681 (2017).
2. "Predicting stable phase monolayer Mo2C (MXene), a superconductor with chemically-tunable critical temperature", J. Lei, A. Kutana, and B.I. Yakobson, **J. of Materials Chemistry C** 5, 3438-3444 (2017).
3. "B_{40}: Stability, reactivity and planar structural precursor", Y Yang, Z. Zhang, E.S. Penev, and B.I Yakobson, ***Nanoscale***, **9**, 1805–1810, DOI: 10.1039/C6NR09385J (2017).
4. "Single-atomic ruthenium catalytic sites on nitrogen-doped graphene for oxygen reduction reaction in acidic medium" C. Zhang, J. Sha, H. Fei, M. Liu, S. Yazdi, J. Zhang, Q. Zhong, X. Zou, N. Zhao, H. Yu, Z. Jiang, E. Ringe, B.I. Yakobson, J. Dong, D. Chen, and J.M. Tour, ***ACS Nano***, **11**, 6930−6941, DOI: 10.1021/acsnano.7b02148 (2017).
5. "Growth mechanism and morphology of hexagonal boron nitride", Zh. Zhang, Y. Liu, Y. Yang, and B.I. Yakobson, ***Nano Lett.*** **16**, 1398−1403, DOI: 10.1021/acs.nanolett.5b04874 (2016).
6. "Substrate-induced nanoscale undulations of borophene on silver", Zh. Zhang, A.J. Mannix, Z. Hu, B. Kiraly, N.P. Guisinger, M.C. Hersam, and B.I. Yakobson, ***Nano Lett.***, **6**, 6622–6627. DOI: 10.1021/acs.nanolett.6b03349 (2016).
7. "Polyphony in B flat", Z. Zhang, E.S. Penev, and B.I. Yakobson, ***Nature Chemistry***, **8**, 525–527, doi:10.1038/nchem.2521 (2016).
8. "Phase crossover in transition metal dichalcogenides nanoclusters", W. Zan, Z. Hu, Z. Zhang, and B.I. Yakobson, ***Nanoscale***, **8**, 19154-19160, DOI: 10.**1039**/c6nr06194j (2016).
9. "Topochemistry of bowtie- and star-shaped metal dichalcogenide nanoisland formation", V.I. Artyukhov, Z. Hu, Z. Zhang, and B.I. Yakobson, ***Nano Lett.*** **16**, 3696–3702, DOI: 10.1021/acs.nanolett.6b00986 (2016).
10. "Solid-vapor reaction growth of transition metal dichalcogenide monolayers", B. Li, Y. Gong, Z. Hu, G. Brunetto, Y. Yang, G. Ye, Z. Zhang, S. Lei, Z. Jin, E. Bianco, X. Zhang, W. Wang, J. Lou, D.S. Galvão, M. Tang, B.I. Yakobson, R. Vajtai, and P.M. Ajayan, ***Angewandte Chemie Int. Ed***., **55**, 10656-10661, DOI: 10.1002/anie.201604445 (2016).
11. "Can two-dimensional boron superconduct?" E.S. Penev, A. Kutana, and B.I. Yakobson, ***Nano Lett.***, **16**, 2522–2526, DOI: 10.1021/acs.nanolett.6b00070 (2016).
12. "Thermomechanical analysis of two-dimensional boron monolayers", T. Tsafack and B.I. Yakobson, ***Phys. Rev. B***, **93**, 165434, DOI: 10.1103/PhysRevB.93.165434 (2016).

***

The Surface Chemistry of Atomic Layer Deposition (ALD) Processes

Francisco Zaera
Department of Chemistry, University of California, Riverside, CA 92521
Email: zaera@ucr.edu

i) Program Scope

The general objective of our project is to develop a molecular-level understanding of the thermal reactions that the organometallic compounds used for atomic layer deposition (ALD) follow on surfaces. ALD is one of the dominant technologies for the growth of nanometer-sized conformal films in many industrial applications. In microelectronics in particular, ALD can be used for the growth of diffusion, adhesion, and protection barriers and of metal interconnects, structures that are central to the buildup of diodes, transistors, and other elements within integrated circuits. More recently, the applications of ALD has been extended to areas related to energy production and use such as solar cells and photovoltaics, batteries, fuel cells, and catalysts and photocatalysts. All these processes require the deposition of isotropic films on complex topographies under mild conditions and with monolayer control. ALD is particularly suited to all those uses, but many questions concerning the underlying surface chemistry need to be answer to improve performance. Our mechanistic studies of ALD reactions are being pursued with the aid of surface-sensitive techniques such as X-ray photoelectron (XPS), low-energy ion scattering (LEIS), temperature programmed desorption (TPD), and infrared (IR) spectroscopies.

ii) Recent Progress

We have identified a number of key issues relevant to the behavior of common organic ligands used to make ALD precursors. Up to now, the work financed by this grant has focused primarily on the chemistry of copper precursors, a metal used in microelectronics applications, even if we have recently expanded that work to also include the deposition of other transition metals. Our studies with copper have illustrated the difficulties that may be encountered when selecting metalorganic compounds of late transition metals for ALD using knowledge from studies from the inorganic-chemistry community exclusively, and have recently led us to the identification of important and perhaps unforeseen factors responsible for the unique way in which some of those precursors bind and are activated on surfaces, following chemistry without precedent in solution. Some of the central observations deriving from our past work have been summarized in the abstracts of previous years, so only the more recent progress will be reviewed here. We have by now studied three generations of copper precursors based on amidinates and related ligands. We have carried out this project in collaboration with Prof. Sean T. Barry of Carleton University, a synthetic organic chemist that has been incorporating the lessons learned from our surface-science studies to develop more sturdy compounds capable of cleaner decomposition on solid surfaces. After having learned that the most labile point of the amidinate precursors is the beta position next to the nitrogen atoms, Prof. Barry proceeded to design a new ligand where all those positions are blocked, that is, where the beta carbons are all substituted and have no hydrogen atoms bonded to them. Our initial results with the resulting copper(I)-N-*tert*-butyl-5,5-dimethyl-2-iminopyrrolidinate show great promise, with initial dehydrogenation delayed by more than 100 K. That research continues to date.

In connection with our work with copper precursors, we have recently identified a new unexpected factor that affects the adsorption and activation of ALD precursors on solid surfaces: the inaccessibility of the metal center(s) to coordinate directly to atoms within those surfaces. This problem proved to be particularly acute with metal amidinates, since those tend to form dimers, tetramers, and other oligomers in the solid state. We have shown, in close collaboration with the theoretical group of Prof. Andrew Teplyakov, that such multi-unit structures are quite stable and survive intact in the gas phase, forcing the precursor to bond to surfaces not through the metal, as often assumed, but via one of the nitrogen atoms in the ligands instead (Figure 1) [1]. The new bonding mode delays any ligand replacement steps within the adsorbed ALD precursor, and results in ligand activation and decomposition. Interestingly, the explanation for this ligand shielding of the metal center seen on surfaces does not seem to be based on steric factors, but rather on the particular stability provided to metal complexes by the multiple bonds that bidentate and π-bonding ligands provide. This new hypothesis needs to be explored further, to test its generality, as other ligands may produce ALD precursors with similar limitations.

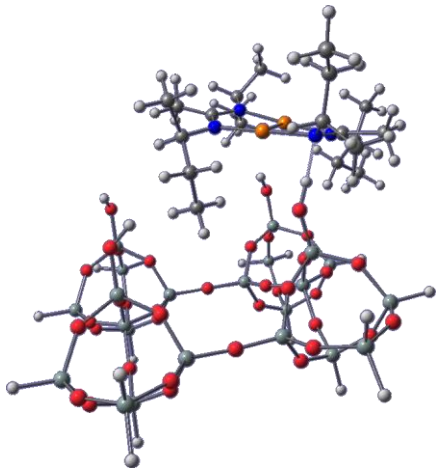

Fig. 1. Calculated structure of Cu(I)-N,N'-di-sec-butyl-acetamidinate adsorbed on OH-terminated silicon oxide surfaces.

We have also been expanding the range of substrates tested for ALD. To that goal, the thermal surface chemistry of copper(I)-N,N'-di-sec-butylacetamidinate, $[Cu(^{s}Bu\text{-}amd)]_2$ was initially characterized on SiO_2 films [2]. Initial adsorption at cryogenic temperatures results in the oxidation of the copper centers, with Cu $2p_{3/2}$ XPS binding energies close to those of a +2 oxidation state, an observation that we interpret as the result of the additional coordination of oxygen atoms from the surface to the Cu atoms of the molecular acetamidinate dimer. Either heating to 300 K or dosing the precursor directly at that temperature leads to the loss of one of its two ligands, presumably via hydrogenation/protonation with a hydrogen/proton from a silanol group, or following a similar reaction on a defect site. By approximately 500 K the Cu $2p_{3/2}$, C 1s, and N 1s XPS data suggest that the remaining acetamidinate ligand is displaced from the copper center and bonds to the silicon oxide directly, after which temperatures above 900 K need to be reached to promote further (and only partial) decomposition of the organic moieties. It was also shown that the uptake of the Cu precursor is self-limiting at either 300 or 500 K, although the initial chemistry is somewhat different at the two temperatures, and that the nature of the substrate also defines reactivity, with the thin native silicon oxide layer always present on Si(100) surfaces being less reactive than thicker films grown by evaporation because of the lower density of surface nucleation sites. The thermal chemistry of Cu(I)-N-sec-butyl-iminopyrrolidinate, one of our 2nd-generation precursors designed by Prof. Barry to minimize ligand decomposition, was characterized on similar silicon oxide films next [3]. Three temperature regimes were identified for that precursor after adsorption at 100 K, as made evident in the TPD shown in Figure 2: (1) molecular desorption at 240 K; (2) protonation of some of the ligands and formation of the corresponding iminopyrrolidine at 300 K; and (3) fragmentation of the remaining ligands to produce H_2, HCN, and butene, which occurs concurrently with the

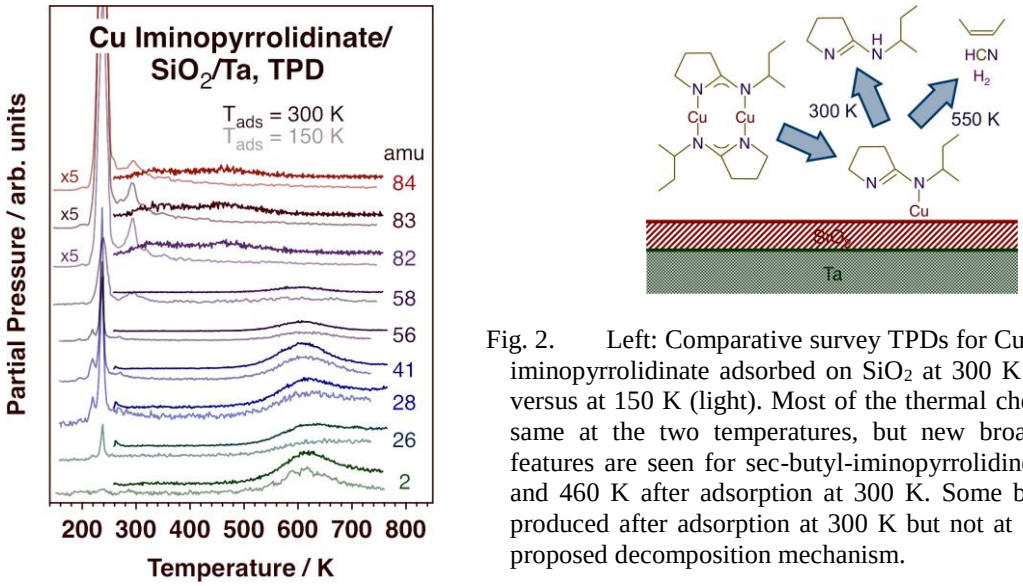

Fig. 2. Left: Comparative survey TPDs for Cu(I)-sec-butyl-iminopyrrolidinate adsorbed on SiO_2 at 300 K (dark traces) versus at 150 K (light). Most of the thermal chemistry is the same at the two temperatures, but new broad desorption features are seen for sec-butyl-iminopyrrolidine around 330 and 460 K after adsorption at 300 K. Some butane is also produced after adsorption at 300 K but not at 100 K. Top: proposed decomposition mechanism.

reduction of the copper ions. Most of the carbon and nitrogen atoms are removed from the surface after the third step, and copper desorbs above 900 K. Similar but enhanced reactivity was observed when the precursor is adsorbed at room temperature, suggesting that the chemistry identified by these TPD experiments is applicable under ALD conditions, but an extended production of sec-butyl-iminopyrrolidine in two broad peaks around 330 and 460 K was seen in that case as well. Self-limiting adsorption, as required for atomic layer deposition (ALD) processes, is seen up to 500 K, but by 550 K continuous copper deposition takes place. In general, the chemistry of this copper ALD precursor is milder and cleaner on silicon oxide than on metals (Figure 2, right panel), as with the other copper precursors, yet it also shows some level of undesirable ligand decomposition leading to the deposition of impurities in the growing films.

The initial work with Cu(I)-sec-butyl-2-iminopyrrolidinate was then extended to other surfaces, including single crystals of transition metals (Ni(110) and Cu(110)), thin oxide films (NiO/Ni(110) and SiO_2/Ta), and oxygen-treated metals (O/Cu(110)) [4]. Decomposition of the pyrrolidinate ligand leads to the desorption of several gas-phase products, including CH_3CN, HCN and butene from the metals and CO and CO_2 from the oxygen-containing surfaces. In all cases dehydrogenation of the organic moieties is accompanied by hydrogen removal from the surface, in the form of H_2 on metals and mainly as water from the metal oxides, but the threshold for this chemistry varies wildly, from 270 K on Ni(110) to 430 K on O/Cu(110), 470 K on Cu(110), 500 K on NiO/Ni(110), and 570 K on SiO_2/Ta (Figure 3, left). Copper reduction is also observed in both the Cu $2p_{3/2}$ XPS and the Cu L_3VV Auger (AES) spectra, reaching completion by 300 K on Ni(110) but occurring only between 500 and 600 K on Cu(110); on NiO/Ni(110), both Cu(I) and Cu(0) coexist between 200 and 500 K, and on SiO_2/Ta a change happens between 500 and 600 K but the reduction is limited, with the copper atoms retaining a significant ionic character (Figure 3, right). Additional experiments to test adsorption at higher temperatures led to the identification of temperature windows for the self-limiting precursor uptake required for ALD between approximately 300 and 450 K on both Ni(110) and NiO/Ni(110); the range on SiO_2 had been previously determined to be wider, reaching an upper limit at about 500 K. Finally, deposition of copper metal films via ALD cycles with O_2 as the co-reactant was successfully accomplished on the Ni(110) substrate.

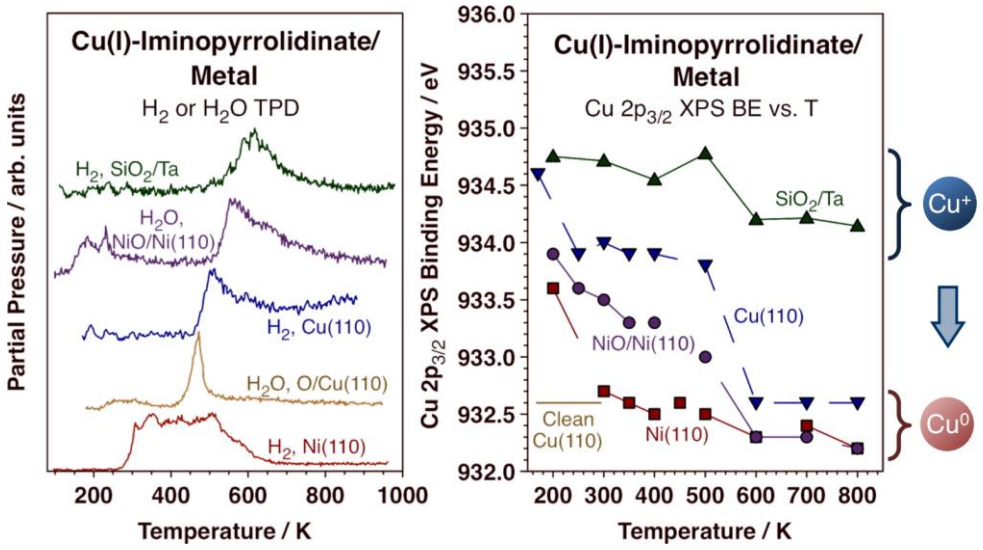

Fig. 3. Left: H_2 (metals, SiO_2) or H_2O (NiO/Ni(110), O/Cu(110)) TPD traces from decomposition of a copper iminopyrrolidinate ALD precursor on five different surfaces, reflecting the kinetics of the surface dehydrogenation steps associated with the decomposition of the ligands. The threshold temperature at which that decomposition starts varies widely, from 270 K on Ni(110) to 550 K on SiO_2/Ta. Right: Cu $2p_{3/2}$ XPS peak binding energies (BEs) as a function of annealing temperature for the same systems highlighting the fact that the reduction of the copper atoms, signified by the shift in binding energies from > 933.6 eV to 932.2–932.6 eV, occurs at the same temperatures as ligand decomposition.

iii) Future Plans

In the next year, we plan to wrap up our work with copper and to extend our project to other metals and other ligands. Because of our interest in ALD applications related to energy problems, we have chosen to start with the deposition of Pt and Ru metals. The specific precursors chosen to initiate this work are methylcyclopentadienyltrimethylplatinum(IV) and tris(2,2,6,6-tetramethyl-3,5-heptanedionato)ruthenium(III), respectively, typical examples for two common families of organic ligands: cyclopentadienyls, which are perhaps the most frequently used ligands that coordinate to metals through pi bonding, and diketonates, another very popular family of bidentate ligands. These should help us test the generality of the initial conclusions reached from our work on Cu ALD in terms of unique reactivity of metalorganic complexes on solid surfaces.

iv) References

[1] B. Chen, Y. Duan, Y. Yao, Q. Ma, J. P. Coyle, S. T. Barry, A. V. Teplyakov, F. Zaera, J. Vac. Sci. Technol., A 35 (2017) 01B124.
[2] Y. Yao, F. Zaera, J. Vac. Sci. Technol., A 34 (2016) 01A101.
[3] Y. Yao, J. P. Coyle, S. T. Barry, F. Zaera, J. Phys. Chem. C 120 (2016) 14149–14156.
[4] Y. Yao, J. P. Coyle, S. T. Barry, F. Zaera, J. Chem. Phys. 146 (2017) 052806.

v) Publications Sponsored by This DOE Grant, 2016-2017

1. Yunxi Yao and Francisco Zaera, Chemistry of Copper Acetamidinate ALD Precursors on Silicon Oxide, *J. Vac. Sci. Technol. A*, **34**, 01A101/1-01A101/8 (2016). ALD SPECIAL ISSUE
2. Yunxi Yao and Francisco Zaera, Adsorption and Thermal Chemistry of Formic Acid on Clean and Oxygen Predosed Cu(110) Single-Crystal Surfaces Revisited, *Surf. Sci.*, **646**, 37–44 (2016). INVITED, Special Issue honoring Richard Lambert.
3. Lei Guo, Xiangdong Qin, and Francisco Zaera, Chemical Treatment of Low-k Dielectric Surfaces for Patterning of Thin Solid Films in Microelectronic Applications, *ACS Appl. Mater. Interfaces*, **8(9)**, 6293-6300 (2016).
4. Menno Bouman and Francisco Zaera, Kinetics of Adsorption of Methylcyclopentadienyl Manganese Tricarbonyl on Copper Surfaces and Implications for the Atomic Layer Deposition of Thin Solid Films, *J. Phys. Chem. C*, **120(15)**, 8232–8239 (2016).
5. Yunxi Yao and Francisco Zaera, Thermal Chemistry of Hydrazine on Clean and Oxygen- and Water-Predosed Cu(110) Single-Crystal Surfaces, *Surf. Sci.*, **650**, 263-271 (2016). INVITED, Special Issue in honor of Robert J. Madix.
6. Yunxi Yao, Jason P. Coyle, Seán T. Barry, and Francisco Zaera, Thermal Decomposition of Copper Iminiopyrrolidinate Atomic Layer Deposition (ALD) Precursors on Silicon Oxide Surfaces, *J. Phys. Chem. C*, **120(26)**, 14149–14156 (2016).
7. Lei Guo, Ilkeun Lee, and Francisco Zaera, Patterning of Solid Films via Selective Atomic Layer Deposition Based on Silylation and UV-Ozonolysis, *ACS Appl. Mater. Interfaces*, **8(30)**, 19836–19841 (2016).
8. Yunxi Yao, Jason P. Coyle, Seán T. Barry, and Francisco Zaera, Effect of the Nature of the Substrate on the Surface Chemistry of Atomic Layer Deposition Precursors, *J. Chem. Phys.*, **146**, 052806 (2017). INVITED, SPECIAL ISSUE ENTITLED "Atomic and Molecular Layer Processing: Deposition, Patterning, and Etching"
9. Bo Chen, Yichen Duan, Yunxi Yao, Qiang Ma, Jason P. Coyle, Seán T. Barry, Andrew V. Teplyakov, and Francisco Zaera, Activation of the Dimers and Tetramers of Metal Amidinate ALD Precursors upon Adsorption on Silicon Oxide Surfaces, *J. Vac. Sci. Technol. A*, **35**, 01B124 (2017). ALD SPECIAL ISSUE

In Situ Visualization and Theoretical Modeling of Early-Stage Oxidation of Metals and Alloys

Guangwen Zhou
Department of Mechanical Engineering, State University of New York, Binghamton, NY 13902

Program Scope

Nearly all metals form spontaneously an oxide skin in ambient conditions. This oxide skin governs the chemical and physical interactions of the metal with the outer environment. Such interactions play a key role in a vast array of technological processes, including acting as a diffusion barrier to protect the materials from corrosion, production of important chemicals in heterogeneous catalysis, and fabrication of gate oxides for electronic devices. A precise knowledge of the oxidation process and atomic structure of the oxide layer is essential to improving existing processes and designing new functional materials. The program exploits the capabilities of imaging, diffraction and spectroscopy of complementary *in situ* techniques including aberration-corrected environmental electron microscopy, ambient-pressure x-ray photoelectron spectroscopy, and scanning tunneling microscopy for dynamically monitoring the evolution of surface structure, composition, and chemistry at practically relevant conditions of temperature and oxygen pressure. The *in situ* reactions are coordinated intimately by a number of theoretical modeling techniques from the density-functional theory to the first-principles thermodynamics by the incorporation of temperature and pressure effect for identifying the critical kinetic and thermodynamic factors controlling the surface oxidation process including adsorption sites, diffusion path, reaction barrier, and surface/interface effects.

Recent Progress

Oxidation is a notoriously complex multiscale process, and much of our current knowledge is based upon work at the mesoscale that is too coarse to reflect the underlying microscopic details. We have undertaken a combined *in situ* microscopy/spectroscopy and model approach aimed at elucidating the atomistic processes ranging from oxygen surface chemisorption to oxide nucleation and growth and then to the dynamic evolution at the buried metal/oxide interface. Below we summarize the major activities and significant results.

- **Atomic-step-induced local nonequilibrium effects on surface oxidation**

Step-crossing barriers are typically considered as a kinetic factor in controlling surface mass transport [1-5]. Using *in situ* low-energy electron microscopy (LEEM) imaging of the oxidation of NiAl(100), we provide direct evidence of the significant effects of atomic steps in controlling the thermodynamic driving force for oxidation. Although the surface steps are only one or a few atoms high, our results show that the inherent barriers associated with step crossing by surface species of oxygen cause a heterogeneous oxygen concentration across the crystal surface, giving rise to local non-equilibrium effects governing oxidation even for surfaces that are globally in equilibrium. The asymmetry in the step-crossing barriers for oxygen atoms crossing up- or down- steps is such that descendant steps exert a local driving force that favors oxidation whereas ascendant steps locally destabilize the surface oxide in their vicinity (Fig. 1). The local differences in the thermodynamic driving force for oxidation due to atomic steps and step bunches gives rise to novel phenomena, such as oscillatory oxide growth and the net translation of surface oxide domains. Our results provide direct insight into the atomic mechanism of step-crossing barriers in controlling the thermodynamic driving force of surface

reactions. The broader applicability of the fundamental insight extracted from the this study can be expected because of the inherent barriers associated with step crossing by surface species and the match between the experimental observation and the prediction by our analytic modeling that is not tied to a specific material system.

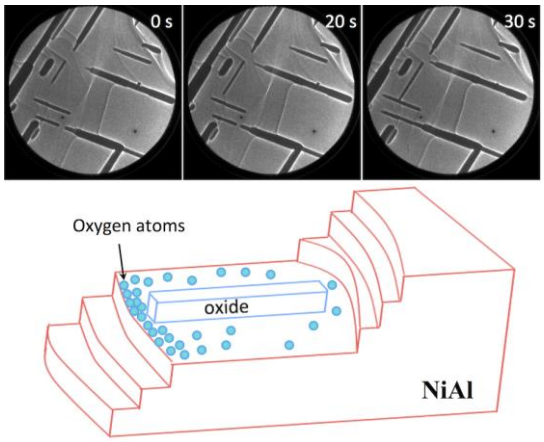

Fig. 1: (Upper panel) Time sequence of LEEM images showing the drifting motion of oxide stripes at pO_2 =1.8×10^{-8} Torr and T=1035 °C. Substrate steps bound the two ends of the oxide stripes; (Lower panel): Pictorial illustration of asymmetric concentrations of oxygen atoms across bunched steps with accumulation of oxygen atoms on the upper terrace adjacent to the step bunch.

- ***In situ* atomic-scale imaging of the metal/oxide interfacial transformation**

The surface oxidation results in the formation of a buried oxide/metal interface. Probing interfacial dynamics *in situ* has always been a major challenge, mainly because of the experimental inaccessibility of buried interfaces. In relation to technologically relevant process such as oxidation, catalysis, and thin film growth, metal/oxide interfaces are in fact highly dynamic in their response to and interaction with the environment. Fundamental understanding of interface dynamics not only requires resolving the local structure at the atomic scale, but also the ability to capture this structural evolution in real time and under reaction conditions. Using environmental TEM that allows for temperature-, time-, and pressure-resolved imaging of gas-surface reactions by introducing a reactive gas to the sample while simultaneously monitoring the structural evolution at the atomic scale, we form Cu_2O/Cu interfaces via *in situ* oxidation of Cu in an oxidizing atmosphere and subsequently probe the atomic mechanisms by which interfacial transformation and grain rotation occur at the interfaces during reduction in a H_2 gas environment. The $Cu_2O \rightarrow Cu$ transformation is observed to occur initially along the Cu_2O/Cu interface in a layer-by-layer manner. The accumulation of oxygen vacancies at the Cu_2O/Cu interface drives the collapse of the Cu_2O lattice near the interface region, which results in a tilted Cu_2O/Cu interface with concomitant Cu_2O island rotation. These results provide new microscopic detail regarding the redox reactions of supported oxides and may have broader implications for manipulating the way that buried interfaces can affect gas-surface reaction kinetics.

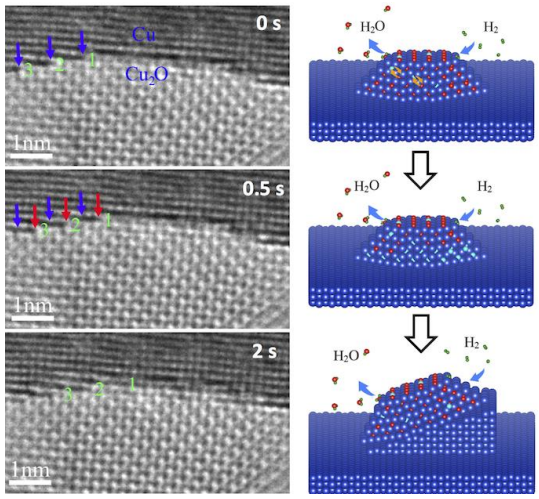

Fig. 2: (Left) HRTEM snapshots showing the $Cu_2O \rightarrow Cu$ conversion at the Cu_2O/Cu interface at T=350°C and pH_2=4×10^{-2} Torr. (Right): Pictorial illustration of the $Cu_2O \rightarrow Cu$ transformation induced Cu_2O island rotation.

- **Facilitating dislocation nucleation through atomic segregation**

Alloying is an established and versatile method to tune the properties of materials, including mechanical strength, ductility and toughness, corrosion resistance, and catalytic

properties. Often, minor compositional modifications that occur locally in a material can lead to drastic changes in properties: at free surfaces these changes can affect corrosion resistance and catalytic function; at grain boundaries they influence fracture strength; at dislocations they alter plastic deformation behavior; and at hetero-phase interfaces they affect adhesion and integrity [6, 7]. Thus, the effects of variations in alloy composition can easily manifest themselves in the macroscopic world through the localized phenomena of segregation, i.e., the enrichment of a material constituent at a free external surface or an internal interface. Because most engineered materials are alloys either by design or by the natural incorporation of impurities that remain after processing, segregation phenomena are of fundamental scientific interest and have enormous consequence across many materials technologies. Using the example of a Cu(Au) solid solution, we demonstrate that compositional variations induced by surface segregation are accompanied by misfit strain and the formation of dislocations in the subsurface region via a surface diffusion and trapping process, and the resulting chemically ordered surface alloy acts as an effective barrier that inhibits subsequent dislocation annihilation at free surfaces. Using dynamic, atomic-scale resolution transmission electron microscopy (TEM) observations and theory modeling, we show that the dislocations are highly active, and we delineate the specific atomic scale mechanisms associated with their nucleation, glide, climb, and annihilation at elevated temperatures. These observations provide an unprecedented level of mechanistic detail on how dislocations nucleate and migrate at hetero-interfaces in dissimilar material systems.

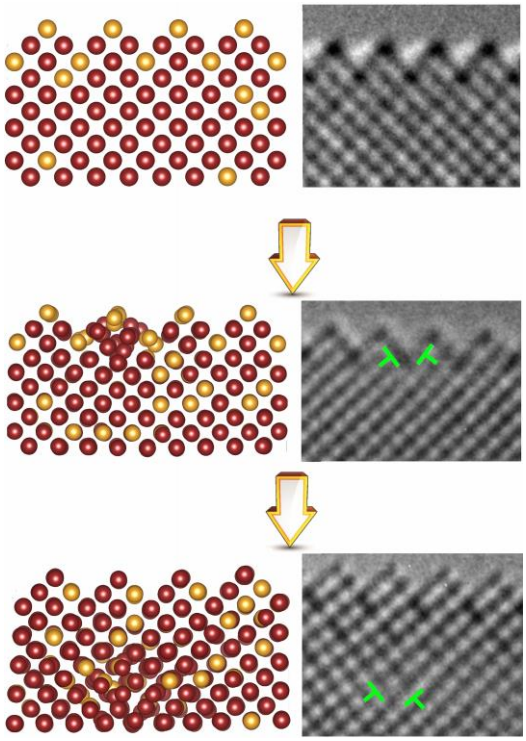

Fig. 3: (Right) *In situ* atomic-scale TEM observation of the birth of misfit dislocations out of a coherent Au/Cu(Au) interface dislocation at 350 °C and 1×10^{-3} Torr of H_2 gas flow, (Left) molecular dynamics and DFT modeling of the near surface dislocation.

Future Plans

Oxygen-chemisorption at a metal surface typically results in a two-dimensionally reconstructed atomic layer that does not bear any resemblance to the corresponding bulk oxides. The monoatomic surface layer is intrinsically connected with the metal support and the strong interfacial interactions can significantly impact a wide range of surface phenomena, such as surface chemical kinetics, catalysis, oxidation and passivation. The variety of possible oxygen chemisorbed phases, as well as – in many cases, unclear nature of the phase transitions between them, may result in spatial variations in the ordered structure, which in turn leads to spatial variations in rates of reactions associated with patches of different phases distributed over the surface. The conditions for mapping ranges of stability of the various phases and for co-existence of different phases and phase transitions in such systems are still not established. Fundamental understanding of the surface region in reaction conditions not only requires resolving the surface

phase, but also the ability to capture the dynamic phase evolution in real time and under the reaction conditions because the surfaces for many technologically relevant processes are in fact highly dynamic in their response to external stimuli. Cu(110) is such a system that first develops an added-row (2×1) reconstruction that transits to the (6×2) reconstruction upon further O adsorption [8-12]. This (2×1)→(6×2) surface phase transition process results in the formation of a large number of (2×1)/(6×2) boundaries. We will employ LEEM to trace out O chemisorption induced phase transitions and map the stability of the O chemisorbed phases with temperature-, time-, and pressure-resolved LEEM imaging of the Cu(110) surface by introducing O_2 at the sample surface while simultaneously monitoring surface phase evolution. The *in situ* LEEM measurements will allow for accurately mapping the ranges of stability for the co-existence of the two ordered phases. In most treatment of surface thermodynamics, the possible co-existence of different phases is not accounted for, nor considered as a criterion for their equilibrium. With *ab initio* calculations based on DFT and thermodynamics considerations, we will further model the stability of the co-existing phases with the presence of (2×1)/(6×2) phase boundaries.

References:

[1] G. Ehrlich, F.G. Hudda, Atomic View of Surface Self-Diffusion: Tungsten on Tungsten, J. Chem. Phys., 44 (1966) 1039-1049.
[2] R.L. Schwoebel, E.J. Shipsey, Step Motion on Crystal Surfaces, J. Appl. Phys., 37 (1966) 3682-3686.
[3] S.J. Liu, H.C. Huang, C.H. Woo, Schwoebel-Ehrlinch Barrier--- From Two to Three Dimensions, Appl. Phys. Lett., 80 (2002) 3295-3297.
[4] Z. Zhang, M.G. Lagally, Atomistic processes in the early stages of thin-film growth, Science, 276 (1997) 377-383.
[5] Q. Zhu, W.A. Saidi, J.C. Yang, Enhanced Mass Transfer in the Step Edge Induced Oxidation on Cu(100) Surface., J. Phys. Chem. C, 121 (2017) 11251-11260.
[6] P.A. Dowben, A. Miller, Surface Segregation Phenomena, CRC Press, 1990.
[7] J.A. Rodriguez, Physical and chemical properties of bimetallic surfaces, Surf. Sci. Rep. , 24 (1996) 223-287.
[8] L. Li, Q.Q. Liu, J. Li, W.A. Saidi, G.W. Zhou, Kinetic barriers of the phase transition in the oxygen chemisorbed Cu(110)-(2x1)-O as a function of oxygen coverage, J. Phys. Chem. C, 118 (2014) 20858-20866.
[9] Q.Q. Liu, L. Li, N. Cai, W.A. Saidi, G.W. Zhou, Oxygen chemisorption-induced surface phase transitions on Cu(110), Surf. Sci., 627 (2014) 75-84.
[10] F. Besenbacher, J.K. Norskov, Oxygen chemisorption on metal surfaces: general trends for Cu, Ni and Ag, Progress in Surface Science, 44 (1993) 5-66.
[11] D.J. Coulman, J. Wintterlin, R.J. Behm, G. Ertl, Novel mechanism for the formation of chemisorption phases: the (2x1)O-Cu(110) "added-row" reconstruction, Phys. Rev. Lett., 64 (1990) 1761-1764.
[12] R. Feidenhans, F. Grey, M. Nielsen, F. Besenbacher, F. Jensen, E. Laegsgaard, I. Stensgaard, K.W. Jacobsen, J.K. Norskov, R.L. Johnson, Oxygen chemisorption on Cu(110): a model for the c(6x2) structure, Phys. Rev. Lett., 65 (1990) 2027-2030.

Publications in the Last Two Years

1. L.F. Zou, C.M. Yang, Y.K. Lei, D. Zakharov, J.M.K. Wiezorek, D. Su, Q.Y. Yin, J. Li, Z.Y. Liu, E.A. Stach, J.C. Yang, L. Qi, G.F. Wang, G.W. Zhou, "*Facilitating dislocation nucleation through atomic segregation*", **Nat. Mater.** (in press)
2. H.L. Qin, X.D. Chen, J. Li, P. Sutter, G.W. Zhou, "*Atomic-step-induced local nonequilibrium effects on surface oxidation"*, **J. Phys. Chem. C** (in press, 2017)
3. D.X. Wu, J. Li, G.W. Zhou, "*Oxygen adsorption at heterophase boundaries of the oxygenated Cu(110)*", **Surf. Sci.** (in press, 2017)
4. L.F. Zou, J. Li, D. Zakharov, E.A. Stach, G.W. Zhou, "*In situ atomic-scale imaging of the metal/oxide interfacial transformation*", **Nat. Commun. 8**, 307 (2017)
5. L.K. Wang, C.Y. Cai, Y.C. Zhou, G.W. Zhou, "*Initial-stage oxidation of $Ni_3Al(100)$ and (110): from Ab Initio thermodynamics",* **J. Phys. Chem. C 121**, 19191-19200 (2017)
6. Q.Q. Liu, H.L. Qin, J. Boscoboinik, G.W. Zhou, "*A comparative study of oxidation of NiAl(100) by molecular oxygen and water vapor using ambient-pressure X-ray photoelectron spectroscopy",* **Langmuir 32**, 11414 (2016)
7. J. Li, G.F. Wang, G.W. Zhou, "*Surface segregation phenomena in extended and nanoparticle surfaces of Cu-Au alloys*", **Surf. Sci.** ***649***, 39 (2016)
8. L.L. Luo, L.F. Zou, D.K. Schreiber, D.R. Baer, M.J. Olszta, S.M. Bruemmer, G.W. Zhou, C.M. Wang, "*In situ atomic scale visualization of surface kinetics driven dynamics of oxide growth on Ni-Cr surface*", **Chem. Commun.** 52, 3300 (2016)
9. L.L. Luo, L.F. Zou, D.K. Schreiber, D.R. Baer, S.M. Bruemmer, G.W. Zhou, C.M. Wang, "*In situ transmission electron microscopy study of surface oxidation for Ni-10Cr and Ni-20Cr alloys*", **Scr. Mater. 114**, 129-132 (2016)
10. Q. Zhu, L.F. Zou, G.W. Zhou, W.A. Saidi, J.C. Yang "*Early and transient stages of Cu oxidation: Atomistic insights from theoretical simulations and in situ experiments*", **Surf. Sci.** ***652***, 98 (2016)
11. J. Li, L. Li, G.W. Zhou, "*The onset of sub-surface oxidation induced by defects in an oxygen chemisorbed layer",* **J. Chem. Phys. 142**, 084701 (2015)
12. L.L. Luo, Y.H. Kang, J.C. Yang, G.W. Zhou, "*Nucleation and growth of oxide islands during the initial-stage oxidation of (100)Cu-Pt alloys"***, J. Appl. Phys. 117**, 065305 (2015)
13. H.L. Qin, X.D. Chen, L. Li, P. Sutter, G.W. Zhou, "*Oxidation-driven surface dynamics on NiAl(100)",* **Proc. Natl. Acad. Sci. 112(2)**, E103-109 (2015)

The path to growth of metal/semiconductor nanocomposite materials by Liquid Phase Epitaxy

PI: Joshua M. O. Zide, University of Delaware, Newark, Delaware 19716

Program Scope

Nanoparticles embedded in semiconductor thin films have shown tremendous potential in device applications ranging from terahertz detection to thermoelectrics. However, the primary way to produce such material systems is by molecular beam epitaxy, which has slow growth rates and is limited in the range of nanocomposites that can be grown; these reasons prevent such a technology from being widely adopted. We have proposed using a combination of inert gas condensation (IGC) and liquid phase epitaxy (LPE) for nanocomposite film growth, such that the particles generated by IGC are included in LPE semiconductor melt. IGC allows for nanoparticles to be generated independent of the semiconductor matrix, increasing the potential variety of metal-semiconductor nanocomposites, both in terms of composition and nanostructure morphology. Semiconductors produced by LPE are well-studied and can be high quality, but are not well-suited for multiple-component systems. The production of thin films (e.g. ErAs:GaAs) by this two-step growth technique can result in better understanding of LPE, which has not been used for the growth of composite materials.

Recent Progress

The first part of this project focused on the growth of binary nanoparticles from pressed powder targets via inert gas condensation. Rietveld refinement of XRD patterns has been used to identify trends in the composition of the powders after growth, which contain ErAs, Er, As, and

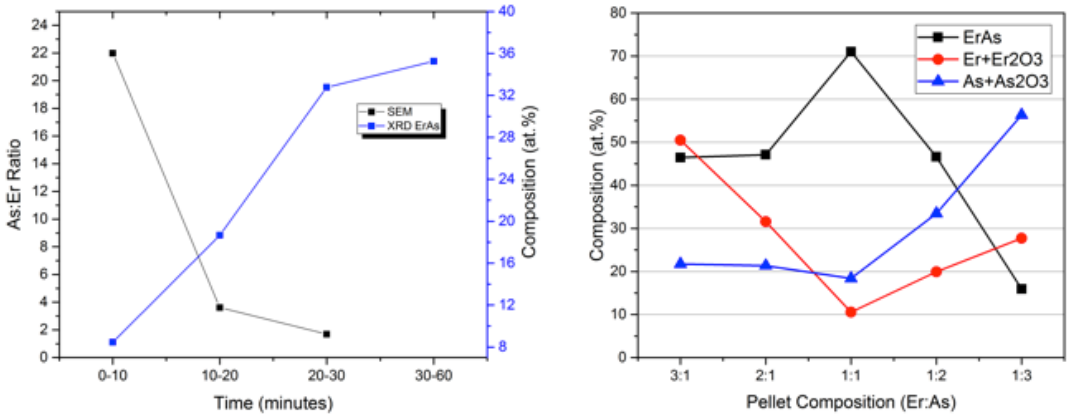

(left) As:Er ratio and ErAs composition of powder collected at various stage of the ablation, showing incongruent ablation that becomes more congruent over time. (right) Powder composition as a function of initial pellet composition showing that stoichiometric pellets produce the highest concentration of ErAs.

oxides of erbium and arsenic. We were previously able to show increases in ErAs composition through the use of high laser fluences, capable of ablating both species, as well as a high He

pressure to promote vapor interaction [1]. Further investigation into the target composition and the ablation process over time have yielded even higher concentrations of ErAs in our resulting powders.

Despite the challenges associated with the growth of non-oxide binary particles from powders with significantly different ablation rates, powders with up to 81.7 at.% ErAs could be synthesized using this technique. We have also demonstrated the flexibility in this growth technique by growing other Ln-V nanoparticles, including TbAs and ErN.

The next step is to incorporate these ErAs nanoparticles into a semiconductor matrix using LPE. Unlike single crystal growth, the growth of nanocomposite thin films by LPE requires the growth melt composition that is supersaturated with both the inclusion phase (ErAs) and also the constituents of the matrix (GaAs) that will form the thin film. Ternary phase diagrams, which are crucial to determining such melt compositions, are scarce and sometimes unreliable. As a result, various melt compositions must be evaluated to grow nanocomposite thin films. X-ray diffraction (XRD), scanning electron microscopy (SEM) and energy dispersive spectroscopy (EDS) have been used to study the compositions, thickness and morphology of both the growth melt solution and nanocomposites grown by LPE.

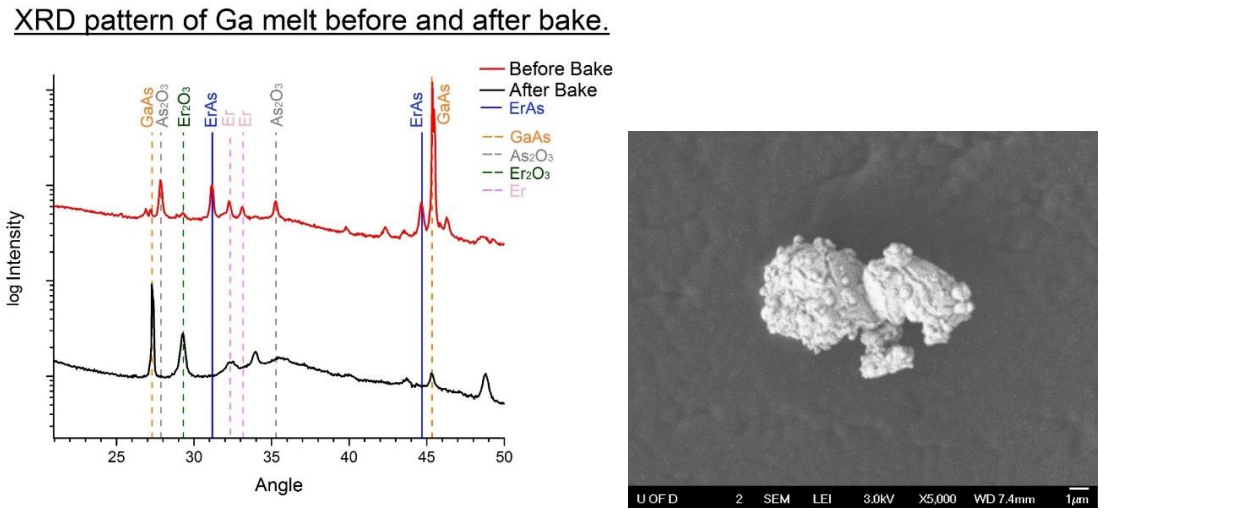

(Left) XRD pattern of Ga melt containing ErAs and GaAs before and after 800°C bake. Most of the ErAs disappears from the melt, while Er_2O_3 seems to increase after the bake. The source of Er_2O_3 is curious, because it could form from either oxidation of ErAs/Er, or the crystallization of amorphous Er_2O_3 that exist in the nanoparticle powder. (Right) SEM image of a large ErAs particle after 800 °C bake in Argon gas, with EDX showing that only small amount of ErAs is present in mostly erbium oxide.

Initially, ErAs nanoparticle powder tested for phase stability with and without a liquid melt, under processing conditions similar to those that would be observed during LPE film growth. We found that these particles tend to oxide in the optimum conditions (800°C) for growing GaAs thin films, causing a mismatch in terms of the growth of the included phase versus the semiconductor matrix. Moreover, there is a small composition window in which ErAs, GaAs and Ga can coexist during the LPE growth, which further restricts the growth perimeters. While oxidation of the particles remains a challenging issue, progress has been made in

determining growth temperatures at which nanoparticle powders can survive while growing thin films of nanocomposite. There is still optimization left in terms of the quality of such nanocomposite thin film, but we have demonstrated that these thin nanocomposite thin films are possible to be grown by LPE.

While there has less progress than expected in the growth of ErAs:GaAs thin films, we have been working hard in the area of Ln-V:III-V materials. Both graduate students on this project were part of the group effort in characterizing ErAs:GaBiAs, TbAs:GaAs and TbAs:InGaAs thin films grown by MBE. Furthermore, one of them was a co-author of a major review paper on Ln-As:GaAs paper, while the other is finishing up on a model that shows that TbAs:InGaAs as a great candidate for thermoelectric devices. In the mean time, our efforts have led to interest in using our LPE approach for the overgrowth of GaAs layer on top of gold contacts, which could be a novel approach for device fabrication.

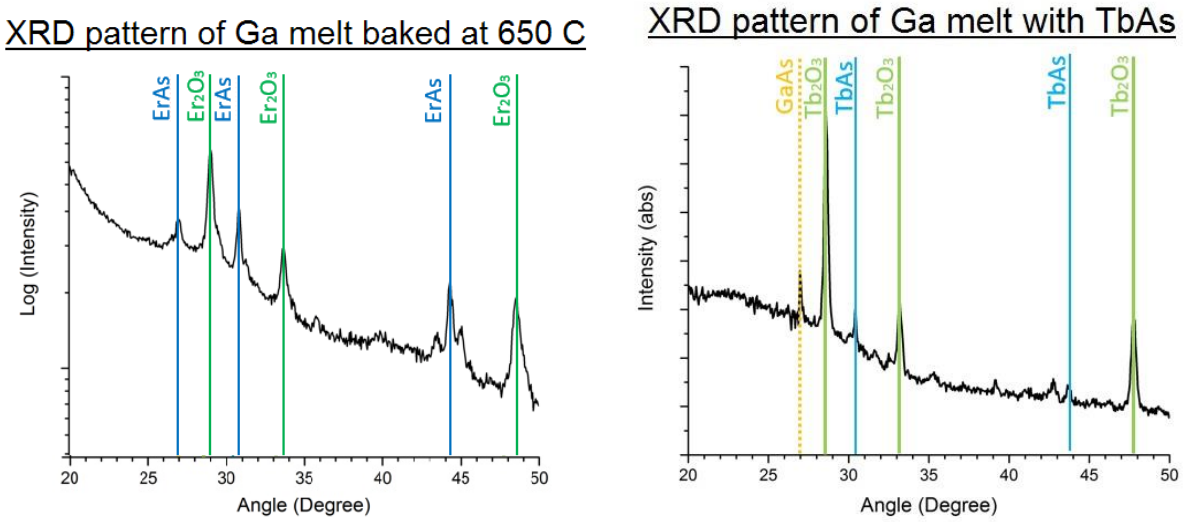

(Left) XRD pattern of Ga melt containing ErAs after 650°C bake. Even though most of Er_2O_3 continue to show up after the bake, there exists higher concentration of ErAs in the melt when compared to higher temperature bake. (Right) XRD pattern of Ga melt containing TbAs after 800°C bake. Similar to ErAs, Tb_2O_3 shows up after the bake, but significant amount of TbAs survived the much higher temperature when compared to the ErAs counterpart.

Future Plans

Through these studies, we have updated and improved upon our understanding of relevant ternary phase diagrams, further refined the growth window for these thin films, and investigated various challenges with the use of LPE for the creation of nanocomposite material systems. In the near future, we are continuing to optimize growth for ErAs:GaAs nanocomposite by 1) reducing roughness of the thin film surface and 2) varying the concentration of ErAs nanoparticles in the thin film. Recently, we found that decreasing the growth rate of ErAs:GaAs in LPE (by reducing the growth temperature and cooling rate) significantly reduces the oxidation of ErAs nanoparticles in the Ga melt, which will help the incorporation of ErAs in GaAs thin

film. Moreover, this drastically reduces the roughness of the thin film, which had plagued the growth of such composite material.

The main goal of this project is provide the material flexibility when selecting the nanoparticles in the semiconductor matrix. As we reported earlier, our lab has the capability to produce TbAs nanoparticles, the only Ln-V material that has been shown to behave like a semiconductor. (3) We have begun branching out from ErAs:GaAs – in part due to the difficulty we have faced growing such thin film - and experimented with TbAs:GaAs. Initial studies have shown that TbAs is more much resistant to oxidation compared to ErAs, even at higher temeratures which improve GaAs thin film growth. Other lanthanides, such as LuAs and ErP, are lattice-matched to GaAs, can be easily grown theoretically with this hybrid growth technique but a huge challenge with using the MBE, showing that LPE might still have an ace up compare to MBE.

While the results of this project are not consistent with our initial expectations, the overall success of this project in terms of developing young scientists has been outstanding. This project has allowed for the training of both two PhD-candidae graduate students, and also five undergraduate students who used their time in the lab to complete their senior research projects and write their senior theses. To this end the project has been successful, as shown by the number of collaborative publications on which these students have been equipped to contribute.

References

[1] M. Lewis, K. Bichoupan, S. I. Shah, and J. M. O. Zide, "Growth of ErAs Nanoparticles by Pulsed Laser Ablation", J. Elec. Mater. **45**, 6247 (2016) doi:10.1007/s11664-016-4775-z

Publications

Publications in 2015-2017

(1) M. Lewis, J. Zide "On the Formation of Binary Particle by Nanosecond Pulsed Laser Ablation of Pressed Powder Targets", *In Preparation*

(2) B. Tew, C. Bomberger, N. Halaszynski, J. Bahk, L. Clinger, T. Favaloro, A. Ramu, A. Shakouri, J. Bowers, J. Zide, "Electron Filtering by TbAs Nanoparticles in $In_{0:53}Ga_{0:47}As$ to Increase Seebeck Coefficient for Wide Temperature Thermoelectrics", *In preparation*

(3) B. Tew, M. Lewis, J. Zide, "On the incorporation of ErAs Nanoparticles in GaAs by Liquid Phase Epitaxy", *In preparation*

(4) C. Bomberger, M. Lewis, L. Vanderhoef, M. Doty, and J. Zide, "Overview of Lanthanide Pnictide Films and Nanoparticles Epitaxially Incorporated into III-V Semiconductors" J. Vac Sci. Tech. B **35**, 030801 (2017).

(5) C. Bomberger, B. Tew, M. Lewis, and J. M. O. Zide, "Growth and Characterization of TbAs Films." Appl. Phys. Lett. **109**, 202104 (2016).

(6) C. Bomberger, J. Nieto-Pescador, M. Lewis, B. Tew, Y. Wang, D. B. Chase, L. Gundlach, and J. M. O. Zide, "Growth and Characterization of ErAs:GaBixAs(1-x)." Appl. Phys. Lett., **109**, 172103 (2016).

(7) M. Lewis, K. Bichoupan, S. I. Shah, and J. M. O. Zide, "Growth of ErAs Nanoparticles by Pulsed Laser Ablation", J. Elec. Mater. **45**, 6247 (2016) doi:10.1007/s11664-016-4775-z

This page is intentionally blank.

Author Index

Participant List

Participant List

Name	Organization	E-Mail Address
Archer, Lynden	Cornell University	laa25@cornell.edu
Arnold, Michael	University of Wisconsin–Madison	msarnold@wisc.edu
Benicewicz, Brian	University of South Carolina	benice@sc.edu
Bent, Stacey	Stanford University	sbent@stanford.edu
Božović, Ivan	Brookhaven National Laboratory	bozovic@bnl.gov
Chambers, Scott	Pacific Northwest National Laboratory	sa.chambers@pnnl.gov
Chi, Miaofang	Oak Ridge National Laboratory	chim@ornl.gov
Clarke, Amy	Colorado School of Mines	amyclarke@mines.edu
De Yoreo, Jim	Pacific Northwest National Laboratory	james.deyoreo@pnnl.gov
Dee, Nicholas	Massachusetts Institute of Technology	nicktdee@mit.edu
Dierolf, Volkmar	Lehigh University	vod2@lehigh.edu
Du, Yingge	Pacific Northwest National Laboratory	Yingge.du@pnnl.gov
Dudney, Nancy	Oak Ridge National Laboratory	dudneynj@ornl.gov
Ediger, Mark	University of Wisconsin–Madison	ediger@chem.wisc.edu
Eom, Chang-Beom	University of Wisconsin–Madison	eom@engr.wisc.edu
Fecko, Christopher	US Department of Energy	christopher.fecko@science.doe.gov
Fedorov, Andrei	Georgia Institute of Technology	AGF@gatech.edu
Fichthorn, Kristen	Pennsylvania State University	fichthorn@psu.edu
Fiechtner, Gregory	US Department of Energy	gregory.fiechtner@science.doe.gov
Geohegan, David	Oak Ridge National Laboratory	geohegandb@ornl.gov
Gersten, Bonnie	US Department of Energy	bonnie.gersten@science.doe.gov
Han, Jung	Yale University	jung.han@yale.edu
Hanrath, Tobias	Cornell University	th358@cornell.edu
Hart, John	Massachusetts Institute of Technology	ajhart@mit.edu
Huang, Hanchen	Northeastern University	huanghanchen@gmail.com
Jain, Himanshu	Lehigh University	h.jain@lehigh.edu
Jin, Rongying	Louisiana State University	rjin@lsu.edu
Kaspar, Tiffany	Pacific Northwest National Laboratory	tiffany.kaspar@pnnl.gov
Kumar, Sanat	Columbia University	sk2794@columbia.edu
Lagally, Max	University of Wisconsin–Madison	lagally@engr.wisc.edu
Li, Dongsheng	Pacific Northwest National Laboratory	dongsheng.li2@pnnl.gov
Liu, Feng	University of Utah	fliu@eng.utah.edu

Liu, Jun	Pacific Northwest National Laboratory	jun.liu@pnnl.gov
Lunt, Richard	Michigan State University	rlunt@msu.edu
Mao, Zhiqiang	Tulane University	zmao@tulane.edu
Markowitz, Michael	US Department of Energy	mike.markowitz@science.doe.gov
Napolitano, Ralph	AMES Laboratory/Iowa State University	ren1@iastate.edu
Navrotsky, Alexandra	University of California, Davis	anavrotsky@ucdavis.edu
Ni, Ni	University of California–Los Angeles	nini@physics.ucla.edu
Olevsky, Eugene	San Diego State University	eolevsky@mail.sdsu.edu
Pechan, Michael	US Department of Energy	michael.pechan@science.doe.gov
Poudeu, Ferdinand	University of Michigan	ppoudeup@umich.edu
Schadler Feist, Linda	Rensselaer Polytechnic Institute	schadl@rpi.edu
Schlom, Darrell	Cornell University	schlom@cornell.edu
Schwartz, Andrew	US Department of Energy	andrew.schwartz@science.doe.gov
Sennett, Michael	US Department of Energy	michael.sennett@science.doe.gov
Shoemaker, Daniel	University of Illinois	dpshoema@illinois.edu
Sushko, Maria	Pacific Northwest National Laboratory	maria.sushko@pnnl.gov
Sutter, Eli	University of Nebraska–Lincoln	esutter@unl.edu
Sutter, Peter	University of Nebraska–Lincoln	psutter@unl.edu
Switzer, Jay	Missouri Univ. of Science and Technology	jswitzer@mst.edu
Thiyagarajan, Pappannan	US Department of Energy	p.thiyagarajan@science.doe.gov
Thornton, Katsuyo	University of Michigan	kthorn@umich.edu
Tringides, Michael	AMES Laboratory	tringides@ameslab.gov
Veith, Gabriel	Oak Ridge National Laboratory	veithgm@ornl.gov
Vetrano, John	US Department of Energy	john.vetrano@science.doe.gov
Voorhees, Peter	Northwestern University	p-voorhees@northwestern.edu
Wang, Cai-Zhuang	AMES Laboratory/Iowa State University	wangcz@ameslab.gov
Wei, Jiang	Tulane University	jwei1@tulane.edu
Xiao, Kai	Oak Ridge National Laboratory	xiaok@ornl.gov
Yakobson, Boris	Rice University	biy@rice.edu
Yoon, Mina	Oak Ridge National Laboratory	myoon@ornl.gov
Young, David	Louisiana State University	dyoung@rouge.phys.lsu.edu
Zaera, Francisco	University of California	zaera@ucr.edu
Zhou, Guangwen	State University of New York	gzhou@binghamton.edu
Zide, Joshua	University of Delaware	zide@udel.edu